

APPENDIX A
CONDITIONING OF PROBABILISTICALLY DERIVED GROUND MOTIONS AT
YUCCA MOUNTAIN

APPENDIX A – CONDITIONING OF PROBABILISTICALLY DERIVED GROUND MOTIONS AT YUCCA MOUNTAIN

A1. INTRODUCTION

This appendix describes work to update results of a probabilistic seismic hazard analysis (PSHA) for Yucca Mountain (CRWMS M&O 1998 [DIRS 103731]; BSC 2004 [DIRS 168030]) such that they reflect new understandings about the geologic setting of the site. New information on the limiting distribution of ground motion that can occur at the site is used to modify (condition) the hazard curves determined in the PSHA. Hazard curve conditioning is carried out using two approaches. One approach, based on geologic observations, laboratory testing of tuff mechanical properties, and ground motion site-response modeling, establishes an upper range of ground motion that has not been experienced at the waste emplacement level since those rocks were deposited about 13 million years ago. A second approach assesses a distribution on extreme stress parameter (stress drop) associated with the stochastic point-source ground motion model. Available data, interpretations, discussions documented in Section A3, and judgment provide the technical basis for an assumed distribution (Section 5.4). Modeling using this distribution is carried out to establish a distribution for the corresponding extreme ground motion appropriate for Yucca Mountain.

The PSHA for Yucca Mountain used a formal expert elicitation process to obtain seismic source, fault displacement, and ground motion interpretations forming the basis for a probabilistic calculation of seismic hazard. Ground motion results were given as the annual frequency of exceedance (AFE) for various levels of 0.3-, 0.5-, 1-, 2-, 5-, 10-, and 20-Hz spectral acceleration, peak ground acceleration (PGA) (100-Hz spectral acceleration), and peak ground velocity (PGV) (BSC 2004 [DIRS 168030], Section 6.5.3). Because investigations to characterize site material properties were limited at the time of the PSHA, ground motion hazard was determined for a hypothetical reference rock outcrop characterized by a shear-wave velocity of 1900 m/sec and a site attenuation kappa of 0.0186 sec (BSC 2004 [DIRS 168030], Section 6.3.3.1.1). Hence, to obtain ground motions for use in design and performance assessment analyses the PSHA results cannot be used directly. The effect of the site materials on ground motion must also be taken into account. A random-vibration-theory-based equivalent-linear site-response model is used for this purpose (BSC 2004 [DIRS 170027], this report).

As part of the PSHA, epistemic uncertainty and aleatory variability in ground motion were assessed and incorporated in the analysis (BSC 2004 [DIRS 168030], Section 6.1.2). The experts provided interpretations of epistemic uncertainty in the median value of ground motion and its standard deviation. Aleatory variability was characterized using untruncated lognormal distributions. Consequently, the PSHA model does not provide an upper bound to ground motion (i.e., a ground motion level for which the AFE is zero and the slope of the hazard curve approaches infinity). As lower and lower AFEs are considered, the level of associated ground motion continues to increase. Because 10 CFR 63 [DIRS 180319] requires demonstration that performance objectives are met for single Category 2 event sequences (i.e., those having at least one chance in 10,000 of occurring before permanent closure) and for a postclosure performance assessment that considers features, events, and processes with a greater than one chance in 10,000 of occurring over 10,000 years, ground motions with AFEs as low as 1×10^{-8} are of interest. Based on the PSHA (Figure A1), ground motion levels with such AFEs are high and

exceed those documented by historical strong motion recordings from tectonic earthquakes (Bommer et al. 2004 [DIRS 184601], Figure 3). For example, for an AFE of 1×10^{-8} the associated horizontal PGA and PGV are 11 g and 1390 cm/sec, respectively (MO03061E9PSHA1.000 [DIRS 163721]).

Deaggregation of the ground motion hazard indicates that, for AFEs of about 1×10^{-5} and lower, the dominant contribution comes from earthquakes within 15 km of Yucca Mountain with M 5.5 to 7 and ground motion that has an epsilon¹ of 1 to 2 or greater (BSC 2004 [DIRS 168030], Section 6.2.2.4). At these AFEs primary contributions to ground motion hazard include earthquakes on the Paintbrush-Stagecoach Road and Solitario Canyon faults (BSC 2004 [DIRS 168030], Section 6.5.4); faults characterized as left-lateral strike-slip or normal mechanism dipping about 60-degrees to the west. The slip rate of these faults range from 0.01-0.05 mm/yr and their closest horizontal distance ranges from 1-10 km (BSC 2004 [DIRS 168030], Table 6). Given the contribution from these local faults it is reasonable to infer that for AFEs of 1×10^{-4} and lower, the earthquakes controlling ground motion hazard occur primarily at distances within 5 km of the site and have magnitudes ranging from M 5-7.5. This conclusion is illustrated schematically in Figure A2 for PGA and Figure A3 for PGV. The uncertainty in the faulting parameters and rates of deformation together with the epistemic uncertainty in the ground motion prediction model, results in the mean hazard exceeding the 85th fractile at an exceedance of about 10^{-6} /yr (Figure A1). The hazard deaggregation for exceedance of about 10^{-7} /yr and less indicate that a majority of the hazard is contributed from exceedance of the 95th percentile (epsilon of 2 or greater) of the ground motion prediction distributions (Figures 6.4.1-10 and 6.4.1-16). In this report, ground motion from these larger and closer events that is far in excess of that recorded historically is termed “extreme”.

Subsequent to the PSHA, scientists have questioned whether the ground motions calculated for low AFEs can be realized at Yucca Mountain (Corradini 2003 [DIRS 171191]; Reiter 2004 [DIRS 170694], Bommer et al. 2004 [DIRS 184601]). This motivated a study (BSC 2005 [DIRS 170137]) in which geologic observations in underground excavations at Yucca Mountain, results of laboratory testing of tuff supplemented by numerical simulations of tuff deformation, and ground motion site-response modeling were used to establish a distribution on the level of horizontal PGV that has not been experienced at the waste emplacement level during the past 12.8 million years. This distribution of PGV was taken as a reasonable limit or bound to ground motions that can occur at Yucca Mountain and used to condition AFEs for horizontal PGV at the waste emplacement level (BSC 2005 [DIRS 170137]). The conditioned hazard curve resulting from this study is used in postclosure analyses (SNL 2007 [DIRS 178851], SNL 2007 [DIRS 176828]).

To enhance the characterization of ground motions at Yucca Mountain with low AFEs, the present study updates the BSC (2005 [DIRS 170137]) analysis and implements a second approach to condition AFEs. The previous analysis is updated based on site-response modeling that uses revised site material properties. Also, an alternative approach is used for incorporating site response in the development of hazard-consistent site-specific ground motions. As in the

¹ Epsilon is the difference between the logarithm of the ground motion amplitude and the mean logarithm of ground motion (for that magnitude and distance), measured in units of the standard deviation of the logarithm of ground motion (McGuire 1995 [DIRS 107483]).

previous site-response modeling (BSC 2004 [DIRS 170027], Section 6.2), aleatory variability in site properties is included. The updated analysis also extends the approach to ground motion measures other than PGV. In addition, constraints on ground motion at the repository waste emplacement level are transformed to constraints on ground motion at the PSHA reference rock outcrop. This allows their use in determining site-specific ground motions for other locations such as the surface facilities area.

The second approach uses a stochastic point-source model (Section 6.3) to determine ground motions for earthquakes controlling Yucca Mountain hazard at low AFEs. A distribution on extreme stress drop, which controls the high frequency level of ground motion, is assessed based on judgment as well as available data. This distribution is used to define a corresponding distribution on extreme ground motion.

Both approaches are used to condition the PSHA ground motion hazard curves. However, constraints from the second approach (i.e., a distribution on extreme stress drop used in the stochastic ground motion model) control the conditioning of the hazard curve. This result is not unexpected as the previous approach only provides information on the upper level of ground motion that has not been experienced, not the level that has occurred or is possible.

In the following sections, first the updated implementation of the approach described in BSC (2005 [DIRS 170137]) is presented. This is followed by a discussion of the approach based on an assessment of a distribution on extreme stress drop used in the stochastic ground motion model that is consistent with the geologic setting of Yucca Mountain. Finally, the use of both approaches jointly to condition the existing PSHA ground motion hazard curves is described.

A1.1 Other Studies

Andrews et al. (2007 [DIRS 184818]) have proposed an upper bound on PGV based on deterministic modeling of fault rupture. For the Solitario Canyon fault, PGV limits of 360 and 570 cm/sec for the horizontal and vertical component respectively were found using limits of crustal stress and maximum possible static stress drop. Two-dimensional geologic structure was assumed with symmetry in the east-west direction. Limits on PGV are found by maximizing constructive interference from the rupture front. Using alternative slip scenarios, limiting PGV hazard was derived. At an exceedance probability of 10^{-8} /yr, the derived horizontal PGV limit is about 50% of the PSHA reference rock outcrop value.

Anderson et al. (2007 [DIRS 184472]) have investigated the ground motions necessary to disturb precariously balanced rocks on the Yucca Mountain crest and vicinity. They concluded that the presence of the precariously balanced rocks shows that the PSHA for Yucca Mountain is conservative and that the aleatory and epistemic uncertainties on the ground motion prediction models may be too large.

A2. UPDATED SHEAR-STRAIN THRESHOLD APPROACH

In BSC (2005 [DIRS 170137]) an analysis was presented that combined geologic observations in the ESF and ECRB cross-drift, laboratory rock mechanics testing of Topopah Spring tuff,

numerical simulations of tuff deformation, and ground motion site response modeling to establish a distribution for the level of horizontal PGV that has not been experienced at the waste emplacement level since soon after the Topopah Spring Tuff was deposited. This analysis is supplemented as part of the work documented in this report, including use of updated site-response model inputs and a revised implementation approach.

A2.1 Previous Work

A key result of this analysis was the determination of a shear-strain threshold that, if exceeded, would be expected to result in wide-spread fracturing of the lithophysal units. Results of unconfined uniaxial compression tests carried out in the laboratory were used to infer the shear-strain threshold at which failure occurred (BSC 2005 [DIRS 170137], Figure 6-5). To enhance confidence in this result, numerical simulations of tuff mechanical deformation were also carried out using validated models. Results of the numerical simulations corroborated the laboratory test results (BSC 2005 [DIRS 170137], Figure 6-6). The numerical simulations also indicated that fracturing in response to shear strains exceeding the threshold would typically result in fractures extending between lithophysae. Because of variability in the test and simulation results, the shear-strain threshold was defined as a triangular distribution extending from 0.09 to 0.25% with a mode of 0.16% (BSC 2005 [DIRS 170137], Figure 6-6).

Given a shear-strain threshold above which fracturing of the lithophysal units of the Topopah Spring Tuff is expected, geologic data gathered in the ESF and ECRB cross-drift were studied to investigate whether such fracturing can be observed. Three types of geologic observations were made. First, fracture data were evaluated to assess their association with deposition/cooling versus mechanical damage subsequent to cooling. Fractures exhibiting rims, borders, and vapor-phase mineral coatings formed early during the cooling of the deposit. Fractures that do not exhibit these features formed either late in the cooling process after the vapor phase had been removed or subsequent to the cooling phase. Based on the assessment, about 70% of the mapped fractures are positively related to cooling with the remainder indeterminate. Also, the vast majority of fractures have no evidence of shear or mechanical degradation (BSC 2005 [DIRS 170137], Section 6.3.1). Second, lithophysae were examined for evidence of damage, especially at locations where fractures intersected them. Only a small percentage of lithophysae are transected by fractures greater than 1 m in length or by shears and none show appreciable effects of damage to their walls (BSC 2005 [DIRS 170137], Section 6.3.2). Third, observations of the relation between fractures and lithophysae were compared to those predicted by numerical simulations. Rather than showing patterns consistent with exceedance of the shear-strain threshold, the relations are consistent with localized fracturing of matrix-groundmass during cooling or minor amounts of extension, probably during structural tilting of the mountain (BSC 2005 [DIRS 170137], Section 6.3.3). Thus, geologic evidence does not support the occurrence of seismically-induced shear strains exceeding the shear-strain threshold for fracturing of lithophysal Topopah Spring tuff.

Ground motion site-response modeling was used to determine the level of horizontal PGV that would be associated with seismically-induced shear strains that exceed the shear-strain threshold for fracturing. Epistemic uncertainty in site material properties was taken into account by carrying out the analysis for four combinations of tuff velocity profile and dynamic material properties characterizing the uncertainty (BSC 2005 [DIRS 170137], Section 6.5). In addition,

for each of the four combinations, two cases of ground motion input to the site response model were analyzed: one representing an earthquake controlling high frequency spectral response and one controlling low frequency response. Site-response modeling was carried out for 4 mean AFEs. Median horizontal PGV and shear strain were averaged over the depth range for the Topopah Spring Tuff lower lithophysal unit. For each AFE, the resulting correspondence between horizontal PGV and shear strain, for each combination of uncertain site properties and structural frequency range, was used to transform the shear-strain threshold distribution into one for horizontal PGV (BSC 2005 [DIRS 170137], Figure 6-8). This resulted in 8 probability distributions for the level of horizontal PGV that has not been experienced at the waste emplacement level, which were treated as being equally likely.

A2.2 Supplemental Work

The original analysis documented in BSC (2005 [DIRS 170137]) is here supplemented to incorporate updated data on site properties, to extend the analysis to ground motion measures other than horizontal PGV, to evaluate the shear strain at the waste emplacement level in terms of ground motion at the PSHA reference rock outcrop, and to include the aleatory variability in shear strain associated with a given value of a ground motion measure.

In BSC (2005 [DIRS 170137], Section 6.5), the association of a value of shear strain with a value of horizontal PGV is based on the results of site-response modeling documented in BSC (2004 [DIRS 170027], Section 6.3.4). Model inputs include velocity profiles as a function of depth and curves representing the variation of shear modulus, normalized to its low strain value, and material damping (BSC 2004 [DIRS 170027], Section 6.2). Since the modeling and analysis described in BSC (2005 [DIRS 170137]) and BSC (2004 [DIRS 170027]), these model inputs have been updated to take into account additional geotechnical data that were collected (Sections 6.4.2 and 6.4.4). The current analysis to determine the distribution of shear strain associated with a given value of a ground motion measure is based on this updated site-response modeling (Section 6.5).

In BSC (2004 [DIRS 170027]), site response was modeled for input control motions with AFEs ranging from 1×10^{-3} to 1×10^{-7} based on results of the PSHA. The correspondence between horizontal PGV and shear strain was determined using results for AFEs of 1×10^{-4} , 1×10^{-5} , 1×10^{-6} , and 1×10^{-7} . To convert the probability distribution for shear-strain threshold to one for horizontal PGV, linear interpolation was used between the values determined at these AFEs (BSC 2005 [DIRS 170137], Section 6.6). For the current analysis, input control motions to site-response modeling were not based on AFEs, but rather were based on PGA. In carrying out the site-response modeling, a range of input control motions ranging from 0.1 g to 10 g was used (Sections 6.1.2, 6.5). Results of this updated site-response modeling form the basis for determining the updated correspondence between values of a ground motion measure and shear strain. As in BSC (2005 [DIRS 170137]), site-response is determined for combinations of repository block (RB) base-case velocity profile and tuff dynamic material property curves. The base-case profiles represent alternate mean velocity and material property profiles necessary to satisfactorily incorporate alternate interpretations of the site characterization data.

In BSC (2005 [DIRS 170137]) the shear strain threshold approach was used to determine a distribution for the level of horizontal PGV that has not been experienced at the waste

emplacement level at Yucca Mountain. In the supplemental work described in this report, the approach has been extended to determine levels of other ground motion measures that have not been experienced. Specifically, the analysis has been extended to address the same suite of ground motion measures that were addressed in the PSHA (i.e., spectral acceleration at 0.3, 0.5, 1, 2, 5, 10, and 20 Hz, PGA (100-Hz spectral acceleration), and PGV).

In BSC (2005 [DIRS 170137]) the shear-strain threshold approach was used to condition the horizontal PGV hazard curve for the waste emplacement level. Based on the shear-strain threshold distribution, a corresponding distribution for the level of horizontal PGV that has not been experienced at the Yucca Mountain waste emplacement level was determined using the site response results. For the supplemental work described in this report, the shear strain threshold is not used directly to assess a limiting distribution on ground motion at the waste emplacement level, but rather to establish the level of ground motion not experienced at the PSHA reference rock outcrop. For a given combination of site-response model inputs (velocity profile, dynamic material property curve set, oscillator frequency range), the median shear strain averaged over the average depth range for the Topopah Spring Tuff lower lithophysal unit (BSC 2005 [DIRS 170137], Section 6.5) is tabulated for a suite of site-response model control motion inputs. This results in a look-up table consisting of median shear strain as a function of ground motion amplitude at the PSHA reference rock outcrop for each combination of site-response model inputs and ground motion measure. Intermediate values are determined by log-log interpolation as needed.

In BSC (2005 [DIRS 170137]), aleatory variability in shear strain was not incorporated in the analysis. For the supplementary work described in this report, aleatory variability is included. Shear strains are taken to be logarithmically distributed with a standard deviation determined on the basis of site-response modeling.

In BSC (2005 [DIRS 170137], Section 6.4), the shear strain threshold is characterized with a triangular distribution to represent uncertainty in its value based on laboratory testing and numerical simulations. The distribution ranged from 0.09 to 0.25% with a mode of 0.16%. For the supplementary work described in this report, a uniform distribution is used. The range of the distribution is maintained at 0.09 to 0.25%.

Details of the analysis are provided in Appendix D.

A3. DISTRIBUTION ON EXTREME STRESS DROP APPROACH

As described above, the shear strain threshold approach to characterizing extreme ground motion provides information on the level of ground motion that has not been experienced at the Yucca Mountain waste emplacement level. While this information is useful and has been employed as a reasonable upper bound for horizontal PGV (BSC 2005 [DIRS 170137]), Section 6.7), it is desirable to better characterize the level of extreme ground motion that is possible at Yucca Mountain. In this section an approach based on constraints at the seismic source is described. An assessment is carried out to determine reasonable distributions of extreme stress drop associated with the stochastic point-source model. The stochastic point-source model is then used to characterize the distribution of extreme ground motion at the PSHA reference rock outcrop. At low AFEs, to preserve the spectral shape of the UHS for the reference rock outcrop,

the extreme-stress-drop-conditioned hazard is developed for PGA and then used to scale the reference rock outcrop UHS for a given AFE. This process retains the inputs of the original PSHA on spectral shape rather than resulting in a purely point-source spectral shape at the low AFEs. Because the unconditioned spectral shapes change little with AFE at low levels (Figure A13), this process is considered to result in reasonable and realistic conditioned hazard reflecting the original ground motion experts' attenuation relations with conditioning applied to the upper tails of their distributions.

It is important to emphasize this approach is not intended to “cap” or “limit” strong ground motions. The approach was developed and implemented to condition the exceedance probability of PSHA reference rock outcrop motions using an assessment regarding extreme values of stress drop applicable to earthquakes potentially affecting the Yucca Mountain normal faulting (extensional) environment. Available information, including data that were not available at the time of the PSHA, is considered in formulating the distribution of extreme stress drop. The distribution is treated as an assumption. Its technical basis is described below and summarized in Section 5.4.

The assumption of a distribution for extreme stress drop is informed by the judgments of experts, but it is not the result of formal expert elicitation processes (Kotra et al. 1996 [DIRS 100909]). As will be described, the advice of acknowledged experts was solicited in a series of workshops and recorded in meeting materials that are attached to this appendix. Ultimately, however, the assumption made and the justification for that assumption, based on available data, interpretations, and judgments, lies with the project. Accordingly, the information given in this appendix supports the technical justification for the assumption given in Section 5.4 of this report.

The stochastic point-source ground motion model is described in Section 6.3. Validation of the model is presented in Section 7. The model uses an ω -square source model (Brune 1970 [DIRS 103315], 1971 [DIRS 131516]) with a single corner frequency and a constant stress drop (Boore 1983 [DIRS 103317], Atkinson 1984 [DIRS 174445]). Based on the model, Equation 6-6 provides an expression for the acceleration spectral density. Source scaling is provided by specifying two independent parameters, the seismic moment (M_0) and the stress drop ($\Delta\sigma$). As defined in the model, the stress drop (and corresponding corner frequency, Equation 6-8) establishes the high-frequency portion of the acceleration spectrum. The stress drop is sometimes referred to as the stress parameter (Boore 1983 [DIRS 103317]) since it directly scales the Fourier amplitude spectrum for frequencies above the corner frequency (Silva 1991 [DIRS 163656], Silva and Darragh 1995 [DIRS 105398]). Model results at high (> 1 Hz) frequency are sensitive to this parameter (Silva 1991 [DIRS 163656]). The interpretation of the parameter as a stress drop implies that earthquake sources are characterized by ω -square scaling and the single-corner-frequency model and thus it has a physical interpretation in source processes. Alternatively, it can be viewed simply as a high frequency scaling factor. In this report, the term “stress drop” is used hereafter for “stress parameter”.

A3.1 Appropriateness of Model to Characterize Extreme Ground Motions

Bommer et al. (2004 [DIRS 184601]) enumerate factors driving and limiting extreme ground motion. In general, three factors are involved: seismic radiation from the source, interaction of

radiation from different parts of the source and along different travel paths, and limitations on the level of motion that can be transmitted by shallow geologic materials.

Validation of the stochastic point-source model (Section 7) provides confidence that it is appropriate for use in characterizing the distribution of extreme ground motion at Yucca Mountain. One aspect of model validation compares predictions of 5%-damped response spectra for a combined stochastic point-source/equivalent-linear site response model to recorded data to assess model bias and variability (Silva et al. 1996 [DIRS 110474], Section 5.12). Combined model bias is slightly positive for frequencies greater than about 10 Hz, indicating a slight under-prediction of ground motions, and is near zero from about 10 Hz to 1 Hz. Below 1 Hz, negative bias indicates the model over-predicts response spectra. The analyses are considered reliable down to about 0.3 Hz at which point the combined model shows about a 40 percent over-prediction. Elimination of the over-prediction when a stochastic finite-source model is coupled with the site-response model (Silva et al. 1996 [DIRS 110474], Section 5.12) suggests that the low-frequency over-prediction is a result of the point-source component of the model, not the site-response component. The validation illustrates the effectiveness of the stochastic point-source model to predict 5%-damped response spectra for recorded strong ground motion. The over-prediction at long period suggests that the application of the model will be conservative relative to an approach using a finite source model.

A3.2 Development of Distributions for Extreme Stress Drop

A3.2.1 Assessment Workshops

Assessment of a distribution for extreme stress drop to characterize extreme ground motion is based on data, interpretations, and judgments. To facilitate this assessment, a series of workshops was held in which project experts in engineering seismology and the use of the stochastic ground motion model, discussed the technical basis for appropriate, reasonable, and defensible values for extreme stress drop. The experts participating in the workshops were Dr. Gail Atkinson, Dr. David Boore, Dr. Arthur McGarr, and Dr. Walter Silva. Dr. John Boatwright, Dr. Thomas Hanks, Dr. Richard Quittmeyer and Dr. Richard Lee also participated in some of the discussions. During the workshops approaches were evaluated to provide a technical basis for developing a distribution on extreme stress drop used in the stochastic ground motion model. The experts are internationally recognized in engineering seismology and geophysics.

The first meeting consisted of discussion of alternate ways to develop values of extreme stress drop. A significant portion of the meeting was dedicated to identification of data needs and new directions for data compilation activities were developed. At a second meeting data were reviewed and approaches to assess a distribution for extreme stress drop were discussed. Following the first two meetings, feedback on the impact of a distribution on extreme stress drop values on the hazard was provided to the experts to understand the impacts of alternate approaches. Finally, each expert had an opportunity to comment on each other's opinion or approach.

The meetings were conducted directly with the participants with the exception of Dr. Atkinson who joined the meetings on two occasions by conference call. All of the meetings were generally begun by Dr. Lee describing the structure and goals of the meetings followed by

presentations by the experts on their preferred approach to develop a limiting distribution on stress drop or to report the results of a special predefined task. Key presentations and documentation of assessments are contained in the attachments to this Appendix.

Following the experts' presentations on approaches to develop a distribution on extreme stress drop, all approaches were discussed as a group and decisions were made to use, refine, or discard each approach. Based on the input provided by the experts, conditioned hazard was evaluated using each expert's extreme stress drop assessment and feedback was provided to all of the experts on the impact of each expert's and the combined experts' input. A final meeting was completed following the feedback and these results are described below. The final distribution on extreme stress drop was then developed based on the input and discussions provided by the experts.

A3.2.1.1 Workshop Expectations

The first workshop was opened with a discussion of the assessment expectations and directions. These expectations and directions were as follows:

- (1) The purpose of the workshops is to provide values of extreme stress drop that could be used to condition seismic hazard at Yucca Mountain.
- (2) This distribution on extreme stress drop is based on currently available information. If additional studies are carried out in the future to enhance the technical basis for the distributions, the workshop results could be updated.
- (3) The workshop results and subsequent distribution on extreme ground motion will be incorporated in the repository ground motion assessment to be carried out in 2007.
- (4) The final product will be developed and owned by the Project and not the individual experts.
- (5) The experts can be proponents of various approaches, but are also expected to serve as evaluators of the relative credibility of alternate approaches.
- (6) The following questions will be asked in advance: (a) what are the appropriate approaches to develop values of extreme stress drop for the repository and (b) what is your estimate for the value or associated distributions and what is the basis?
- (7) The expert will provide a value and/or a continuous or discrete distribution on extreme stress drop and multiple approaches can be incorporated in the expert's response.
- (8) Any dependencies related to the assessed extreme stress drop value, such as earthquake magnitude/moment, source depth, mechanism, fault slip-rate, or hazard return period, should be described.

A3.2.1.2 Workshop Proceedings

This section summarizes the workshop proceedings. The summaries are not intended to be comprehensive, but rather focus on key discussions and assessments. Key presentations are included as attachments to this Appendix.

Workshop of January 25, 2007

Attendees: Dr. Boore, Dr. McGarr, Dr. Silva, Dr. Hanks, Dr. Ake, Dr. Lee

The purpose of this workshop was to initiate the assessment and have a general discussion of approaches that could be used to develop a distribution on extreme stress drop. Impromptu presentations/discussions were given by three of the experts (Attachment A-1). Overall project goals, purpose and structure of the workshops, and the primary seismic source contributors (faults) to low AFE ground motions were discussed.

Dr. Silva discussed the structural characterization of Yucca Mountain for ground motion evaluations and the implications for design ground motions. Dr. Silva also presented summaries of stress drops and their distributions inferred from strong motion recordings in the eastern and western United States and noted a tendency of stress drop to decrease with increasing magnitude.

Dr. Boore summarized work-in-progress by Dr. James Dewey and himself comparing measurements of m_b and M_s values worldwide in which high m_b relative to M_s could be an indicator of high stress drop. Based on a review of the data it was concluded that inferences or generalizations on stress drop models that could fit the data were at best weakly constraining stress drop. Following additional discussion, a consensus developed that these relationships were of limited use at this time because of the complexities and bias in a high frequency magnitude measurement. Dr. Boore agreed to review the data again with his co-investigator and possibly add additional catalog data.

Dr. McGarr introduced the relationship between apparent stress (τ_a) and stress drop ($\Delta\sigma$) developed by Singh and Ordaz (1994 [DIRS 184394]):

$$\frac{\tau_a}{\Delta\sigma} = 0.233 \quad \text{(Equation A-1)}$$

Dr McGarr observed that laboratory and earthquake data suggest that $\tau_a < \sim 10$ MPa (100 bars) which may suggest an extreme value of about 400 bars on stress drop. It was pointed out that the Singh and Ordaz relationship was dependent on source spectral shape (ω^2) and that other source spectral models should be employed as a check. It was agreed that additional source models, such as the 2-corner model of Atkinson (1993 [DIRS 184793]), should be considered. Data on apparent stress should also be reviewed.

Other meeting notes/comments:

In reference to the limited availability of stress drop data, Dr. Hanks noted that there is an insufficient number of inferred values to justify an extreme value based on the maximum values observed. Based on the recurrence rate of earthquakes at Yucca Mountain, at $10^{-8}/\text{yr}$ 100 to 1000 observations would be needed to observe an extreme stress drop. It was also agreed that, because of the difficulty of inferring stress drop for smaller earthquakes, stress drops for only $M > 5$ should be considered, although Dr. Silva noted that stress drop appeared to be stable for a magnitude range of **M** 1 to **M** 8 (about 10 orders in seismic moment).

A discussion ensued on possible source mechanism dependence of stress drop and no consensus was reached on whether that dependence was present.

It was agreed that the group should consider the available data on stress drop from different tectonic environments because useful consistencies may be observed.

Workshop of February 13, 2007

Attendees: Dr. Atkinson, Dr. Boore, Dr. McGarr, Dr. Silva , Dr Hanks, Dr Ake, Dr. Lee, Dr. Quittmeyer, Dr. Boatwright

Presentations and Discussions

The purpose of this workshop was to provide results of the follow-up investigations and initiate the first round of expert positions on stress drop. Presentations were given by each of the experts (Attachment A-2).

Dr Silva reviewed stress drop from the literature and Pacific Engineering and Analysis special studies. Models for western North America (WNA) earthquakes suggest a depth dependency in stress drop with stress drop lower for shallow earthquakes. In inferring stress drop, Dr Silva isolates the effects of Q , κ , and site conditions on spectra, and for larger earthquakes notes that shallow slip dominates the spectra and stress drop decreases for increasing magnitude. For similar analysis of central and eastern United States (CEUS) earthquakes he sees the same magnitude dependency with stress drop but with a higher median stress drop for the EUS. Dr. Silva reviewed stress drop inferences from earthquake data reported for earthquakes occurring in Korea, Greece, Italy and Turkey and believes that the inferences are biased because of the lack of consistency in site corrections and geometrical attenuation incorporated in those studies. Dr. Silva noted that using a deterministic approach to model the probabilistic ground motions for Yucca Mountain at annual exceedances of 10^{-7} to 10^{-8} requires source representations with a stress drop on the order of 2500 bars.

Dr Silva's stress drop results were summarized as follows (Table A-1):

Table A-1. Summary of Stress Drop Data

Earthquake Geographic Region	Magnitude Range (M)	Number of observations (n)	Median Stress drop- μ_{ln} (bars)	Stress drop Sigma (σ_{ln})	Stress drop Range (bars)
Western US	5-7.5	15	42	0.55	13-100
Korea	5-7	7	47	1.00	10-130
Korea	2-7	296	56	.93	5-1350
Central and Eastern US	2-5	122	36	.83	4-314
Central and Eastern US	4-5	16	110	.57	49-314
Central and Eastern US	4-8	36	170	.60	55-800
Central and Eastern US	4-7	25	145	.57	55-500
Greece	5-7	18	63	.57	32-290
Italy	4-6.5	9	181	.31	116-340
Italy/3	4-6.5	9	60	.31	38-113

Source: Dr. Silva presentation at Workshop 1 (see Attachment 1)

Inferences on stress drop drawn from the Italian data were questioned by the experts because the authors did not incorporate site effects. Inferences on stress drop from the Korean earthquakes are also questioned because they occurred offshore and therefore their distance and magnitudes are more uncertain.

Dr. Silva summarized stress drop by region as follows (Table A-2):

Table A-2. Regional Summary of Stress Drop Data

Earthquake Geographic Region	Magnitude Range (M)	Number of observations (n)	Median Stress drop (bars)	Stress drop Sigma (σ_{in})	Stress drop Range (bars)	2σ
All	4-7.5	81	82	0.78	10-500	391
Western US + Greece	5-7.5	33	52	0.59	13-290	170
Central and Eastern US	4-7	33	125	0.56	49-500	383

Note: Values from Table A-1 that are considered by Dr. Silva to be unreliable are not included in this table. For example, a stress drop value of 800 bars for the Central and Eastern US that was inferred from intensity data is not included.

Source: Dr. Silva presentation at Workshop 1 (see Attachment 1)

Dr. Hanks noted that in Andrews (2007 [DIRS 184349]), directivity is important to the occurrence of large ground motions and that the limiting stress drop logic should have a dependency on exceedance probability. Dr. Silva believes that rupture directivity may be accounted for in an average horizontal component in the single corner stochastic ground motion model due to the negative low-frequency bias. Dr. Silva also raised an issue with Andrews (2007 [DIRS 184349]) results because that model has not been either validated or calibrated with data nor fit to any single observed earthquake. Validations are considered essential to assess reasonableness of parameters, model accuracy, as well as any model bias.

Dr. McGarr made a presentation on stress drop constraints based on seismic and laboratory observations. Dr. McGarr showed that with the exception of one borehole recording in Long Valley caldera, their collected observations suggest that apparent stress is relatively low, $\tau_a < 10$ MPa (100 bars) and with the exception of one station recording, there were no obvious moment dependencies (McGarr and Fletcher, 2003 [DIRS 170693]). McGarr and Fletcher (2003 [DIRS 170693]) compiled over 200 inferred values of apparent stress for earthquakes from magnitudes ranging from $M < -3$ to $M > 7$ with apparent stresses ranging from 0.001- 10 MPa. For earthquake magnitudes $M > 5$, apparent stress drop ranged from 1-10 MPa (10-100 bars).

Using the single-corner model of the amplitude spectrum, Dr. McGarr illustrated the Singh and Ordaz relationship using the definition of radiated energy in terms of stress drop and spectral velocity:

$$E_s = \frac{\tau_a M_0}{\mu} = 4\rho\beta R^2 \int_0^{\infty} V(\omega, \omega_0)^2 d\omega \quad (\text{Equation A-2})$$

For a single corner model Dr. McGarr showed that Equation A-2 reduces to:

$$\tau_a = 0.23\Delta\sigma$$

And thus for a single-corner model, stress drop has a relatively simple theoretical relationship to apparent stress.

To illustrate parallels between laboratory induced shear ruptures and large earthquakes, Dr. McGarr compared inferences on maximum fault rupture slip-rate to show that for seismic moment ranging from laboratory data to large earthquake data, slip rates seem to have a similar distribution. Also, maximum observed slip (m) followed a simple trend suggesting that scaling relationships should be consistent between laboratory stick-slip experiments and large earthquakes. Using stick-slip laboratory data by Lockner and Okubo (1983 [DIRS 170902]), Dr. McGarr showed that both laboratory data and earthquake data followed the Singh and Ordaz relationship (Equation A-1). Further, Dr. McGarr argues that laboratory and earthquake data suggest that apparent stress is independent of magnitude and normal stress but dependent on loading stresses. Dr. McGarr noted that the Singh and Ordaz (1994 [DIRS 184394]) relationship (Equation A-1) was developed for a single-corner source model without directivity effects. Dr. McGarr believes that this is the best approach to characterize extreme stress drop.

Dr. Boore revisited the work being carried out with Dr. Dewey comparing m_b and M_S and noted that there were cases such as the Cape Mendocino earthquake that had a relatively high stress drop but low m_b relative to M_S . Dr. Boore concluded that there was too much variability in m_b/M_S measurements and that this approach would not be fruitful to characterize extreme values of stress drop. Dr. Boatwright agreed, mentioning that although the method was appealing because of the large number of measurements there was a Mammoth Lakes earthquake exhibiting the same characteristics as the Cape Mendocino earthquake and in his opinion variability in 1 sec source spectrum is not a good indicator of higher frequency motions.

Dr. Boore presented his investigation of the Singh and Ordaz relationship for a suite of 2-corner source models and found that with one exception the ratio of effective stress to stress drop was significantly lower for the equivalent 2-corner case:

$$\left(\frac{\tau_a}{\Delta\sigma} \right)_{2c} < \left(\frac{\tau_a}{\Delta\sigma} \right)_{1c}$$

That is, one would underestimate the stress drop if the Singh and Ordaz relationship were used to convert an apparent stress to stress drop if the spectrum had the form of a 2-corner model. Using preferred 2-corner source models, Dr Boore illustrated the magnitude dependency of the correction and finds that $\tau_a/\Delta\sigma$ it can be as small as 0.09 or 0.06 for WNA or ENA double-corner models respectively.

Dr Atkinson discussed various comparisons or inferences on stress drop for earthquakes in the EUS vs WUS. She noted that stress drop is about a factor of 2 higher in the EUS and the distributions exhibited a sigma of about a factor of 2. Dr. Atkinson does not believe there is a justifiable physical extreme value that could be placed on stress drop based on current data, although she felt that truncating the distribution on stress drop was acceptable.

Expert Assessments

Based on Dr. McGarr's judgment of a maximum apparent stress for Yucca Mountain of about 10 MPa, Dr. Silva used the Singh and Ordaz single-corner relationship and Dr. Boore's two-corner adjustment to the Singh and Ordaz relationship to develop extreme values of stress drop of 500 and 1000 bars. Dr. Silva added a + 50% variability with weights of 0.2 and 0.8 applied to the two-corner and one-corner source models respectively.

Dr. Atkinson stated that she believes there is a physical limit on stress drop but felt that there was no defensible basis for providing values at this time.

Dr. McGarr believes that very controlled laboratory experiments of stick-slip behavior are most useful to develop extreme values of stress drop. Based on the laboratory measurements of apparent stress and stress drop of Lockner and Okubo (1983 [DIRS 170902]), Dr. McGarr notes that the average $\tau_a/\Delta\sigma$ compares well with the theoretical relationship developed by Singh and Ordaz. Dr. McGarr adjusts the laboratory measurements to the normal stresses (on preferentially oriented faults) measured at 6.8 km depth at the KTB site in Germany. He notes that the adjustments result in stress drops and apparent stresses typical of those observed for mid-crustal earthquakes. Dr. McGarr believes that the normal stress on optimally oriented faults is much lower at Yucca Mountain than the KTB site based on work of Brace and Kohlstedt (1980 [DIRS 184351]) and therefore the KTB site provides conservative estimates for Yucca Mountain. Based on the distribution of laboratory inferred and depth corrected stress drop determinations, Dr. McGarr recommends extreme stress drop values of +1, +2 and +5 σ values from the log-normal (base 10) distribution with a geometric mean of 11.5 MPa and a log-normal standard deviation of 0.11. These extreme values are 150, 190 and 407 bars with relative weights of 0.2, 0.5, and 0.3 respectively.

There were several questions and comments following Dr. McGarr's assessment. Dr. Boore stated that he did not understand the relationship between high-frequency stress drop and crustal strength. Dr. Ake asked how higher inferred stress drops are explained, to which Dr. McGarr responded that those values do not apply to Yucca Mountain, an extensional environment.

Dr. Boore selected his lower range on extreme stress drop of 800 bars to be about the historically largest inferred stress drop, acknowledging that this basis could change the limit over time. The highest weighted value was 1000 bars based on the 10 MPa apparent stress limit and the two-corner source model. Dr. Boore's largest estimate was based on a 50% increase on the 1000 bar value. Dr. Boore provided weights on the three values of 0.2, 0.6 and 0.2 respectively.

The experts' assessments are summarized in Table A-3.

Table A-3. Initial Expert Assessments of Extreme Stress Drop Distribution

Expert	Extreme Stress Drop ($\Delta\sigma$, bars)	Weight	Basis
Dr. Silva	1000	0.8	Maximum apparent stress of 10 MPa and 2-corner model
	500	0.2	Maximum apparent stress of 10 MPa and 1-corner model
	Factors of 50% about above estimates	Relative weights of 0.2, 0.6, and 0.2	Represents uncertainty in assessments
Dr. McGarr	150	0.2	Laboratory data extrapolated to mid-crustal depths
	190	0.5	
	407	0.3	
Dr. Atkinson	---	---	Although one likely exists, it is not possible to define a physically based limit to extreme stress drop at this time.
Dr. Boore	800	0.2	Lower limit based on highest inferred stress drop from recorded events
	1000	0.6	Maximum apparent stress of 10 MPa and 2-corner model
	1500	0.2	50% increase to above estimates

Note: In evaluating the impacts of the four assessments on seismic hazard for the reference rock outcrop, Dr. Atkinson's assessment was conservatively interpreted to mean that there is no limit to extreme stress drop.

There were several general comments and issues raised during the meeting. Several experts and observers mentioned that an evaluation of the stress drops reported in the literature may require careful scrutiny because the site response and crustal model may not have been carefully incorporated in the evaluation of the stress drop. Also, the stress drop should be reviewed for all tectonic environments. Dr. Hanks argued that the assessment on extreme values of stress drop should have been asked in the context of differing probabilities, such as what are the extreme values for 10^{-1} , 10^{-2} and 10^{-3} /yr?

Workshop of March 8th, 2007

Attendees: Dr. Boore, Dr. McGarr, Dr. Silva, Dr. Lee,

In this workshop results of stochastic point-source modeling, using the initial assessments of the distribution of extreme stress drop for Yucca Mountain, were examined in terms of their implications for conditioning of the PSHA reference rock outcrop PGA hazard curve. Following this discussion, some additional aspects of the technical bases for assessments were discussed. Key presentations are provided in Attachment A-3 to this appendix.

Impact of Expert Assessments on PGA Hazard for the Reference Rock Outcrop

Dr. Silva presented PGA hazard results for reference rock outcrop conditions based on the preliminary values of extreme stress drop assessed at the workshop of February 13, 2007. The

results of the expert's assessments were illustrated by showing the unconditioned PGA hazard curve, and a conditioned mean hazard curve for each expert (using that expert's distribution) and the mean conditioned hazard curve using equal weight for each expert. The method to condition the original hazard curves based on the assessed distribution of extreme stress drop is presented in Section A3.2.2. In addition to the stress drop-based conditioned hazard, Dr. Silva also presented comparisons with the site strain-threshold-based conditioned hazard and illustrated that the site and source hazard operator on the unconditioned hazard curve is an associative operation.

Several issues were indicated in Dr. Silva's evaluation of the distribution on extreme ground motion in the context of extreme stress drop. For evaluating a reference rock PGA distribution given a distribution on extreme stress drop:

- (1) The variability in the PGA distribution is significantly impacted by the effect of varying stress drop, source depth, κ and the velocity profile. The total sigma including these variations was 0.76 (natural-log). Since these parameters are reflected in the aleatory variability about the median attenuation relations used in developing the reference rock outcrop hazard, and therefore already accommodated, it was agreed the distribution on the extreme ground motions should be tightened significantly.
- (2) Treatment of Dr. Atkinson's assessment as "no response" or as a weight of 1.0 on the unconditioned hazard curve has a significant impact on the overall conditioned hazard curve when combined equally with the other experts' assessments.

Other Considerations

Dr. McGarr revisited some of his considerations on rock strength from the previous workshop and argues that rock shear strength at 8 km is about 54 MPa for optimally oriented faulted rock. He estimates that τ_a is about 6% of rock strength, so 10MPa is a very conservative number for Yucca Mountain apparent stress. Dr. McGarr also increased the laboratory stress drop database to 23 values.

Following Dr. McGarr's discussion on rock strength, it was agreed that the assessments of extreme stress drop would only consider already fractured rock in apparent stress evaluations. Rupture of fresh, unfractured crustal rock would require much higher stresses to reach failure and would be unnecessarily conservative for the already faulted Yucca Mountain environment. This is a critical assumption in establishing values for extreme stress drop and all the experts were in agreement regarding the appropriateness of the assumption.

There was general discussion on various high-stress drop values in the literature and it was agreed that Dr. Silva and Dr. Boore would review and, if appropriate, revise some stress drop interpretations in the literature. Dr. McGarr would review apparent stress values from extensional environments.

Workshop of April 4th, 2007

Attendees: Dr. Boore, Dr. McGarr, Dr. Silva, Dr. Atkinson (by conference call), Dr. Boatwright, Dr. Ake, Dr. Quittmeyer, Dr. Lee

During this workshop, the implications of initial assessed distributions of extreme stress drop were again evaluated. Updated results on stress drop values for some European earthquakes were also discussed. With this additional information, the experts then finalized their assessments. Key presentations are provided in Attachment A-4 to this appendix.

Additional Feedback and Information

Dr. Silva summarized the updated conditioned hazard curves for each of the experts and the mean hazard using three experts as compared to using all four experts. Dr. Silva also summarized the impact of limiting variability in the structural model and source depth in the development of the conditioned hazard. Dr. Silva also introduced a single limiting distribution on extreme stress drop that contains the input from three of four experts.

Dr. Silva summarized his evaluations of stress drop for a suite of earthquakes in Italy and Montenegro and found that by incorporating improved site and geometrical corrections, the median stress drops for reverse and normal earthquakes were reduced significantly from 438 to 80 and 182 to 37 bars respectively (Table A-4).

Table A-4. European Earthquake Stress Parameter Update

Earthquake	Date MM/DY/YR HRMN	M	Mechanism	$\Delta\sigma$ (bars)	
				Original	Revised
Fruili	05/06/76 2000	6.20	reverse	780	139.6
Fruili	06/09/76 1848	4.40	reverse	353	75.4
Fruili	06/09/76 1716	4.65	reverse	242	87.4
Fruili	06/11/76 1631	5.20	reverse	325	47.6
Fruili	06/11/76 1635	5.30	reverse	406	102.3
Fruili	09/15/76 0315	5.90	reverse	430	40.0
Fruili	09/15/76 0921	5.90	reverse	386	56.7
Montenegro	04/15/79 0619	6.63	reverse	932	171.8
			mean (ln) =	438.2	80.4
			σ (ln) =	0.45	0.51
Valernia	09/19/79 2135	5.8	normal	116	26.4
Irpinia	11/23/80 1834	6.8	normal	131	73.3
Irpinia	11/23/80 1835	6.3	normal	340	69.3
Umbria	04/29/84 2135	5.6	normal	210	67.6

Earthquake	Date MM/DY/YR HRMN	M	Mechanism	$\Delta\sigma$ (bars)	
				Original	Revised
Lazio-Abru	05/07/84	5.9	normal	172	89.8
Lazio-Abru	05/11/84 1041	5.5	normal	178	34.1
Lazio-Abru	05/11/84 1126	4.7	normal	190	9.1
Lazio-Abru	05/11/84 1314	4.8	normal	166	29.0
Lazio-Abru	05/11/84 1639	4.8	normal	205	19.6
			mean (ln) =	181.6	37.4
			σ (ln) =	0.31	0.76

Source: reverse mechanism; Cocco and Rovelli (1989 [DIRS 184795])
normal mechanism; Rovelli et al. (1988 [DIRS 182048])

Dr Silva also discussed a trend to lower stress drop for increasing magnitude for both WUS and EUS earthquakes. Dr. Silva also discussed the hazard model impacts of considering alternate models for ground motion variability.

Final Expert Assessments

Based on the feedback and additional information, each of the experts was given the opportunity to revise their assessment of extreme stress drop.

Dr. McGarr stated that he was comfortable with values he provided to the group at the last meeting.

Dr. Atkinson revised her assessment to provide a distribution. Her assessment was based on the judgment that a lognormal distribution on stress drop is justified and that the regulatory requirement to consider events with one chance in 10,000 of exceedance in 10,000 years is an adequate and justifiable basis for developing an extreme value on stress drop in the context of project performance goals. The regulatory requirement directs that events with lower probabilities do not need to be considered in evaluation of postclosure performance. Dr. Atkinson argues that if the product of the event occurrence probability and the stress drop probability is less than $10^{-8}/\text{yr}$, the project need not consider that occurrence. Dr. Atkinson argued that the probability of an earthquake close to the repository to be on the order of $10^{-4}/\text{yr}$ or less, and by accepting a $3.7\text{-}\sigma$ on the lognormal distribution, results in a value of 440 bars (median of 80 bars and a $\sigma_{\ln} = 0.46$).

Dr. Silva reversed his 1-corner and 2-corner class weights on his belief that the 2-corner model did not adequately fit observed earthquake spectra.

Dr. Boore modified his extreme stress drop estimates slightly by taking the geometric mean of the 1- and 2-corner correction to the Singh and Ordaz relationship with uncertainties of 50%.

The final expert assessments are summarized in Table A-5.

Table A-5. Final Expert Assessments of Extreme Stress Drop Distribution

Expert	Extreme Stress Drop ($\Delta\sigma$, bars)	Weight	Basis
Dr. Silva	1000	0.2	Maximum apparent stress of 10 MPa and 2-corner model
	500	0.8	Maximum apparent stress of 10 MPa and 1-corner model
	Factors of 50% about above estimates	Relative weights of 0.2, 0.6, and 0.2	Represents uncertainty in assessments
Dr. McGarr	150	0.2	Laboratory data extrapolated to mid-crustal depths; geometric mean + 1 σ
	190	0.5	Laboratory data extrapolated to mid-crustal depths; geometric mean + 2 σ
	407	0.3	Laboratory data extrapolated to mid-crustal depths; geometric mean + 5 σ
Dr. Atkinson	440	1	3.7 σ on lognormal stress drop which has a AFE of 10 ⁻⁴ , which meets external event screening criteria.
Dr. Boore	413	0.2	-50%
	620	0.6	Geometric mean of 1- and 2-corner model correction
	930	0.2	+50%

A3.2.1.3. Assumed Distribution on Extreme Stress Drop for Hazard Conditioning

The technical bases described below form the underpinning of the experts' assessments of extreme stress drop, which ranged from 150 bars to 1000 bars (Table A-5). These bases provide the rationale for an assumption that extreme stress drop is characterized by a log-normal distribution with a value of 400 bars and σ_{ln} of 0.6 (mean of 480 bars). In using this assumed distribution to condition extreme ground motions (Section A4), the distribution is approximated by three values: 150 bars, 400 bars, and 1100 bars, with weights of 0.2, 0.6, and 0.2, respectively.

As one component of the technical basis for this assumption, controlled laboratory experiments of stick-slip behavior are used to assess an extreme value of stress drop (Appendix A, Section A3.2.1.2). Based on the laboratory measurements of apparent stress and stress drop of Lockner and Okubo (1983 [DIRS 170902]) there is agreement with the theoretical apparent stress and stress drop relationship developed by Singh and Ordaz (1994 [DIRS 184394]): $\tau_a/\Delta\sigma = 0.233$, in which τ_a is apparent stress and $\Delta\sigma$ is stress drop. When the laboratory measurements of apparent stress are conservatively corrected to the normal stresses (on preferentially oriented faults) measured at seismic depths, the resulting stress drops and apparent stresses are typical of those observed for mid-crustal earthquakes. Because laboratory stick-slip experiments provide a controlled environment for inferring apparent stress and stress drop, these measurements provide a reasonable basis for assessing extreme stress drop. The stress-corrected laboratory

inferred values of stress drop can be represented as a log-normal distribution with a median of about 115 bars.

Apparent stress from a global data base was also considered in evaluating extreme stress drop. McGarr and Fletcher (2003 [DIRS 170793]) compiled over 200 inferred values of apparent stress for crustal earthquakes with magnitudes ranging from $-3 < \mathbf{M} < 7$ and with apparent stresses ranging from 0.01 to 100 bars. For earthquake magnitudes $\mathbf{M} > 5$, the apparent stress ranged from 10 to 100 bars. Taking an apparent stress drop of 100 bars as a reasonable upper limit and using the relationship of Singh and Ordaz (1994 [DIRS 184394]), a value for extreme stress drop of about 500 bars is obtained.

Consideration was also given to the impact of a double-corner source representation on the relationship of Singh and Ordaz (1994 [DIRS 184394]) (Section A3.2.1.2). For a double-corner source representation, the corresponding value of extreme stress drop inferred from a 100 bar upper limit to apparent stress is about 1000 bars (Section A3.2.1.2). This value is given less weight, however, as the single-corner representation is preferred.

Another component of the technical basis for the assumed distribution of extreme stress drop is based on the historical record of stress drops inferred from global earthquakes producing strong ground motion and laboratory results combined with regulatory requirements from 10 CFR 63 [DIRS 180319]. Consideration of the historical record, taking into account tectonic environment, analysis details that differ from study to study, corrections for site amplification, and correlations with magnitude and focal depth supports the conclusion that stress drop is lognormally distributed with a median of about 80 bars and a standard deviation of about 0.46. Based on this distribution, a value of extreme stress drop is defined consistent with the regulatory requirement to consider features, events, and processes with one chance in 10,000 of occurring in 10,000 years. Based on the assessments in the PSHA for Yucca Mountain, a recurrence interval of 10,000 years is conservatively adopted for moderate magnitude earthquakes on fault sources close to the site. Hazard deaggregation shows such earthquakes dominate the hazard for Yucca Mountain at low AFEs. Combining this probability of recurrence with a 3.7σ value of stress drop from the log-normal distribution gives a combined annual probability of 10^{-8} or less. This value of stress drop is 440 bars.

A4. APPROACH TO CONDITIONING REFERENCE ROCK OUTCROP HAZARD

To condition the hazard curve for the PSHA reference rock outcrop, the distribution on extreme stress drop must be mapped into a distribution of extreme ground motion for the reference rock outcrop. A point-source stochastic ground motion model (Section 6.3) is used to map the distribution on extreme stress drop into reference rock outcrop ground motions. An operator in the form of a complementary cumulative distribution function (CCDF) is developed using the corresponding distribution on extreme ground motion. This operator is applied to the reference rock outcrop hazard curve for every level of motion. This operation effectively conditions the hazard curve to accommodate the assessed distribution on extreme stress drop.

In addition to the hazard conditioning provided by an assessment of a distribution for extreme stress drop, conditioning of the reference rock outcrop hazard is also developed based on the

shear-strain threshold approach (Section A2.2). In this alternate approach geologic, rock mechanics, and site-response modeling are used to establish a level of ground motion that has not been exceeded at the repository waste emplacement (BSC, 2005 [DIRS 170137]). The shear-strain threshold approach to conditioning the hazard is analogous to the approach taken with the stress drop conditioning.

A4.1 Conditioning Based on a Distribution on Extreme Stress Drop

Distributions on extreme ground motions are developed based on the distribution on extreme stress drop by using a stochastic point-source ground motion model and accounting for the expected variability in geologic conditions. For a given distribution on extreme stress drop, the corresponding distribution of extreme ground motion values would not be exceeded.

To condition the hazard curve, the extreme stress drop operator is given by:

$$P[x > x']^C = P[x_m > x' | \Delta\sigma_m]P[x > x'] \quad (\text{Equation A-3})$$

in which:

$P[x > x']^C$ is the conditioned hazard curve for the reference rock outcrop and ground motion x ;

$P[x_m > x' | \Delta\sigma_m]$ is the CCDF of extreme ground motion values (x_m) at the reference rock outcrop determined using the combined point-source and site response models with parameter distributions, conditional on extreme stress drop $\Delta\sigma_m$;

and

$P[x > x']$ is the unconditioned (original) reference rock outcrop hazard curve for motion x .

The extreme stress drop operator approach follows from the approach taken in BSC (2005)[DIRS 170137]).

A4.2 Conditioning Based on a Distribution on Shear-Strain Threshold

For this approach the reference rock outcrop distribution of extreme ground motions is developed based on the distribution of shear-strains that have not been experienced at the repository waste emplacement level (BSC 2005 [DIRS 170137]). A site-response model is used to relate ground motions at the reference rock outcrop to shear-strains at the repository waste emplacement level and accounts for the uncertainty and variability in site materials. For a given shear-strain threshold, the corresponding distribution of ground motion values would not be exceeded.

To condition the reference rock outcrop hazard curve based on the distribution of shear-strain threshold at the repository waste emplacement level, the hazard operator is given by:

$$P[x > x']^C = \sum_i P[\gamma_m > \gamma | x_i] P[x_i] \quad (\text{Equation A-4})$$

in which:

$P[x > x']^C$ is the conditioned hazard curve for the reference rock outcrop and ground motion x ;

$P[\gamma_m > \gamma | x_i]$ is the CCDF for shear strains at the waste emplacement level conditional on ground motion x_i at the reference rock outcrop with γ_m the non-exceeded shear strain value,

and

$P[x_i]$ is the probability of reference rock outcrop motion x_i and the range of summation index i , is over all ground motion values defining the hazard curve.

This approach to condition the reference rock outcrop hazard differs from BSC (2005 [DIRS 170137]) in which a CCDF for shear strains at the waste emplacement level was applied directly to a hazard curve determined for the waste emplacement level. The approach adopted here is more exact in that the hazard is accumulated by applying the CCDF to the probability of occurrence of a level of motion, integrated over all levels of the reference rock outcrop motions (hazard curve). As discussed in Section A2.2, material properties in the tuff have been updated since BSC (2005 [DIRS 170137]) and consequently predicted distributions of ground-motion-related shear strains differ from those used previously. A comparison of the updated conditioned hazard and BSC (2005 [DIRS 170137]) results is presented in the Section A4.5.

A4.3 Stochastic Point-Source Model Parameter Values

The stochastic point-source ground motion model is used to develop reference rock outcrop distributions of extreme ground motion using the assumed distribution of extreme stress drop based on the experts' assessments. The point-source ground motion parameters used to develop the distribution of ground motion are listed in Table A-6. The bases for parameter values are described in Section 6.4.7. Because the hazard deaggregation indicates that extreme ground motions are controlled by moderate magnitude earthquakes in the vicinity of the site (Figure 6.4.1-10, Figure 6.4.1-16), the source distance is taken as 1 km with a source depth of 8 km. The point-source depth of 8 km is adopted as an average (median) hypocentral or asperity depth for active regions (McGuire et al. 2001 [DIRS 157510]) (Section 4.1.2). The addition of a shallower depth, e.g., 4 km, as used in the shallow bound for the parameter randomization illustrated in Figure A7 and A8, would result in little impact on predicted motions as its contribution to extreme ground motions would receive significantly less weight than the average depth of 8 km, based on regional seismicity. Additionally, there is an observed correlation between level of strong ground motion, for a given M and D , and depth of slip. This correlation is seen, especially at high frequencies (> 0.5 to 1.0 Hz), in both finite- and point-source modeling of recorded motions (e.g., Silva et al. 1996 [DIRS 110474]). In general, earthquakes that are dominated by deep slip or deep asperities produce significantly larger motions, for the same M and D , than shallow-slip-dominated earthquakes. Considering shallow-slip-dominated earthquakes as those with more than 20% moment released over the top 5 km, point-source stress

drops computed for moderate to large earthquakes available in 1997 show a clear separation with depth (Silva et al. 1996 [DIRS 110474]). As Table A-1 shows, over all earthquakes, the median stress drop is about 50 bars with a variability of about 0.5 (ln). Separating the earthquakes using the deep versus shallow slip criterion results in about a factor of two in stress drop, 60 bars and 30 bars, respectively and with a reduced variability of about 0.4 (ln). The reduced variability suggests epistemic uncertainty of about 0.3 (ln) masquerading as aleatory variability when combining the two distributions. Increased knowledge has reduced the variability, suggesting the inclusion of a shallow depth point-source would reduce the extreme stress drop distribution by a factor of two. These trends in ground motion or stress drop with depth of slip are also accommodated in recently developed empirical attenuation relations accommodating active region earthquakes available through 2002 (NGA). Depth to top-of-rupture has been added as an independent variable resulting in increased motions with increased depth, conditional on M, D, rupture mechanism, and site condition. As with the point-source stress drop, the inclusion of depth to top-of-rupture significantly reduced the aleatory variability about median predictions.

Since the change in stress drop is directly proportional to a change in ground motion, a 100% change in stress drop results in about a 70% to 80% change in ground motions for frequencies above the corner frequency (Silva et al. 1996 [DIRS 110474]). The corner frequency for M 6.0 to 6.5 is about 0.3 Hz ($\Delta\sigma = 50$ bars), as a result, for a 4 km point-source depth, the combination of a lower extreme stress drop distribution coupled with a relative weight of less than 0.5 would result in extreme motions lower than those computed for a depth of 8 km for frequencies exceeding about 0.3 Hz.

The distribution for extreme stress drop discussed in Section A3.2.1.3 is approximated by three values: 150, 400, and 1100 bars with weights of 0.2, 0.6, and 0.2, respectively.

Table A-6. Point-Source Model Parameters for Extreme Stress Drop Conditioning.

Parameter	Values																					
Magnitude, M , [Weight]	6.0 [0.5], 6.5 [0.5]																					
Extreme Stress Drop, $\Delta\sigma$ (bars) [Weight]	150 [0.2], 400 [0.6], 1100 [0.2]																					
Site attenuation, κ (seconds)	0.02																					
Regional attenuation, $Q(f)^{\dagger}$	$250f^{0.4}$																					
Source distance (km)	1.0																					
Source depth (km)	8.0																					
Crustal velocity profile: Thickness (km), V_S (km/sec), V_P (km/sec)	<table> <tbody> <tr> <td>0.78</td> <td>1.9</td> <td>3.2</td> </tr> <tr> <td>0.60</td> <td>2.1</td> <td>3.6</td> </tr> <tr> <td>1.50</td> <td>2.9</td> <td>5.0</td> </tr> <tr> <td>2.20</td> <td>3.4</td> <td>5.8</td> </tr> <tr> <td>10.70</td> <td>3.5</td> <td>6.2</td> </tr> <tr> <td>16.00</td> <td>3.8</td> <td>6.5</td> </tr> <tr> <td>---</td> <td>4.6</td> <td>7.8</td> </tr> </tbody> </table>	0.78	1.9	3.2	0.60	2.1	3.6	1.50	2.9	5.0	2.20	3.4	5.8	10.70	3.5	6.2	16.00	3.8	6.5	---	4.6	7.8
0.78	1.9	3.2																				
0.60	2.1	3.6																				
1.50	2.9	5.0																				
2.20	3.4	5.8																				
10.70	3.5	6.2																				
16.00	3.8	6.5																				
---	4.6	7.8																				

Source: Section 6.4.7

A4.4 Appropriate Inclusion of Variability

Given the intended purpose of the stochastic point-source model results (i.e., to condition the reference rock outcrop hazard curves from the PSHA), it is necessary to consider what parameter variability it is appropriate to include in the modeling. In characterizing ground motion for the PSHA, the experts relied on two general classes of data: empirical ground motion attenuation curves and numerical simulations. Because the ground motion attenuation curves were derived from a set of data that implicitly included variability in source depth, regional attenuation, site attenuation, velocity profile, and stress drop, this variability is included in the PSHA results. Variability was also explicitly included in the numerical simulations that supported ground motion characterization during the PSHA.

Also, because the ground motion estimate is conditional on defined parameters for the extreme motions (i.e., a specified stress drop and source depth), the variability in ground motion estimation using the point-source model due to the randomness in these parameters should not be included. Accordingly, a reduced value of the standard deviation in the natural logarithm of PGA equal to 0.15 was used to avoid double counting the effects of variability. This value is based on the composition of total standard deviation presented in Figure A6. Note that the results are not sensitive to variations in the value of sigma in the range of 0.1 to 0.4 as shown in Figures A8 and A10.

Although not included in the final modeling to condition the PSHA hazard curves, modeling that included variability was carried out to examine its relative effects and the sensitivity of the results. The range in predicted response spectra for a nearby source using the stochastic ground motion model is illustrated in Figure A4 for a range of stress drop values. Acceleration spectra are shown for a suite of stress drops ranging from 50 to 2500 bars for a magnitude (**M**) 6.5 at a distance of 1 km and depth of 8 km. The range in predicted median PGA increases from about .3g (50 bars) to over 6g (2500 bars). The range in predicted median PGV increases from about 25 cm/sec (50 bars) to over 300 cm/sec (2500 bars).

To examine the relative effects of parameter variability, modeling was carried out for an **M** 6.5 event with stress drop of 1000 bars at a distance of 1 km and a depth of 8 km. Variability in stress drop, source depth, kappa and the velocity profile was modeled. The sigma(ln) for stress drop and source depth was taken as 0.5 and for kappa as 0.3. Variability in velocity profile was treated analogously with its treatment in site-response modeling. Based on these inputs, an approximate factor of 2-range in spectral acceleration is observed between the median and 84th percentile spectra (Figure A5). Figure A6 illustrates the composition of total sigma by oscillator frequency, indicating that variations in source depth and stress drop are the largest components of spectra variability.

Figure A7 illustrates point A spectral acceleration for an **M** 6.5 with stress drop of 1000 bars at a distance of 1 km and depth of 8 km using depth randomization only. This reduces the sigma on predicted spectral values to about 0.5.

A4.5 Hazard Conditioning Results

A4.5.1 Conditioned Hazard Based on Distribution on Extreme Stress Drop

Using the methodology described in Section A4.1, reference rock outcrop mean PGA hazard is conditioned using the distribution of extreme ground motion derived from the distribution of extreme stress drop (Section A3.2.1.3). The stochastic point-source model is run using the parameter values given in Table A-6. This results in ground motion predictions for PGA and PGV for six $M-\Delta\sigma$ cases. The PGA and PGV determined for each of the six cases form the basis for extreme ground motion distributions to condition the results from the PSHA. The distribution is taken as lognormal with a $\sigma(\ln)$ of 0.15. Conditioning is carried out for each of the six cases using Equation A-3 and the resulting conditioned PGA and PGV hazard curves are combined for each ground motion measure using the weights in Table A-6. The conditioned PGA hazard curve is then used to scale UHS from the PSHA. This approach preserves the spectral shape from the PSHA for the reference rock outcrop. Preservation of this shape is desirable as it is a key output of the PSHA and represents the interpretations developed through the expert elicitation process. Hazard curves for spectral acceleration at oscillator periods of 0.05, 0.1, 0.2, 0.5, 1, 2, and 3.3 sec are then determined using interpolation. Details of the modeling and analysis are presented in Appendix D (CALCULATIONS/ Constraints of Site A Hazard Curves for Extreme Ground Motion).

Figure A8(a) illustrates the reference rock outcrop unconditioned and conditioned PGV hazard curves for a suite of ground motion σ ranging from 0.1-0.4, including the base-case of 0.15. Note that, for the range shown, the effect of ground motion σ is small. Figures A8(b) and (c) illustrate the extreme-stress-drop-conditioned hazard for PGA and 1-Hz spectral acceleration respectively. For mean PGVs less than about 60 cm/sec (AFEs greater than about 8×10^{-5}), the conditioned hazard is identical to the unconditioned hazard, consistent with the operator approach taken in Section A4.1. For PGVs greater than about 60 cm/sec (AFEs less than about 8×10^{-5}) the conditioned and unconditioned hazard increasingly diverge with increasing ground motion. For increasing PGV, the slope of the conditioned hazard increases continuously relative to the slope of the unconditioned hazard resulting in a decrease in mean PGV from about 1200 cm/sec to about 480 cm/sec at $10^{-8}/\text{yr}$ (60% reduction in PGV). We note that at $10^{-8}/\text{yr}$ the mean hazard is still increasing and has not reached a maximum, suggesting that the breadth of the uncertainty in the estimate of extreme stress drop will result in increasing hazard at even lower AFEs.

The results demonstrate that the assessment of values of extreme stress drop have a significant effect on the unconstrained hazard for AFEs less than about 10^{-4} to $10^{-5}/\text{yr}$. Variability in predicted reference rock outcrop ground motion using the stochastic point-source ground motion model would be significant ($\sigma \sim 0.7$) if distributions for all model input parameters were sampled. However, for the range of σ shown in Figure A8, the effects of ground motion σ have a relatively weak impact on the conditioned hazard. At a probability of exceedance of $10^{-8}/\text{yr}$, the effect on the conditioned hazard is less than about 5% on ground motion (Figure A8).

A4.5.2 Conditioned Hazard Based on Repository Waste Emplacement Level Non-Exceedance Distributions on Shear Strain

The shear-strain threshold approach is implemented by associating the distribution of shear-strain values averaged over the depth of the Topopah Spring lower lithophysal zone, as calculated using the site-response model, with the corresponding levels of ground motion input at the control point (the reference rock outcrop). The catalog of site-response modeling results produced in developing amplification functions for the repository waste emplacement level (Section 6.5.3.1) forms the basis for this analysis. The analysis is carried out for the four combinations of RB velocity profile and tuff dynamic material property curves for each ground motion measure. Once the relation between control motion amplitude and RB shear-strain is established, the probability that a ground motion amplitude at the control point will produce a shear-strain in excess of the shear-strain threshold at the Topopah Spring lower lithophysal zone is assessed taking shear strains as log-normally distributed with a $\sigma(\ln)$ determined from the results of site-response modeling. This probability is multiplied by the probability of the given control point ground motion level (Equation A-4), which is determined from the PSHA hazard curve through differencing. This process is carried out for the upper and lower limit of the shear-strain threshold distribution (0.09 and 0.25%) and the results are averaged with equal weight. Results for each combination of RB velocity profile and tuff dynamic material property curves are averaged using the same weights as in determining RB site-specific ground motions. Details of the analysis are presented in Appendix D (CALCULATION/ Constraints of Site A Hazard Curves for Extreme Ground Motion).

The updated approach to conditioning reference rock outcrop hazard using the shear-strain threshold (Equation A-4) differs from that used in BSC (2005 [DIRS 170137]) as described in Section A4.2. In addition, the shear-wave velocity and strain-dependent material properties above the reference rock outcrop have been updated since the BSC (2005[DIRS 170137]) work was completed (Sections A2.2 and 6.4). Consequently, a comparison of the results developed in BSC (2005 [DIRS 170137]) and the revised approach using updated site properties is in order.

Figure A9(a) illustrates the conditioned repository waste emplacement level mean PGV hazard curve using the method described in Section A4.2, but using shear strains from BSC (2005 [DIRS 170137]). Figure A9(a) also displays the BSC (2005 [DIRS 170137]) conditioned PGV hazard. Using the previous site response results, the updated methodology shows somewhat lower rates of PGV exceedance above about 2×10^{-8} /yr as compared to BSC (2005 [DIRS 170137]), but higher rates at lower AFEs because of the inclusion of shear strain variability. Figure A9(b) illustrates the conditioned mean PGV hazard for the waste emplacement level using the approach in Section A4.2 and updated site properties. The impact of the updated site properties is to increase the waste emplacement level AFEs, especially for exceedances less than about 10^{-7} /yr. Comparing Figures A9(a) and A9(b) at an AFE of 10^{-8} shows PGV increases from about 500 cm/sec to about 700 cm/sec. The conditioning described in BSC (2005 [DIRS 170137]) determined a corresponding PGV of about 400 cm/sec. The effect of shear-strain sigma is illustrated in Figure A9(c) using the previous site response results (BSC 2005 [170137]). A four-fold increase in sigma from 0.1 to 0.4 does not significantly increase the conditioned PGV hazard for AFEs greater than about 10^{-7} /yr. The effect of base-case models in velocity and strain-dependent properties (epistemic uncertainty) and BSC (2005 [DIRS 170137]) shear-strains is illustrated in Figure A9(d). Finally, the effect of updated base-case models in

velocity and strain-dependent properties (epistemic uncertainty and deterministic variability) and updated shear-strains is illustrated in Figure A9(d). As compared to the conditioned BSC (2005 [DIRS 170137]) PGV hazard, the revised approach and the updated properties and corresponding waste emplacement level shear-strains significantly reduce the effect of shear-strain threshold conditioning.

Shear-strain-threshold-conditioned ground motion hazard curves for the reference rock outcrop, using the methodology described in Section A4.2, are illustrated in Figures A10(a), A10(b) and A10(c) for PGV, PGA and 1-Hz Sa respectively. For shear-strain-threshold conditioning, the sensitivity of the conditioned hazard to different values of $\sigma(\ln)$ for the distribution of shear strain is also displayed on the figures. In addition to the base-case value determined from the results of site-response modeling, values of 0.1, 0.2, and 0.4 are investigated. Note that the shear-strain-threshold-conditioned hazard shows a weaker dependence on the σ used in the point-source model than the extreme-stress-drop approach, however the overall effect of the conditioning is significantly less than for the extreme stress drop approach. For an annual exceedance of 10^{-8} the shear strain threshold conditioned PGV hazard is reduced from about 1200 cm/sec to about 1100 cm/sec or about 10%. This reduction is less than the stress drop reduction and is substantially less than the reduction observed in BSC (2005 [DIRS 170137]) owing to the more refined site-specific data and consequent reduction in predicted waste emplacement level shear-strains and to the conditioning approach (Section A4.2).

A4.5.3 Combined Extreme-Stress-Drop and Shear-Strain-Threshold Conditioned Hazard

Reference rock outcrop hazard conditioned using both the extreme stress drop approach and the shear strain threshold approach is illustrated in Figures A11(a), A11(b), and A11(c) for PGV, PGA, and 1-Hz SA, respectively. The effects of ground motion σ are also illustrated in Figure A11. From Figure A10 and A11, the shear strain threshold conditioning has a marginal impact on the unconditioned hazard as compared to the extreme stress drop method. The final conditioned mean hazard curves are illustrated in Figures A12(a), A12(b) and A12(c) for PGV, PGA and 1-Hz SA respectively.

A4.5.4 Conditioned Uniform Hazard Spectra

The conditioned horizontal component UHS for the reference rock outcrop, based on combined conditioning using the extreme stress drop and shear strain threshold approaches, are illustrated in Figures A13(a) through A13(f) for AFEs of 10^{-3} , 10^{-4} , 10^{-5} , 10^{-6} , 10^{-7} and 10^{-8} respectively. For AFEs of 10^{-3} and 10^{-4} (Figures A13(a) and A13(b)) the UHS for conditioned and unconditioned hazard are approximately equal. For decreasing AFEs of 10^{-5} (Figure A13(c)), 10^{-6} (Figure A13(d)), 10^{-7} (Figure A13(e)), and 10^{-8} (Figure A13(f)), UHS for the conditioned hazard is increasingly lower than the unconditioned UHS.

A5. CONCLUSIONS

Two approaches are used to condition ground motion hazard for the reference rock outcrop at Yucca Mountain. One approach uses an assumed distribution for extreme stress drop— those stress drops that produce ground motion far in excess of levels recorded historically (Section

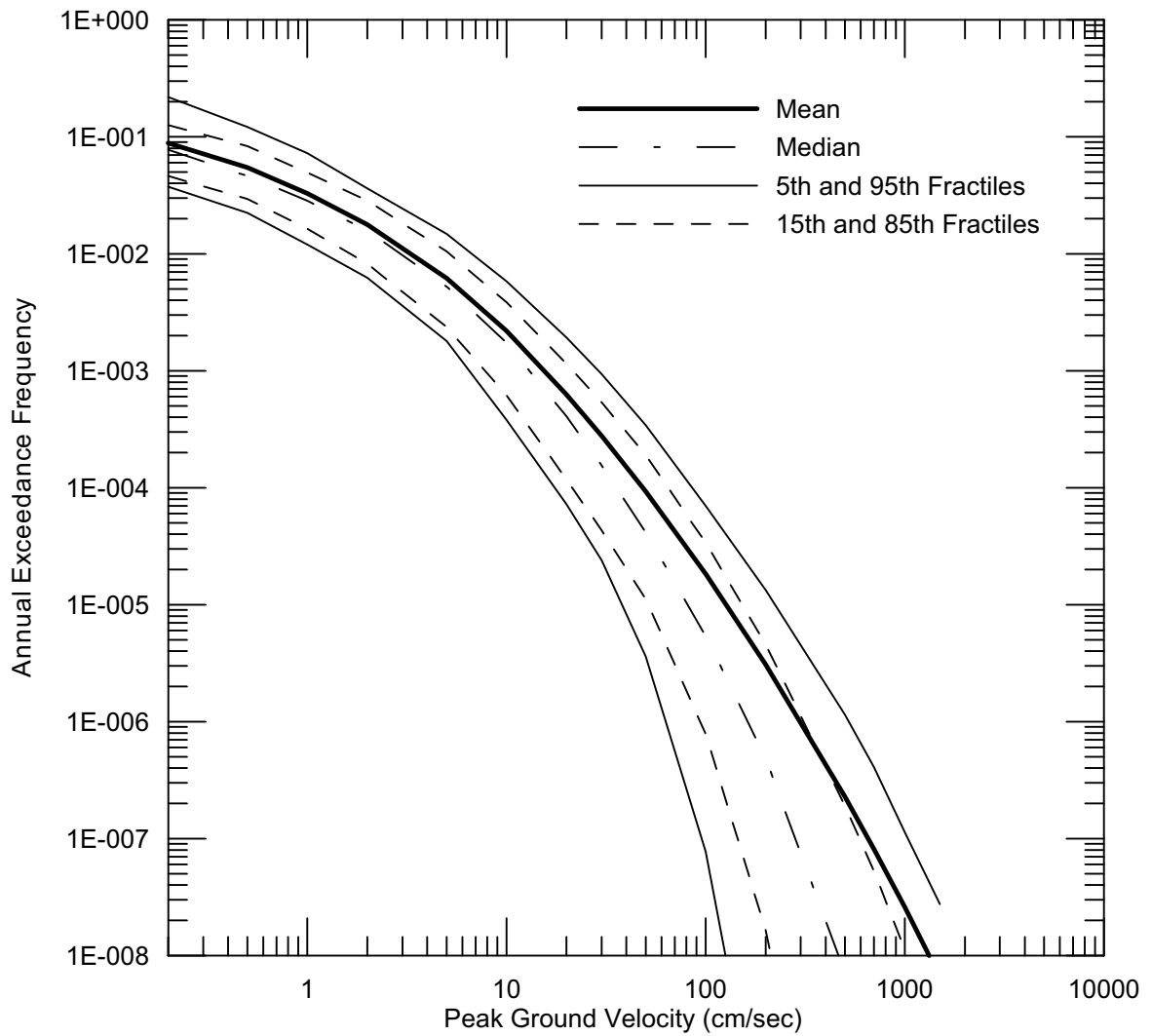
A3.2.1.3, Section 5.4). The assumption is based on available data, interpretations, and judgment and is informed by discussions among experts during a series of workshops held to address the issue. This distribution on extreme stress drop is used in the stochastic point-source ground motion model to determine a distribution of extreme ground motion that conditions the ground motion hazard determined during the PSHA. This approach complements an approach used to condition the hazard based on repository level observations of unfractured rock, (i.e., the distribution on non-exceeded shear-strain developed in BSC (2005 [DIRS 170137])). That approach has also been updated in this study with a refined analytical approach and updated site properties used in site-response modeling. Both approaches are used to condition reference rock outcrop seismic hazard, although with the updated site properties the shear-strain threshold approach has only marginal affect at low exceedance rates.

The stress drop approach applies a distribution on extreme stress drop, used in the stochastic point-source ground motion model, to develop distributions of extreme ground motion at the reference rock outcrop that are used to condition the reference rock outcrop PGA and PGV hazard. The conditioned PGA hazard is the then used to scale the UHS from the PSHA. Scaling of the PSHA UHS is used to preserve the spectral shape of the UHS determined through the PSHA. The assumed distribution on extreme stress drop is lognormal with a mean of 480 bars, a median of 400 bars and a $\sigma_{ln}=0.6$.

The distribution on extreme stress drop provides a practical and justifiable limit on the distribution of reference rock outcrop ground motion for low AFEs ($<10^{-4}$). The extreme stress drop approach significantly reduces the AFE of reference rock ground motions for exceedances less than about $10^{-5}/\text{yr}$. The non-exceedance distribution on shear-strain (shear strain threshold) approach, also incorporated here using a refined methodology and updated site properties, results in significantly less reduction of reference rock outcrop ground motions.

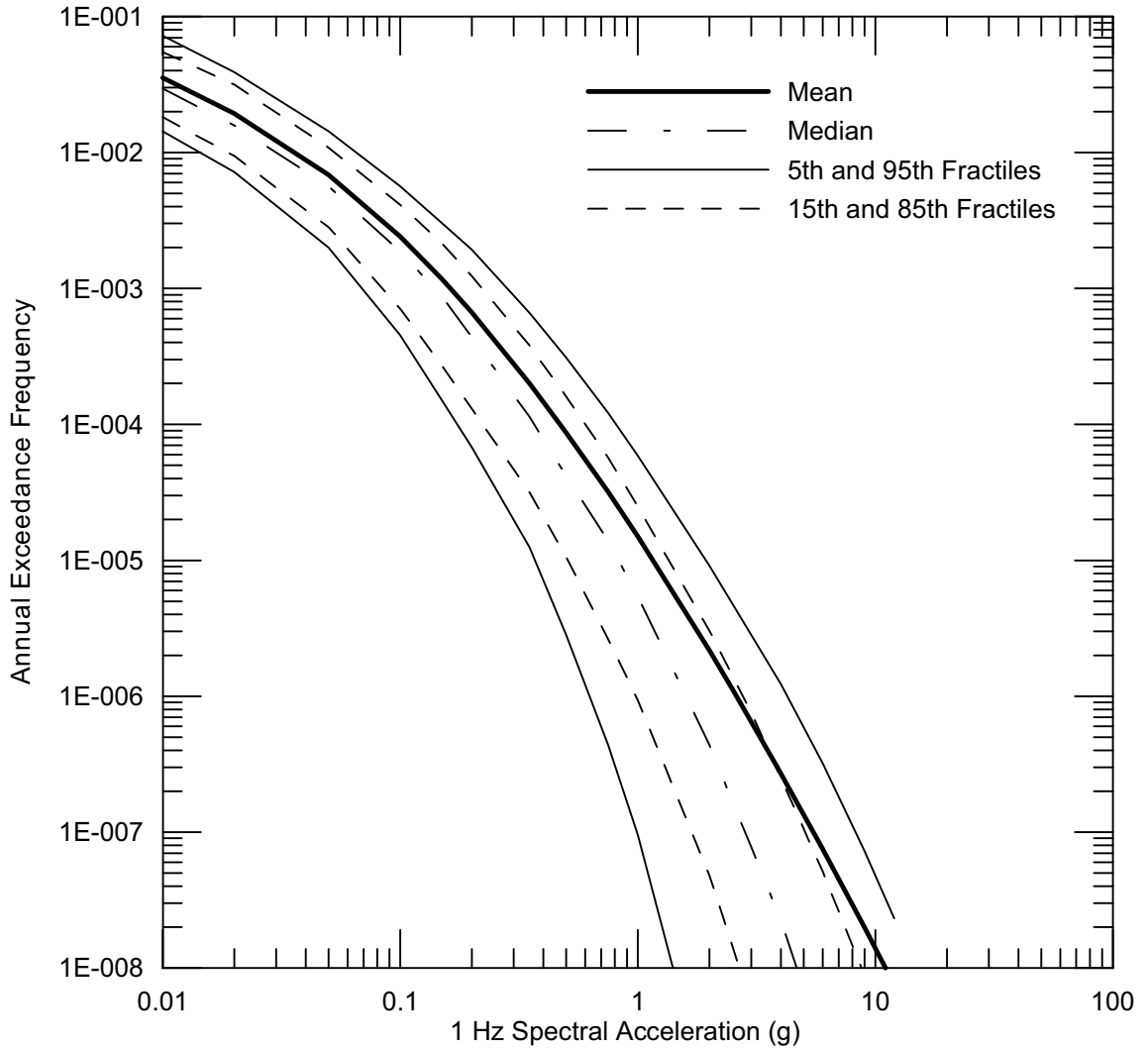
Attachments

1. January 25, 2007 presentations/reports/attendees
2. February 13, 2007 presentations/reports/attendees
3. March 8, 2007 presentations/reports/attendees
4. April 4, 2007 presentations/reports/attendees



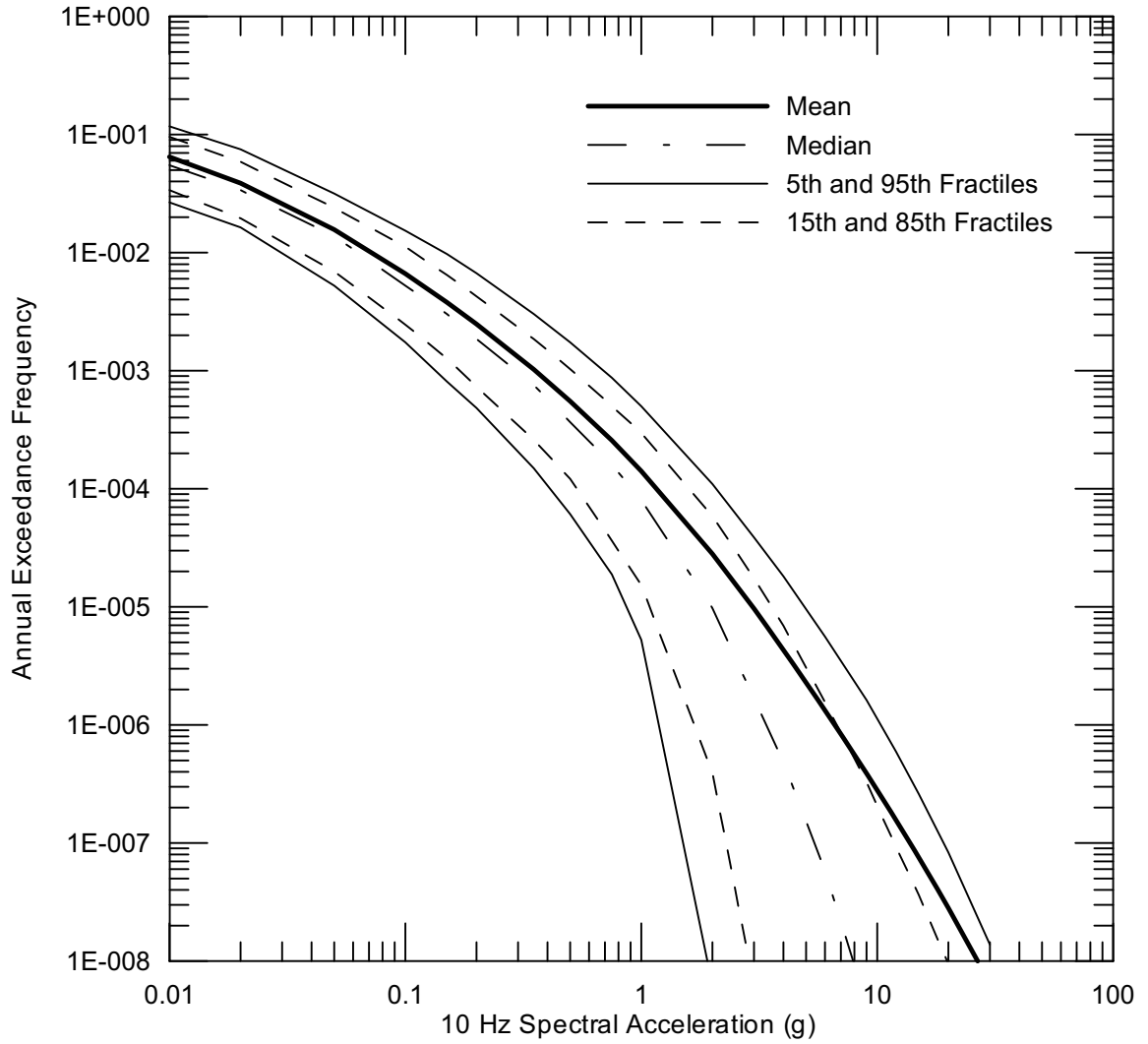
Source: DTN: MO03061E9PSHA1.000 [DIRS 163721]

Figure A1(a). Mean and Fractile Hazard at the PSHA Reference Rock Outcrop for Peak Horizontal Ground Velocity



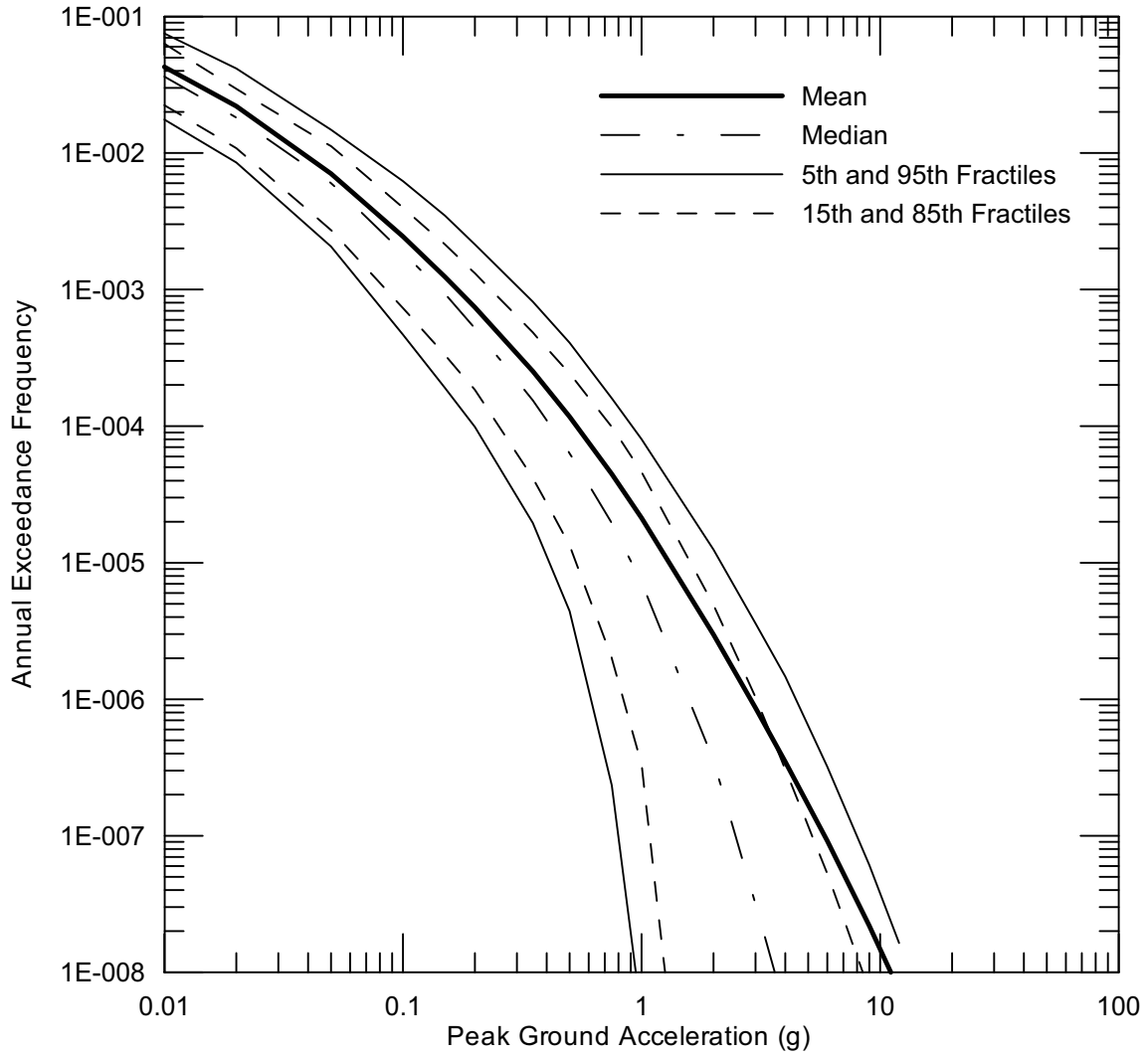
Source: DTN: MO03061E9PSHA1.000 [DIRS 163721]

Figure A1(b). Mean and Fractile Hazard at the PSHA Reference Rock Outcrop for 1-Hz Horizontal Spectral Acceleration



Source: DTN: MO03061E9PSHA1.000 [DIRS 163721]

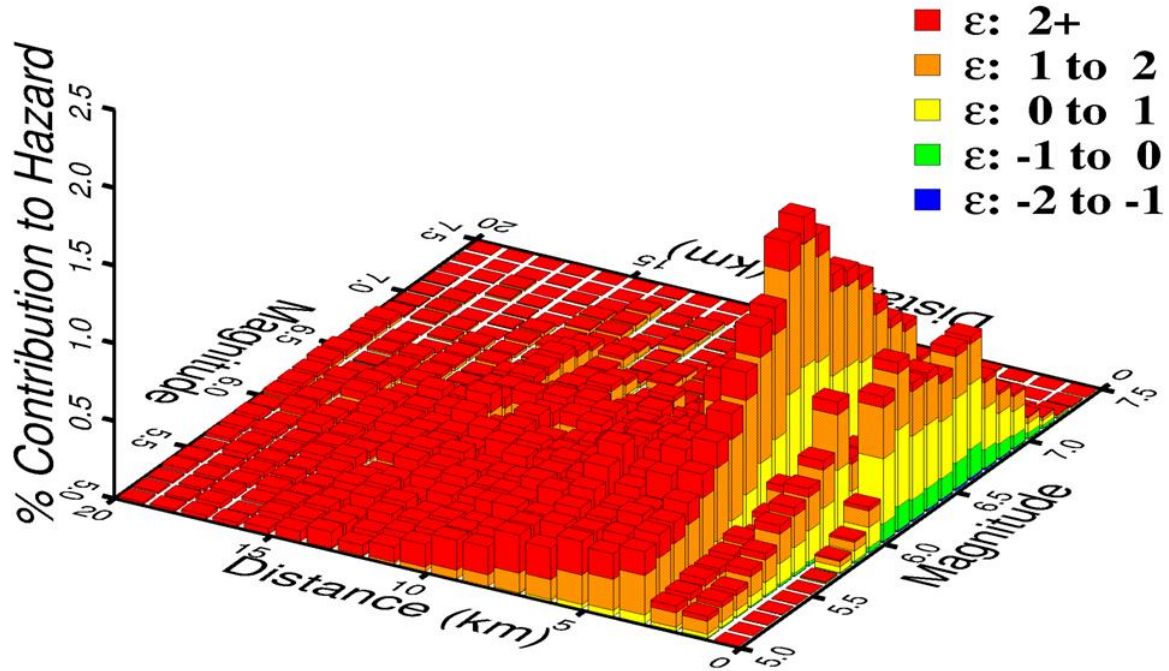
Figure A1(c). Mean and Fractile Hazard at the PSHA Reference Rock Outcrop for 10-Hz Horizontal Spectral Acceleration



Source: DTN: MO03061E9PSHA1.000 [DIRS 163721]

Figure A1(d). Mean and Fractile Hazard at the PSHA Reference Rock Outcrop for Peak Horizontal Ground Acceleration

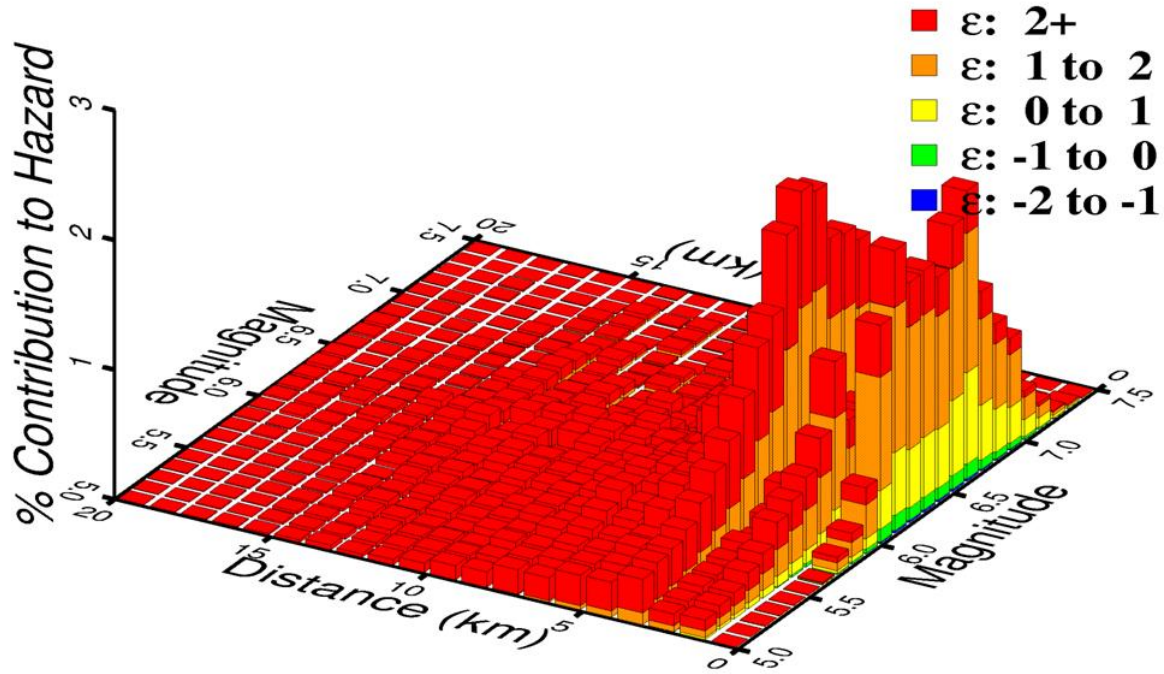
1E-4 Hazard,PGA Horiz., All Teams



Source: Schematic illustration only

Figure A2(a). Schematic Mean Hazard Deaggregation for the PSHA Reference Rock Outcrop for Peak Horizontal Ground Acceleration for an AFE of 10^{-4}

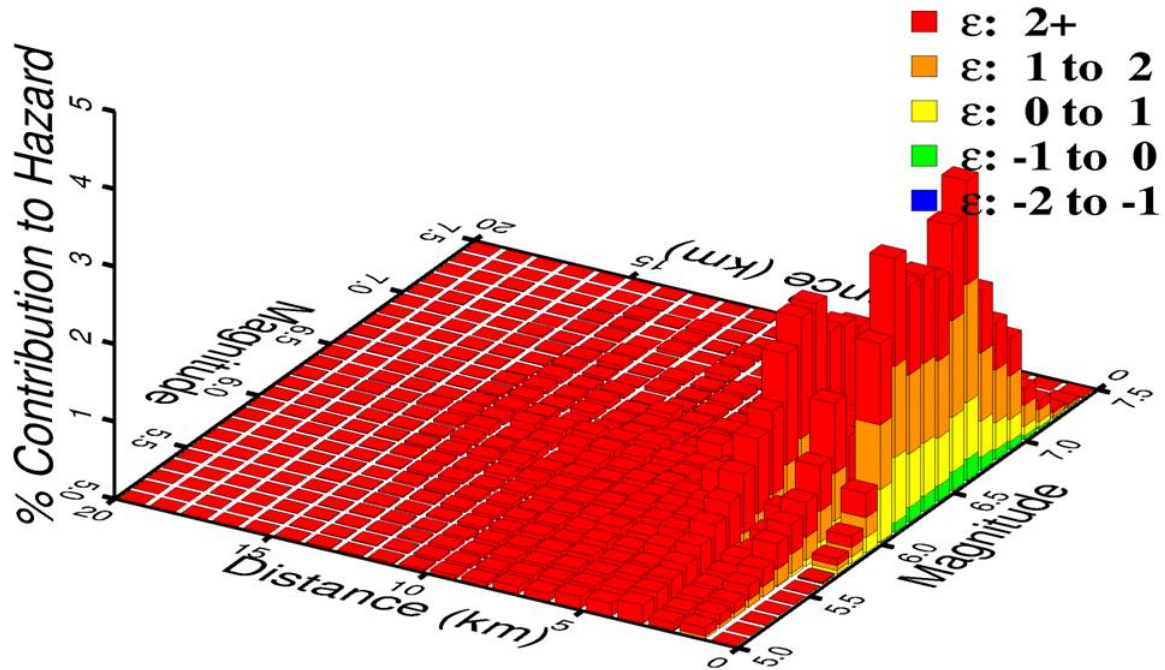
1E-5 Hazard, PGA Horiz., All Teams



Source: Schematic illustration only

Figure A2(b). Schematic Mean Hazard Deaggregation for the PSHA Reference Rock Outcrop for Peak Horizontal Ground Acceleration for an AFE of 10^{-5}

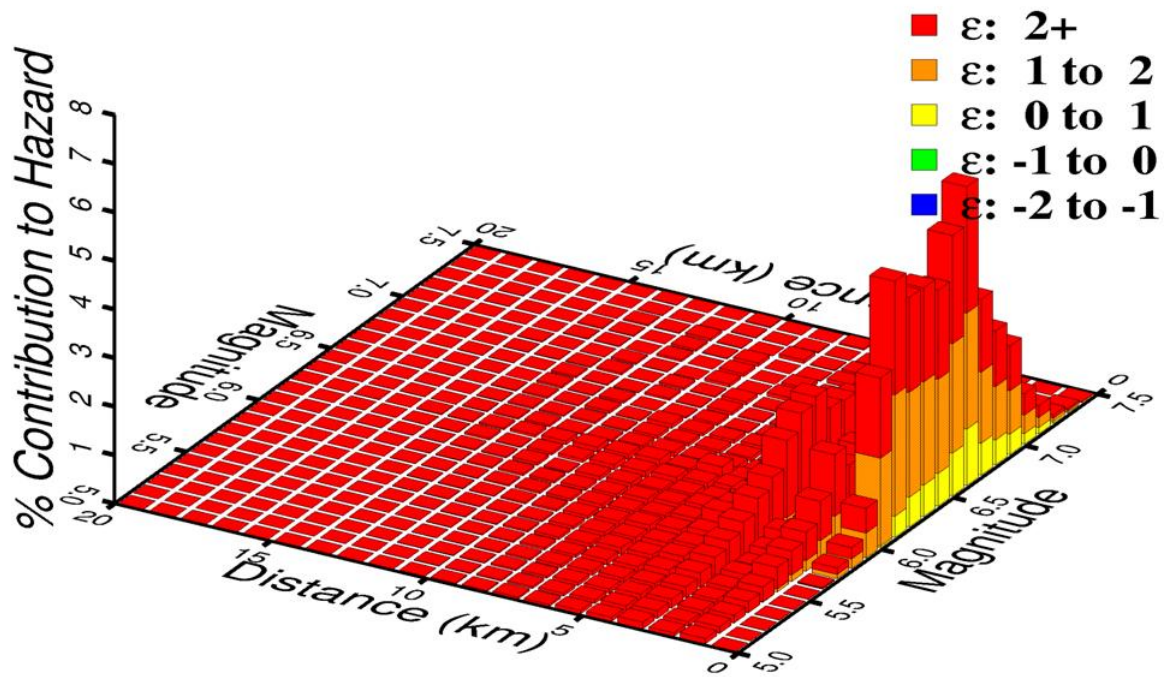
1E-6 Hazard, PGA Horiz., All Teams



Source: Schematic illustration only

Figure A2(c). Schematic Mean Hazard Deaggregation for the PSHA Reference Rock Outcrop for Peak Horizontal Ground Acceleration for an AFE of 10^{-6}

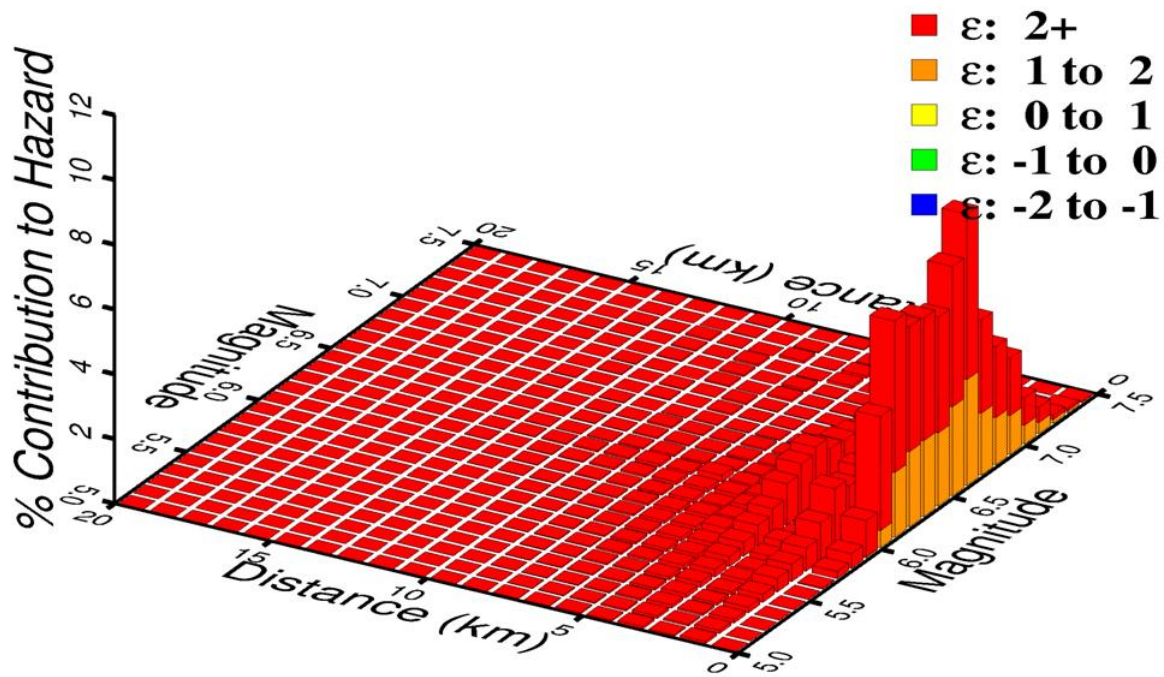
1E-7 Hazard, PGA Horiz., All Teams



Source: Schematic illustration only

Figure A2(d). Schematic Mean Hazard Deaggregation for the PSHA Reference Rock Outcrop for Peak Horizontal Ground Acceleration for an AFE of 10⁻⁷

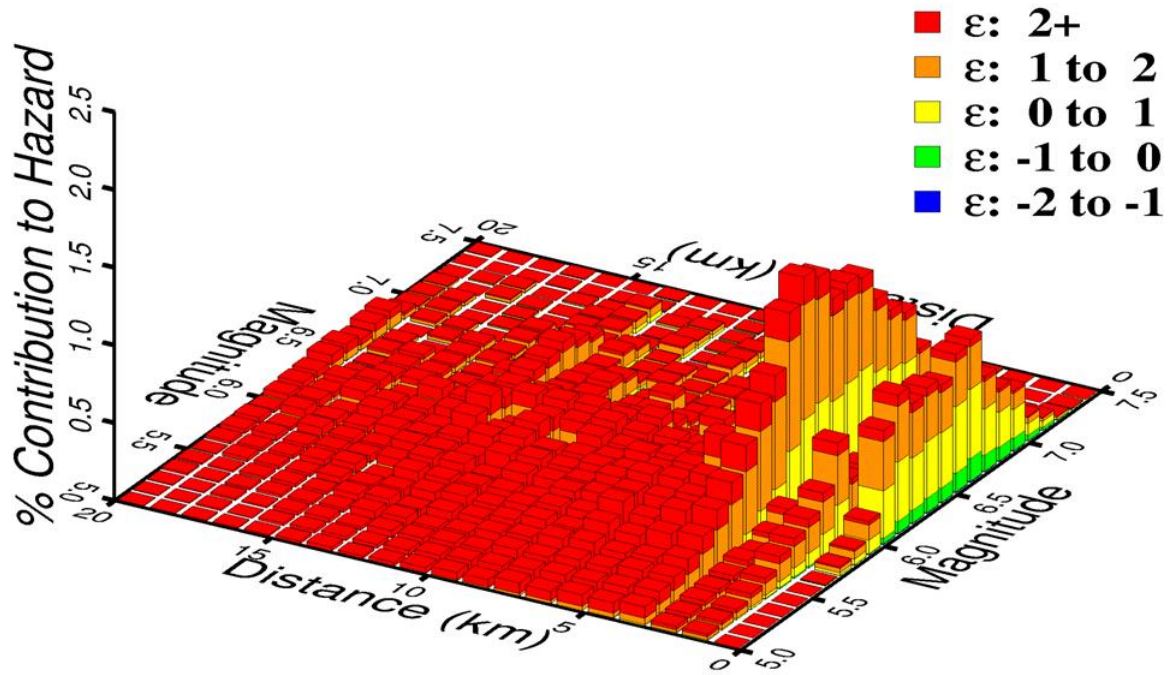
1E-8 Hazard, PGA Horiz., All Teams



Source: Schematic illustration only

Figure A2(e). Schematic Mean Hazard Deaggregation for the PSHA Reference Rock Outcrop for Peak Horizontal Ground Acceleration for an AFE of 10^{-8}

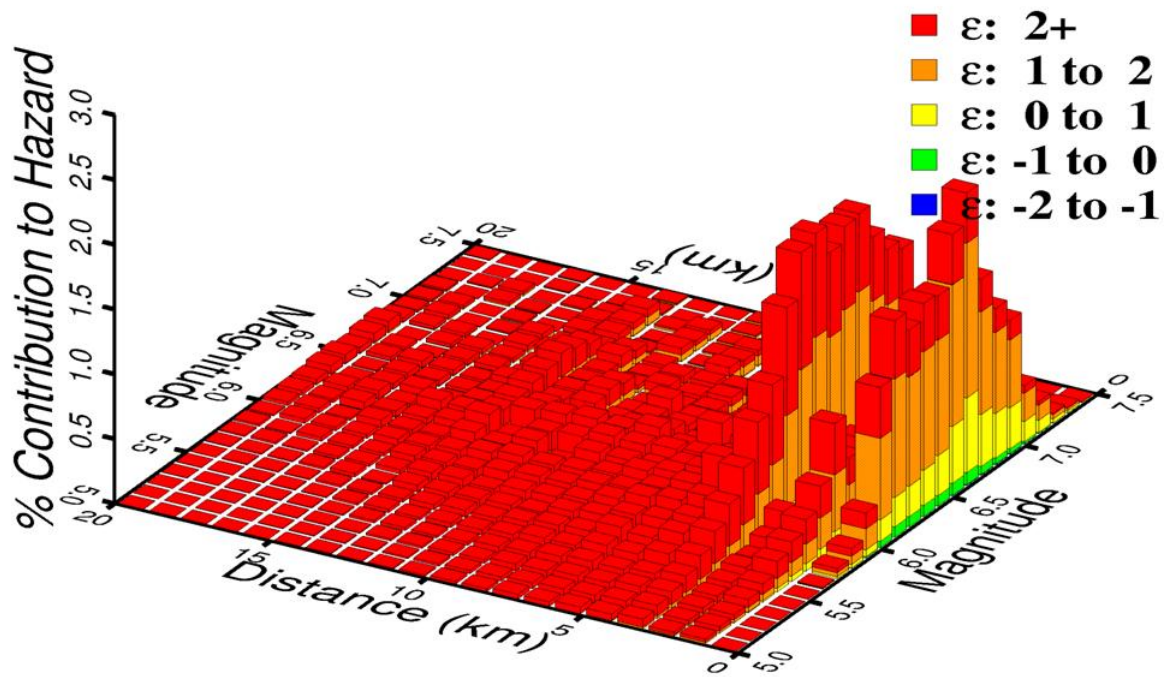
1E-4 Hazard,PGV Horiz., All Teams



Source: Schematic illustration only

Figure A3(a). Schematic Mean Hazard Deaggregation for the PSHA Reference Rock Outcrop for Peak Horizontal Ground Velocity for an AFE of 10^{-4}

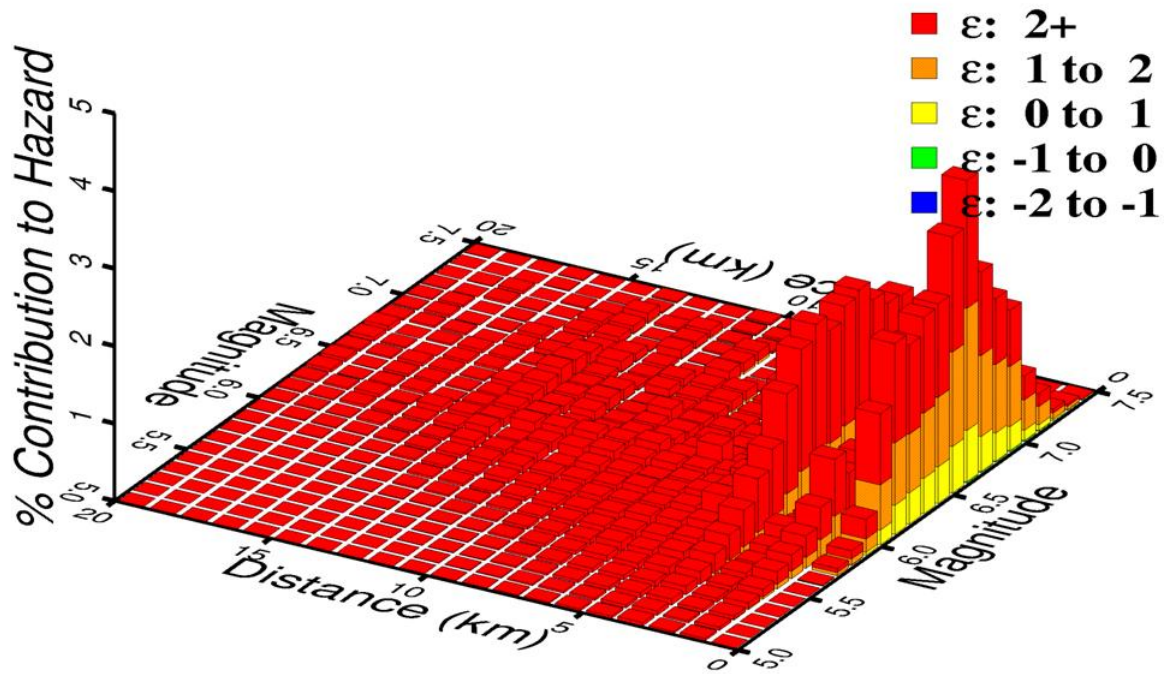
1E-5 Hazard, PGV Horiz., All Teams



Source: Schematic illustration only

Figure A3(b). Schematic Mean Hazard Deaggregation for the PSHA Reference Rock Outcrop for Peak Horizontal Ground Velocity for an AFE of 10^{-5}

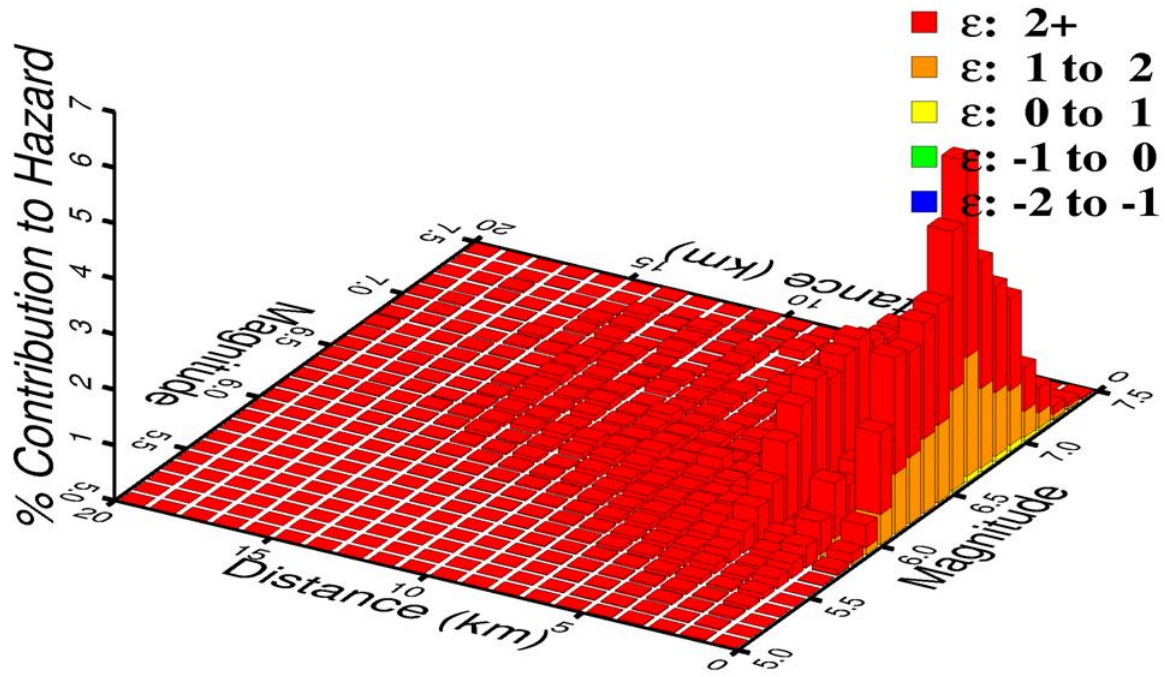
1E-6 Hazard, PGV Horiz., All Teams



Source: Schematic illustration only

Figure A3(c). Schematic Mean Hazard Deaggregation for the PSHA Reference Rock Outcrop for Peak Horizontal Ground Velocity for an AFE of 10^{-6}

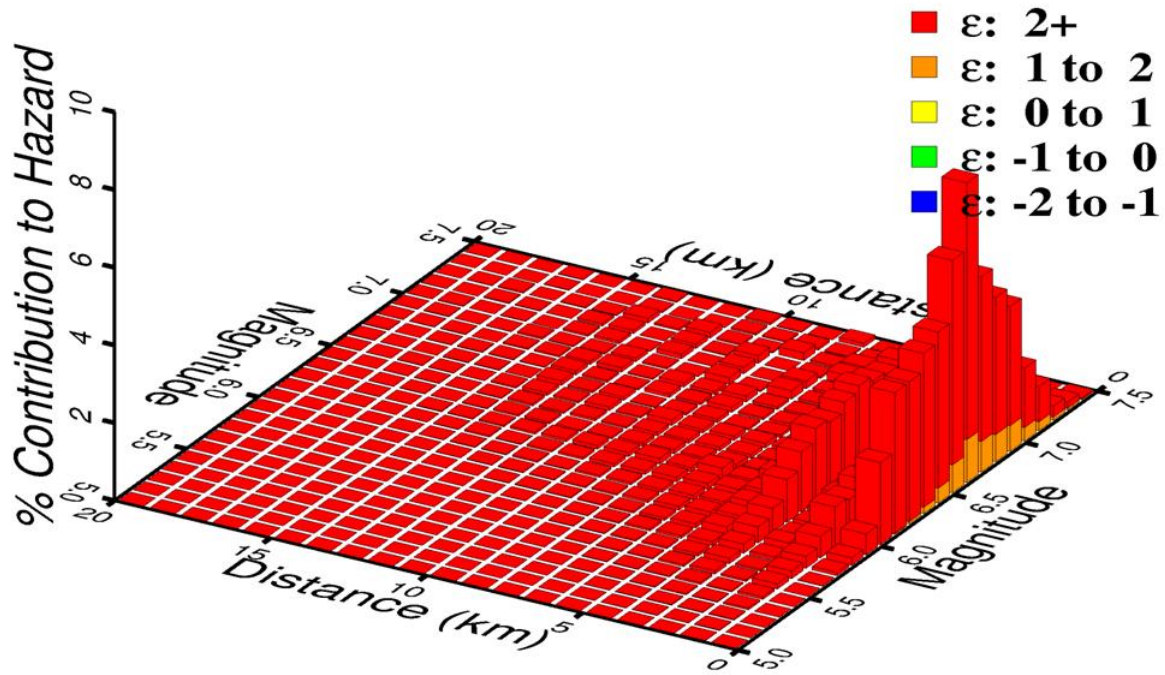
1E-7 Hazard, PGV Horiz., All Teams



Source: Schematic illustration only

Figure A3(d). Schematic Mean Hazard Deaggregation for the PSHA Reference Rock Outcrop for Peak Horizontal Ground Velocity for an AFE of 10^{-7}

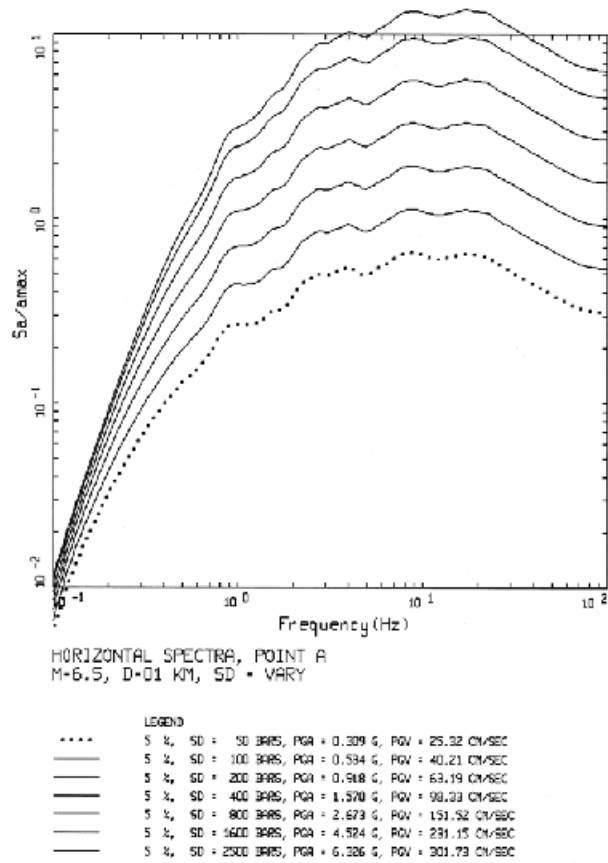
1E-8 Hazard, PGV Horiz., All Teams



Source: Schematic illustration only

Figure A3(e). Schematic Mean Hazard Deaggregation for the PSHA Reference Rock Outcrop for Peak Horizontal Ground Velocity for an AFE of 10^{-8}

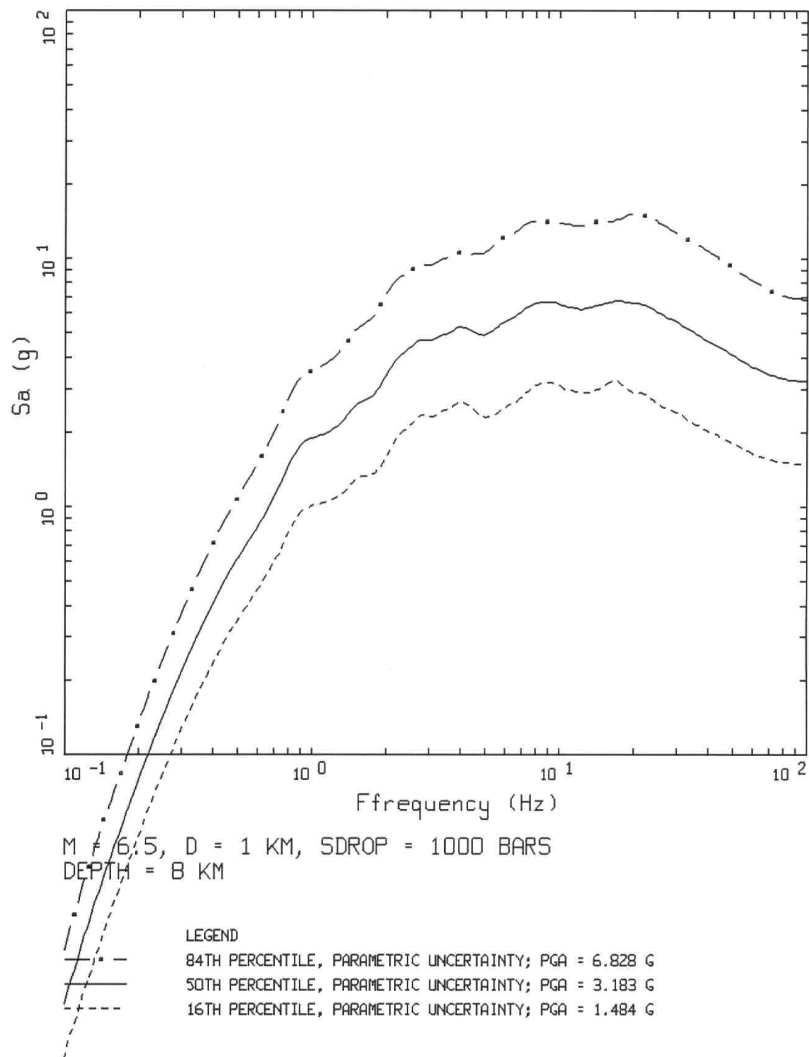
INTENTIONALLY LEFT BLANK



Source: Appendix D, Table D-1

NOTE: Acceleration spectra are shown for a suite of stress drop values ranging from 50 to 2500 bars for an **M** 6.5 earthquake at a distance of 1 km and depth of 8 km.

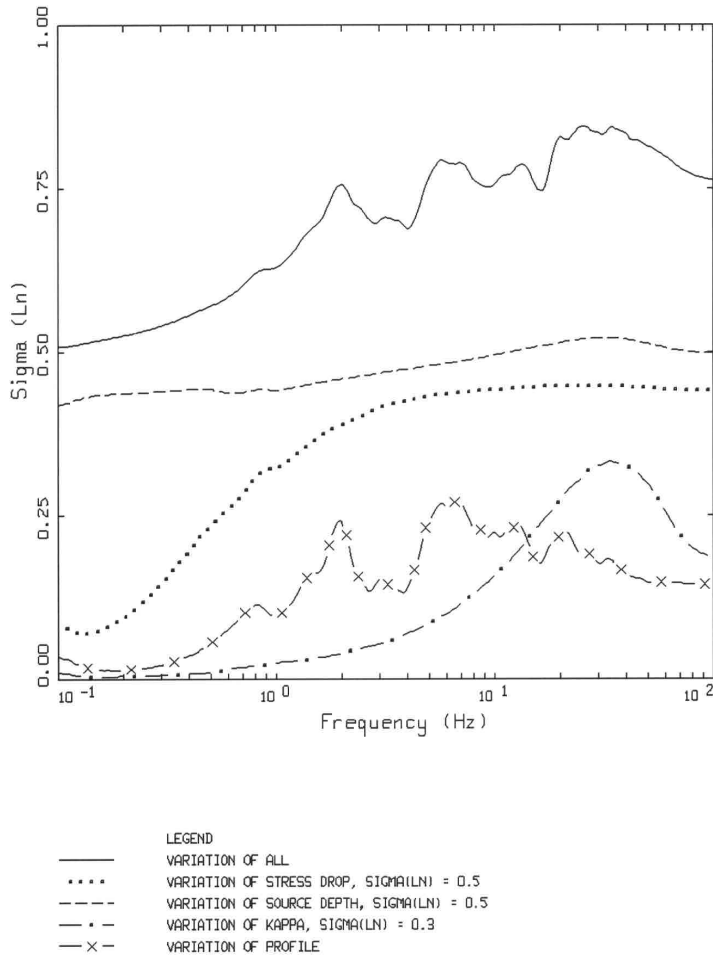
Figure A4. Range in predicted response spectra for a nearby source using the point-source model.



Source: Appendix D, Table D-1

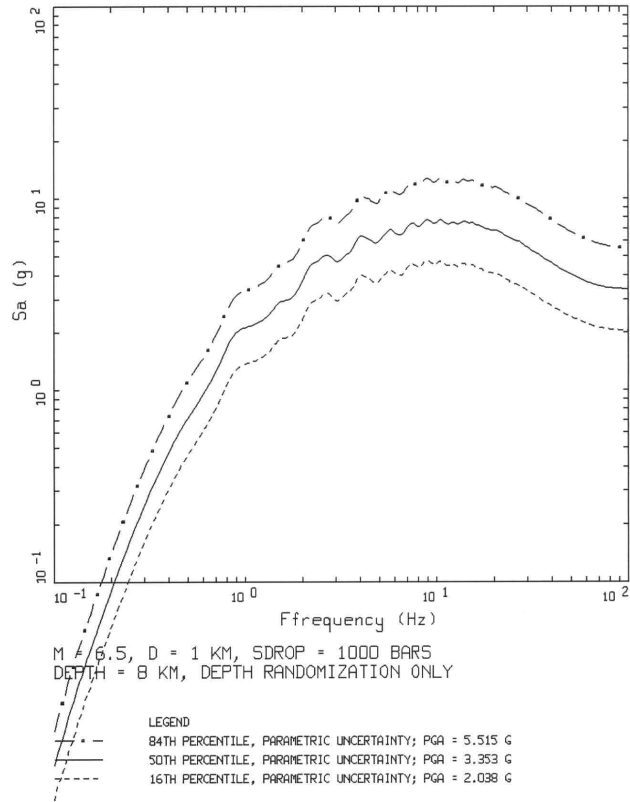
NOTE: Model variability includes stress drop ($\sigma(\ln) 0.5$), source depth ($\sigma(\ln) 0.5$), kappa ($\sigma(\ln) 0.3$) and the velocity profile (Section 6.4.2.9). Total sigma is about 0.7.

Figure A5. PSHA Reference Rock Outcrop 16th, median and 84th percentile spectral acceleration for an **M** 6.5 earthquake with stress drop of 1000 bars at a distance of 1 km and depth of 8 km using the point-source model.



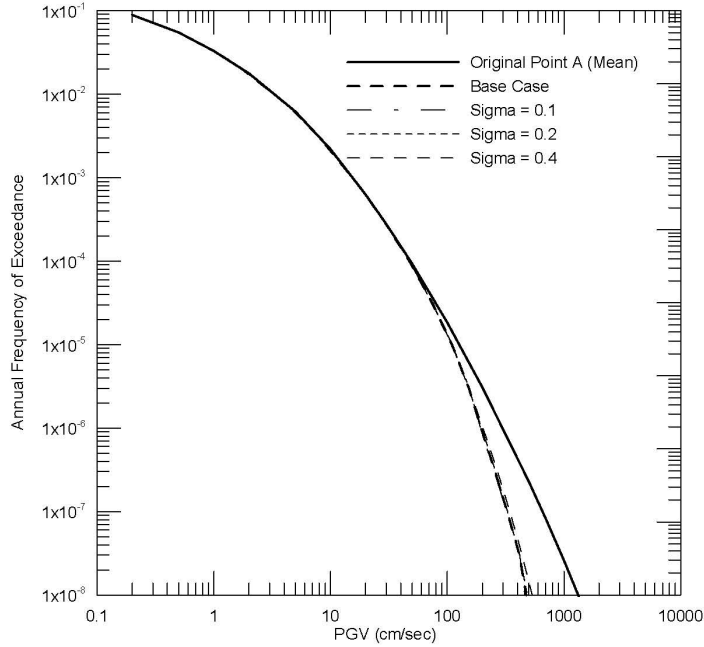
Source: Appendix D, Table D-1

Figure A6. Composition of total sigma in single corner stochastic model by oscillator frequency, with variations in source depth, stress drop, kappa and velocity profile.



Source: Appendix D, Table D-1

Figure A7. PSHA Reference Rock Outcrop 16th, median, and 84th percentile spectral acceleration for an **M** 6.5 earthquake with stress drop of 1000 bars at a distance of 1 km and depth of 8 km using depth randomization only in point-source modeling. Sigma on predicted spectral values is reduced to about 0.5.

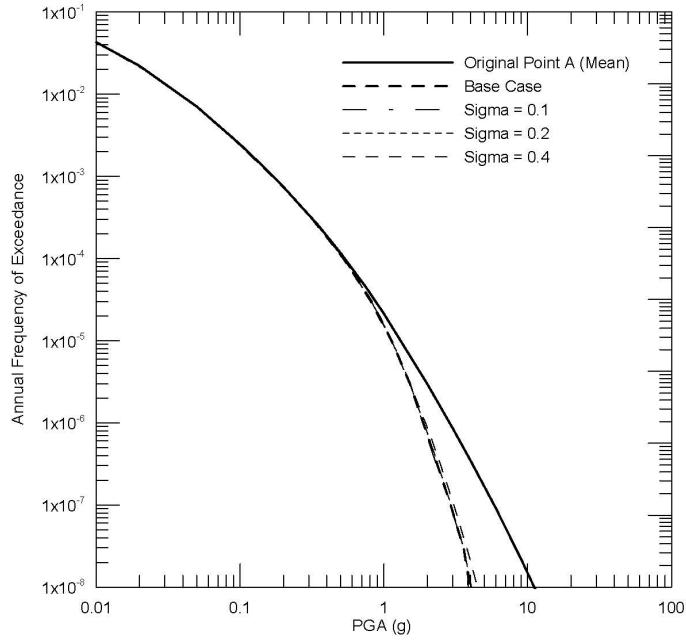


Point A PGV Mean Hazard Curve
versus
Stress Conditioned Hazard Curves

Source: Appendix D, Table D-1

NOTE: Base case sigma is 0.15.

Figure A8(a). PSHA Reference Rock Outcrop extreme-stress-drop conditioned and unconditioned PGV hazard for a suite of ground motion sigma ranging from 0.1-0.4.

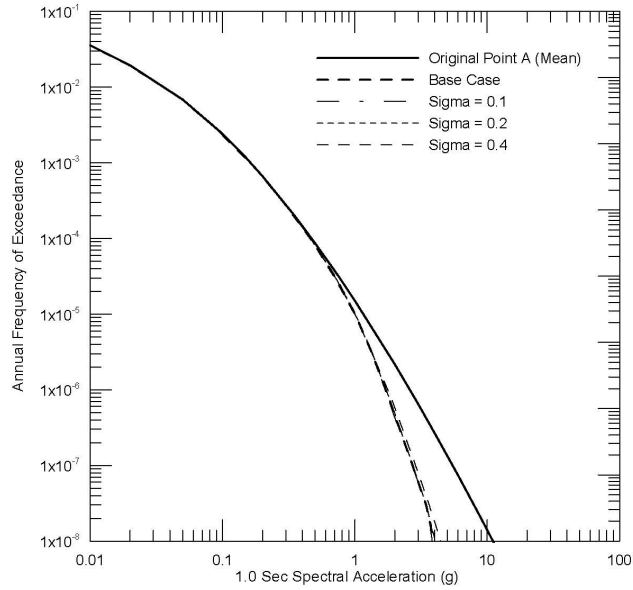


Point A PGA Mean Hazard Curve
versus
Stress Conditioned Hazard Curves

Source: Appendix D, Table D-1

NOTE: Base case sigma is 0.15.

Figure A8(b). PSHA Reference Rock Outcrop extreme-stress-drop conditioned and unconditioned PGA hazard for a suite of ground motion sigma ranging from 0.1-0.4.

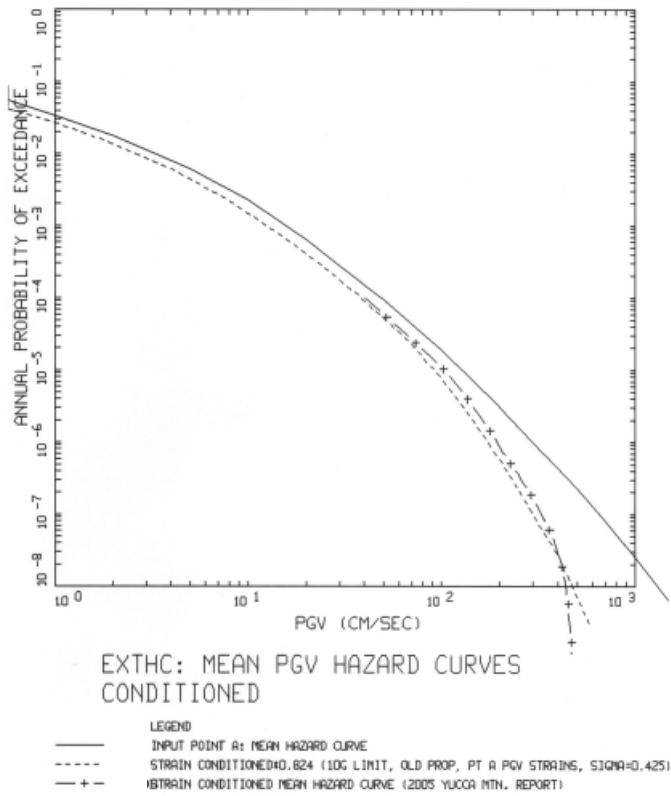


Point A 1.0 Second SA Mean Hazard Curve
versus
Stress Conditioned Hazard Curves

Source: Appendix D, Table D-1

NOTE: Base case sigma is 0.15.

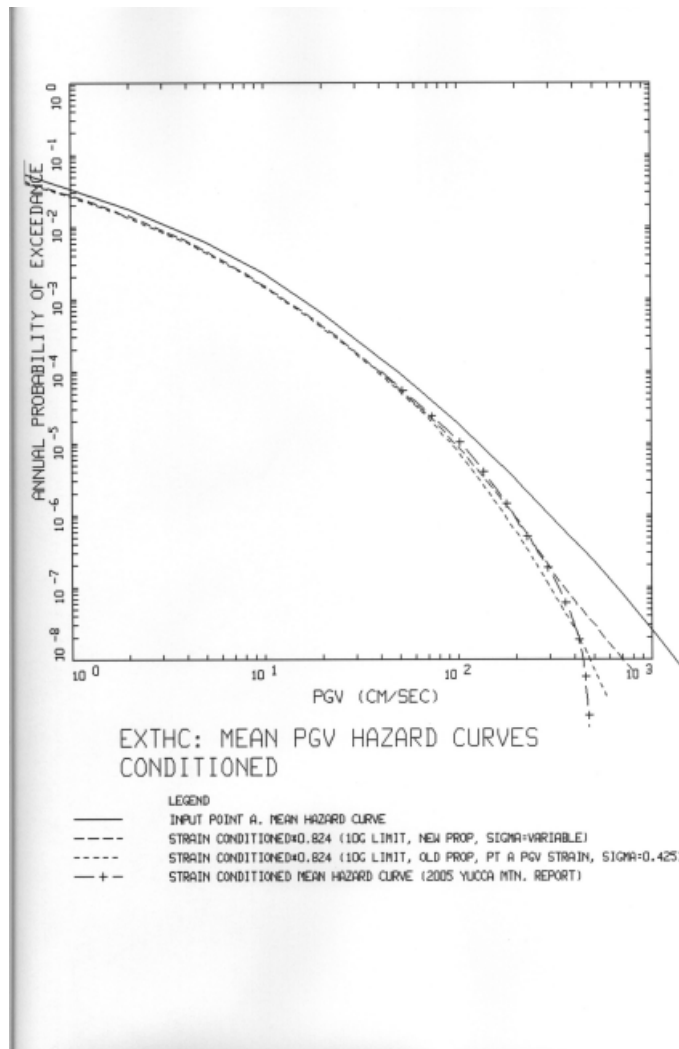
Figure A8(c). PSHA Reference Rock Outcrop extreme-stress-drop conditioned and unconditioned 1.0-Hz spectral acceleration hazard for a suite of ground motion sigma ranging from 0.1-0.4.



Source: Appendix D, Table D-1

NOTE: The short-dash line represents the conditioned hazard using shear strains and PGV from BSC (2005 [DIRS 170137]), a shear strain sigma of 0.425, and a 0.824 factor to convert hazard for the reference rock outcrop to hazard at the waste emplacement level. The factor of 0.824 is based on site response modeling from BSC (2004 [DIRS 170027]) for AFEs of 10^{-4} , 10^{-5} , 10^{-6} , and 10^{-7} . The solid line is the PSHA Reference Rock Outcrop mean PGV hazard. The long-dash-plus line is the conditioned hazard from BSC (2005 [DIRS 170137]).

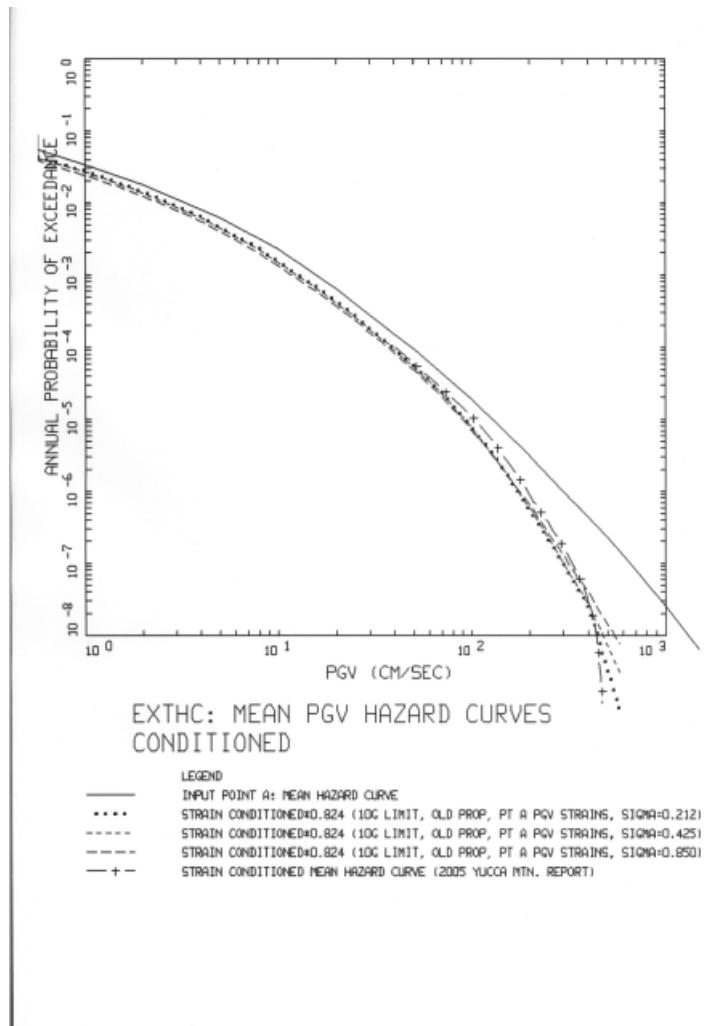
Figure A9(a). Repository waste emplacement level shear-strain-threshold conditioned mean PGV hazard using the methodology described in Section A4.2: Results for shear strains from BSC (2005 [DIRS 170137]) are compared to results using the methodology in BSC (2005 [DIRS 170137]).



Source: Appendix D, Table D-1

NOTES: The short-dash line represents the conditioned hazard using shear strains and PGV from BSC (2005 [DIRS 170137]), a shear strain sigma of 0.425, and a 0.824 factor to convert hazard for the reference rock outcrop to hazard at the waste emplacement level. The long-dash line represents the same case, except shear strain values from this report are used. The solid line represents the PSHA Reference Rock Outcrop mean PGV hazard. The dash-plus line represents conditioned hazard from BSC (2005 [DIRS 170137]).

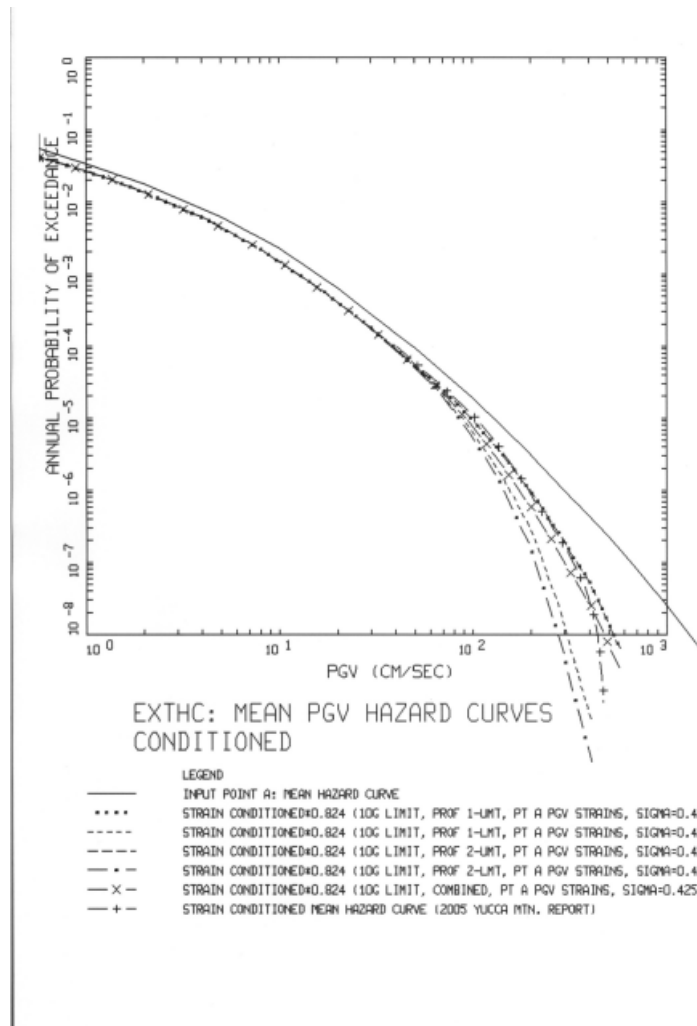
Figure A9(b). Repository waste emplacement level shear-strain-threshold conditioned mean PGV hazard using the methodology described in Section A4.2: Results using shear strains from BSC (2005 [DIRS 170137]) are compared to results using shear strains developed in this report.



Source: Appendix D, Table D-1

NOTE: The dotted line represents the conditioned hazard using shear strains and PGV from BSC (2005 [DIRS 170137]), a shear strain sigma of 0.212, and a 0.824 factor to convert hazard for the reference rock outcrop to hazard at the waste emplacement level. The short-dash and long-dash lines represent the same case, except shear strain sigma is changed to 0.425 and 0.850, respectively. The solid line represents the PSHA Reference Rock Outcrop mean PGV hazard. The dash-plus line represents conditioned hazard from BSC (2005 [DIRS 170137]).

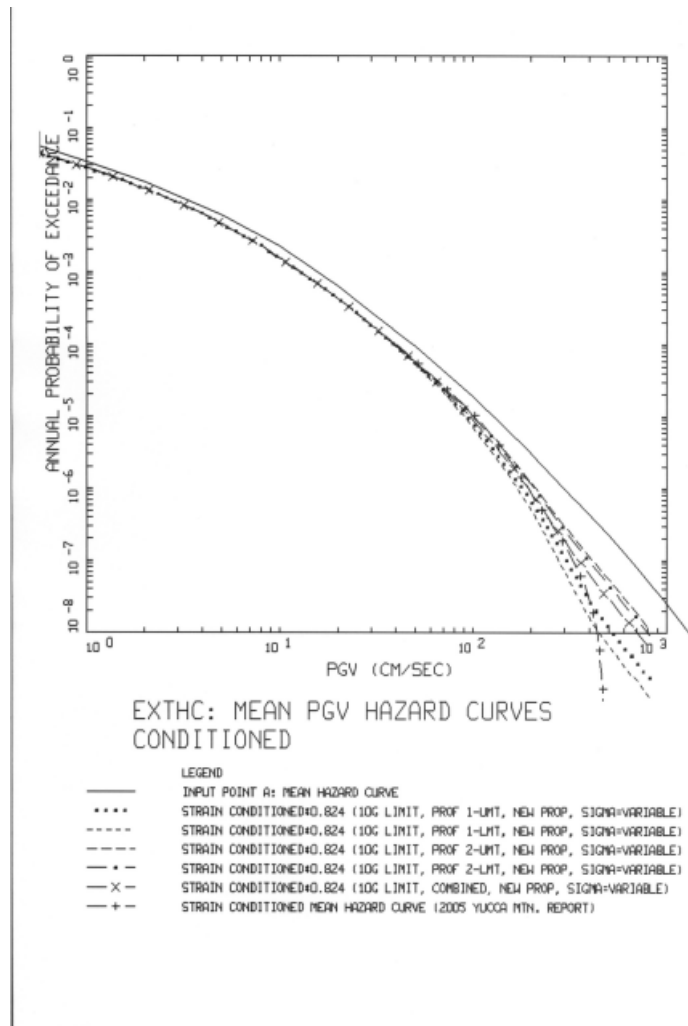
Figure A9(c). Repository waste emplacement level shear-strain-threshold conditioned mean PGV hazard using the methodology described in Section A4.2: Results for three values of shear-strain sigma.



Source: Appendix D, Table D-1

NOTE: The dotted, short-dash, long-dash, dash-dot, and dash-X lines represent conditioned hazard for different combinations of velocity profile and dynamic material property curves using shear strains and PGV from BSC (2005 [DIRS 170137]), a shear strain sigma of 0.425, and a 0.824 factor to convert hazard for the reference rock outcrop to hazard at the waste emplacement level. The dotted line is for base case velocity profile 1 and upper mean tuff (UMT) dynamic property curves (BSC 2004 [DIRS 170027]). The short-dash line is from profile 1 and lower mean tuff (LMT) curves. The long-dash line is for profile 2 and UMT curves. The dash-dot line is for profile 2 and LMT curves. The dash-X curve represents the mean of the four combinations using equal weighting. The solid line represents the PSHA Reference Rock Outcrop mean PGV hazard. The dash-plus line represents conditioned hazard from BSC (2005 [DIRS 170137]).

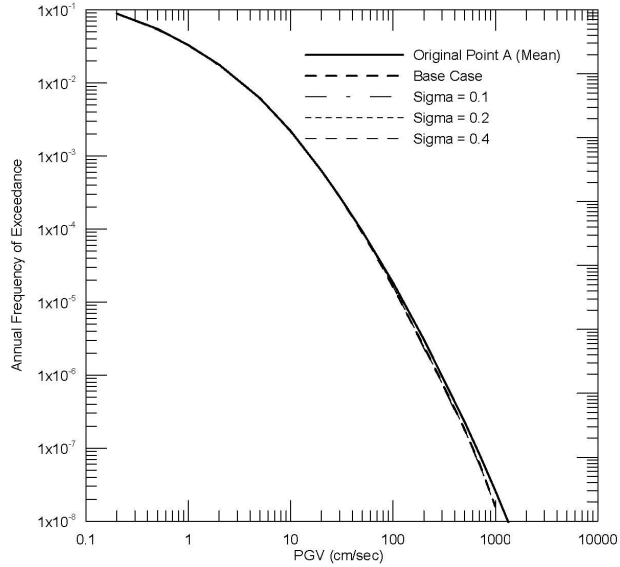
Figure A9(d). Repository waste emplacement level shear-strain-threshold conditioned mean PGV hazard using the methodology described in Section A4.2: Effects of epistemic uncertainty in material properties for properties from BSC (2004 [DIRS 170027]).



Source: Appendix D, Table D-1

NOTE: The dotted, short-dash, long-dash, dash-dot, and dash-X lines represent conditioned hazard for different combinations of velocity profile and dynamic material property curves using shear strains and PGV from this report, a shear strain sigma of 0.425, and a 0.824 factor to convert hazard for the reference rock outcrop to hazard at the waste emplacement level. The dotted line is for base case velocity profile 1 and upper mean tuff (UMT) dynamic property curves (Section 6.4). The short-dash line is from profile 1 and lower mean tuff (LMT) curves. The long-dash line is for profile 2 and UMT curves. The dash-dot line is for profile 2 and LMT curves. The dash-X curve represents the mean of the four combinations using equal weighting. The solid line represents the PSHA Reference Rock Outcrop mean PGV hazard. The dash-plus line represents conditioned hazard from BSC (2005 [DIRS 170137]).

Figure A9(e). Repository waste emplacement level shear-strain-threshold conditioned mean PGV hazard using the methodology described in Section A4.2: Effects of epistemic uncertainty and deterministic variability in material properties for properties from Section 6.4.

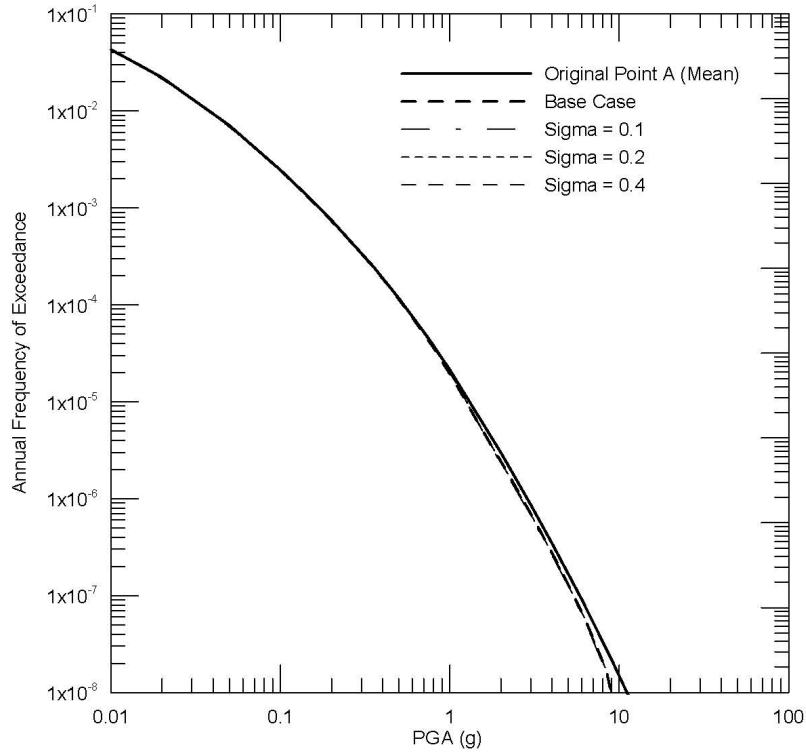


Point A PGV Mean Hazard Curve
versus
Strain Conditioned Hazard Curves

Source: Appendix D, Table D-1

NOTE: Base case shear strain sigma is determined from site-response modeling.

Figure A10(a). Shear-strain-threshold conditioned PSHA Reference Rock Outcrop PGV hazard using the methodology described in Section A4.2. The conditioned hazard dependence on shear strain sigma is also illustrated.

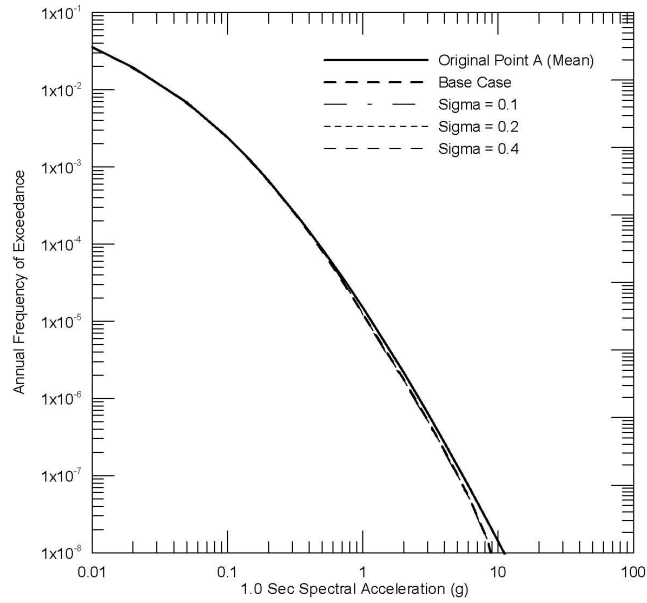


Point A PGA Mean Hazard Curve
versus
Strain Conditioned Hazard Curves

Source: Appendix D, Table D-1

NOTE: Base case shear strain sigma is determined from site-response modeling.

Figure A10(b). Strain conditioned PSHA Reference Rock Outcrop PGA hazard using the methodology described in Section A4.2. The conditioned hazard dependence on shear strain sigma is also illustrated.

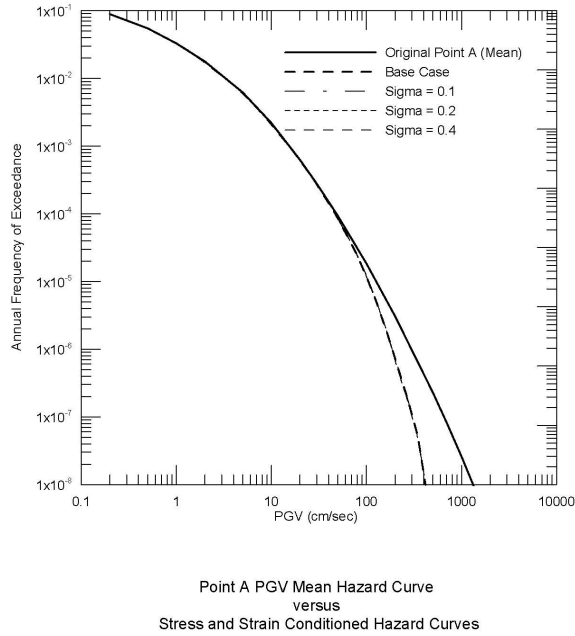


Point A 1.0 Second SA Mean Hazard Curve
versus
Strain Conditioned Hazard Curves

Source: Appendix D, Table D-1

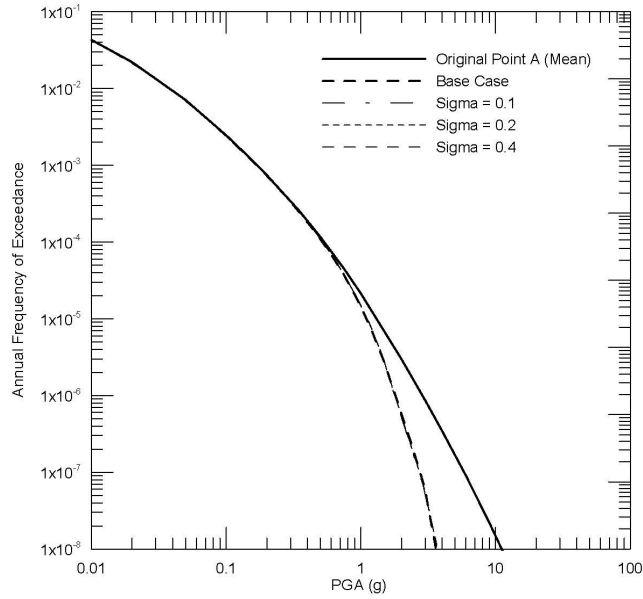
NOTE: Base case shear strain sigma is determined from site-response modeling.

Figure A10(c). Strain conditioned PSHA Reference Rock Outcrop 1.0-second spectral acceleration hazard using the methodology described in Section A4.2. The conditioned hazard dependence on shear strain sigma is also illustrated.



Source: Appendix D, Table D-1

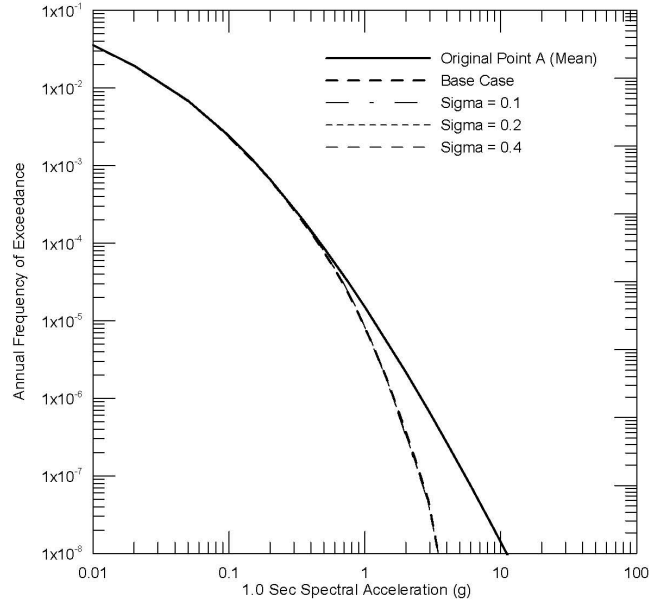
Figure A11(a). Extreme-stress-drop and shear-strain-threshold conditioned PGV hazard using the methodology described in Sections A4.1 and A4.2. The effects of ground motion and shear strain sigma are also illustrated.



Point A Mean Hazard Curve
versus
Stress and Strain Conditioned Hazard Curves

Source: Appendix D, Table D-1

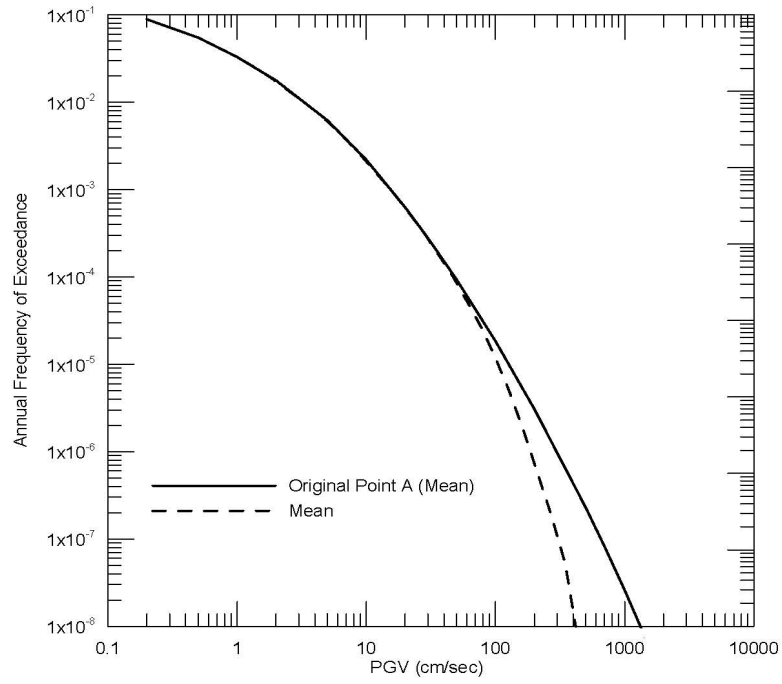
Figure A11 (b). Extreme-stress-drop and shear-strain-threshold conditioned PGA hazard using the methodology described in Sections A41 and A4.2. The effects of ground motion and shear strain sigma are also illustrated.



Point A 1.0 Second SA Mean Hazard Curve
versus
Stress and Strain Conditioned Hazard Curves

Source: Appendix D, Table D-1

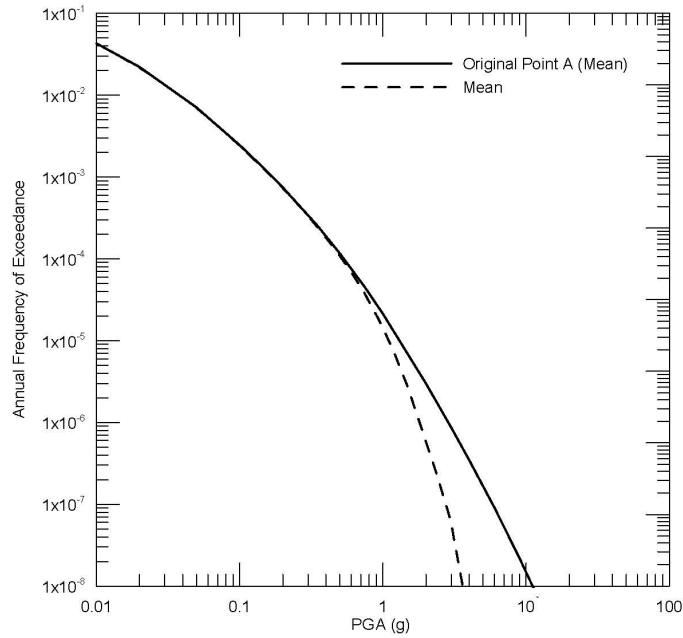
Figure A11(c). Extreme-stress-drop and shear-strain-threshold conditioned 1-second spectral acceleration hazard using the methodology described in Sections A4.1 and A4.2. The effects of ground motion and shear strain sigma are also illustrated.



Point A PGV Mean Hazard Curve
versus
Base Conditioned Hazard Curves used in 2007 Analyses

Source: Appendix D, Table D-1

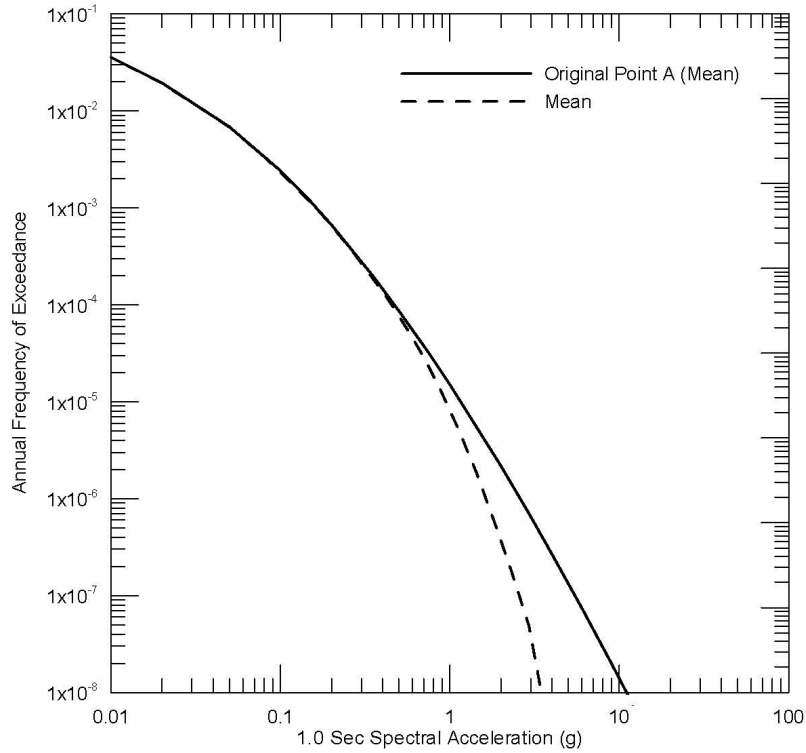
Figure A12(a). Conditioned PSHA Reference Rock Outcrop mean horizontal PGV hazard.



Point A PGA Mean Hazard Curve
versus
Base Conditioned Hazard Curves used in 2007 Analyses

Source: Appendix D, Table D-1

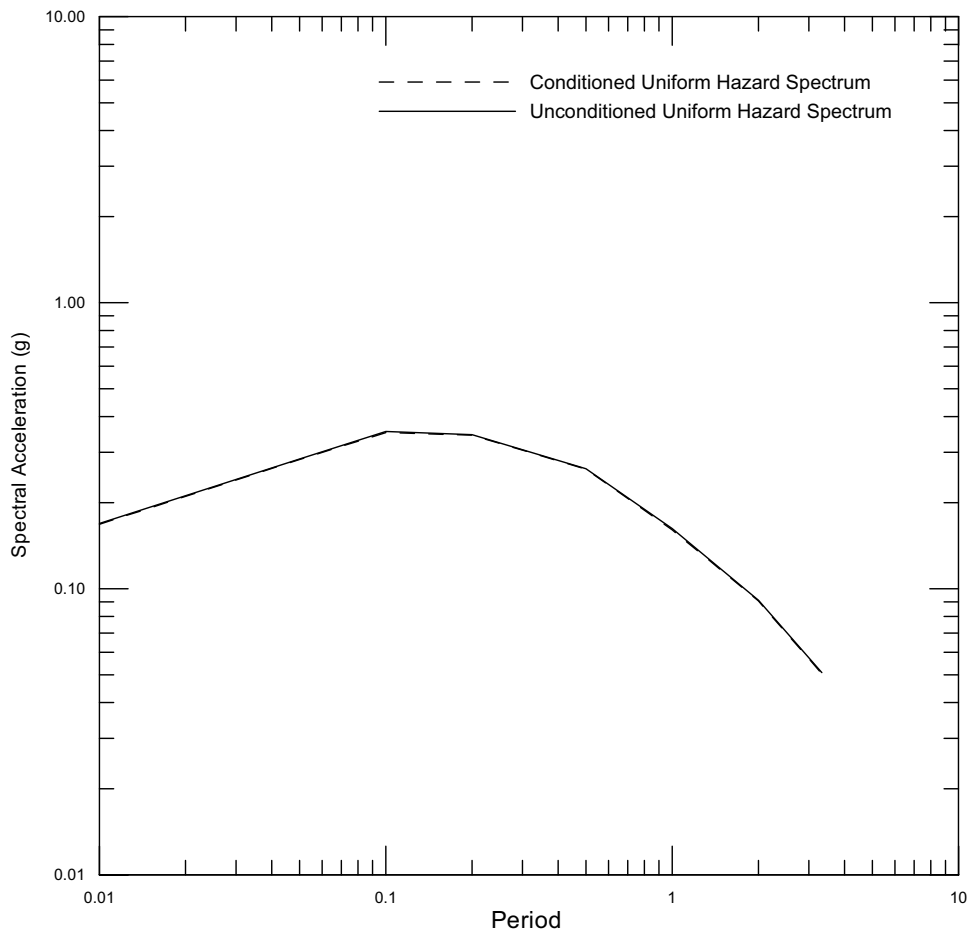
Figure A12 (b). Conditioned PSHA Reference Rock Outcrop mean horizontal PGA hazard.



Point A 1.0 Second SA Mean Hazard Curve
versus
Base Conditioned Hazard Curves used in 2007 Analyses

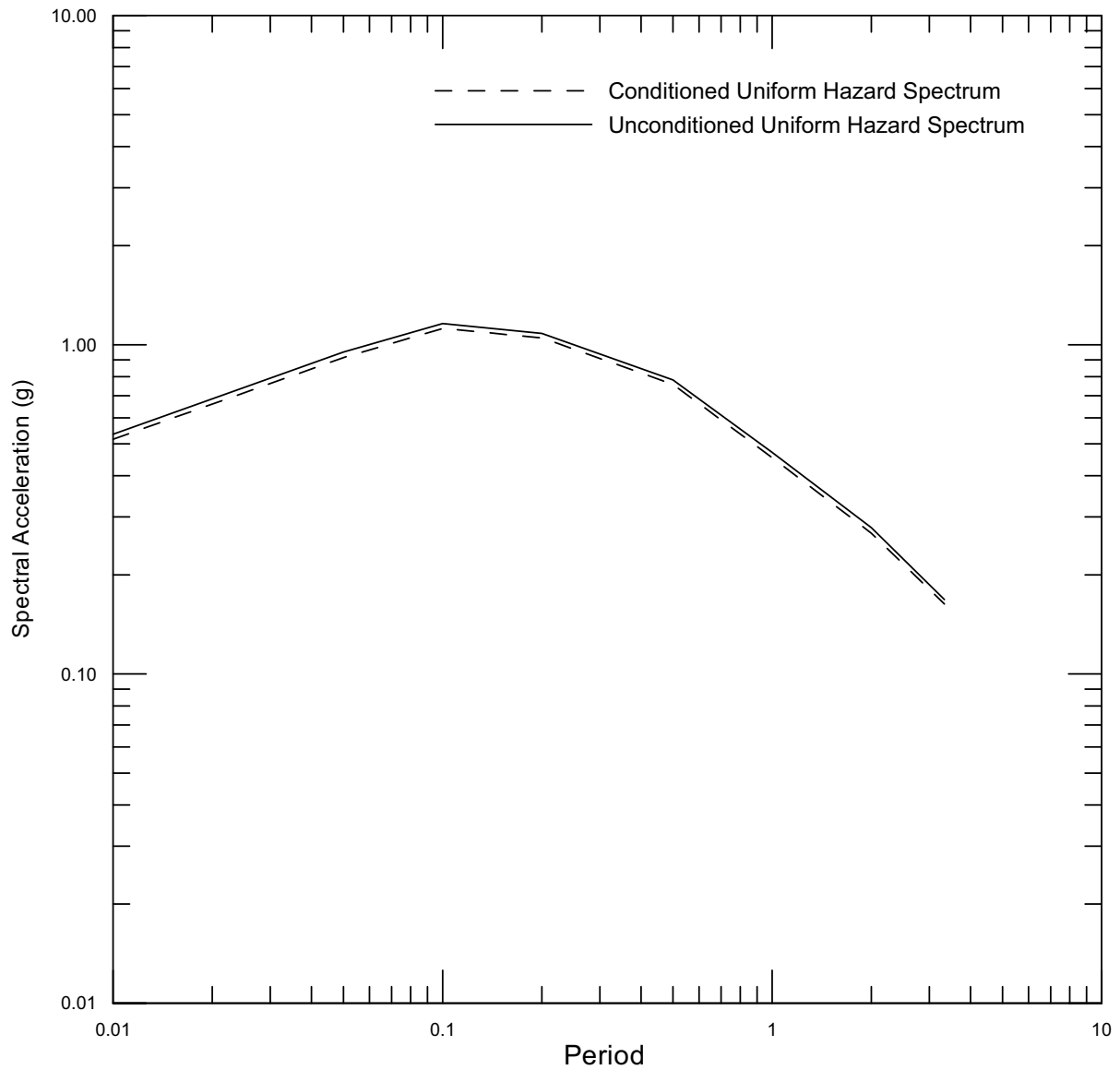
Source: Appendix D, Table D-1

Figure A12(c). Conditioned PSHA Reference Rock Outcrop mean horizontal 1-second spectral acceleration hazard.



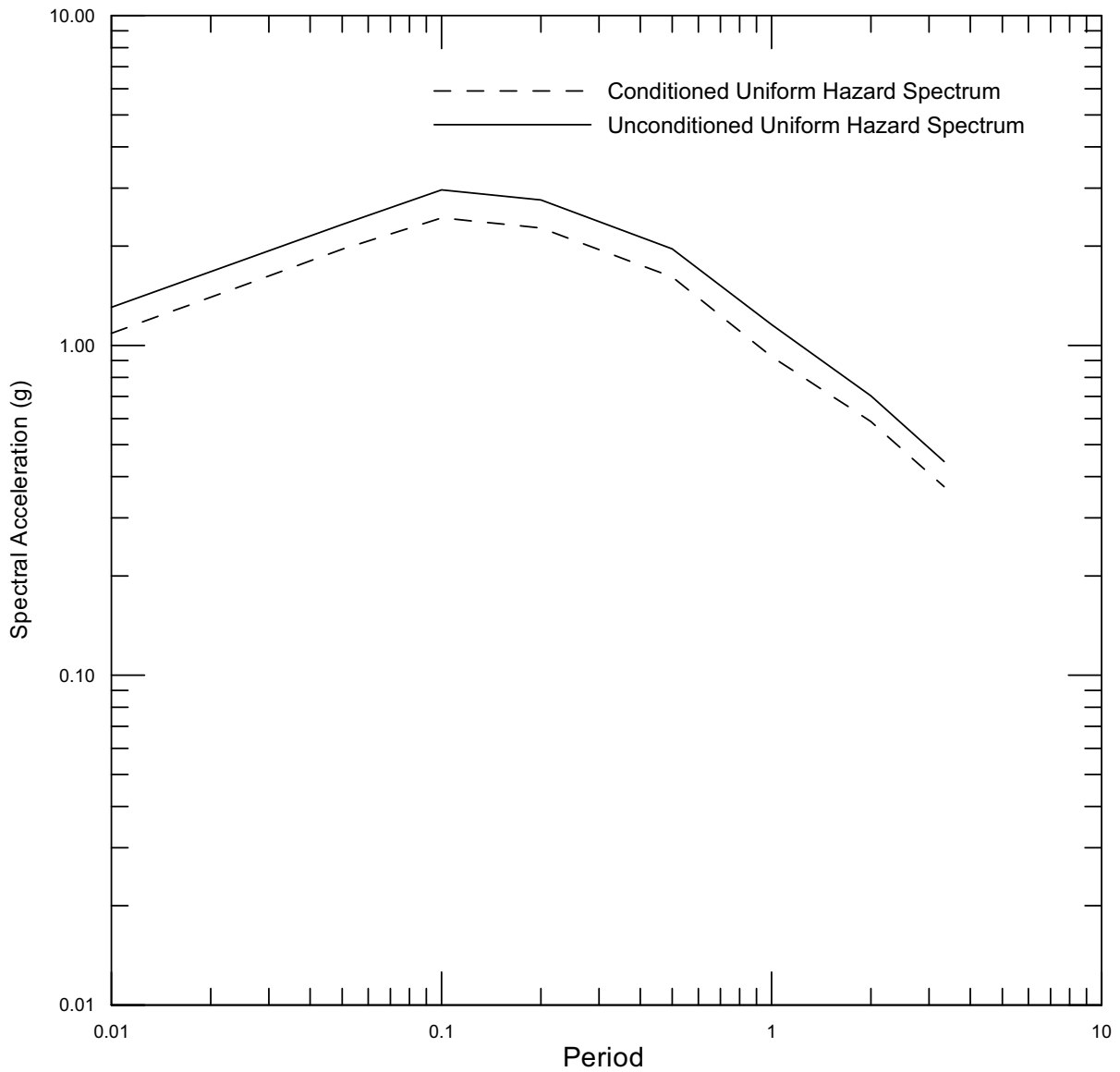
Sources: MO0211REDES103.000 [DIRS 170424] (unconditioned), Appendix D, Table D-1 (conditioned)

Figure A13 (a). The PSHA Reference Rock Outcrop uniform hazard spectra based on the extreme-stress-drop and shear-strain-threshold conditioned and unconditioned hazard for an AFE of 10^{-3} .



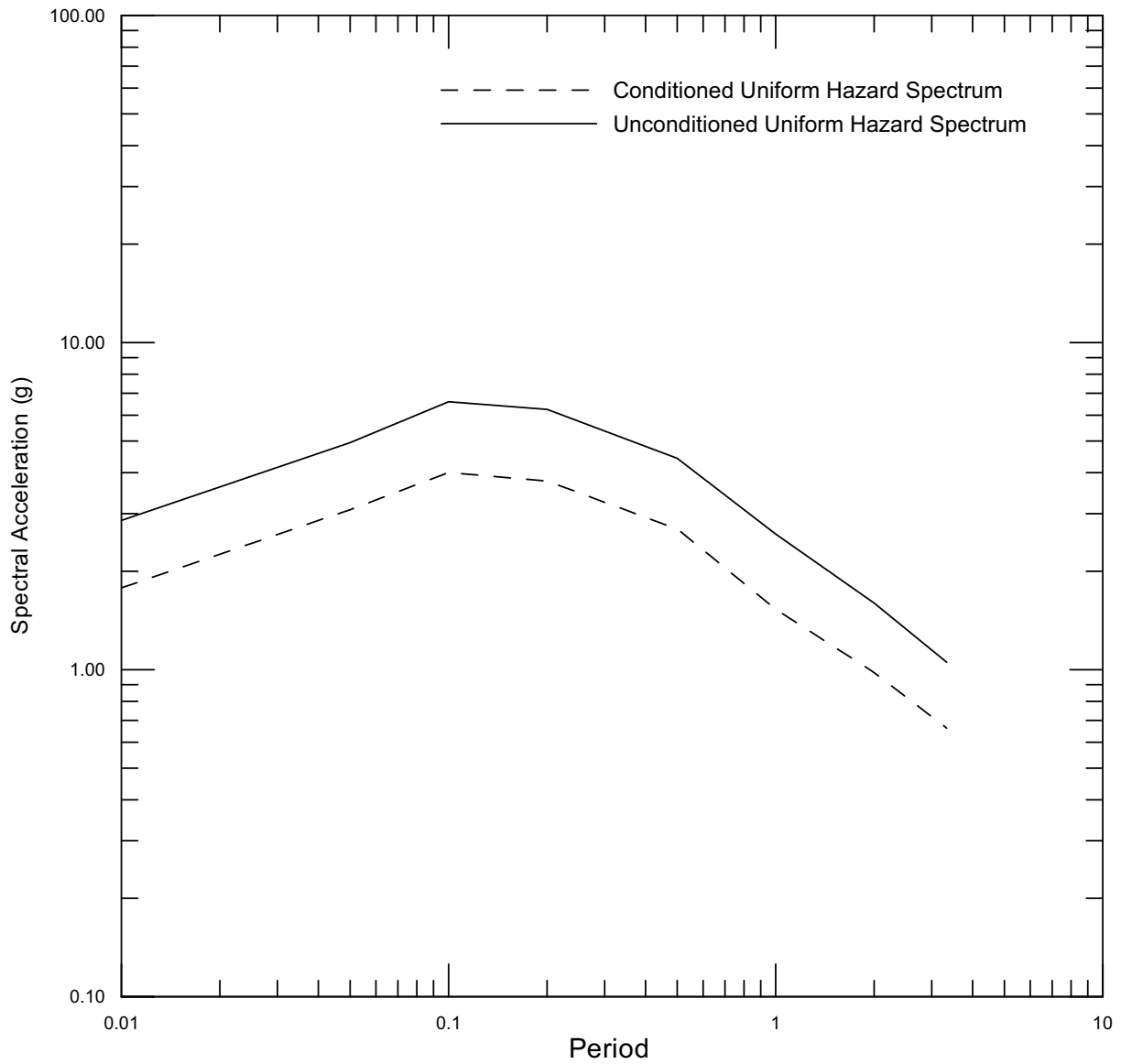
Sources: MO0211DERES104.000 [DIRS 170423] (unconditioned), Appendix D, Table D-1 (conditioned)

Figure A13(b). The PSHA Reference Rock Outcrop uniform hazard spectra based on the extreme-stress-drop and shear-strain-threshold conditioned and unconditioned hazard for an AFE of 10^{-4} .



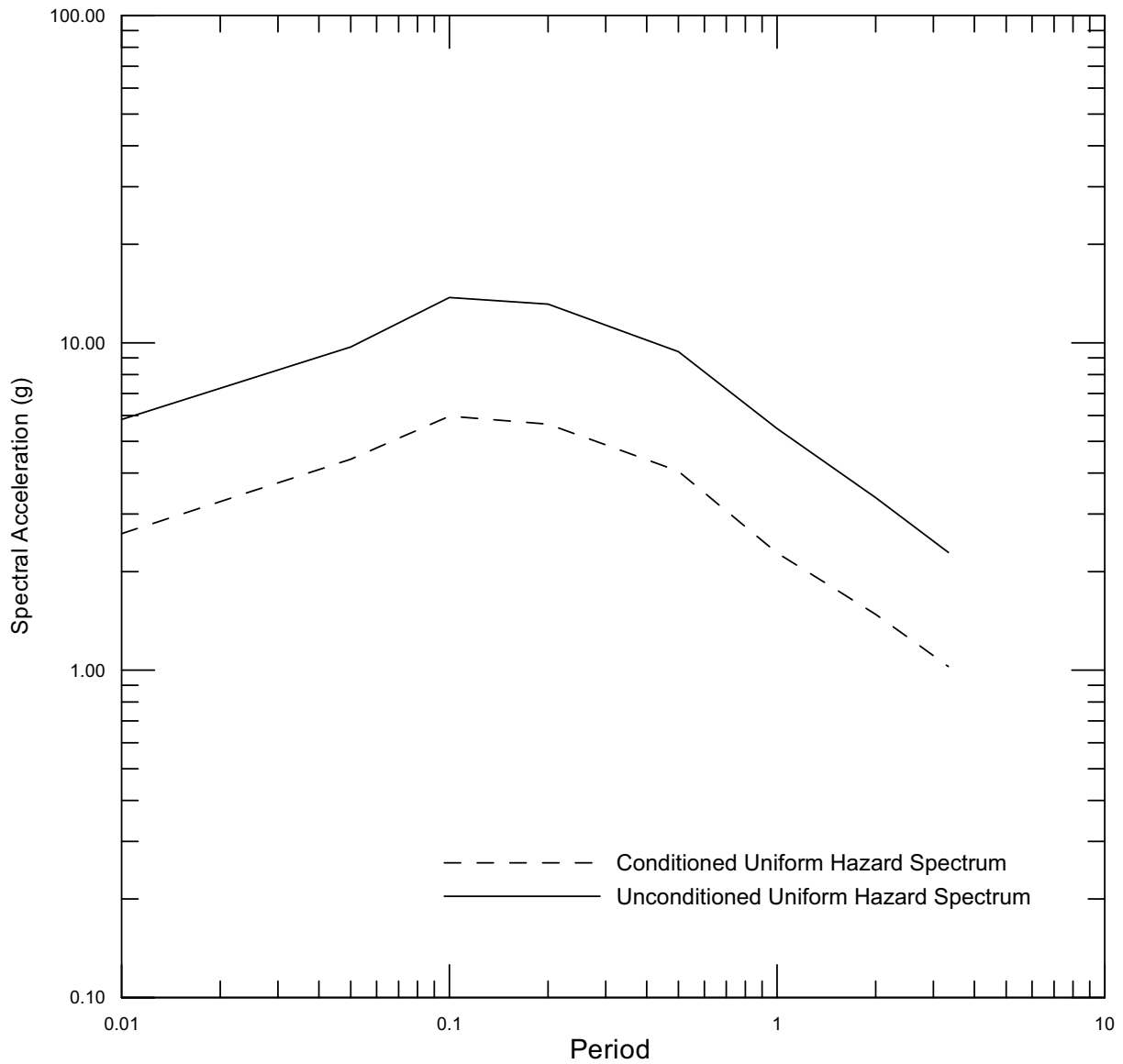
Sources: MO0308UNHAZ105.000 [DIRS 170425] (unconditioned), Appendix D, Table D-1 (conditioned)

Figure A13(c). The PSHA Reference Rock Outcrop uniform hazard spectra based on the extreme-stress-drop and shear-strain-threshold conditioned and unconditioned hazard for an AFE of 10^{-5} .



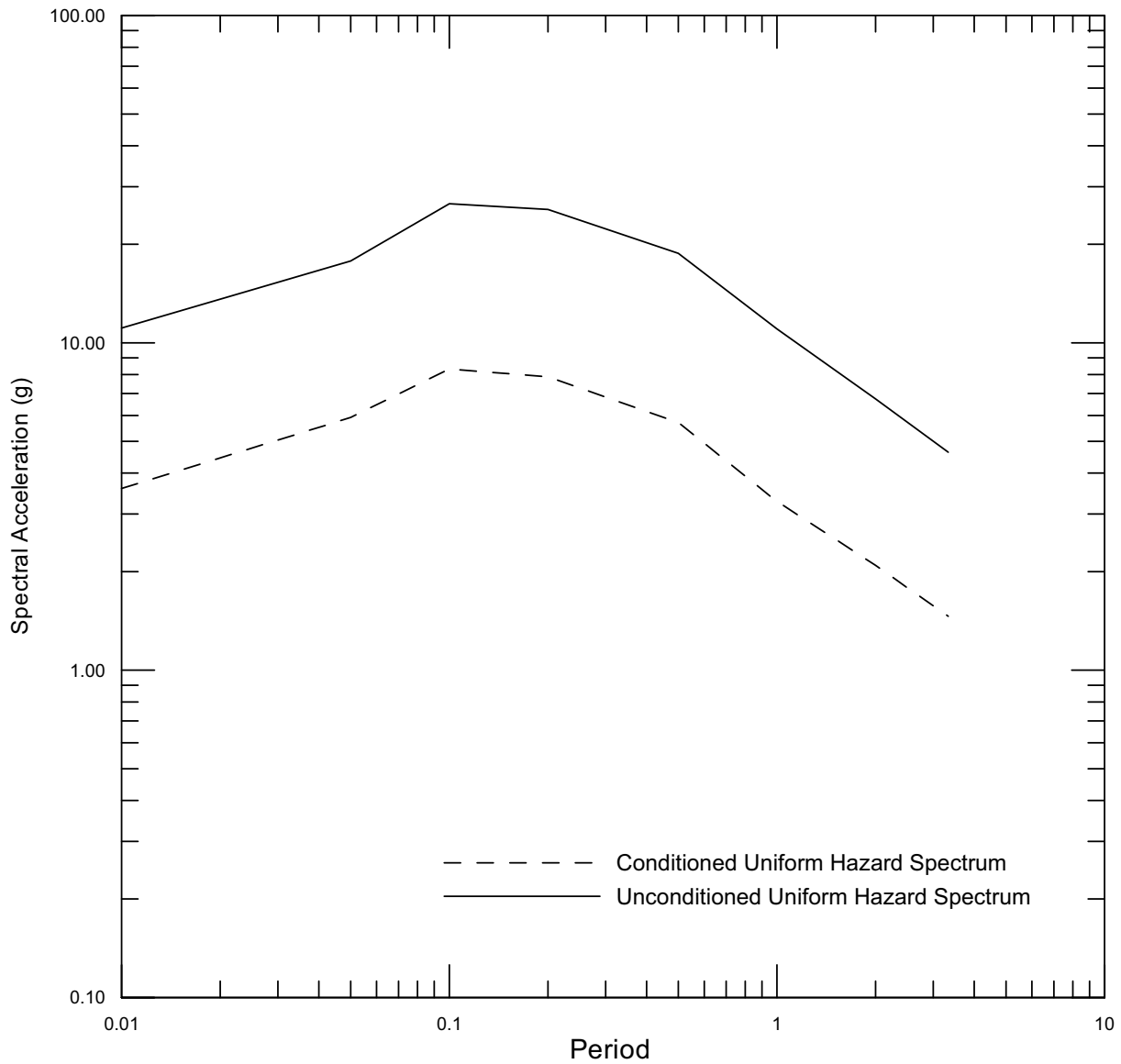
Sources: MO0206UNHAZ106.001 [DIRS 163723] (unconditioned), Appendix D, Table D-1 (conditioned)

Figure A13(d). The PSHA Reference Rock Outcrop uniform hazard spectra based on the extreme-stress-drop and shear-strain-threshold conditioned and unconditioned hazard for an AFE of 10^{-6} .



Sources: MO0209UNHAZ107.000 [DIRS 163724] (unconditioned), Appendix D, Table D-1 (conditioned)

Figure A13(e). The PSHA Reference Rock Outcrop uniform hazard spectra based on the extreme-stress-drop and shear-strain-threshold conditioned and unconditioned hazard for an AFE of 10^{-7} .



Sources: MO03061E9PSHA1.000 [DIRS 163721] (unconditioned), Appendix D, Table D-1 (conditioned)

Figure A13(f). The PSHA Reference Rock Outcrop uniform hazard spectra based on the extreme-stress-drop and shear-strain-threshold conditioned and unconditioned hazard for an AFE of 10^{-8} .

Meeting 1/25/07

Background Material by R. Lee and W. Silva

Informational Meeting

- Discussion of approaches to limit stress parameter
- Additional data and analysis needs
 - What is required to develop maxima

What is desired from Experts?

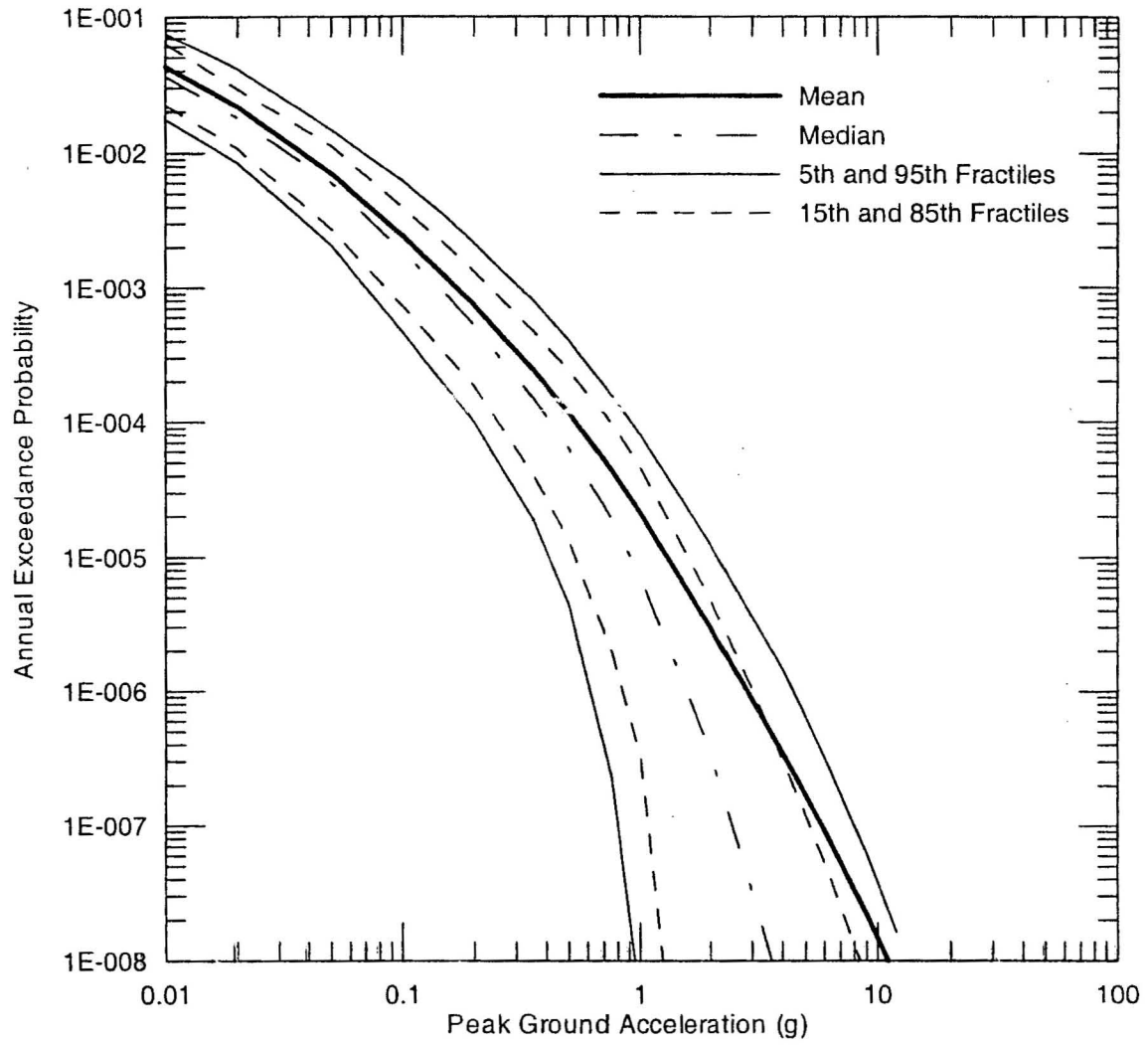
- Upper bound/limitation on stress parameter and its variability
 - Point estimate(s) or distribution(s)
 - Dependencies (e.g., magnitude/moment, depth, mechanism, fault slip-rate, hazard return period)
 - focus on M 6.5, normal faulting

YMP Hazard Deaggregations

- 10^{-6} to 10^{-7} /yr 1-2.5 and 5-10 Hz contributions from M 5-7.5, 0-15 km; mode: M 6.5
- Primary contributions from: (1) Paintbrush Canyon-Stagecoach Rd; (2) Solitario Canyon faults; and (3) coalesced faults.
- All left-lateral strike-slip/Normal dipping 60 degrees to west

Primary Contributing Sources

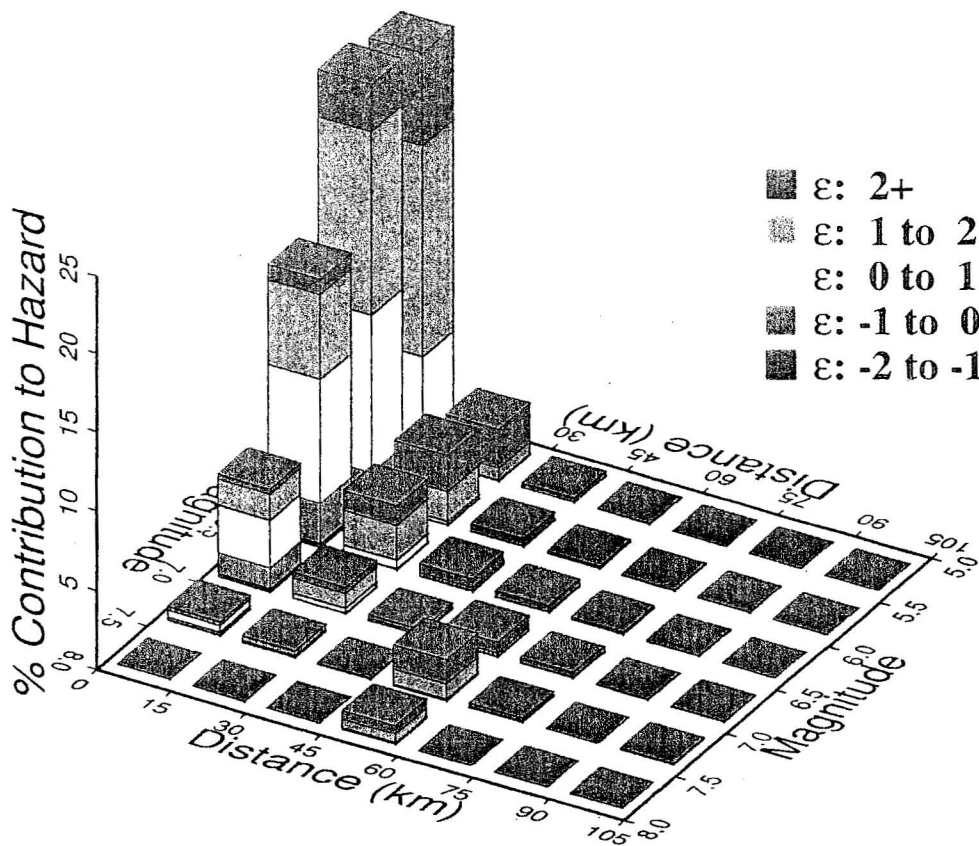
Fault	slip rate (mm/yr)	L (km)	R (km)	dip (deg)
SC	.01-.03	16-19	1	60
PC	.002-.017	12-19	4	60
SR	.016-.05	4-10	10	60



DTN: MO03061E9PSHA1.000

Figure 6.2-1. Hazard Curve at Point A for Peak Horizontal Ground Acceleration

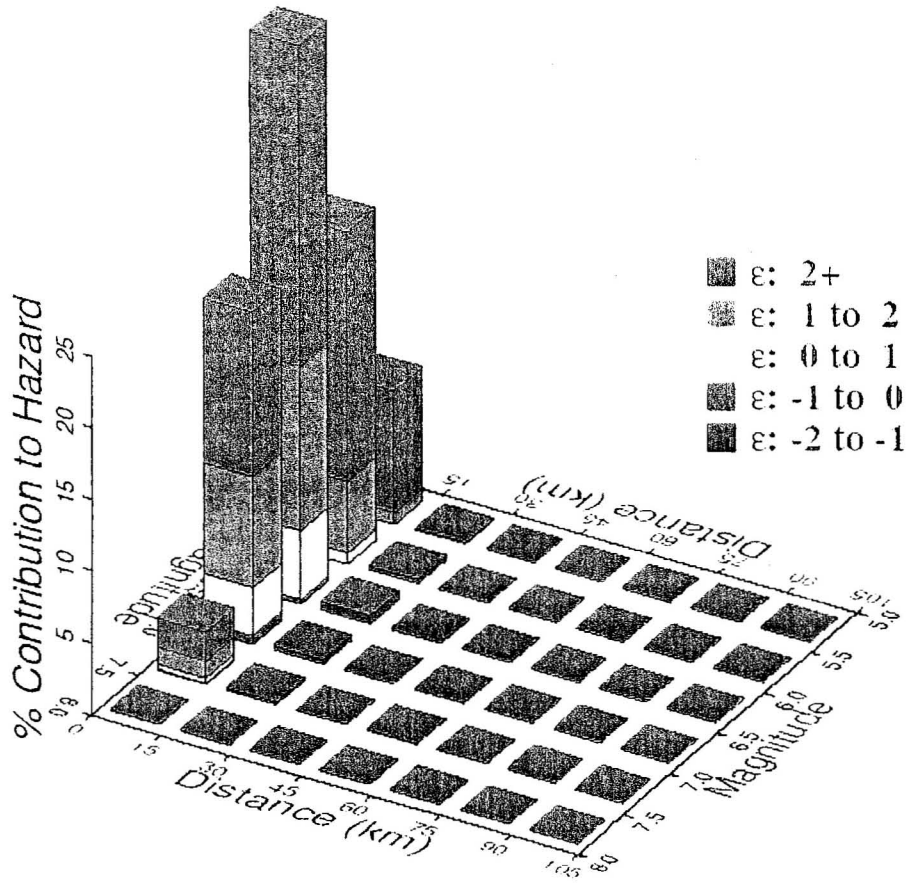
5E-4 Hazard, 5-10 Hz Horizontal



Source: Toro (2003, SR-104, page 1)

Figure 6.2-11. Contribution to Mean Hazard by Magnitude, Distance, and Epsilon (ϵ) for the 5-10 Hz Horizontal Ground Motions, 5×10^{-4} Annual Exceedance Probability

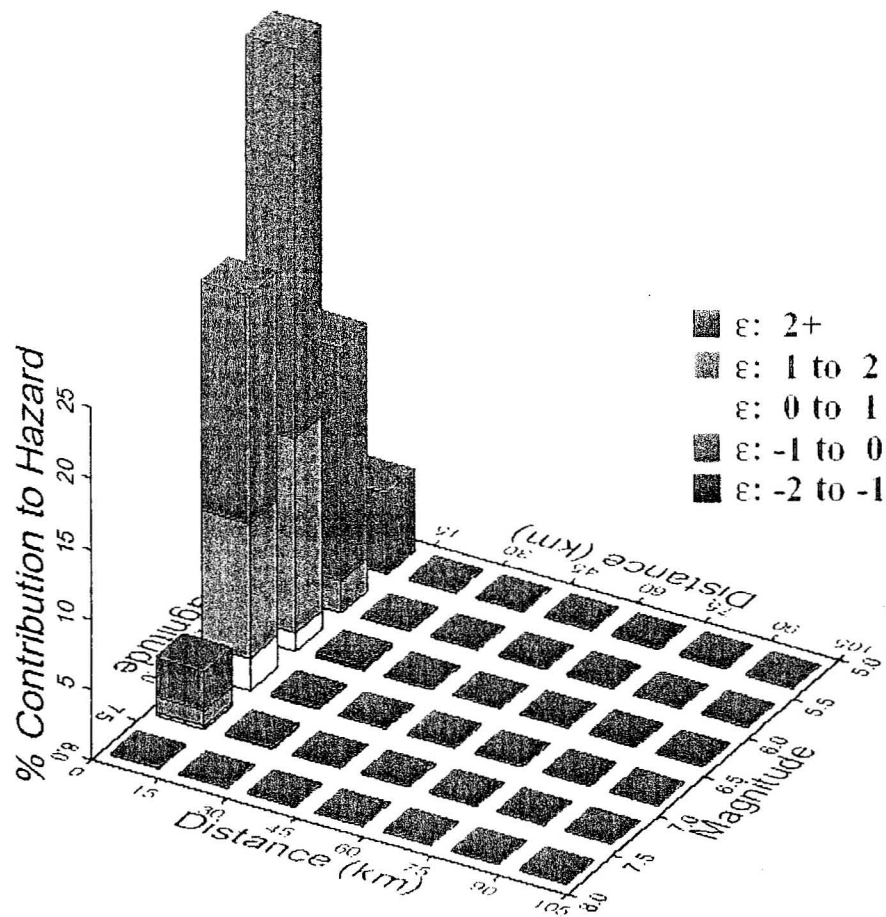
1E-6 Hazard, 5-10 Hz Horizontal



Source: Toro (2003, SR-67, page 1)

Figure 6.2-12. Contribution to Mean Hazard by Magnitude, Distance, and Epsilon (ϵ) for the 5-10 Hz Horizontal Ground Motions, 10^{-6} Annual Exceedance Probability

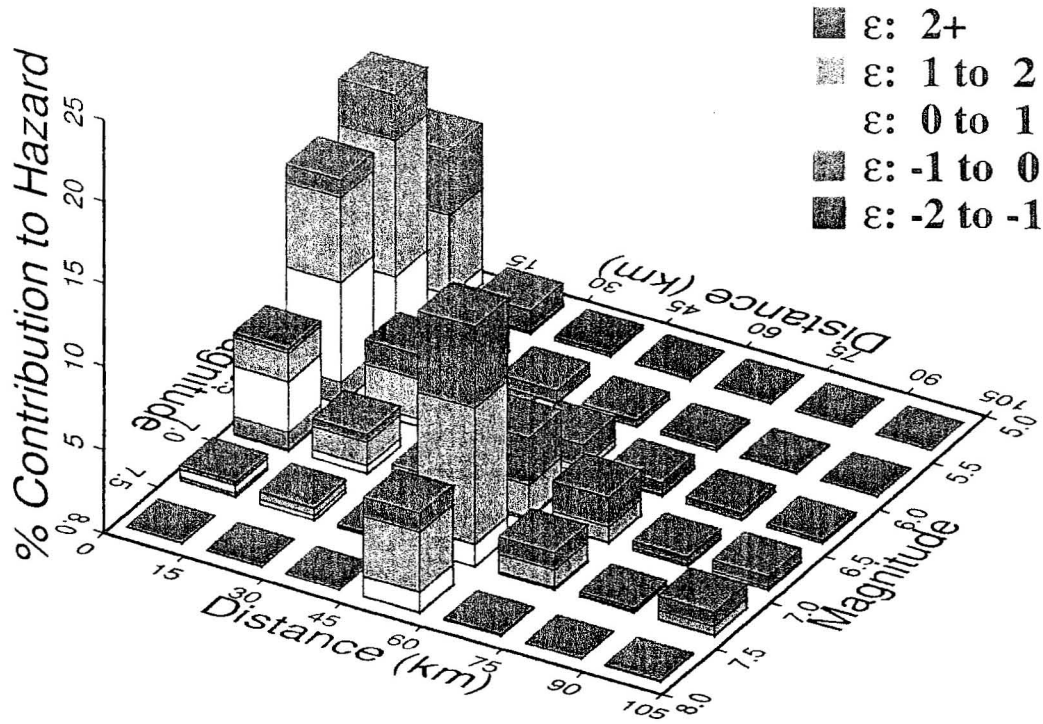
1E-7 Hazard, 5-10 Hz Horizontal



Source: Toro (2003, SR-138, page 6)

Figure 6.2-13. Contribution to Mean Hazard by Magnitude, Distance, and Epsilon (ϵ) for the 5-10 Hz Horizontal Ground Motions, 10^{-7} Annual Exceedance Probability

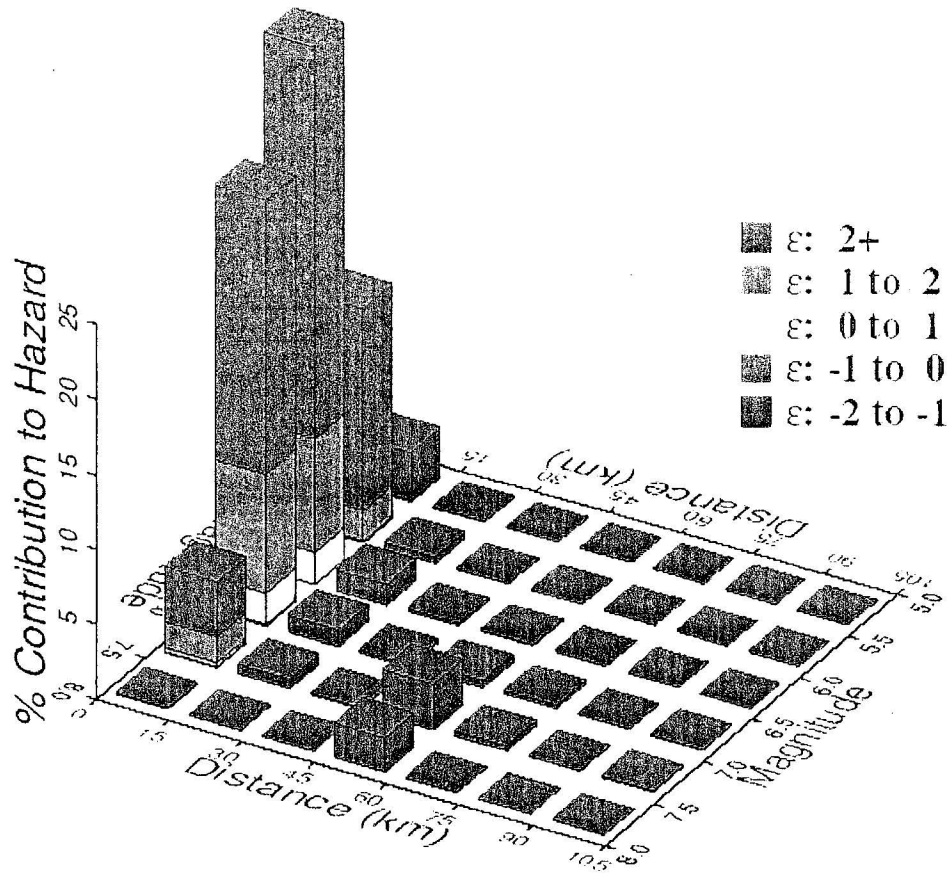
5E-4 Hazard, 1-2 Hz Horizontal



Source: Toro (2003, SR-104, page 2)

Figure 6.2-14. Contribution to Mean Hazard by Magnitude, Distance, and Epsilon (ϵ) for the 1-2 Hz Horizontal Ground Motions, 5×10^{-4} Annual Exceedance Probability

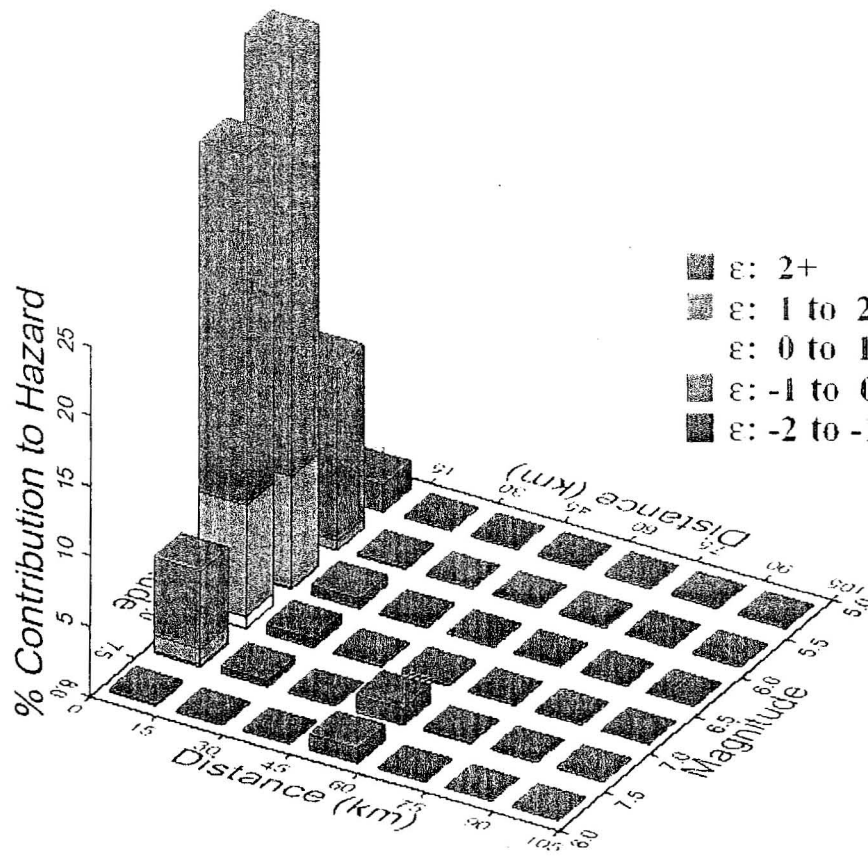
1E-6 Hazard, 1-2 Hz Horizontal



Source: Toro (2003, SR-65, page 1)

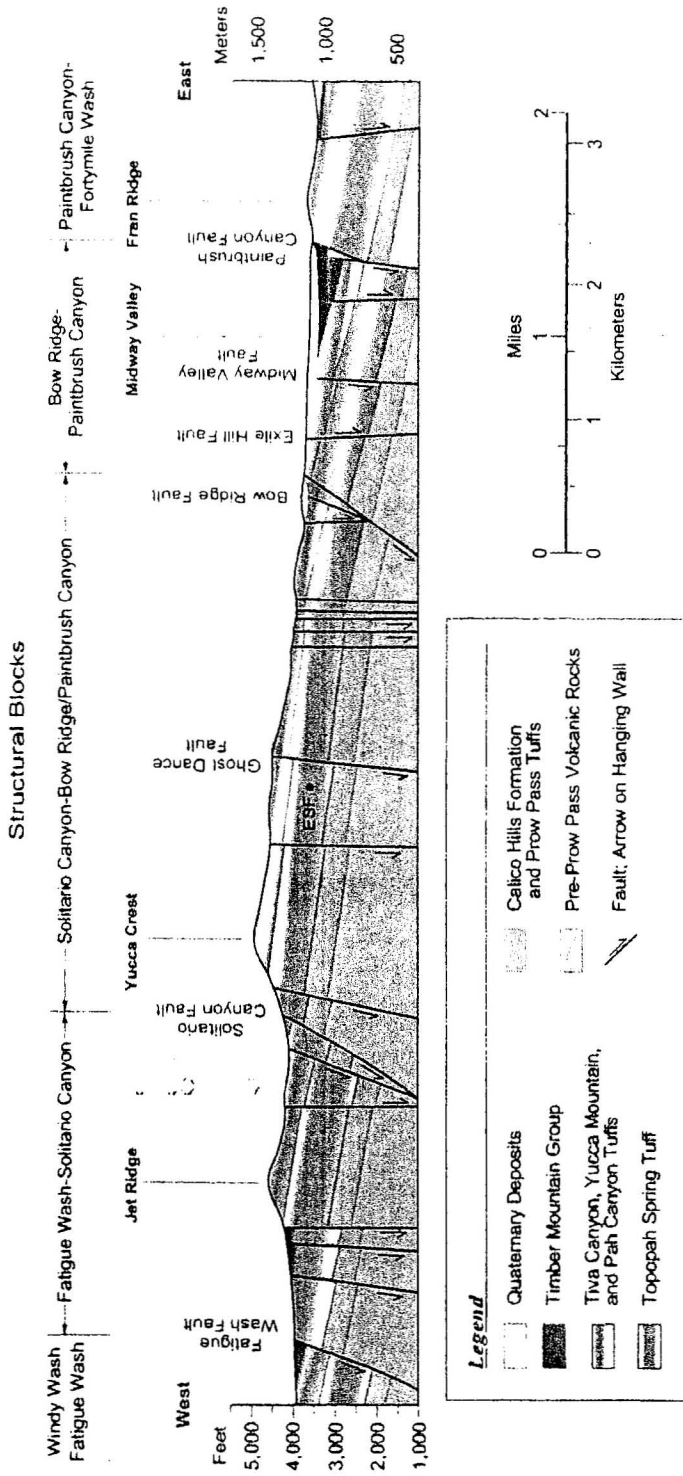
Figure 6.2-15. Contribution to Mean Hazard by Magnitude, Distance, and Epsilon (ϵ) for the 1-2 Hz Horizontal Ground Motions, 10^{-6} Annual Exceedance Probability

1E-7 Hazard, 1-2 Hz Horizontal



Source: Toro (2003, SR-138 page 4)

Figure 6.2-16. Contribution to Mean Hazard by Magnitude, Distance, and Epsilon (ϵ) for the 1-2 Hz Horizontal Ground Motions, 10^{-7} Annual Exceedance Probability



DTN: GS990908314224.010

Figure 6.2-54. Northeast-Southwest Schematic Cross-Section Through Yucca Mountain along the Enhanced Characterization of the Repository Block Cross-Drift

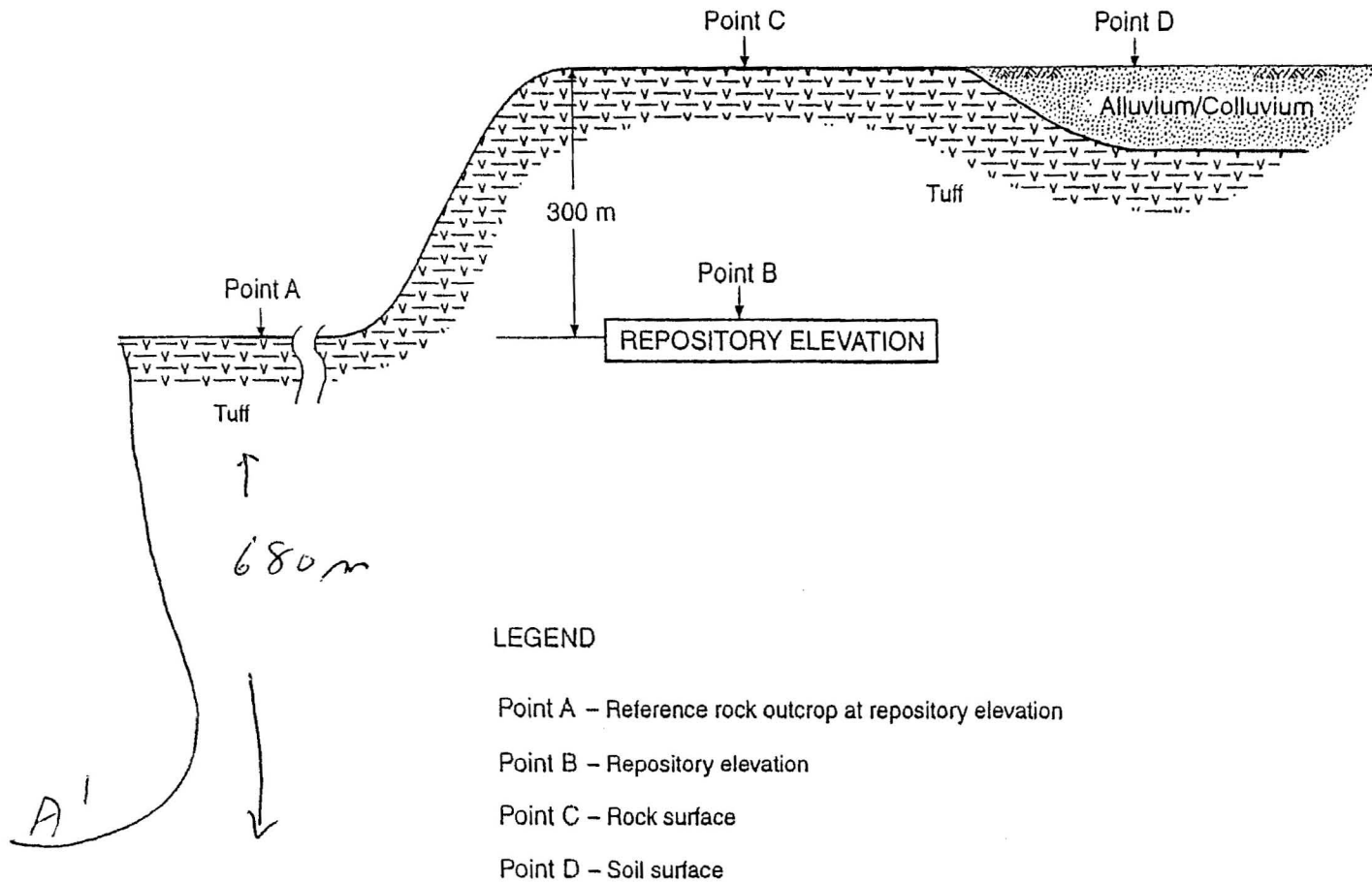
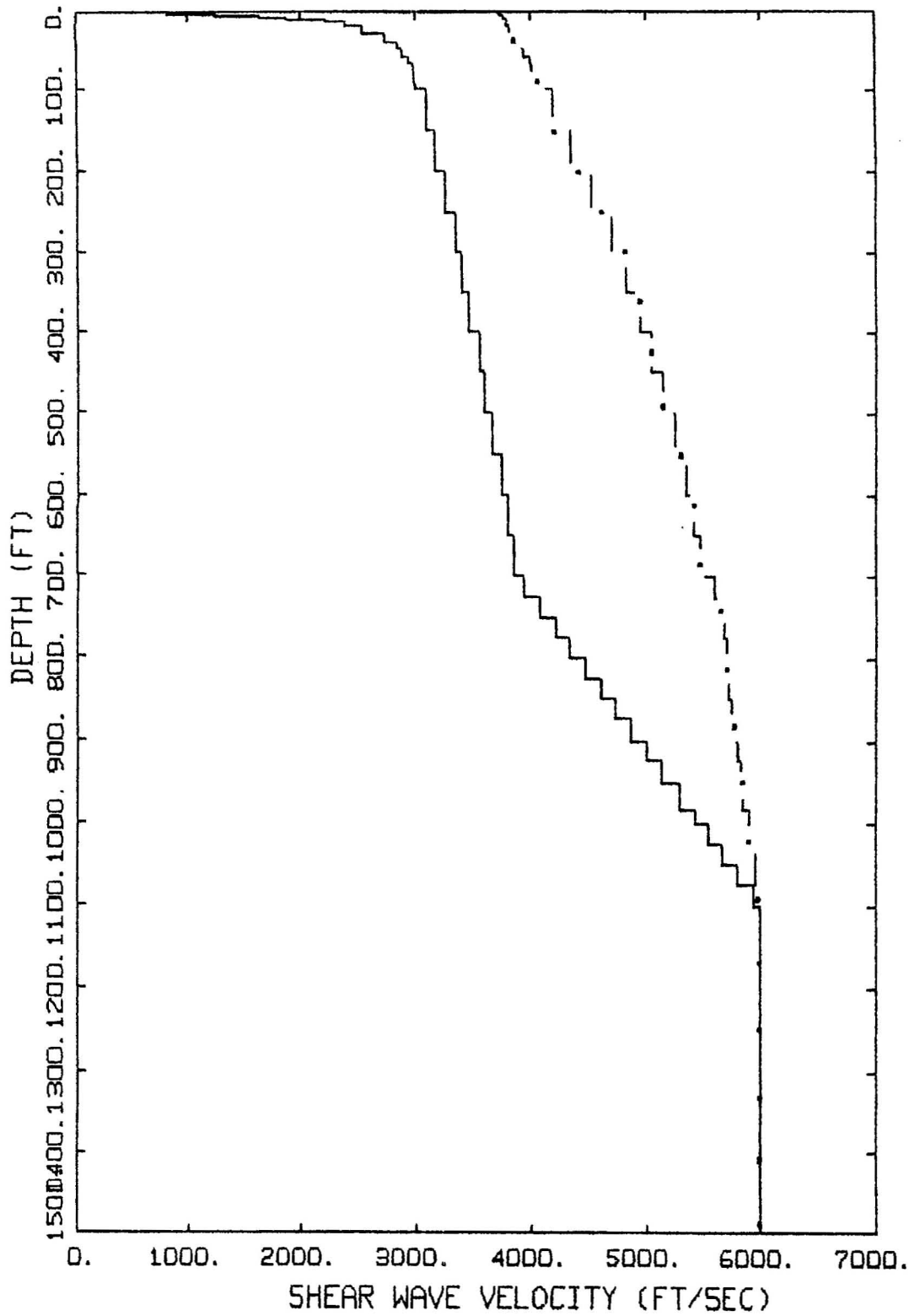


Figure 1. Locations of Specified Seismic Design Ground Motion Inputs



VELOCITY PROFILE
REPOSITORY BLOCK

LEGEND
 ——— BASE CASE
 - . - UPPER RANGE

Crustal Model At Point A

Thickness (km)	V _s (km/sec)	V _p (km/sec)	Density (cgs)
0.08	1.9	3.2	2.4
0.60	2.1	3.6	2.4
1.50	2.9	5.0	2.5
2.20	3.4	5.8	2.7
10.70	3.5	6.2	2.8
16.00	3.8	6.5	2.9
-	4.6	7.8	3.3

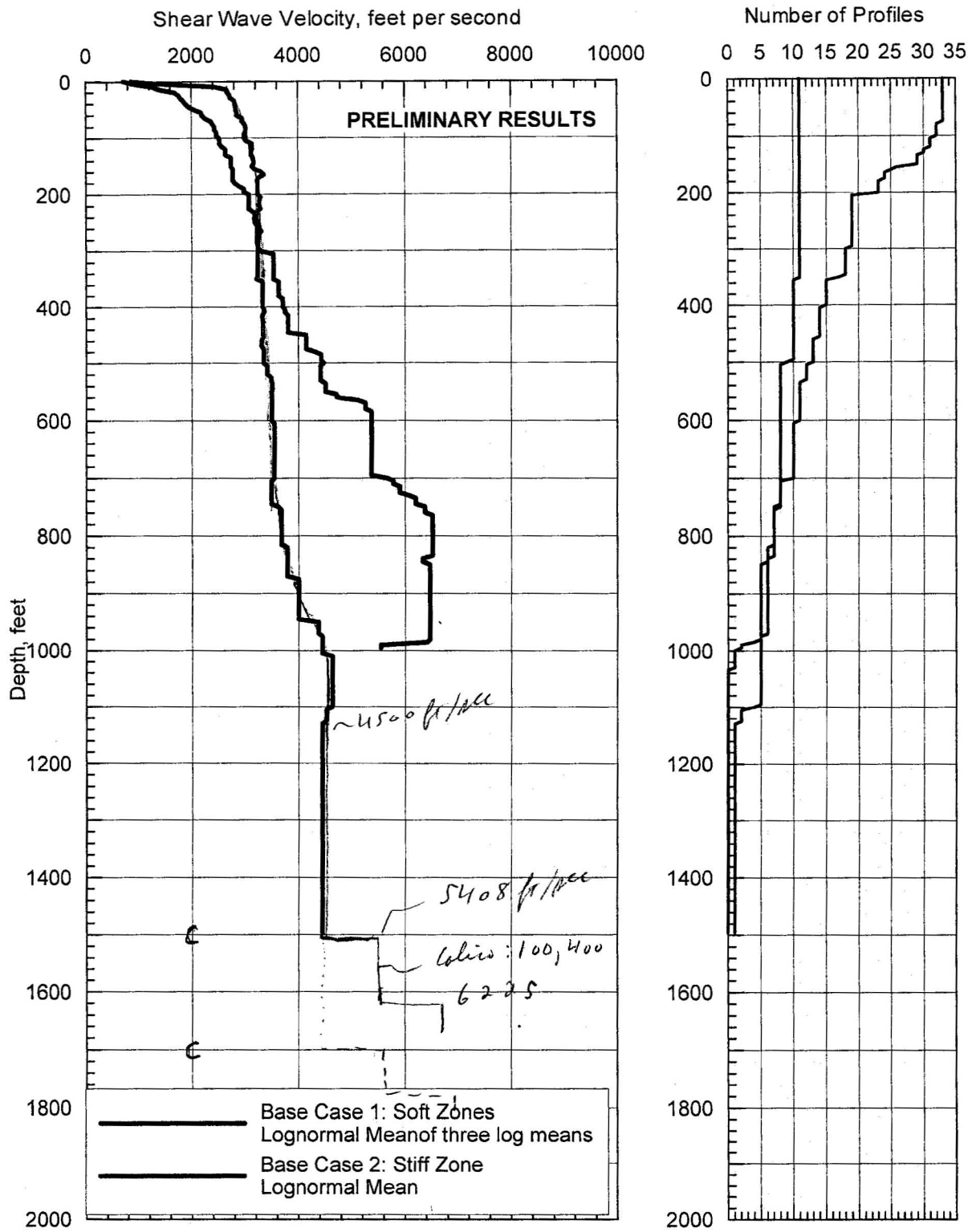
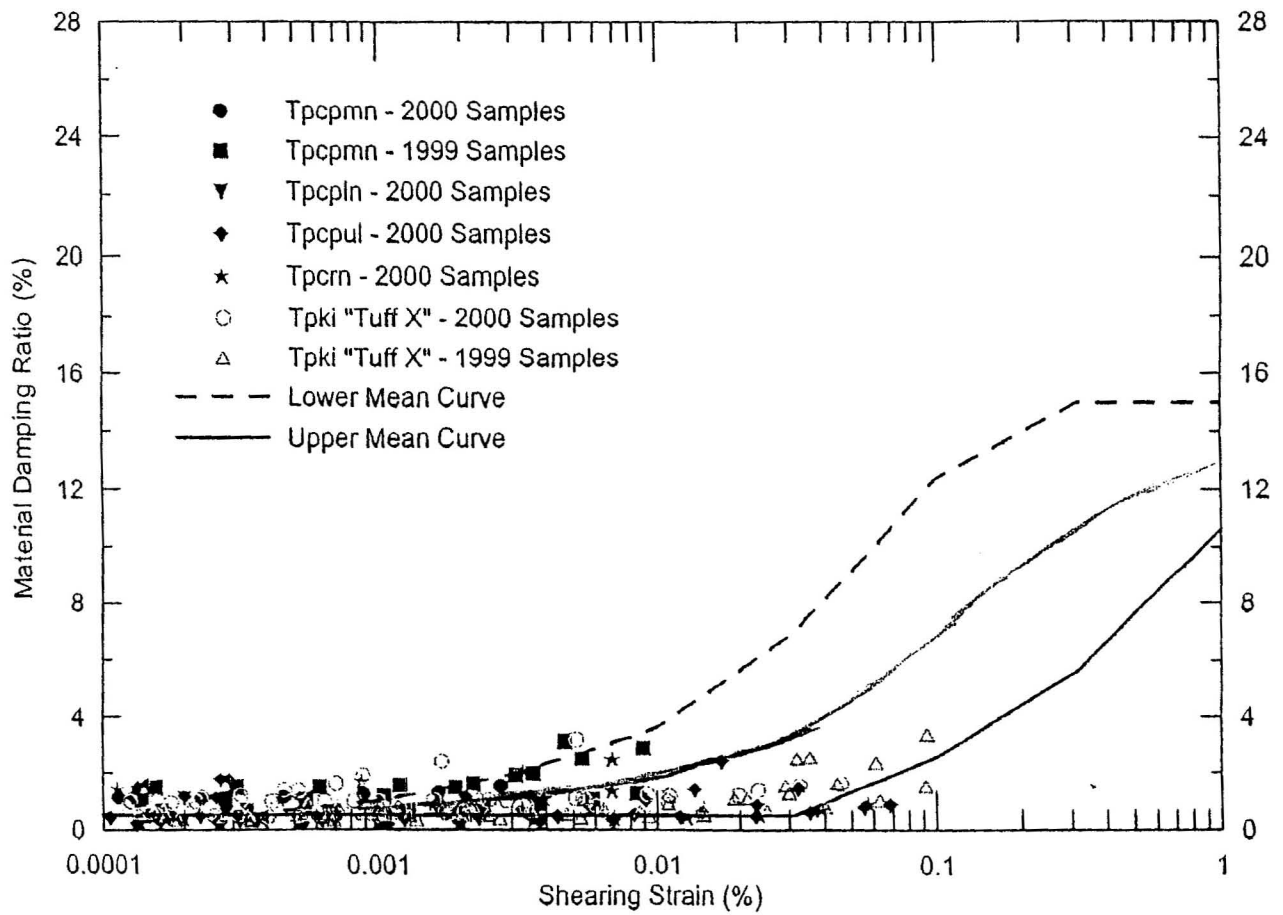
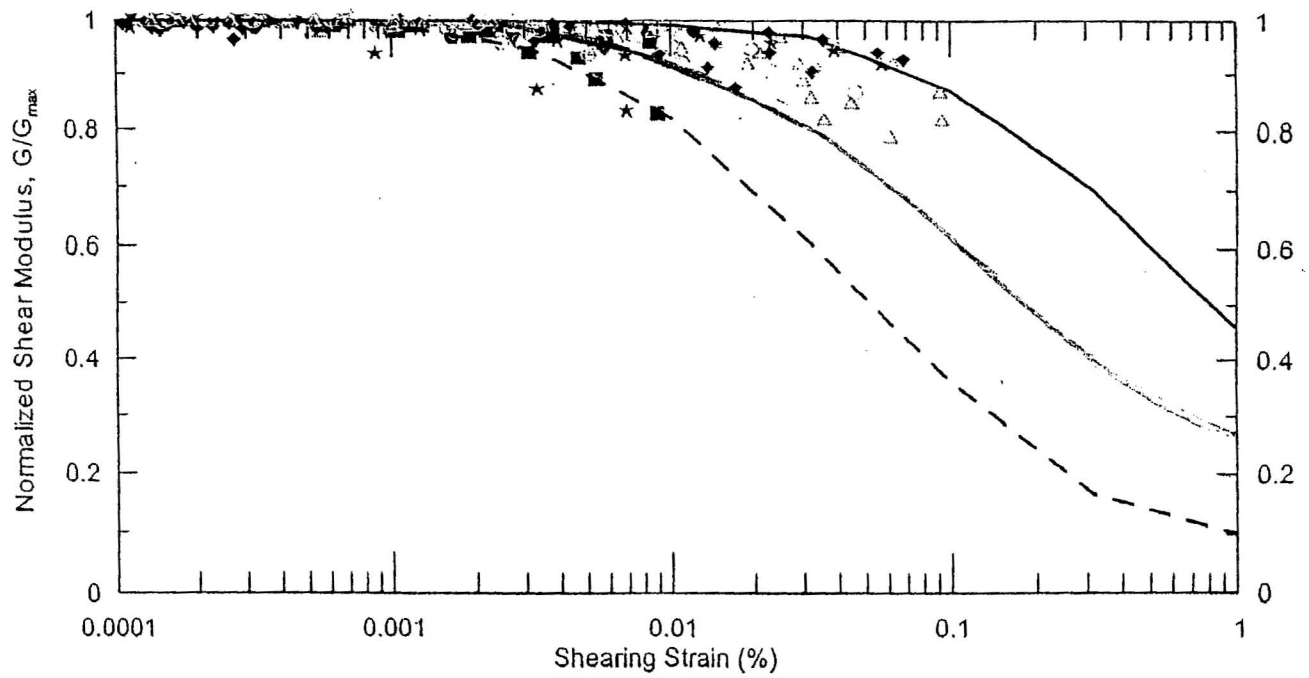


Figure: Comparison of base case profiles developed for the "soft" and "stiff" zones at the Repository Block.

Calico	:	5408 ft/sec	,	5,600
Proton	:	6225	"	6,000
Bal	:	6616	"	6,500
TRAM	:	6902	"	6,700

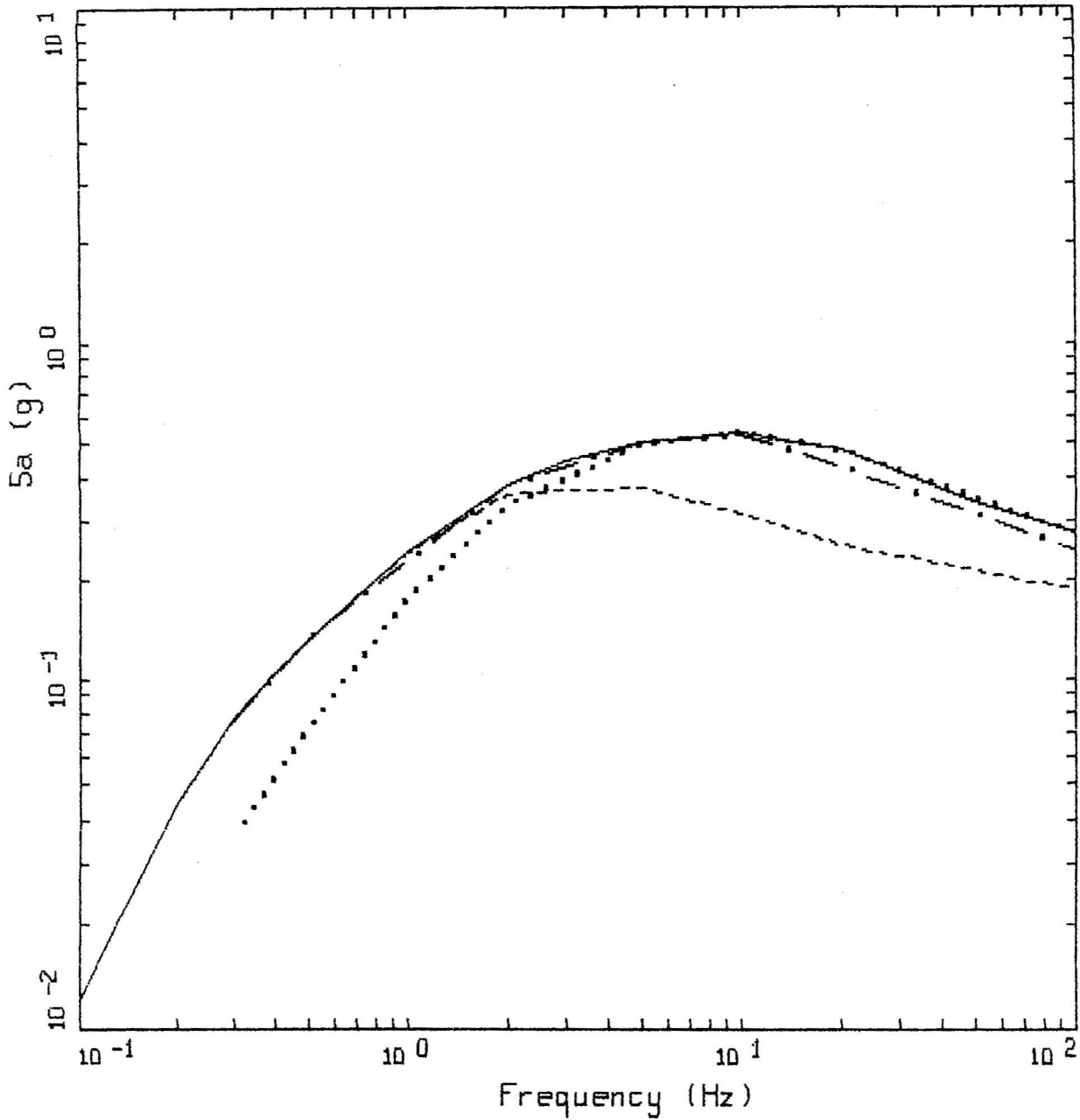


Unit	thick	Velocity
Calico	400 ft, 121.9 m	5,600 ft/sec, 1707 m/sec
Now	500 ft, 152 m	6,000 ft/sec, 1829 m/sec
Bull	500 ft, 152 m	6,500 ft/sec, 1981 m/sec
Tram	1000 ft, 305 m	6,700 ft/sec, 2042 m/sec
	2400 ft, 732 m	6,900 ft/sec, 1920 m/sec



Laboratory Test Results for all Tuffs from 1999 and 2000 Tests and Mean Curves

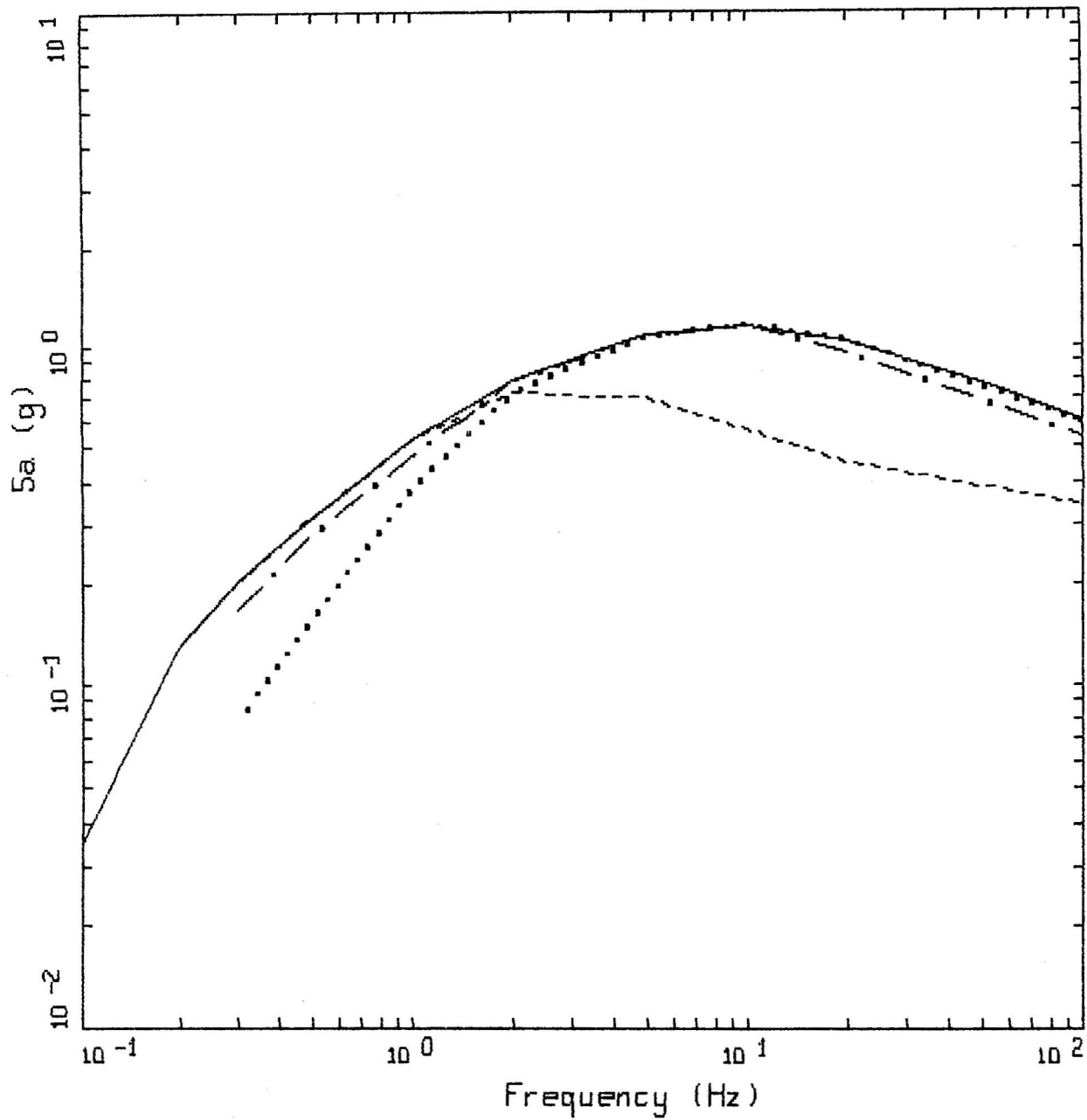
FRACTH



Y02 UHS AND DESIGN SPECTRA
SITE "A"

LEGEND

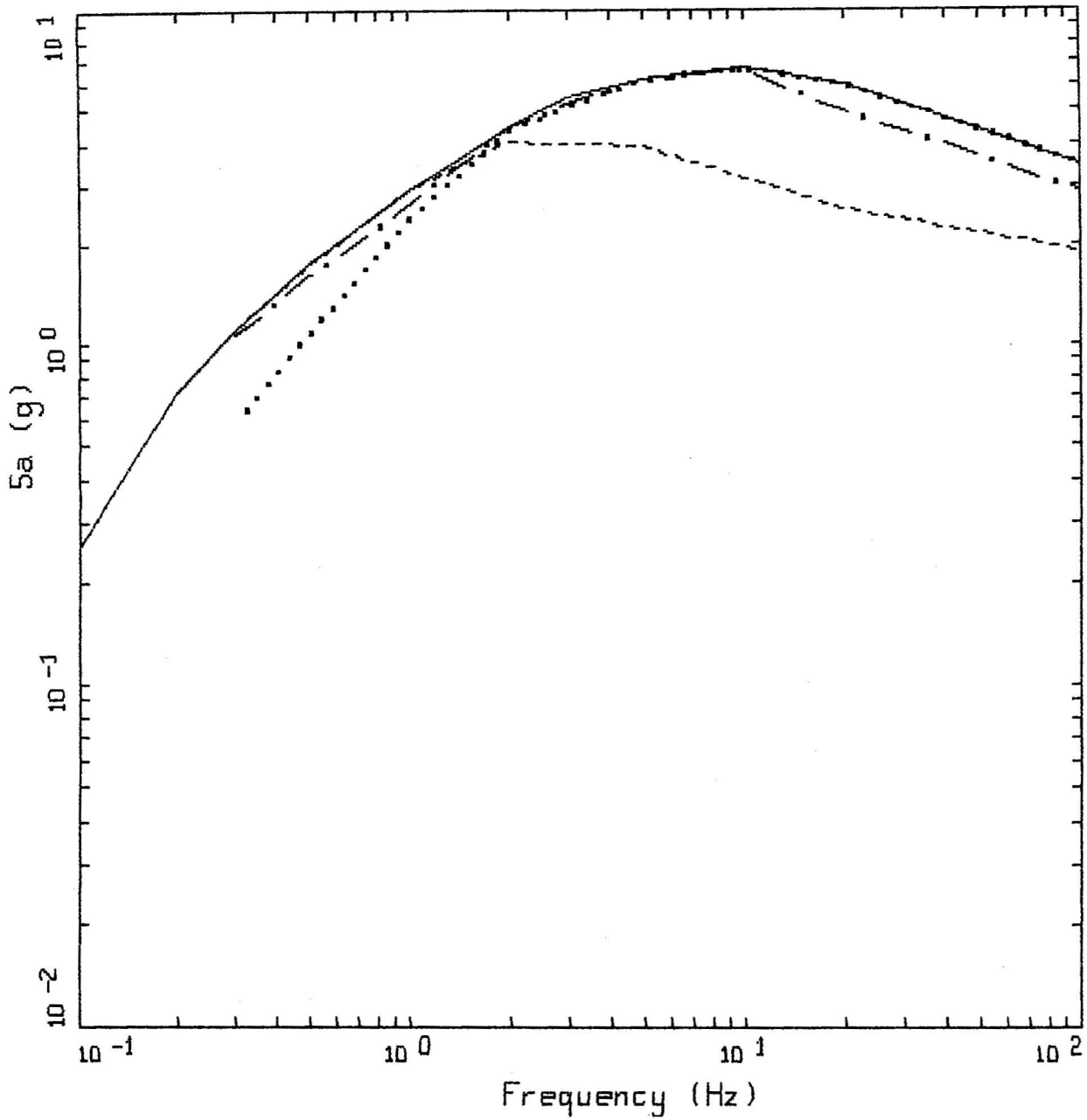
- . — HORIZONTAL 5E-4 UNIFORM HAZARD SPECTRUM; PGA = 0.245 G
- HORIZONTAL 5E-4 UNIFORM HAZARD SPECTRUM 1-2HZ; PGA = 0.186 G
- HORIZONTAL 5E-4 UNIFORM HAZARD SPECTRUM 5-10HZ; PGA = 0.273 G
- HORIZONTAL 5E-4 ENVELOPED UNIFORM HAZARD SPECTRUM; PGA = 0.273 G



Y02 UHS AND DESIGN SPECTRA
SITE "A"

LEGEND

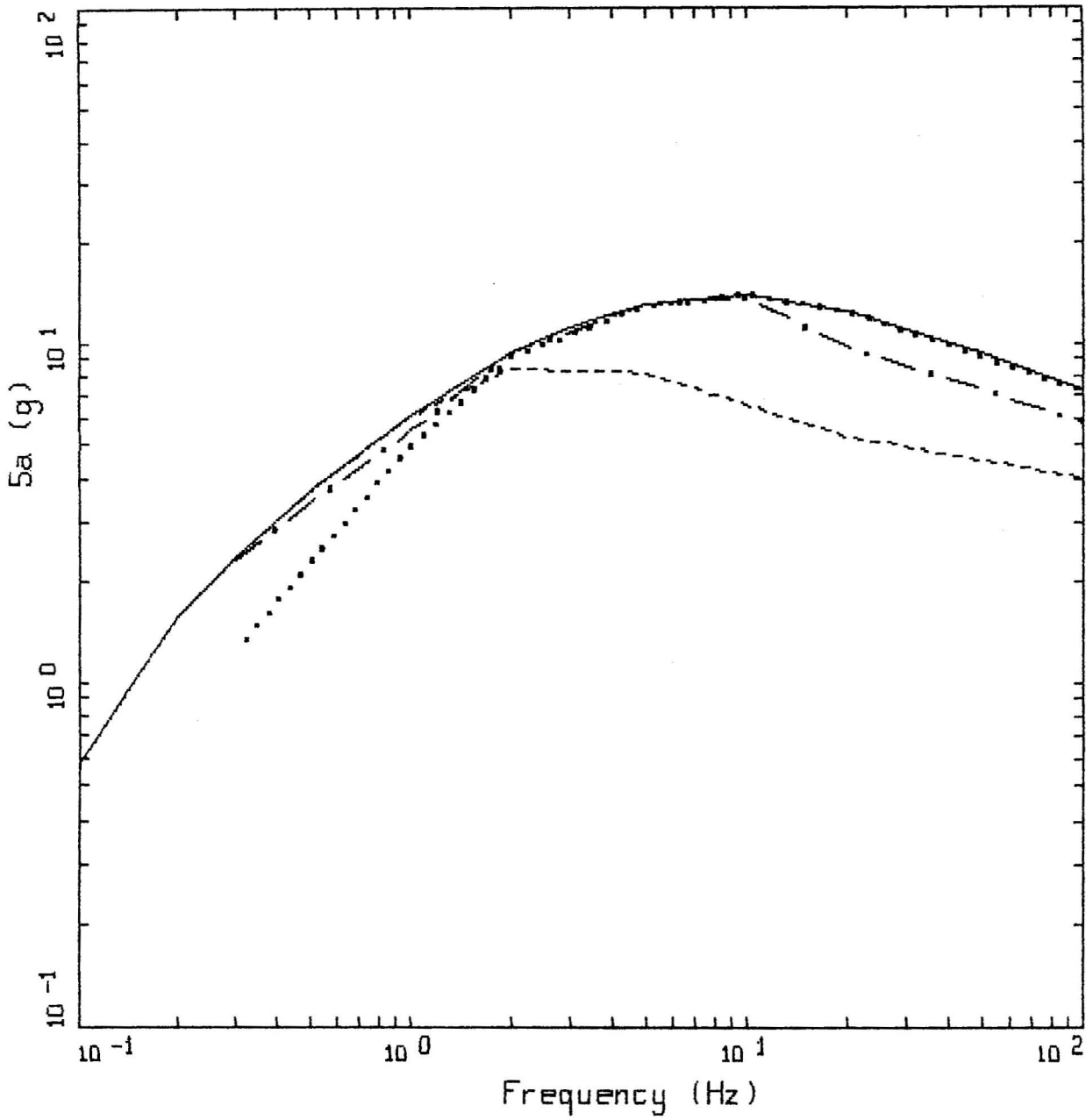
- · — HORIZONTAL 10-4 UNIFORM HAZARD SPECTUM; $PGA = 0.534\text{ G}$
- - - - HORIZONTAL 10-4 UNIFORM HAZARD SPECTUM 1-2HZ; $PGA = 0.341\text{ G}$
- · · · HORIZONTAL 10-4 UNIFORM HAZARD SPECTUM 5-10HZ; $PGA = 0.594\text{ G}$
- — — HORIZONTAL 10-4 ENVELOPED UNIFORM HAZARD SPECTUM; $PGA = 0.594\text{ G}$



Y02 UHS AND DESIGN SPECTRA
SITE "A"

LEGEND

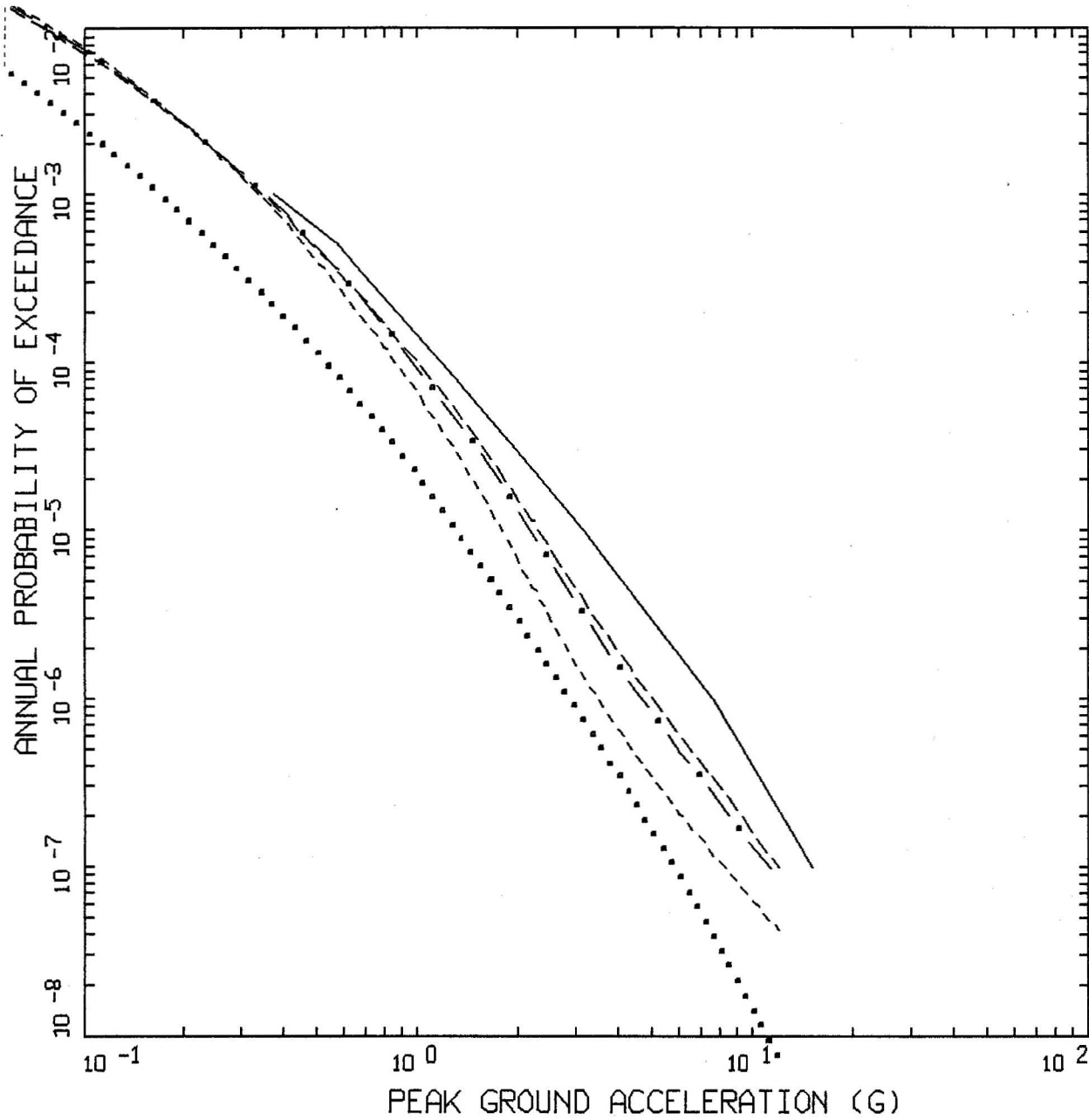
- · — HORIZONTAL 10-6 UNIFORM HAZARD SPECTRUM; PGA = 2.860 G
- HORIZONTAL 10-6 UNIFORM HAZARD SPECTRUM 1-2HZ; PGA = 1.901 G
- HORIZONTAL 10-6 UNIFORM HAZARD SPECTRUM 5-10HZ; PGA = 3.437 G
- HORIZONTAL 10-6 ENVELOPED UNIFORM HAZARD SPECTRUM; PGA = 3.437 G



Y02 UHS AND DESIGN SPECTRA
SITE "A"

LEGEND

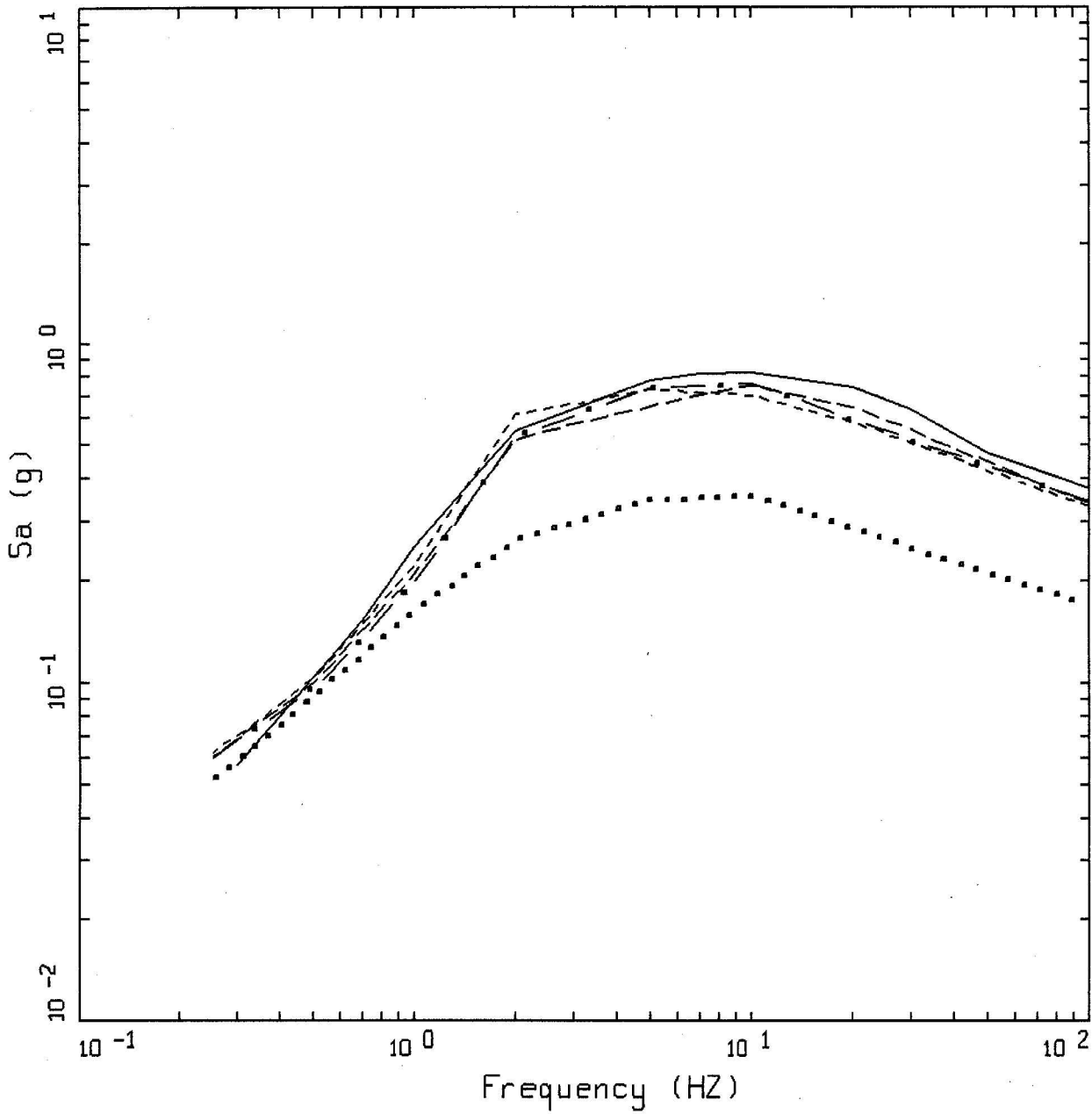
- · — HORIZONTAL 10⁻⁷ UNIFORM HAZARD SPECTUM; PGA = 5.828 G
- HORIZONTAL 10⁻⁷ UNIFORM HAZARD SPECTUM 1-2HZ; PGA = 3.989 G
- HORIZONTAL 10⁻⁷ UNIFORM HAZARD SPECTUM 5-10HZ; PGA = 7.210 G
- HORIZONTAL 10⁻⁷ ENVELOPED UNIFORM HAZARD SPECTUM; PGA = 7.210 G



YUCCA.06: MEAN HAZARD CURVES
 PGA, SOILUHSI (FRACT=9)

LEGEND

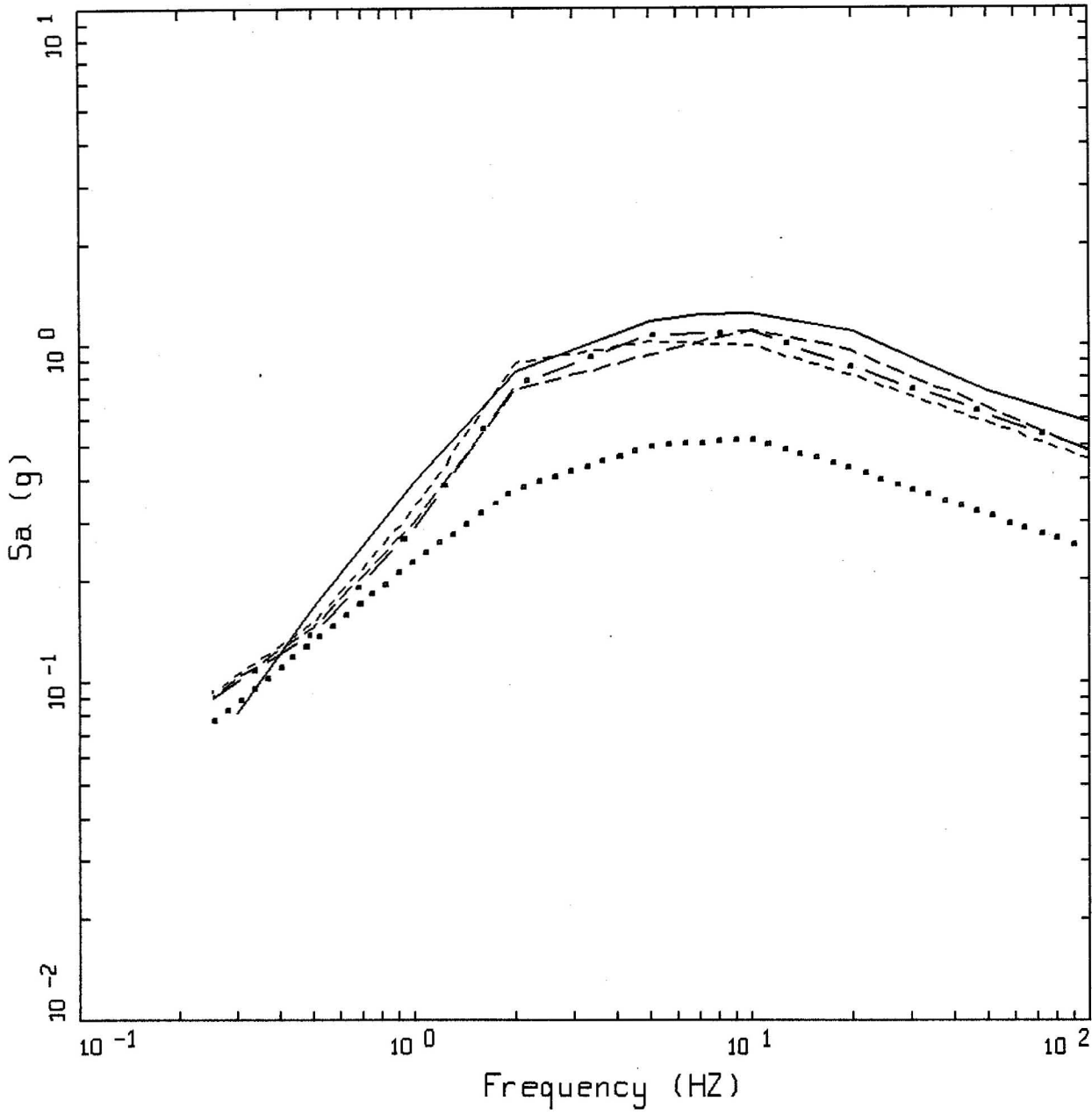
- · — POINT D, APPROACH 3, 35 FEET SOIL
- - - - POINT D, APPROACH 3, 110 FEET SOIL
- - - - POINT E, APPROACH 3, 0-15 FEET SOIL
- POINT D/E, APPROACH 2B
- POINT A



YUCCA.06: MEAN UHS 10-3
 POINT D/E, SOILUHS (FRACT=9)

LEGEND

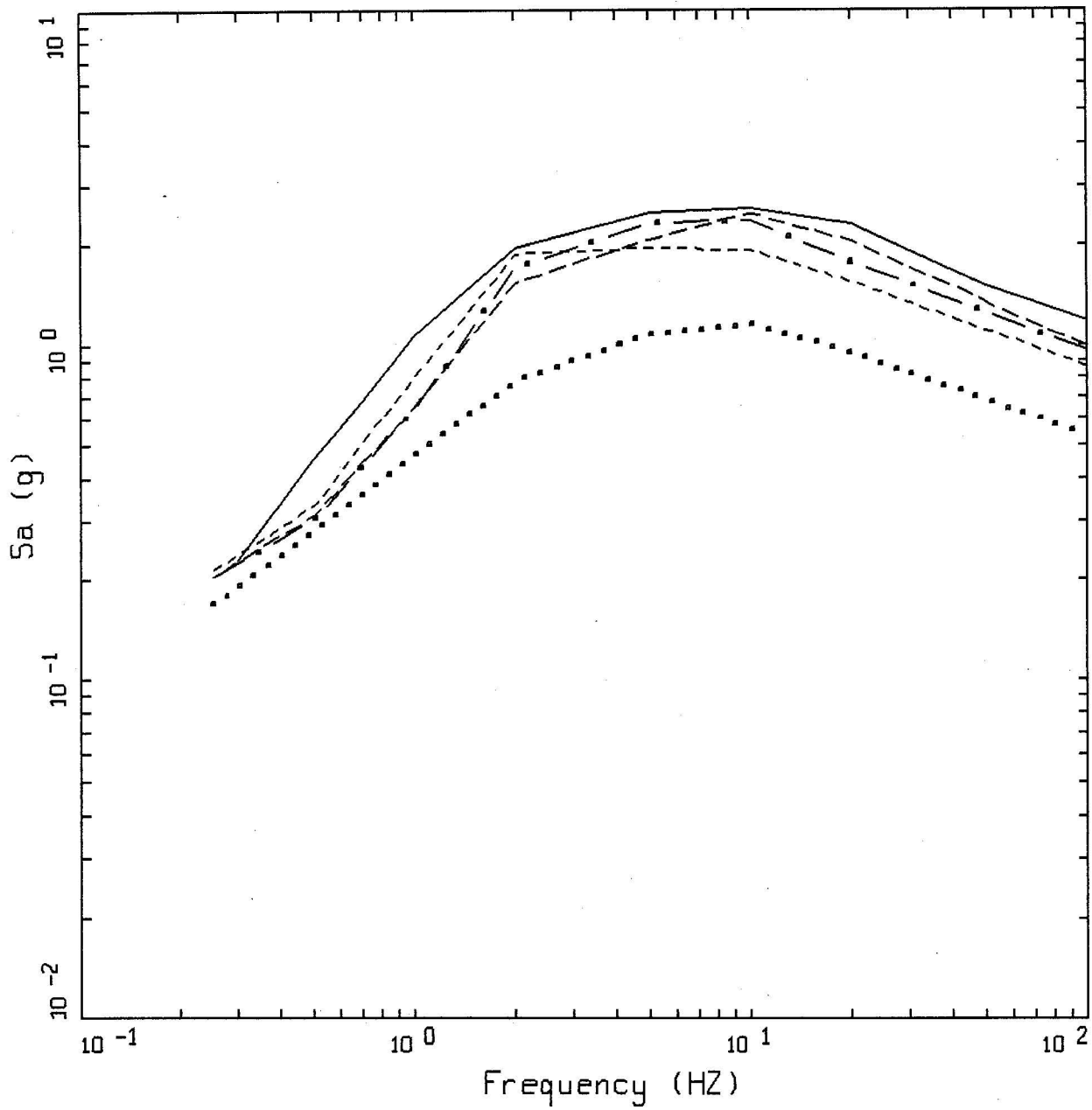
- . - . 5 %, POINT D, APPROACH 3, 35 FEET SOIL
- - - - 5 %, POINT D, APPROACH 3, 110 FEET SOIL
- - - - 5 %, POINT E, APPROACH 3, 0-15 FEET SOIL
- 5 %, POINT D/E APPROACH 2B
- 5 %, POINT A



YUCCA.06: MEAN UHS 5X10⁻⁴
 POINT D/E, SOILUHS (FRACT=9)

LEGEND

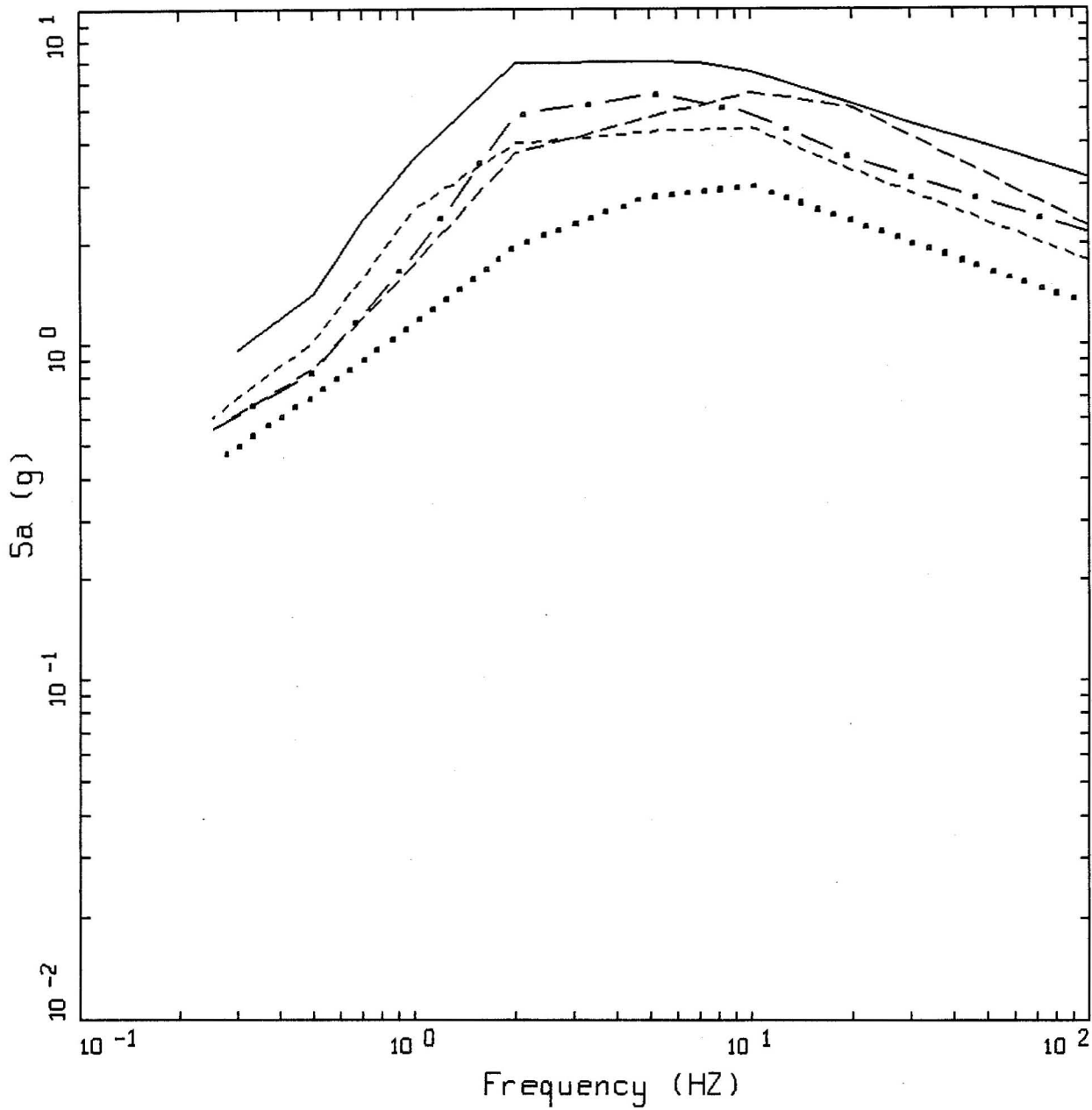
- · — 5 %, POINT D, APPROACH 3, 35 FEET SOIL
- - - - 5 %, POINT D, APPROACH 3, 110 FEET SOIL
- · - · 5 %, POINT D, APPROACH 3, 0-15 FEET SOIL
- 5 %, POINT D/E APPROACH 2B
- 5 %, POINT A

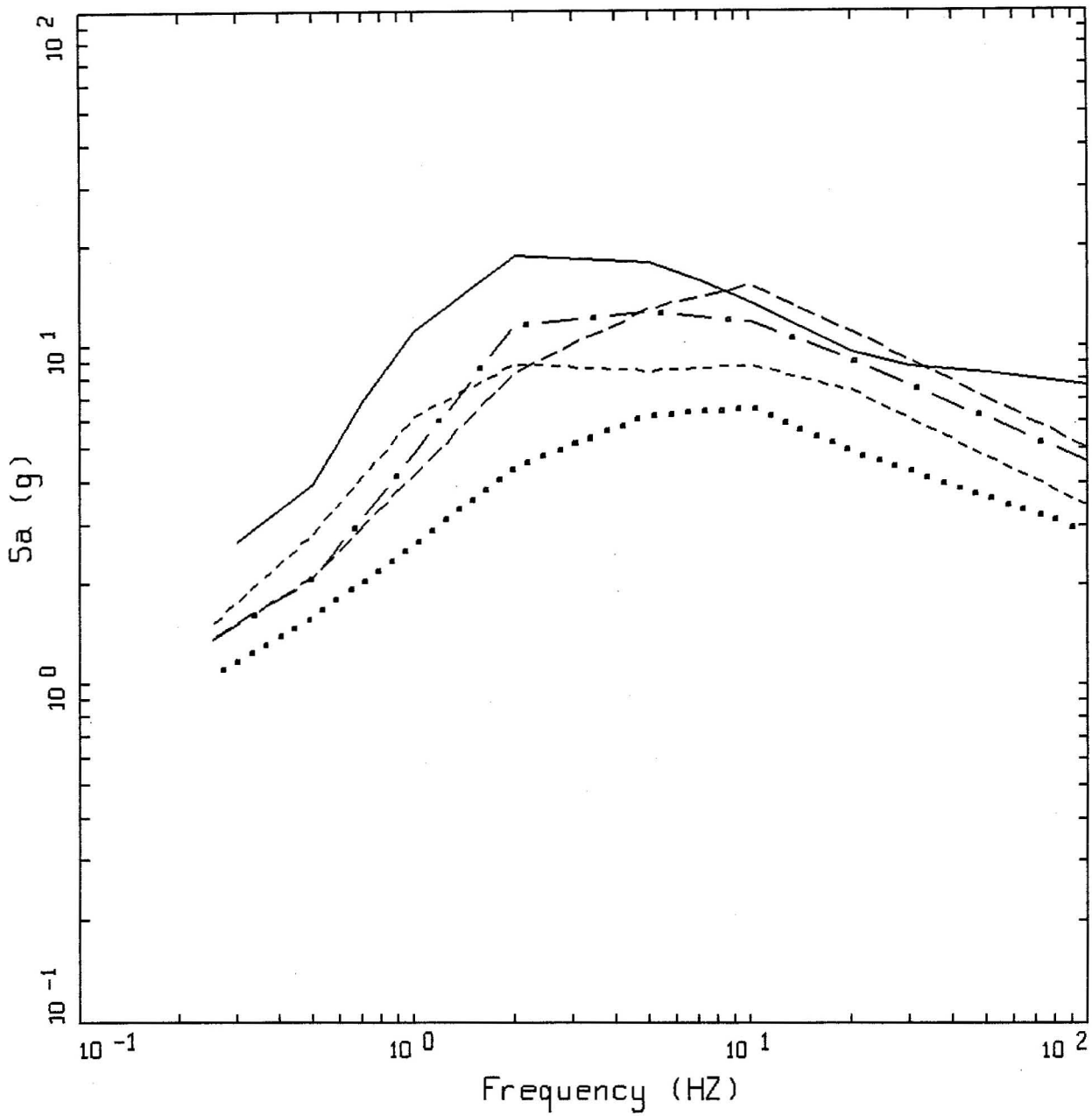


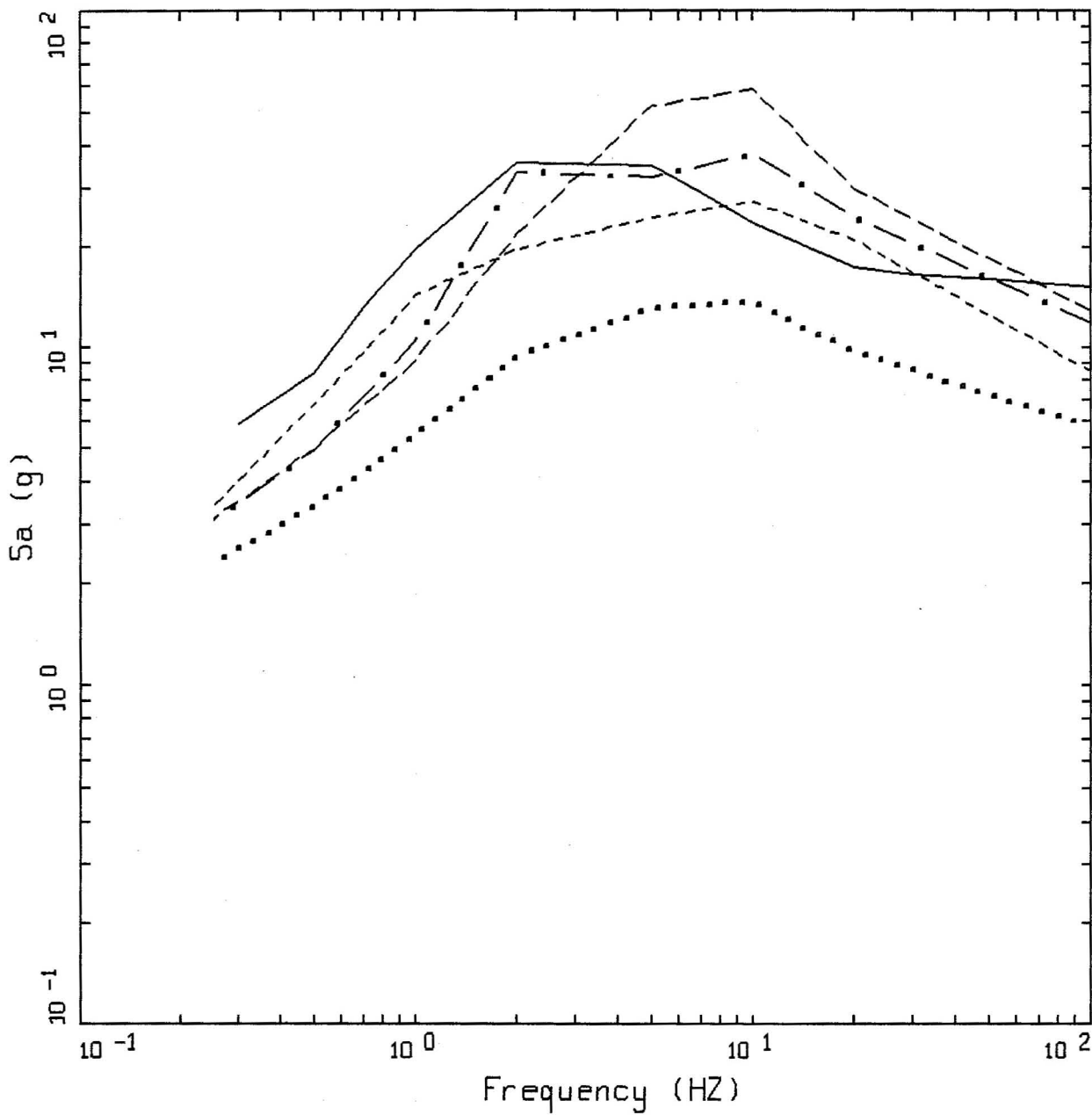
YUCCA.06: MEAN UHS 10-4
 POINT D/E, SOILUHS (FRACT=9)

LEGEND

- . - . 5 %, POINT D, APPROACH 3, 35 FEET SOIL
- - - - 5 %, POINT D, APPROACH 3, 110 FEET SOIL
- - - - 5 %, POINT D, APPROACH 3, 0-15 FEET SOIL
- 5 %, POINT D/E APPROACH 2B
- 5 %, POINT A



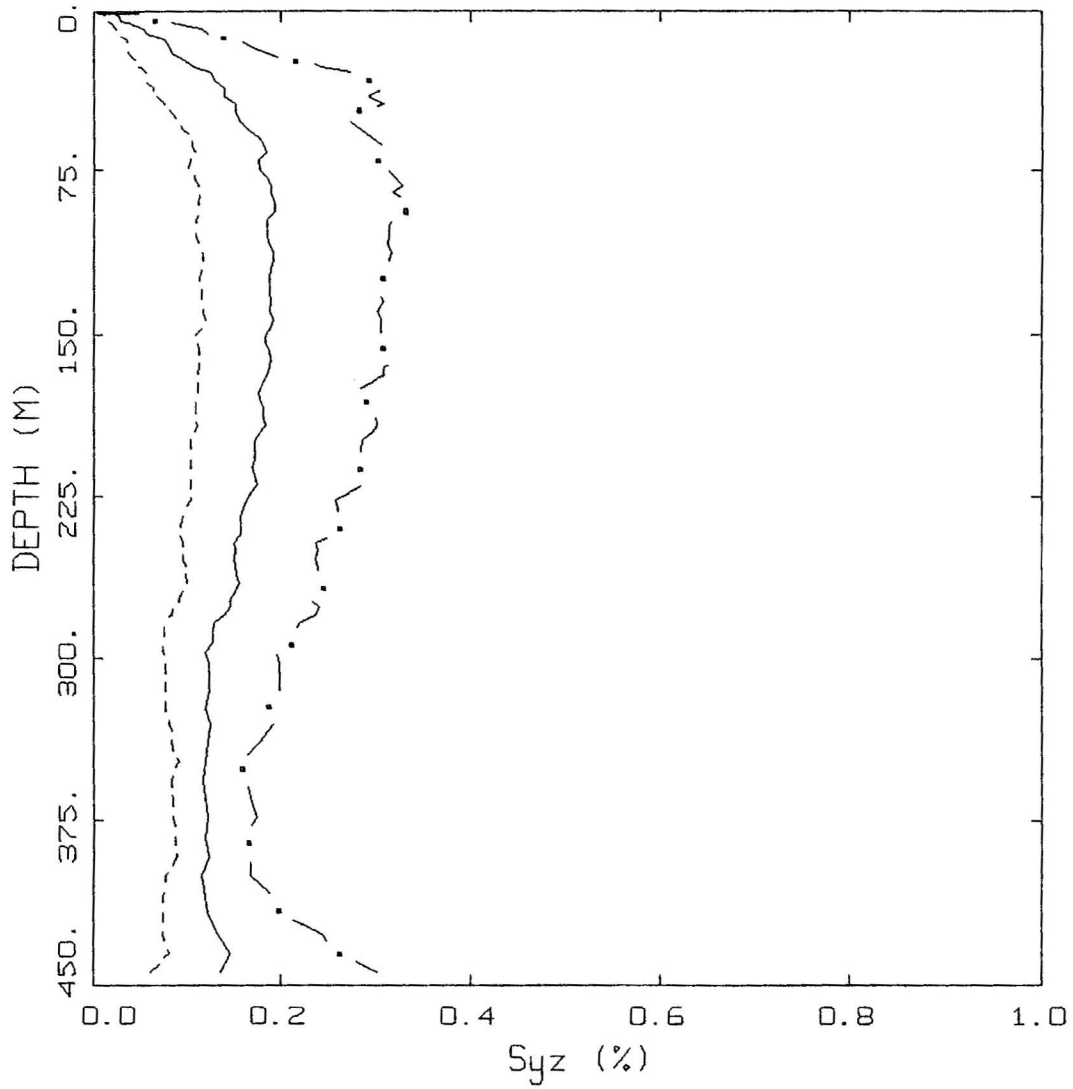




YUCCA.06: MEAN UHS 10-7
 POINT D/E, SOILUHS (FRACT=9)

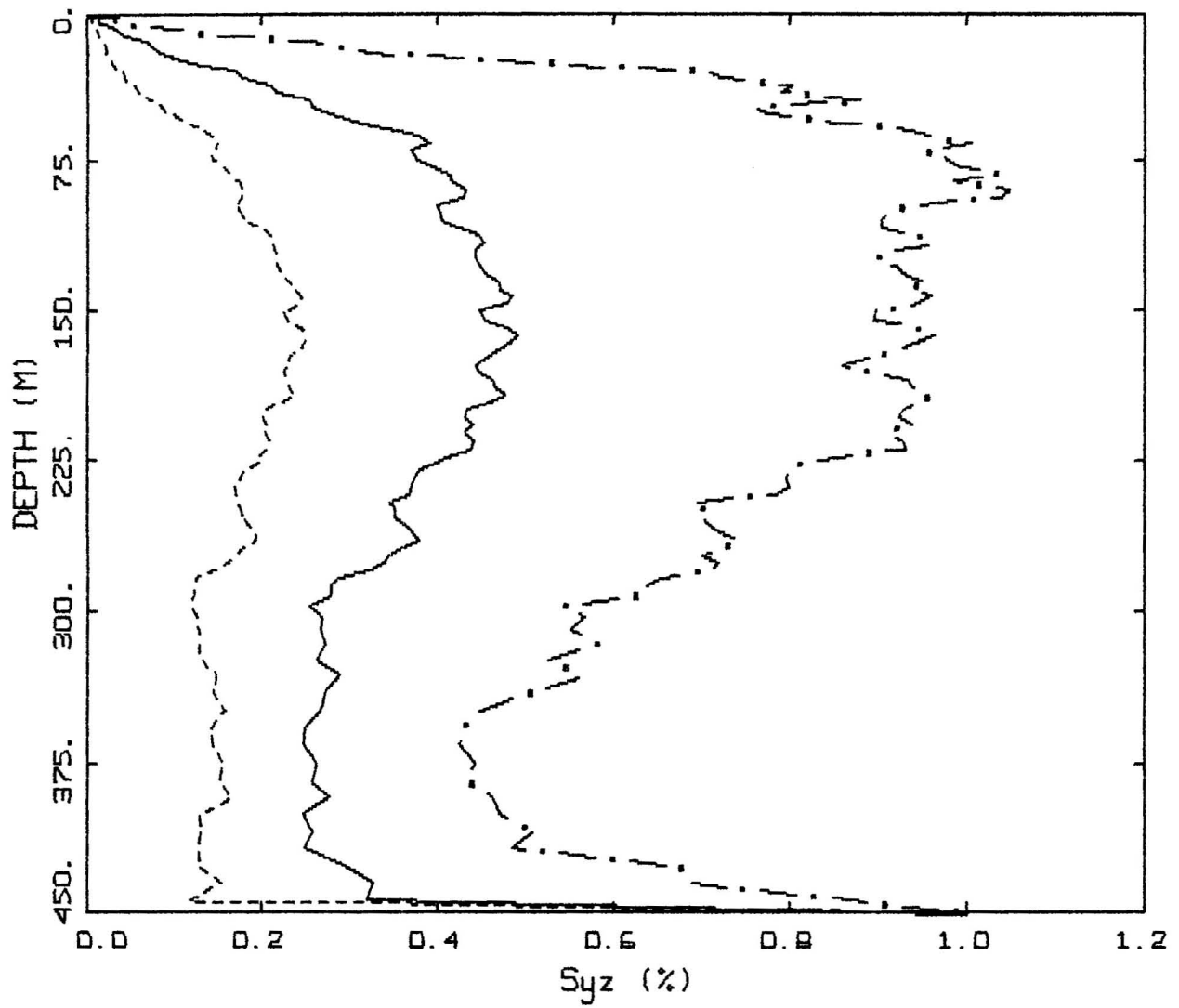
LEGEND

- 5 %, POINT D, APPROACH 3, 35 FEET SOIL
- 5 %, POINT D, APPROACH 3, 110 FEET SOIL
- - - - 5 %, POINT D, APPROACH 3, 0-15 FEET SOIL
- 5 %, POINT D/E APPROACH 2B
- 5 %, POINT A



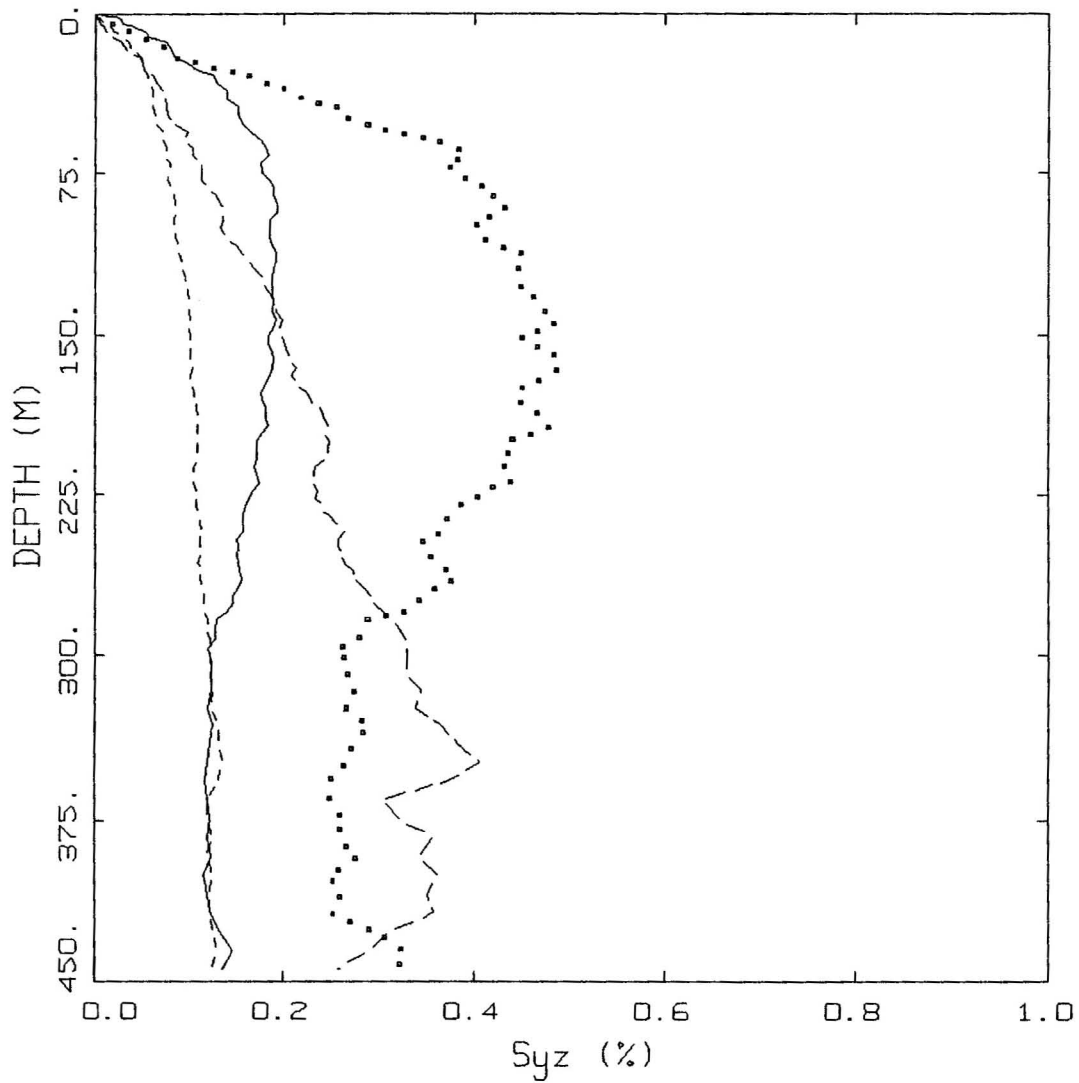
Y02 B 300M TOTAL P1 10-6 5-10HZ HSHH INCIDENCE = 0 DEG
 UMT, MM

LEGEND
 - . - 84TH PERCENTILE
 ——— MEDIAN
 - - - 16TH PERCENTILE



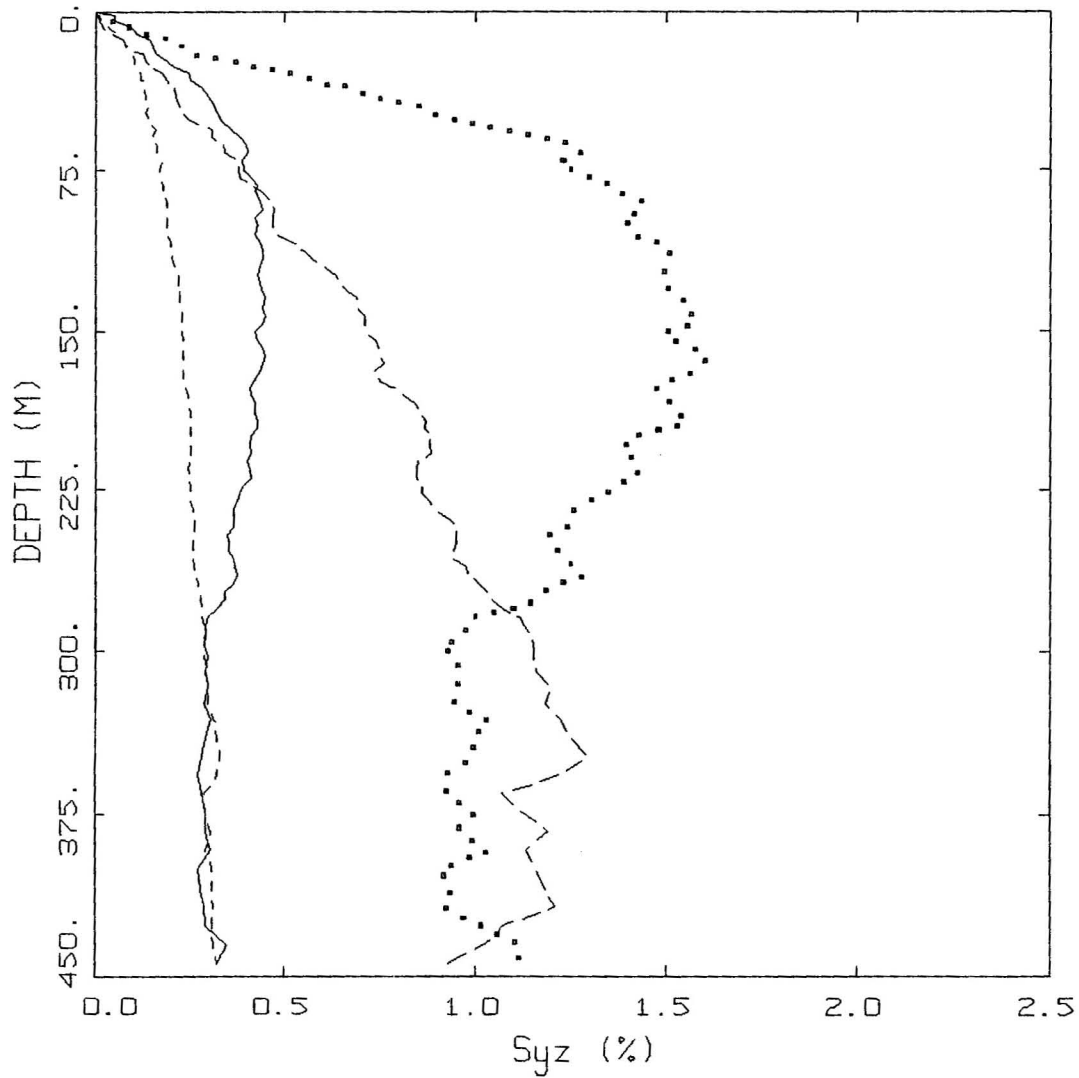
Y02 B 300M TOTAL P1 10-6 5-10HZ HSHH INCIDENCE = 0 DEG
LMT, MM

LEGEND
 - . - 84TH PERCENTILE
 ——— MEDIAN
 - - - 16TH PERCENTILE



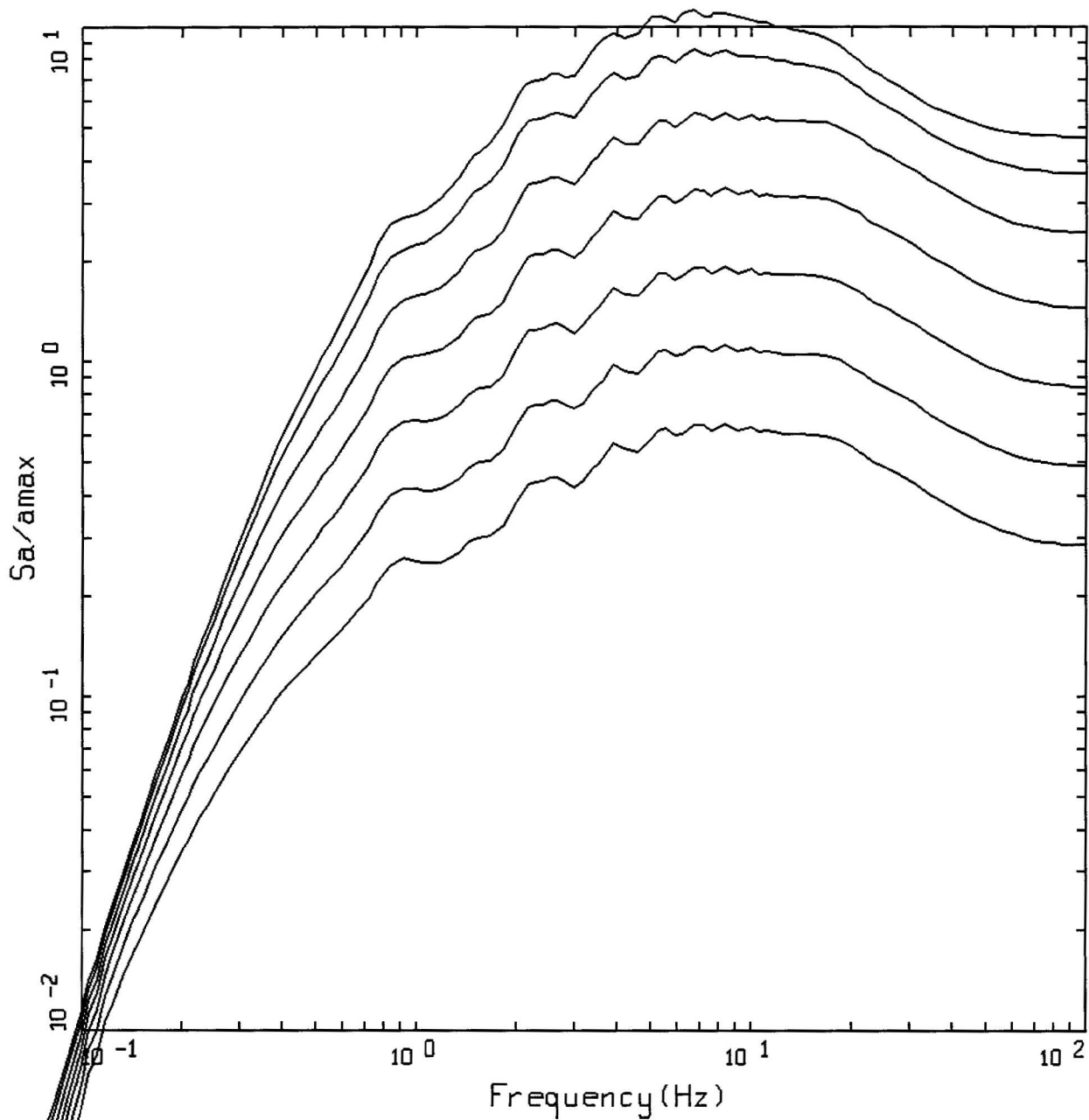
Y02 B 300M TOTAL 10-6 HSHH INCIDENCE = 0 DEG
MM, SYZ STRAIN, 5-10HZ

LEGEND
 ——— MEDIAN; P1, UMT
 MEDIAN; P1, LMT
 - - - - MEDIAN; P2, UMT
 - . - . MEDIAN; P2, LMT



Y02 B 300M TOTAL 10-7 HSHH INCIDENCE = 0 DEG
MM, SYZ STRAIN, 5-10HZ

- LEGEND
- MEDIAN; P1, UMT
 - MEDIAN; P1, LMT
 - MEDIAN; P2, UMT
 - . - . - MEDIAN; P2, LMT



HORIZONTAL SPECTRA, POINT A(6,000FT/SEC OUTCROP)
M=6.5, D=01 KM, SD = VARY

LEGEND

- 5 %, SD = 50 BARS, PGA = 0.279 G, PGV = 25.80 CM/SEC, MAX STRAIN = 0.008 %
- 5 %, SD = 100 BARS, PGA = 0.481 G, PGV = 40.79 CM/SEC, MAX STRAIN = 0.013 %
- 5 %, SD = 200 BARS, PGA = 0.826 G, PGV = 63.80 CM/SEC, MAX STRAIN = 0.022 %
- 5 %, SD = 400 BARS, PGA = 1.414 G, PGV = 98.80 CM/SEC, MAX STRAIN = 0.036 %
- 5 %, SD = 800 BARS, PGA = 2.381 G, PGV = 151.10 CM/SEC, MAX STRAIN = 0.056 %
- 5 %, SD = 1600 BARS, PGA = 3.615 G, PGV = 222.40 CM/SEC, MAX STRAIN = 0.080 %
- 5 %, SD = 2500 BARS, PGA = 4.675 G, PGV = 282.00 CM/SEC, MAX STRAIN = 0.120 %

1/24/2007

POINT A UHS			
APE	PGA(g)	PGV(cm/sec)	
10^{-4}	0.53	48.0	
10^{-5}	1.20	127.0	
10^{-6}	2.86	301.0	
10^{-7}	5.84	655.0	
M 6.5, D = 1 km, H = 8 km			
$\Delta\sigma$ (bars)	PGA(g)	PGV(cm/sec)	γ %
50	0.289	25.80	0.008
100	0.48	40.79	0.013
200	0.83	63.80	0.022
400	1.41	98.80	0.036
800	2.38	151.10	0.056
1600	3.62	222.40	0.080
2500	4.68	282.00	0.120

Seismicity of Nevada and some parts of the Great Basin

167

are typically from stations more than one focal depth from the epicenter, earthquake focal depth is frequently poorly constrained. In general, the most accurate earthquake depths for this region have been obtained from data derived from detailed microearthquake surveys and telemetered local networks. Such studies have been conducted in Nevada by Oliver and others (1966), Westphal and Lange (1967), Stauder and Ryall (1967), Ryall and Savage (1969), Gumper and Scholz (1971), Ryall and Malone (1971), Hamilton and others (1971), Smith and others (1971), Fischer and others (1972), Papanek and Hamilton (1972), Ryall and Priestley (1975), Rogers and Lee (1976), Rogers and others (1977), Ryall and Vetter (1982), Tarr and Rogers (1986), and Rogers and others (1987). Although considerable additional study of individual active zones will be necessary before confidence can be acquired concerning earthquake depths in this region, hypocenters appear to display some consistent general characteristics.

Great Basin earthquakes are rarely deeper than 20 km. For

most seismic zones in the Great Basin, more than 95 percent of the events occur in the upper 15 km (Ryall and Savage, 1969; Rogers and others, 1987). Within the upper 15 km of the crust, hypocenter concentrations display considerable variability (Fig. 5; Stauder and Ryall, 1967; Ryall and Savage, 1969; Okaya and Thompson, 1985; Richins and others, 1985). Modal depths of background microearthquakes or aftershocks may occur at any depth between about 1 and 15 km. In contrast, mainshock focal depth occurs in the range 8 to 16 km for the best-determined values (Doser and Smith, 1985; Doser, 1986, 1987, 1988; Baker and Doser, 1988). This observation has been one of the chief arguments supporting the existence of a brittle-ductile crustal boundary at this depth in the Great Basin (Anderson, 1971; Tocher, 1975; Smith and Bruhn, 1984). Because mainshock events commonly initiate near the base of the brittle upper crust between 10 and 15 km, Smith and Bruhn (1984) infer that maximum strength of the brittle crust occurs at the brittle-ductile boundary.

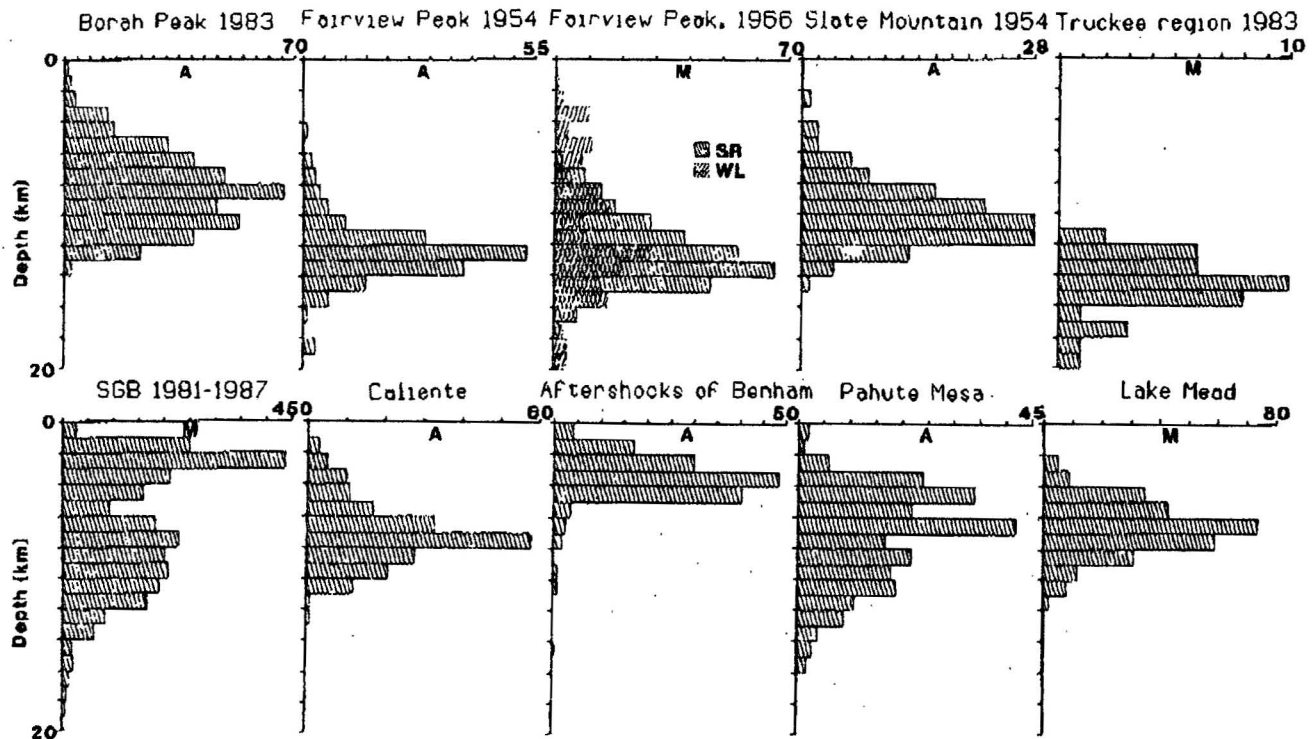


Figure 5. Depth-of-focus histograms for aftershock studies (labeled A) and microearthquake studies (labeled M) for various regions in the Great Basin. We plot numbers of earthquakes versus depth of focus for events in the range 0.0 to 20.0 km. For all but one of the data sets, less than 1 percent of the estimated depths are greater than 20 km. About 8 percent of the Fairview Peak depths computed by Westphal and Lange (1967) are greater than 20 km. References are: Borah Peak 1983—Charley Langer (written communication, 1987); Fairview Peak 1954, Slate Mountain 1954, and Caliente 1966—Ryall and Savage (1969); Fairview Peak 1966—Stauder and Ryall (SR) (1967) and Westphal and Lange (WL) (1967); Truckee region 1983—Hawkins and others (1986); southern Great Basin (SGB)—Rogers and others (1987) and Harmsen and Rogers (1987); Benham and other Nevada Test Site (NTS) nuclear test aftershocks—Hamilton and others (1971); aftershocks of Pahute Mesa (NTS) nuclear tests of 1976—Rogers and others (1977); and Lake Mead earthquakes of 1972 and 1973—Rogers and Lee (1976). Depths are relative to the mean surface level for each study area.

TOTAL P.02

**YUCCA MOUNTAIN
RECURRENCE INTERVALS FOR LOCAL FAULTS**

Expert Team	Bow Ridge Fault	Solitario Canyon Fault	Paintbrush Canyon/ Stagecoach Road Faults
AAR	70 – 200 ky 120 ky preferred	35 – 100 ky 60 ky preferred	5 – 40 ky 20 ky preferred
ASM	71 – 188 ky 120 ky preferred	31 – 78 ky 51 ky preferred	17 – 42 ky 27 ky preferred
DFS	100 – 140 ky	50 – 70 ky	None
RYA	75 ky (?)	90 ky	50 / 25 ky
SBK	100 – 140 ky	None	40 ky
SDO	100 – 140 ky	35 ky (minimum)	21 – 118 / 10 – 35 ky
Average Minimum	88	38	14
Average Maximum	160	82	62
Average of Preferred/Mean	112	65	38

88 ky
 $88 \times 10^3 \text{ yo/yr}$
 $2.1 \times 10^{-5} \text{ yr/yr}$

JAKE

STATIC (crawler), NORMAL

Best Ln(SSD) Summary Stats

Mean	2.915464
Standard Error	0.149722
Median	2.909962
Mode	3.670715
Standard Deviation	0.873023
Sample Variance	0.762169
Kurtosis	0.048846
Skewness	-0.417662
Range	3.976562
Minimum	0.792766
Maximum	4.769328
Sum	99.12577
Count	34

18.45 Bars

WNA

Stress Parameters

Set	Stress Drop (bars)	σ_{In}
All	46.9	0.47
Shallow Slip	30.6	0.37
Deep Slip	56.6	0.38
	$\Delta\sigma$ (bars)	
M	WUS	CEUS
5.5	80	160
6.5	65	120
7.5	45	90
8.5	35	70
6.5	NS SS OB RV	
	50 60 70 80	

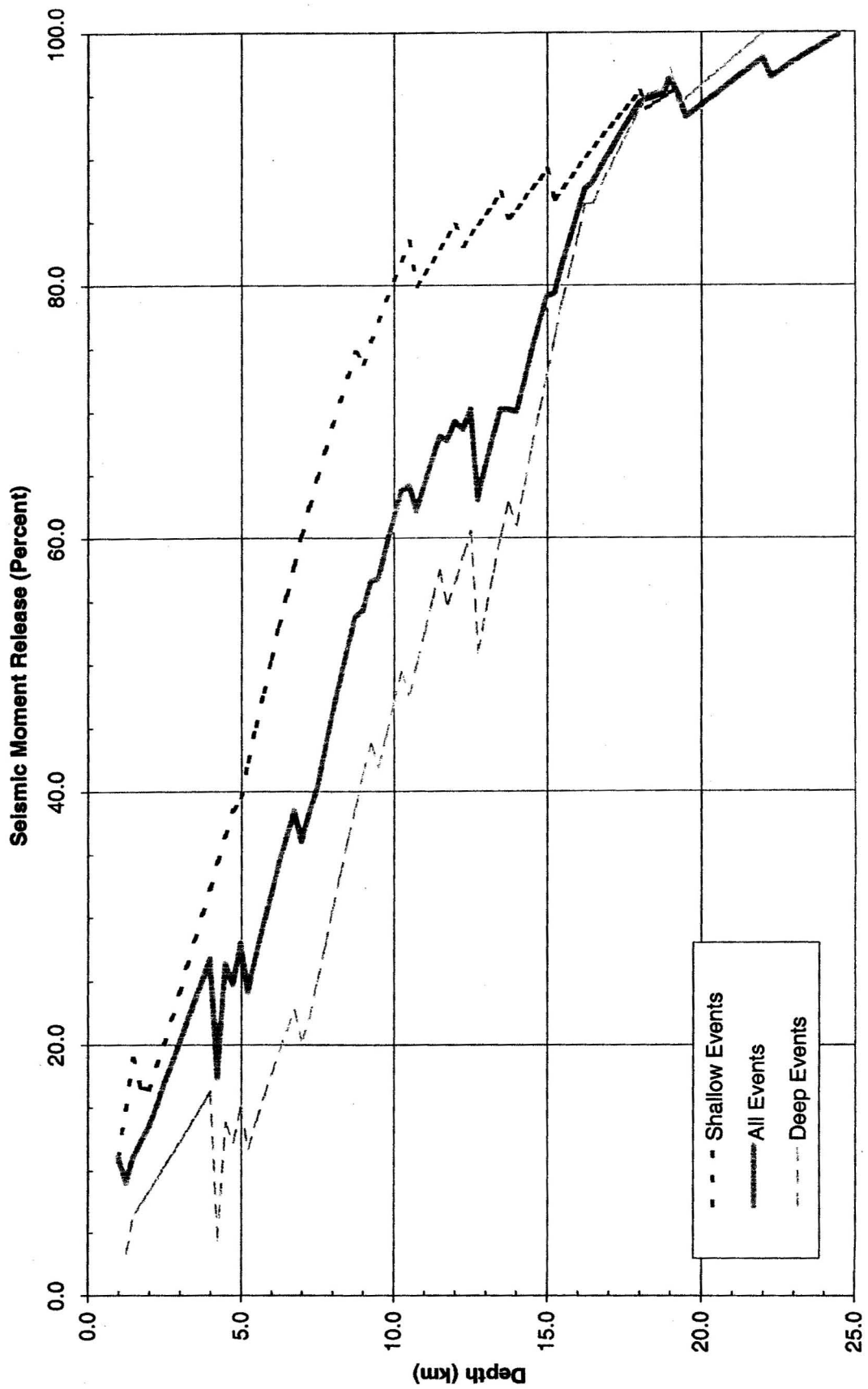
Table 5.39 Stress Drop Summary

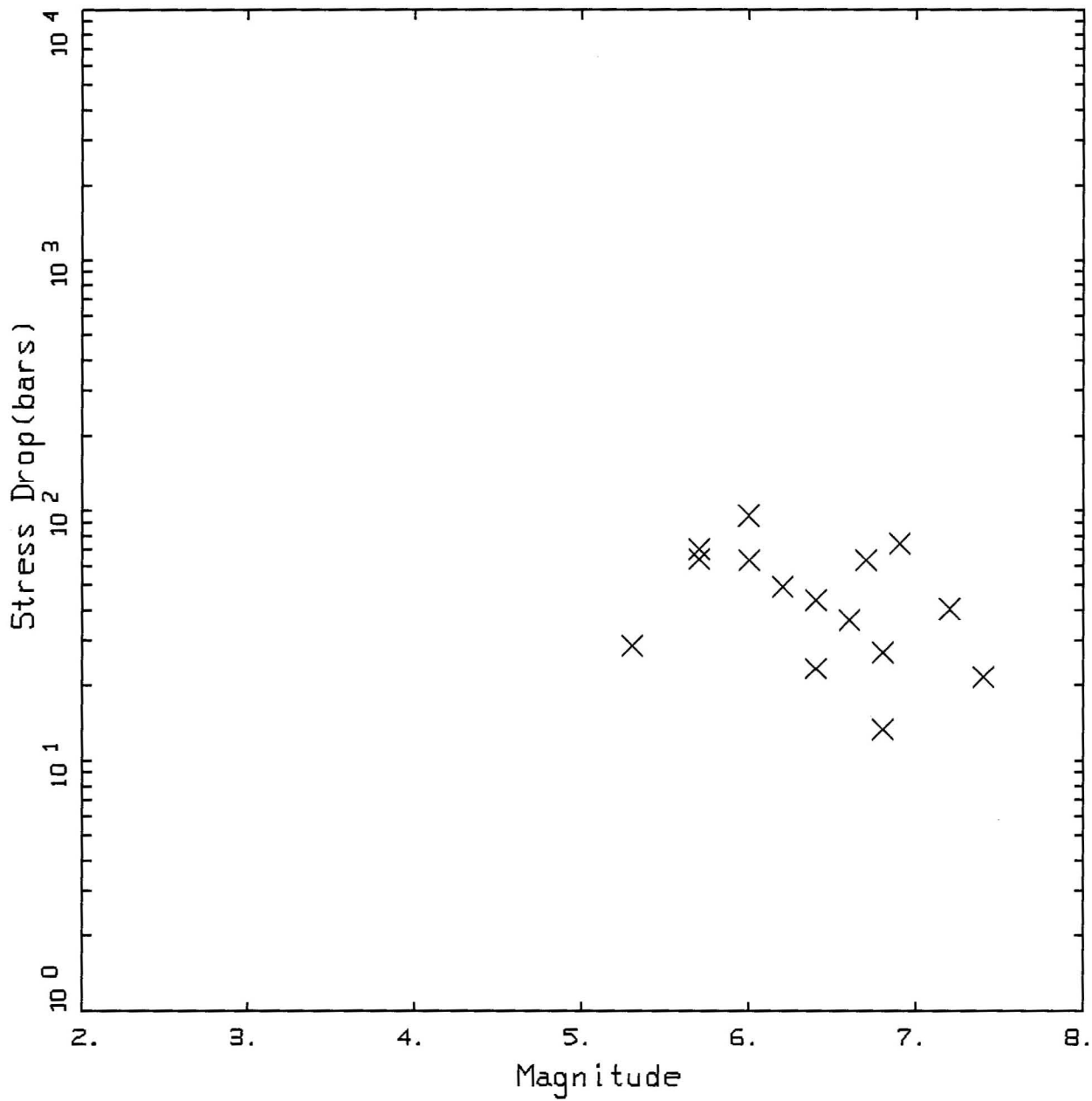
Earthquake	Date	M	Stress Drop Inversion (bars)	Stress Drop SE (bars)	N
San Fernando	1971	6.6	36.1	1	39
S Tabas, Iran	1978	7.4	21.5	1	4
Coyote Lake	1979	5.7	70.1	2	10
S Imperial Valley	1979	6.4	23.2	1	35
Imperial Valley(AS)	1979	5.3	28.7	1	16
Morgan Hill	1984	6.2	49.0	1	29
S Nahanni	1985	6.8	13.4	1	3
North Palm Springs	1986	6.0	62.8	1	29
Whittier Narrows	1987	6.0	95.7	1	88
S Superstition Hills(B)	1987	6.4.(6.7)	43.4 (26.6)	1	12
Saguenay	1988	5.8	572.2	22	22
Loma Prieta	1989	6.9	73.7	1	53
Little Skull Mtn.	1992	5.7	63.7	2	8
A		4.4	34.0	1	5
B		4.2	46.0	2	3
S Landers	1992	7.2	40.7	1	57
Cape Mendocino	1992	6.8	27.2	1	5
Northridge	1994	6.7	62.9	1	94

WNA AVG* = 46.9

Excludes* Saguenay, Nahanni, and aftershocks

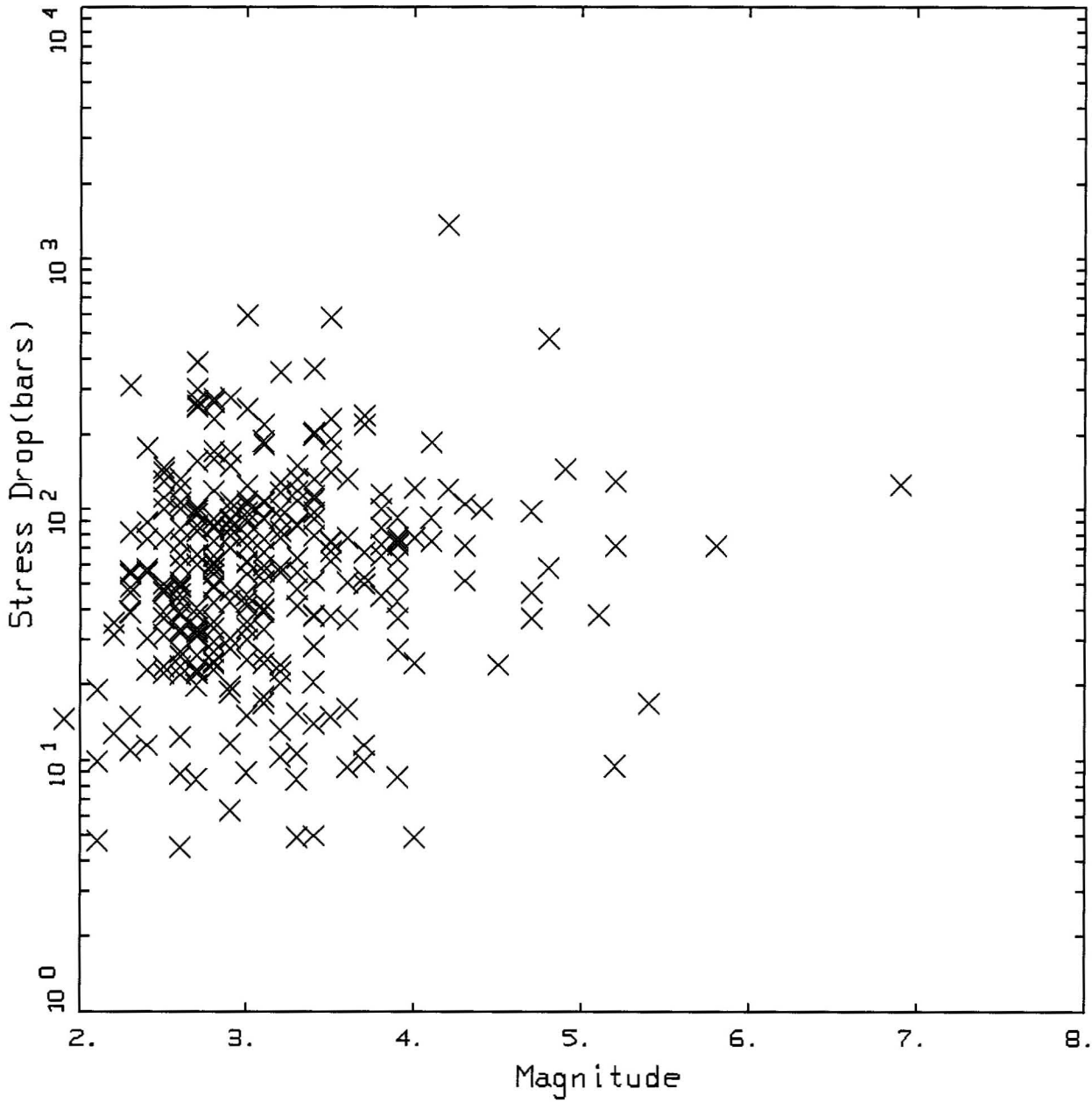
Moment Release vs. Depth: Median





WUS STRESS PARAMETERS

X X LEGEND
 WUS, MEDIAN = 41.7 BARS, SIGMA = 0.55



KOREA STRESS PARAMETERS

× × LEGEND
 KOREA, MEDIAN = 56.5 BARS, SIGMA = 0.94

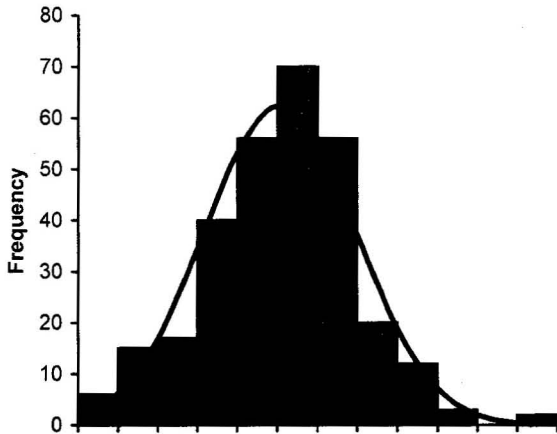
Test | Continuous summary descriptives

Variable | LN Stress Drop (Bars)

Performed by | Ky Lang

Date |

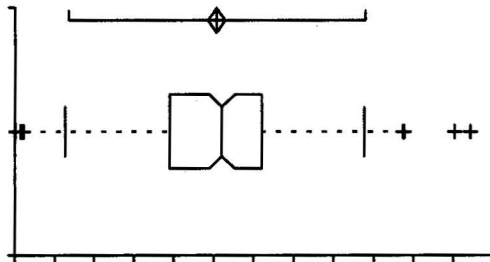
14 December 2006



n | 297 (cases excluded: 1 due to mis

Mean | 4.03430 **56**
95% CI | 3.92604 to 4.14257

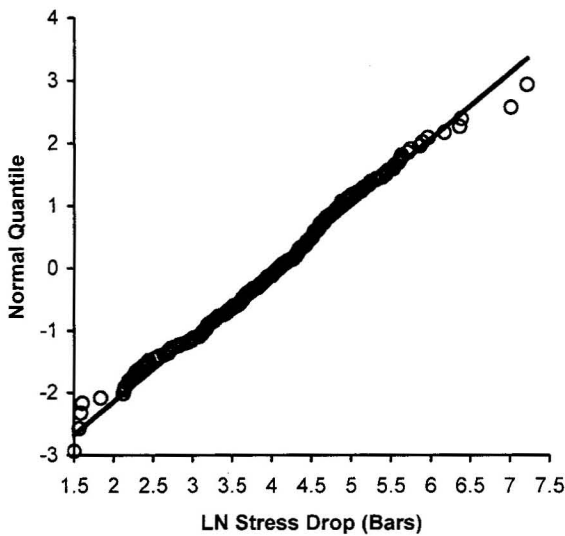
Variance | 0.898884
SD | 0.948095
SE | 0.055014
CV | 24%



Median | 4.10264
95.2% CI | 3.94739 to 4.26970

Range | 5.7101
IQR | 1.1542

Percentile	
2.5th	2.13356
25th	3.44999
50th	4.10264
75th	4.60417
97.5th	5.88078

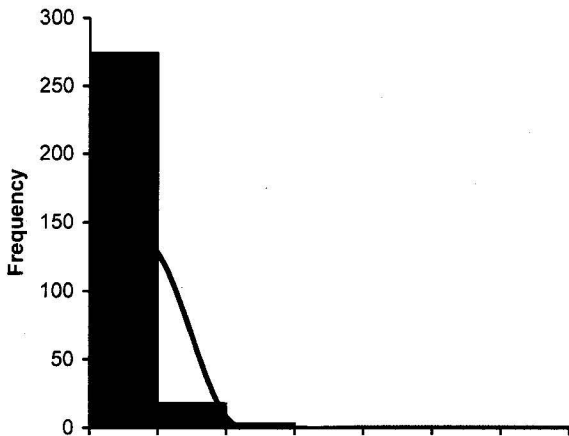


	Coefficient	p
Shapiro-Wilk	0.9905	0.0509
Skewness	-0.0778	0.5775
Kurtosis	0.5082	0.1023

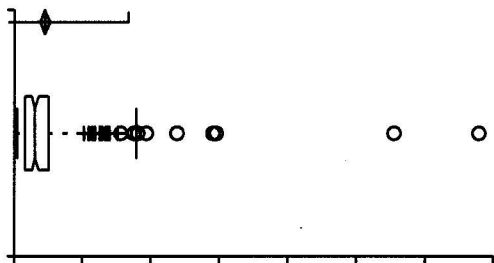
Test | Continuous summary descriptives

Variable SD (est)
Performed by Ky Lang

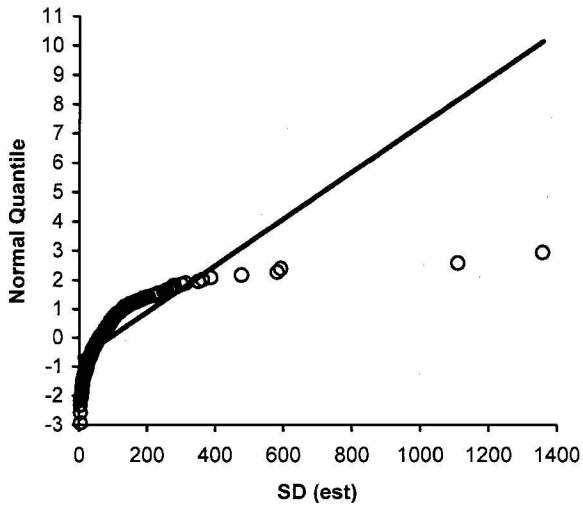
Date 14 December 2006



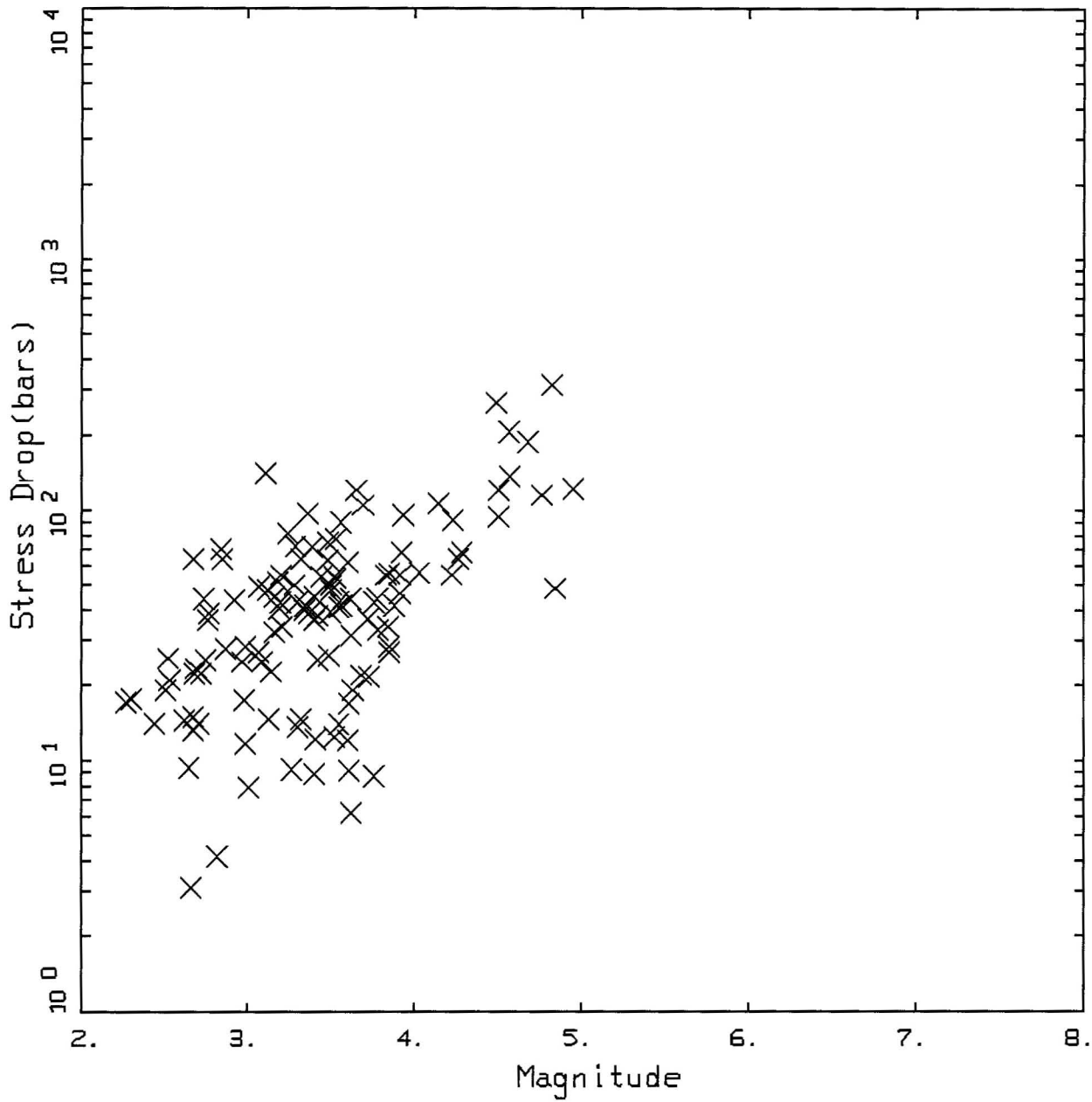
n	297 (cases excluded: 1 due to mis
Mean	89.39697
95% CI	75.10388 to 103.69006
Variance	15665.841308
SD	125.163259
SE	7.262709
CV	140%



Median	60.50000
95.2% CI	51.80000 to 71.50000
Range	1354.0000
IQR	68.4000
Percentile	
2.5th	8.44500
25th	31.50000
50th	60.50000
75th	99.90000
97.5th	358.13500

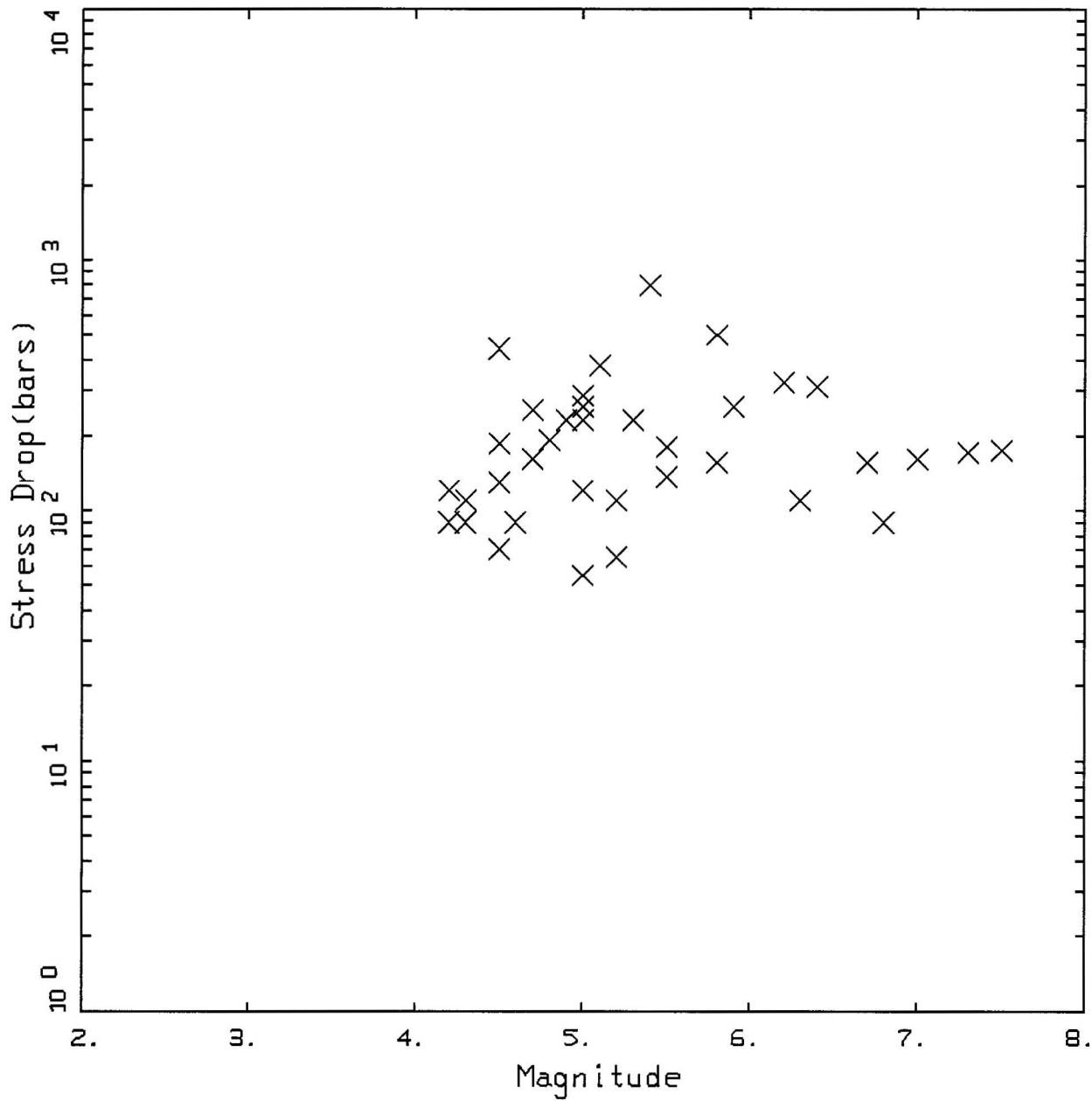


	Coefficient	p
Shapiro-Wilk	0.4956	<0.0001
Skewness	6.1201	<0.0001
Kurtosis	51.1950	<0.0001



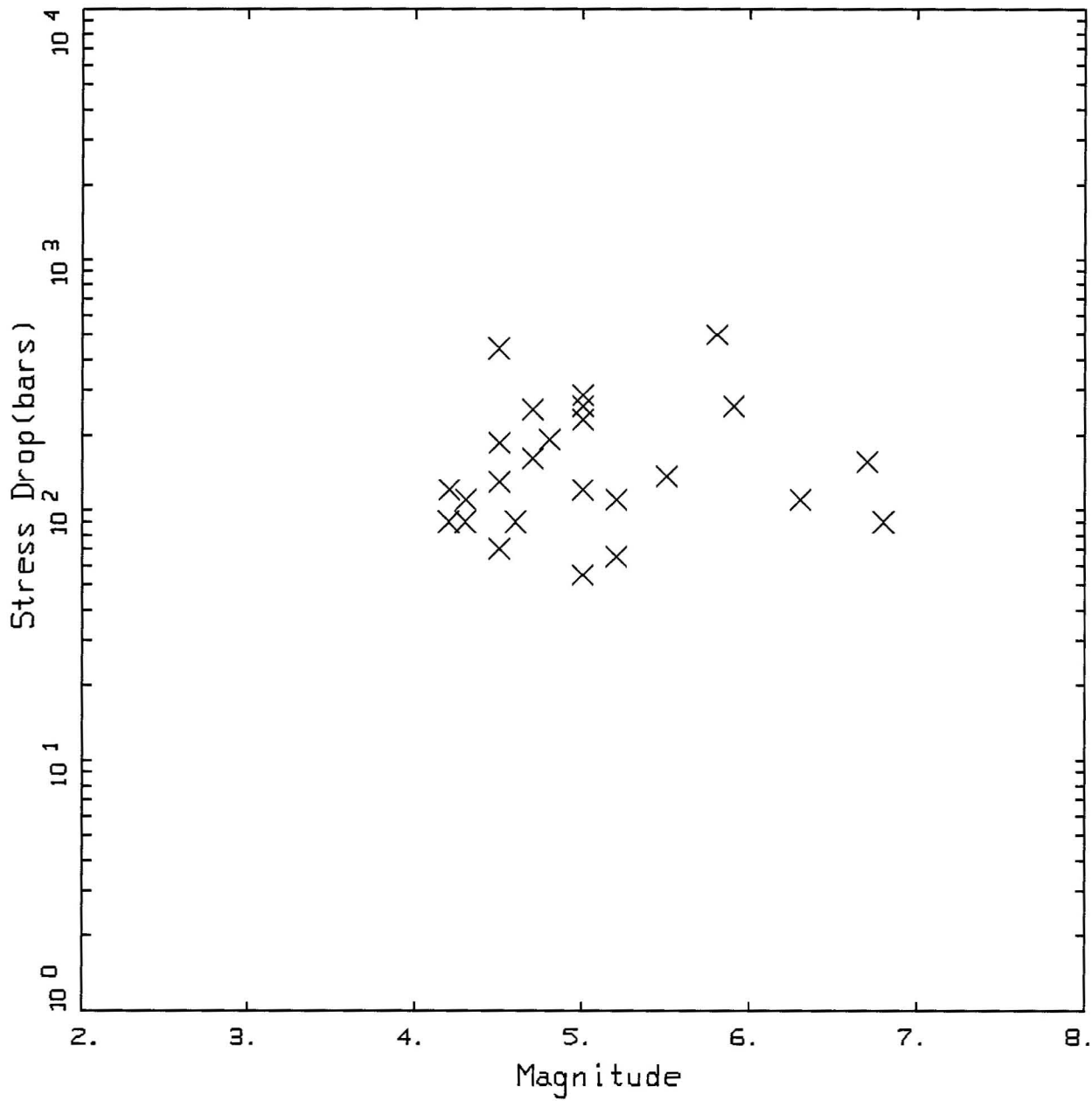
CEUS STRESS PARAMETERS

X X LEGEND
 CEUS, MEDIAN = 35(110)BARS, SIGMA = 0.83(0.57), (M>4)



CEUS STRESS PARAMETERS

× × LEGEND
 CEUS, MEDIAN = 166.8 BARS, SIGMA = 0.62



CEUS STRESS PARAMETERS

X X LEGEND
 CEUS, MEDIAN = 145.6 BARS, SIGMA = 0.57

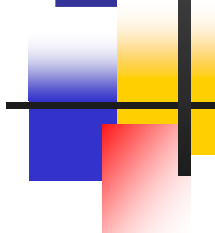
- Meeting 2/13/07 presentation by W. Silva

Stress Parameter Statistics

Region	M	n	$\Delta\sigma(\text{bars})$	σ_{In}	range
WUS	5-7.5	15	42	.55	13-100
Korea	5-7	7	47	1.00	10-130
Korea	2-7	296	56	.93	5-1350
CEUS	2-5	122	36	.83	4-314
CEUS	4-5	16	110	.57	49-314
CEUS.06	4-8	36	170	.60	55-800
CEUS.06	4-7	25	145	.57	55-500
Greece	5-7	18	63	.57	32-290
Italy	4-6.5	9	181	.31	116-340
Italy/3	4-6.5	9	60	.31	38-113

Combined Stress Parameter Statistics

Region	M	n	μ_{In}	e^{μ}	σ_{In}	range	2σ
All*	4-7.5	81	4.41	82	.78	10-500	391
WUS+Greece							
	5-7.5	33	3.96	52	.59	13-290	170
CEUS	4-7	33	4.83	125	.56	49-500	383



Some thoughts on stress parameter

Gail M. Atkinson



Background

- An important issue in the examination of extreme ground motion potential is the statistical distribution of the high-frequency source-spectral level of the ground motion. This high-frequency level is often interpreted in terms of stress drop. According to the Brune point-source model, the Fourier acceleration spectrum at distances near the source is given by (Brune, 1970; Boore, 1983):

$$A_{ij}(f) = C M_0 (2 \pi f)^2 / [R (1 + (f/f_0)^2)]$$



Consequence

- at high frequencies, well above f_0 , the high-frequency spectral level is given by the constant:

$$A_{hf} = C M_0 (2 \pi)^2 f_0^2 / R$$



Caveat

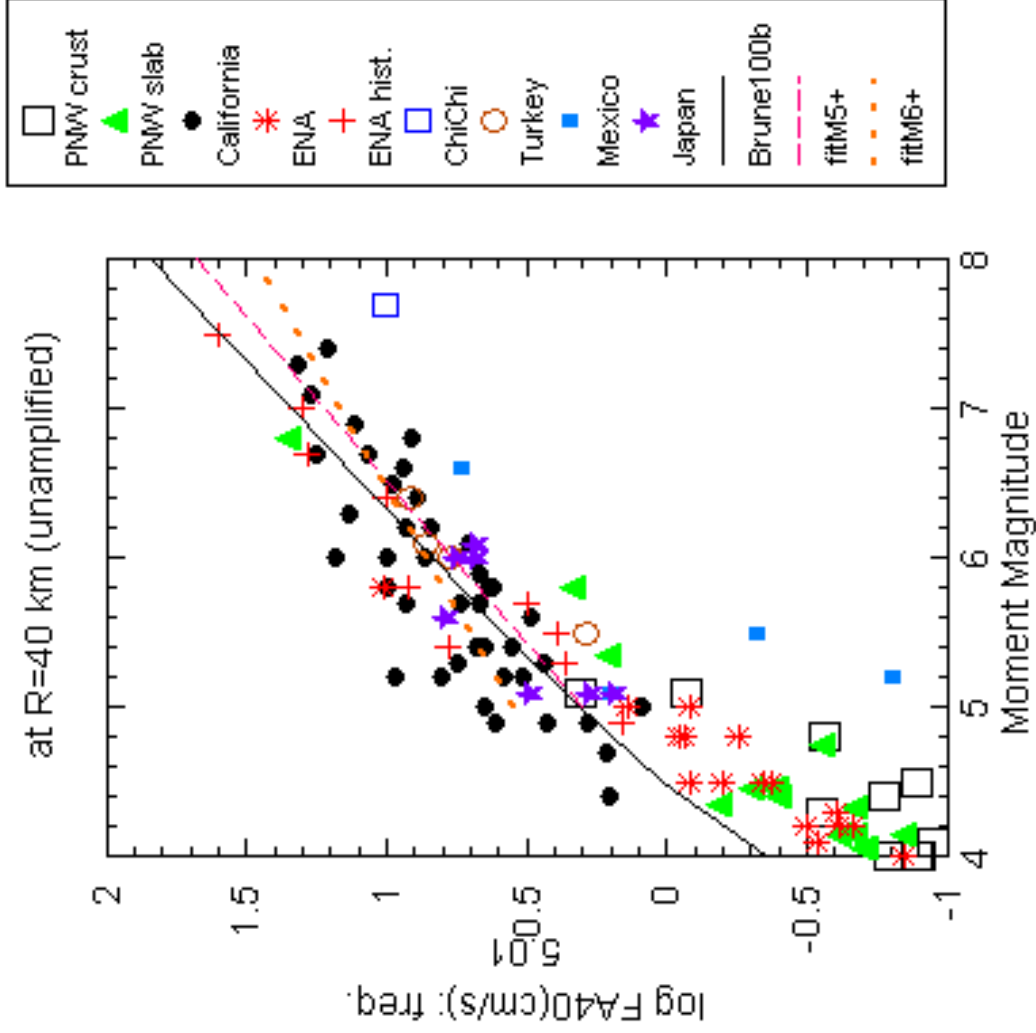
- In this expression, it is implicitly assumed that any effects of amplification on the spectrum (such as that due to travel through the crustal velocity gradient) have been removed (eg. such as by division of the spectra by the appropriate frequency-dependent amplification factors). This assumption is implied by the fact that we are equating the observed spectrum at some distance R to that at the source, where the attenuation from the source to the observation point has been modeled by the simple $1/R$ operator that applies to direct-wave geometric spreading. We are also assuming $1/R$ is appropriate to some distance (and this may not be true).



Rule of Thumb

- Hanks and McGuire (1981) made the observation that the above expression (combined with some equations from random process theory linking frequency domain to time domain amplitudes) appears to explain observed peak ground accelerations in California, if a constant stress drop of 100 bars is assumed.

Comparison of HF spectral amplitudes across regions



Some data
on Ahf at
40 km:
All data
points
come from
regressions
of $A(f)$ vs.
dist. to get
near-src
Ahf



Notes on plot

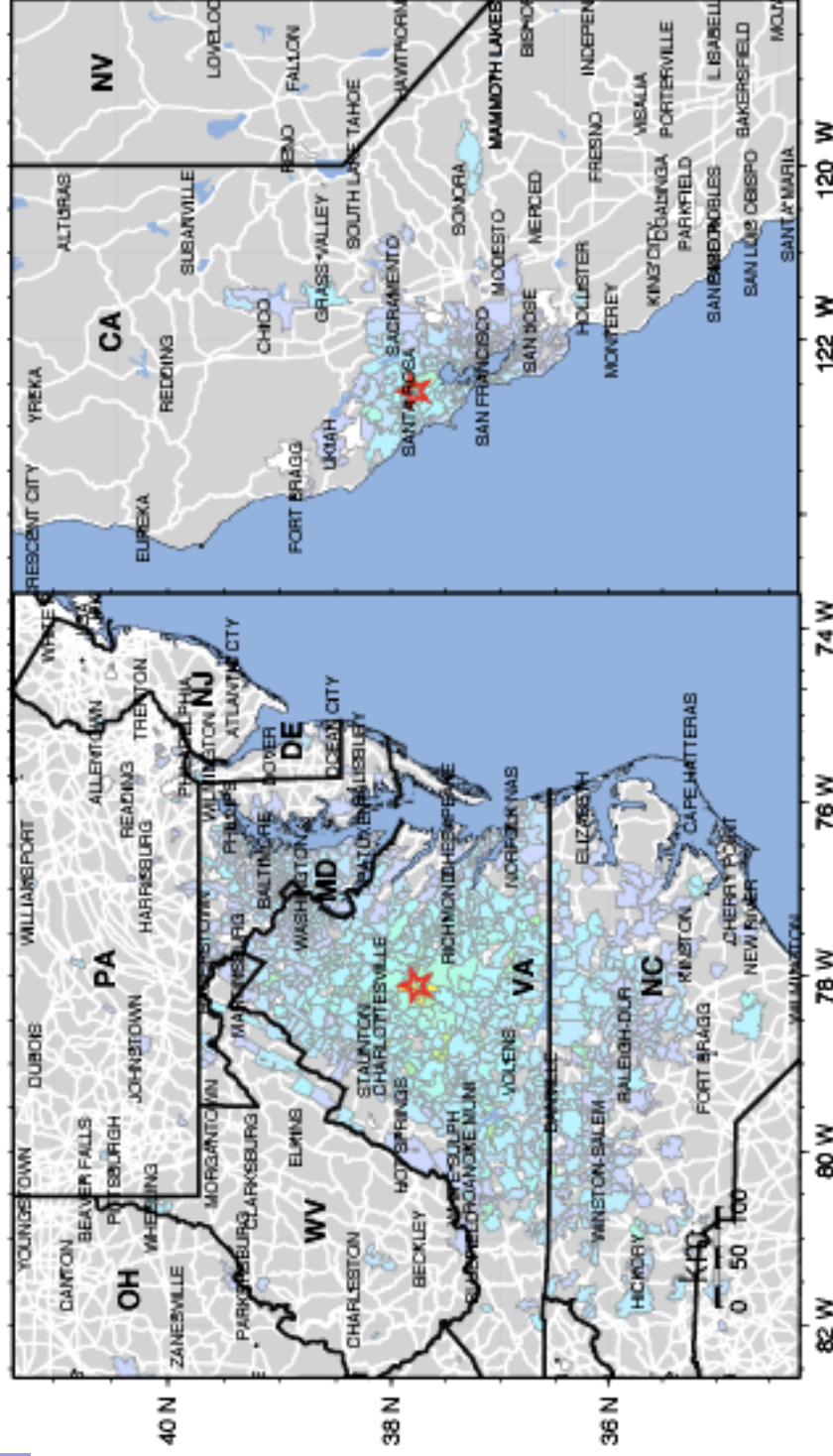
- A best-fit line of FA versus **M** (pink dashed line) for **M** ≥ 5 is given by:
- $\log \text{FA}(40) = -1.99 + 0.46 \mathbf{M}$
where the residuals have a standard deviation of 0.28 log units. If we focus on just the data for **M** ≥ 6, we eliminate a few anomalously low points and obtain (dotted orange line):
- $\log \text{FA}(40) = -1.00 + 0.31 \mathbf{M}$
with a significantly lower standard deviation of 0.17 (factor of 1.5). This line also shows the decreasing stress drop trend at larger magnitudes more clearly. (This trend is a consequence of modeling an extended source as a point-source.)



Some problems with drawing conclusions from the plot of Ahf(40)

- Near-source amplitudes are defined at 40 km (due to lack of close data in many regions for larger events)
- Recent data suggest faster near-source attenuation in ENA vs. WNA ($R^{*-1.3}$ vs. R^{*-1}), in first 70 km, so a comparison at 40 km may be misleading (Atkinson, 2004)
- I now think ENA stress is about a factor of 2 or 3 higher than WNA, with a more rapid attenuation in ENA resulting in similar apparent values near 40 km. See DYFI data for corroboration of these trends.

Comparison of DYFI data from 2 M4.3 events: VA vs. CA



INTENSITY	I	II-III	IV	V	VI	VII	VIII	IX	X+
SHAKING	Not felt	Weak	Light	Moderate	Strong	Very strong	Severe	Violent	Extreme
DAMAGE	none	none	none	Very light	Light	Moderate	Moderate/Heavy	Heavy	Very Heavy

M4.2 Columbia VA vs. M4.4 Santa Rosa CA

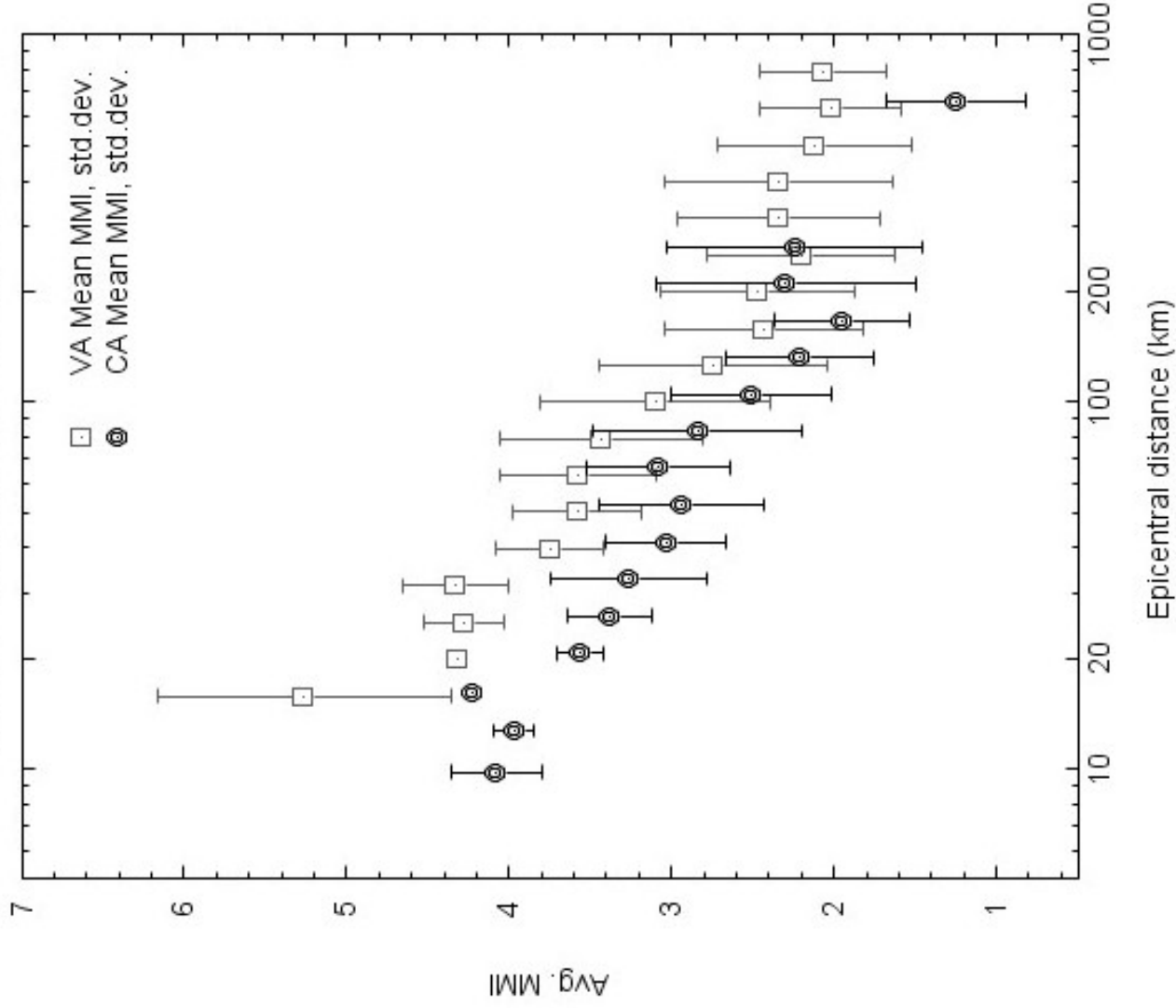


Illustration of ENA vs. CA attenuation, based on DYFI



Initial conclusions (needing more data analysis to verify)

- Stress parameters are probably about 50 to 100 bars for WNA, vs. 100-200 bars for ENA, as an average
- Stress might depend on depth (eg. Saguenay was deep, with large stress), but systematic info. on depth effect is limited
- Standard deviation is probably about a factor of 1.5 to 2
- No evidence of upper limit on stress parameter to my knowledge

Relation between apparent stress (σ_A) and the equivalent point-source stress parameter ($\Delta\sigma$).

Notes by David M. Boore

I use these definitions:

$$\sigma_A = \frac{\mu E_S}{M_0} \quad (1)$$

where μ is shear modulus, E_S is the radiated seismic energy, and M_0 is the seismic moment.

$\Delta\sigma$ is the parameter that determines the level of the flat portion of the acceleration source spectrum for an ω^2 source spectrum, regardless of whether it is a single-corner frequency or a more complicated spectrum. This can be confusing but is essential to understand for the analysis herein. Consider a single-corner-frequency, ω^2 source spectrum, for which the moment-rate spectrum is given by:

$$\dot{M}_0(f) = M_0 \left(\frac{1}{1 + (f/f_C)^2} \right) \quad (2)$$

The acceleration spectrum goes as $f^2 \dot{M}_0(f)$. At high frequencies, the acceleration spectra (A_{HF}) is given by the following equation:

$$A_{HF} \approx M_0 f_C^2 \quad (3)$$

Using the Brune relation between corner frequency, radius, and stress,

$$f_C = 0.49 \beta \left(\frac{\Delta\sigma}{M_0} \right)^{1/3} \quad (4)$$

and thus the high-frequency spectral level can be parameterized by a variable having the units of stress; I call this the “stress parameter”:

$$\Delta\sigma = \frac{1}{(0.49)^3} \frac{M_0 f_C^3}{\beta^3} \quad (5)$$

Now consider the more complicated source spectrum used by Atkinson and Boore (1995) and by Atkinson and Silva (2000).

$$\dot{M}_0(f) = M_0 \left(\frac{1 - \varepsilon}{1 + (f/f_A)^2} + \frac{\varepsilon}{1 + (f/f_B)^2} \right) \quad (6)$$

The parameters ε , f_A , and f_B are functions of seismic moment; see Tables 2 and 3 in Boore (2003) for a convenient summary of various source spectral scaling relations, including the functions for the three parameters ε , f_A , and f_B .

At high frequencies the acceleration spectrum goes as

$$A_{HF} \approx M_0 \left((1 - \varepsilon) f_A^2 + \varepsilon f_B^2 \right) \quad (7)$$

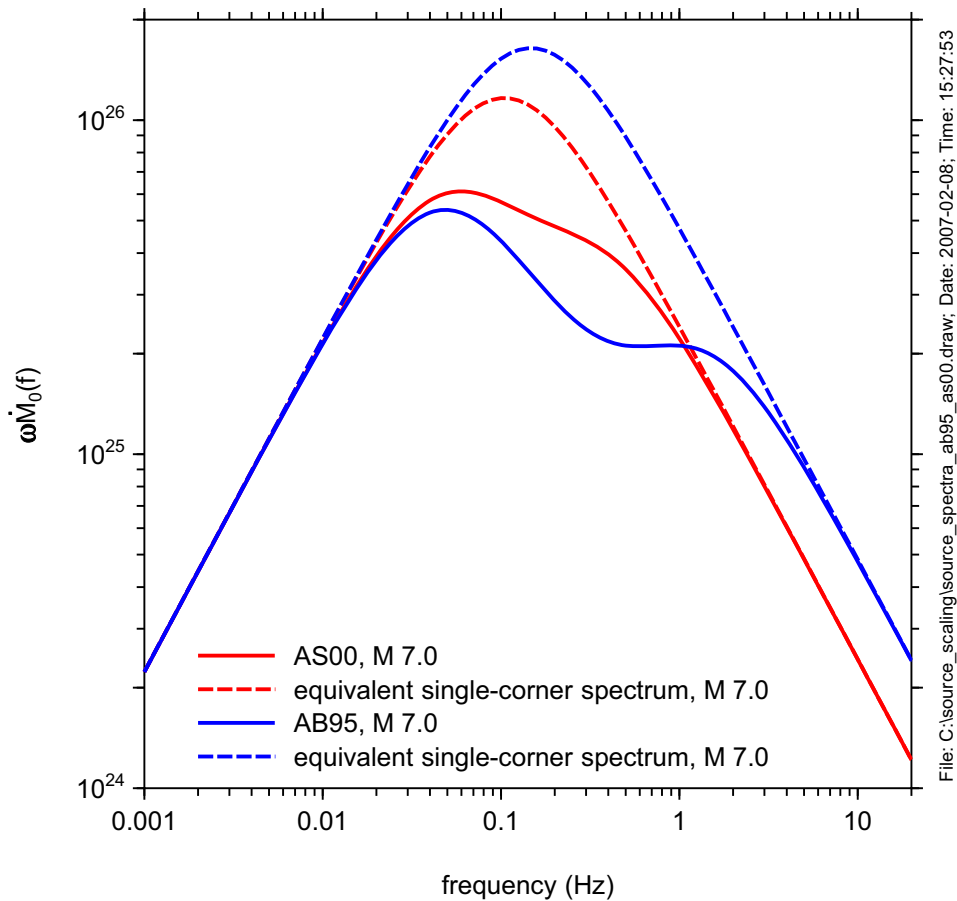
Note that a stress parameter is not used to specify the high-frequency spectral level. But an equivalent single-corner-frequency stress parameter can be defined by equating the spectral levels given in equations (3) and (7). This gives

$$f_C = \sqrt{(1 - \varepsilon) f_A^2 + \varepsilon f_B^2} \quad (8)$$

and using equation (4), we have

$$\Delta\sigma = \frac{1}{(0.49)^3} \frac{M_0}{\beta^3} \left[(1 - \varepsilon) f_A^2 + \varepsilon f_B^2 \right]^{3/2} \quad (9)$$

It is very important to realize that a spectrum given by using equation (8) in equation (2) will give a spectrum equal to that given by equation (6) only for low frequencies and high frequencies. In particular, the portion of the equivalent single-corner-frequency spectrum in the range between the corners f_A and f_B will overestimate the double-corner frequency spectrum. This is shown in the figure below; which plots $\omega\dot{M}_0(f)$ for the Atkinson and Boore (1995) and the Atkinson and Silva (2000) source spectra, as well as the single-corner-frequency approximations.



Because the energy is proportional to the integral of the square of $\omega\dot{M}_0(f)$, it is clear from the figure above that the energy for the double-corner model will be less than from the equivalent single-corner model, and therefore the ratio of apparent stress to the effective stress parameter will be less than for the single-corner-frequency model.

With the definition given in equation (9) for $\Delta\sigma$ (the single-corner-frequency equivalent stress parameter for the double-corner-frequency model), I now proceed to derive the relation between σ_A and $\Delta\sigma$. To do this, I use equation (16) of Singh and Ordaz (1994) (correcting a minor typo by adding the dot diacritical mark to M_0):

$$E_s = \frac{4\pi}{5\rho\beta^3} \int_0^{\infty} f^2 \dot{M}_o^2(f) df \quad (10)$$

Using Gradshteyn and Ryzhik (1965) to evaluate the integral in equation (10) leads to the following equations:

Single-corner model:

$$\frac{\sigma_A}{\Delta\sigma} = (0.49)^3 \frac{\pi^2}{5} = 0.23 \quad (11)$$

Double-corner model:

$$\frac{\sigma_A}{\Delta\sigma} = (0.49)^3 \frac{\pi^2}{5} \frac{(1-\varepsilon)^2 f_A^3 + \varepsilon^2 f_B^3 + 4(1-\varepsilon)\varepsilon \frac{(f_A f_B)^2}{(f_A + f_B)}}{\left((1-\varepsilon)f_A^2 + \varepsilon f_B^2\right)^{3/2}} \quad (12)$$

I have evaluated these equations as a function of **M** for the AB95 and the AS00 source models. Here are the results:

AS00 model:

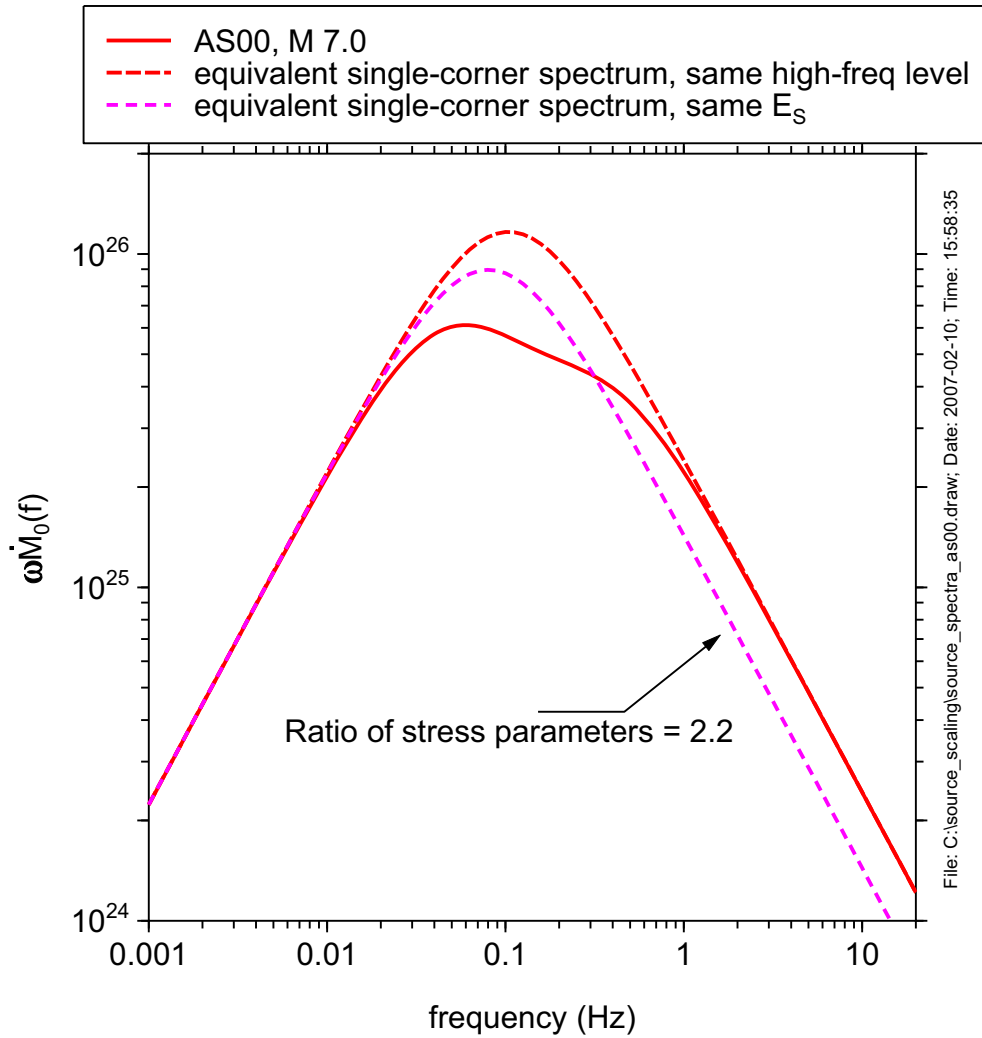
M	M0	fa	fb	eps	fc	Sig_a	Dsigma	sig_a/ds ds/sig_a	
4.00	1.12E+22	1.574	5.998	0.385	3.919	23.006	133.908	0.172	5.82
4.25	2.66E+22	1.183	4.742	0.332	2.899	21.087	128.501	0.164	6.09
4.50	6.31E+22	0.889	3.750	0.287	2.144	19.327	123.238	0.157	6.38
4.75	1.50E+23	0.668	2.965	0.248	1.585	17.718	118.135	0.150	6.67
5.00	3.55E+23	0.502	2.344	0.214	1.172	16.249	113.202	0.144	6.97
5.25	8.41E+23	0.378	1.854	0.185	0.866	14.913	108.446	0.138	7.27
5.50	2.00E+24	0.284	1.466	0.159	0.640	13.699	103.872	0.132	7.58
5.75	4.73E+24	0.213	1.159	0.138	0.473	12.599	99.482	0.127	7.90
6.00	1.12E+25	0.160	0.916	0.119	0.350	11.602	95.275	0.122	8.21
6.25	2.66E+25	0.121	0.724	0.103	0.259	10.701	91.251	0.117	8.53
6.50	6.31E+25	0.091	0.573	0.089	0.191	9.887	87.406	0.113	8.84
6.75	1.50E+26	0.068	0.453	0.077	0.141	9.153	83.737	0.109	9.15
7.00	3.55E+26	0.051	0.358	0.066	0.104	8.491	80.240	0.106	9.45
7.25	8.41E+26	0.038	0.283	0.057	0.077	7.894	76.909	0.103	9.74
7.50	2.00E+27	0.029	0.224	0.049	0.057	7.358	73.739	0.100	10.02
7.75	4.73E+27	0.022	0.177	0.043	0.042	6.875	70.724	0.097	10.29
8.00	1.12E+28	0.016	0.140	0.037	0.031	6.441	67.859	0.095	10.53
8.25	2.66E+28	0.012	0.111	0.032	0.023	6.052	65.138	0.093	10.76
8.50	6.31E+28	0.009	0.087	0.027	0.017	5.702	62.554	0.091	10.97

AB95 model:

M	M0	fa	fb	eps	fc	Sig_a	Dsigma	sig_a/ds ds/sig_a	
4.00	1.12E+22	1.897	4.764	0.938	4.637	50.602	221.844	0.228	4.38
4.25	2.66E+22	1.396	4.276	0.650	3.544	47.832	234.806	0.204	4.91
4.50	6.31E+22	1.027	3.837	0.450	2.685	43.406	242.134	0.179	5.58
4.75	1.50E+23	0.756	3.443	0.312	2.023	38.333	245.632	0.156	6.41
5.00	3.55E+23	0.556	3.090	0.216	1.519	33.237	246.571	0.135	7.42
5.25	8.41E+23	0.409	2.773	0.150	1.138	28.461	245.822	0.116	8.64
5.50	2.00E+24	0.301	2.489	0.104	0.851	24.169	243.977	0.099	10.09
5.75	4.73E+24	0.221	2.234	0.072	0.636	20.415	241.435	0.085	11.83
6.00	1.12E+25	0.163	2.004	0.050	0.475	17.191	238.460	0.072	13.87
6.25	2.66E+25	0.120	1.799	0.035	0.355	14.455	235.228	0.061	16.27
6.50	6.31E+25	0.088	1.614	0.024	0.265	12.152	231.857	0.052	19.08
6.75	1.50E+26	0.065	1.449	0.017	0.197	10.225	228.422	0.045	22.34
7.00	3.55E+26	0.048	1.300	0.012	0.147	8.618	224.972	0.038	26.10
7.25	8.41E+26	0.035	1.167	0.008	0.110	7.282	221.540	0.033	30.42
7.50	2.00E+27	0.026	1.047	0.006	0.082	6.171	218.147	0.028	35.35
7.75	4.73E+27	0.019	0.940	0.004	0.061	5.248	214.805	0.024	40.93
8.00	1.12E+28	0.014	0.843	0.003	0.046	4.481	211.521	0.021	47.20
8.25	2.66E+28	0.010	0.757	0.002	0.034	3.843	208.299	0.018	54.21
8.50	6.31E+28	0.008	0.679	0.001	0.025	3.311	205.143	0.016	61.97

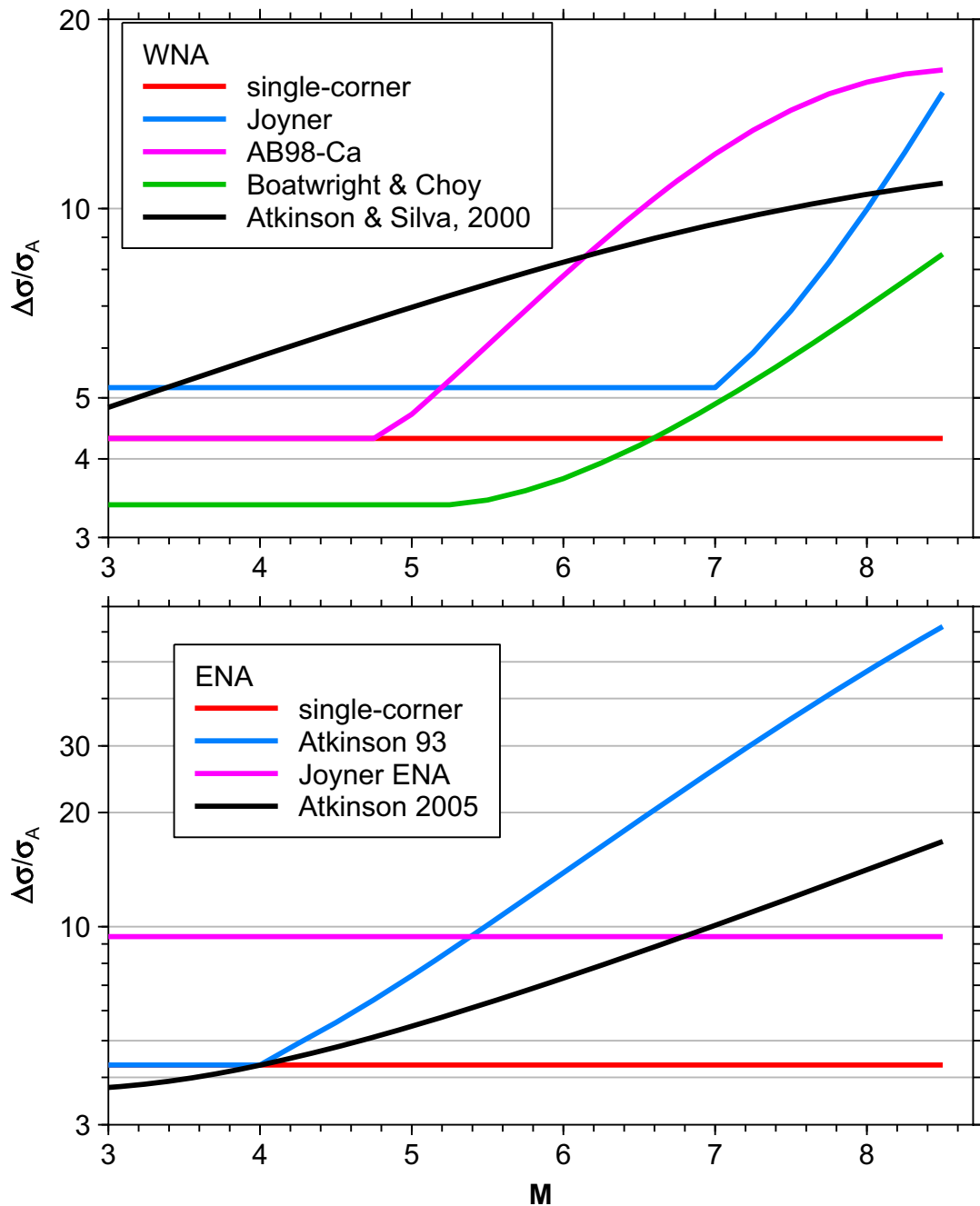
What does this mean? If one wanted to convert an observed value of σ_A to $\Delta\sigma$, using the single-corner frequency relation of $1/0.23 = 4.31$ would seriously underestimate the actual equivalent stress parameter if the spectrum had the form of the double corner spectrum assumed by AB95 and by AS00. The underestimation is much worse for the AB95 model than for the AS00 model, but even the latter would give an underestimation of more than a factor of 2 for earthquakes greater than 6.5.

Another way of looking at the situation is to ask how the spectral shape of a single-corner and double corner model compare if the energies are the same. This is shown in the following figure. The key lesson is that if the energy is used to define the high-frequency spectral level, the level will be significantly underestimated if a single-corner frequency model is assumed but the actual spectrum corresponds to a double-corner frequency model. The high-frequency spectral level is defined in terms of an equivalent stress parameter in the stochastic model, and the stress parameter will generally be underestimated if the actual spectrum is a double-corner spectrum. In the last section of this note I discuss the ratio of stresses for a variety of models.



Ratio for many models:

In order to compute the ratio of equivalent stress parameter to apparent stress for the models contained in my SMSIM software, I was forced to do numerical integration (which turned out to be quite straightforward, using Numerical Recipes QROMO with functions MIDPNT and MIDINF, as described on p. 138 of Press et al. (1992). Here are the results, separated into models for ENA and for WNA:



File: C:\source_scaling\delta_sigma_apparent_ratio.draw; Date: 2007-02-20; Time: 18:32:23

All but one of the two-corner models give ratios larger than for the single-corner model for $M > 4.0$, and the one exception gives ratios greater than the single-corner model for $M > 6.6$. The double-corner models to which I would give the most weight are those by Atkinson and Silva for WNA and Atkinson (2005) for ENA. These indicate that $\Delta\sigma/\sigma_A$ can be as large as 11 and 17 for WNA and ENA, respectively.

References

Atkinson, G.M. and D.M. Boore (1995). Ground motion relations for eastern North America, *\bssa{85}{17--30}*

Atkinson, G.M. and W. Silva (2000). Stochastic modeling of California ground motions, *\bssa{90}{255--274}*

Boore, D. M. (2003). Prediction of ground motion using the stochastic method, *\pageoph{160}{635--676}*

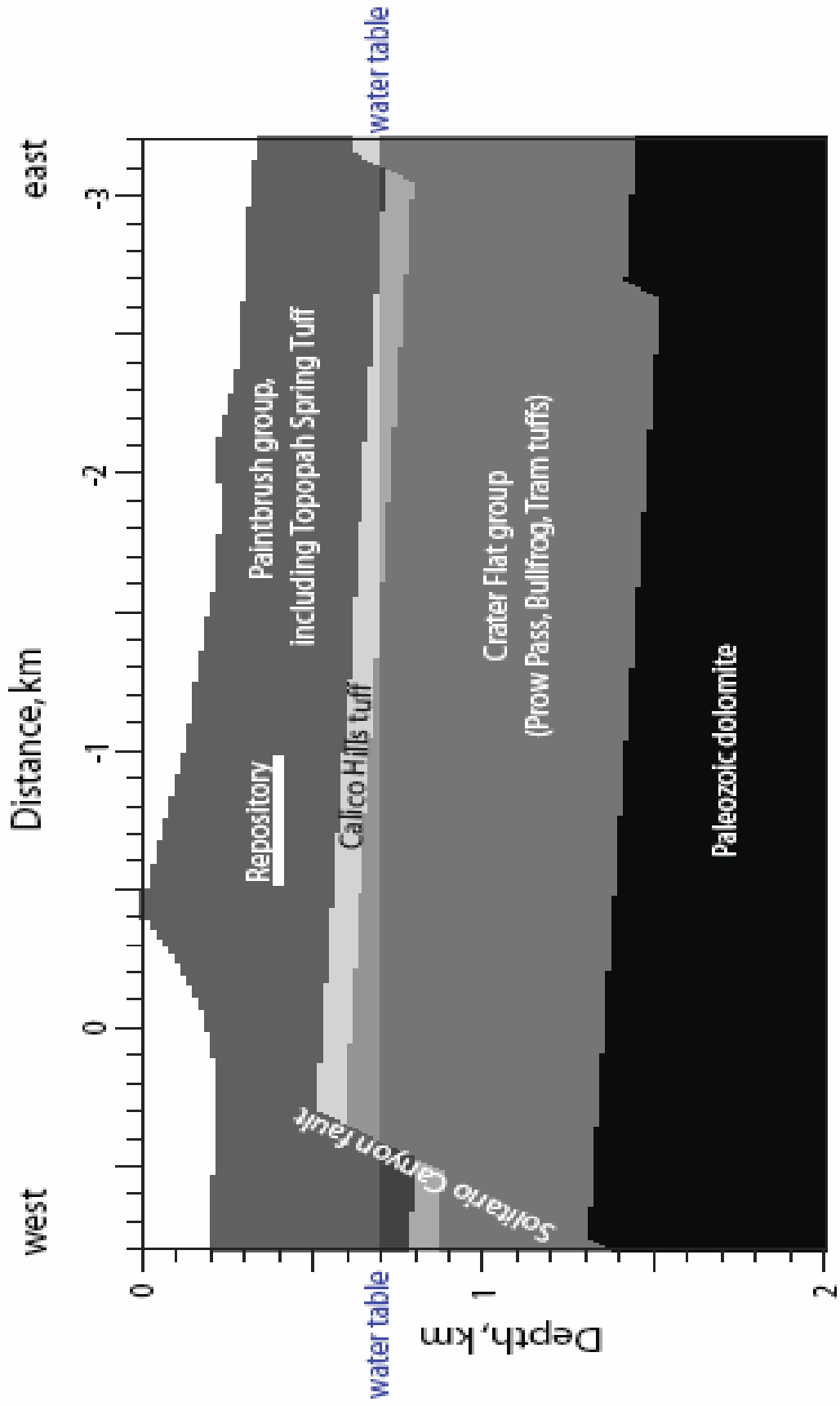
Press, W.H., S.A. Teukolsky, W.T. Vetterling, and B.P. Flannery (1992). *{\it Numerical Recipes in FORTRAN: The Art of Scientific Computing}*, Cambridge University Press, Cambridge, England, 963 pp.

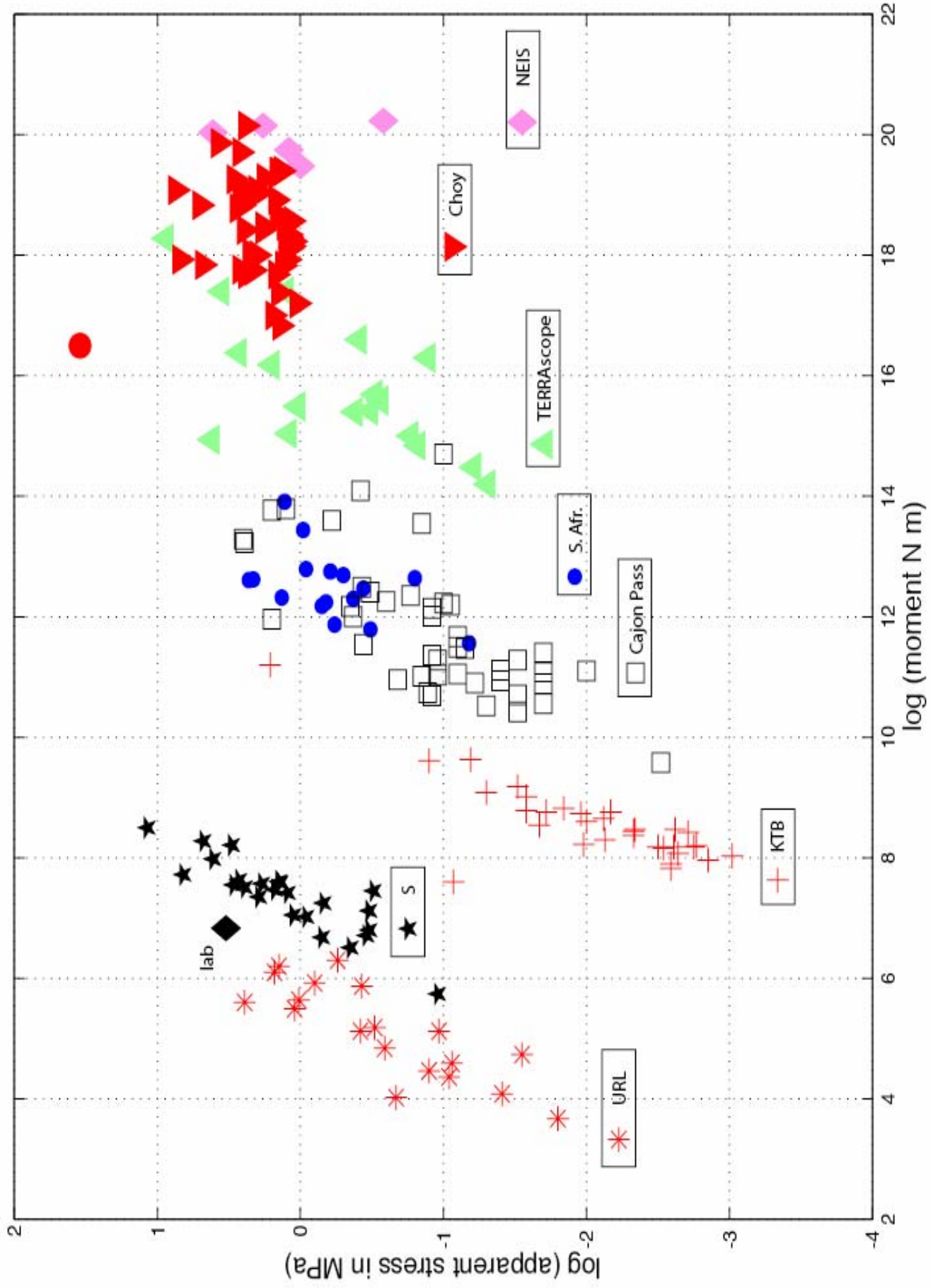
Singh, S. K. and M. Ordaz (1994). Seismic energy release in Mexican subduction earthquakes, *\bssa{84}{1533--1550}*

Constraints on stress parameter based on seismic and laboratory observations

A. McGarr







$$A(\omega) = CM_0 S(\omega, \omega_0) P(\omega, \omega_m) \frac{e^{-\omega R / 2Q\beta}}{R} \quad (5)$$

$$C = \frac{R_{\theta\phi} (FS)(PRTTN)}{4\pi\rho\beta^3} \quad (6)$$

$$S(\omega, \omega_0) = \frac{\omega^2}{1 + (\omega / \omega_0)^2} \quad (7)$$

$$P(\omega, \omega_m) = [1 + (\omega / \omega_m)^{2s}]^{-1/2} \quad (8)$$

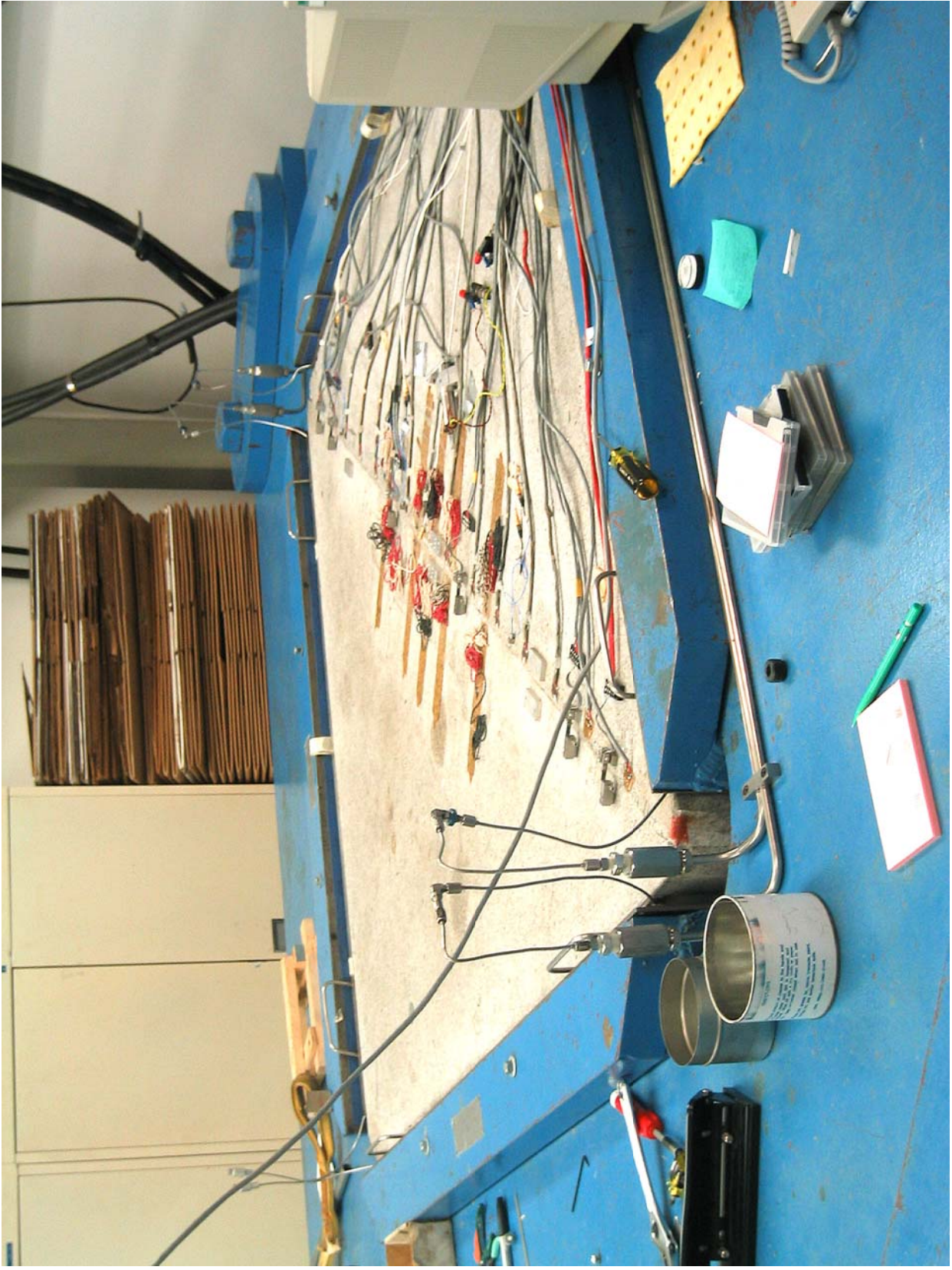
$$\omega_0 = 3.08\beta(\Delta\sigma / M_0)^{1/3} \quad (9)$$

$$V(\omega, \omega_0) = A(\omega, \omega_0) / \omega = \frac{\sqrt{0.4} M_0 \omega_0^2}{4\pi\rho\beta^3 R} \frac{\omega}{\omega^2 + \omega_0^2} \quad (10)$$

$$E_S = 4\rho\beta R^2 \int_0^\infty V(\omega, \omega_0)^2 d\omega \quad (11)$$

$$E_S = 0.233 M_0 \Delta\sigma / G \quad (12)$$

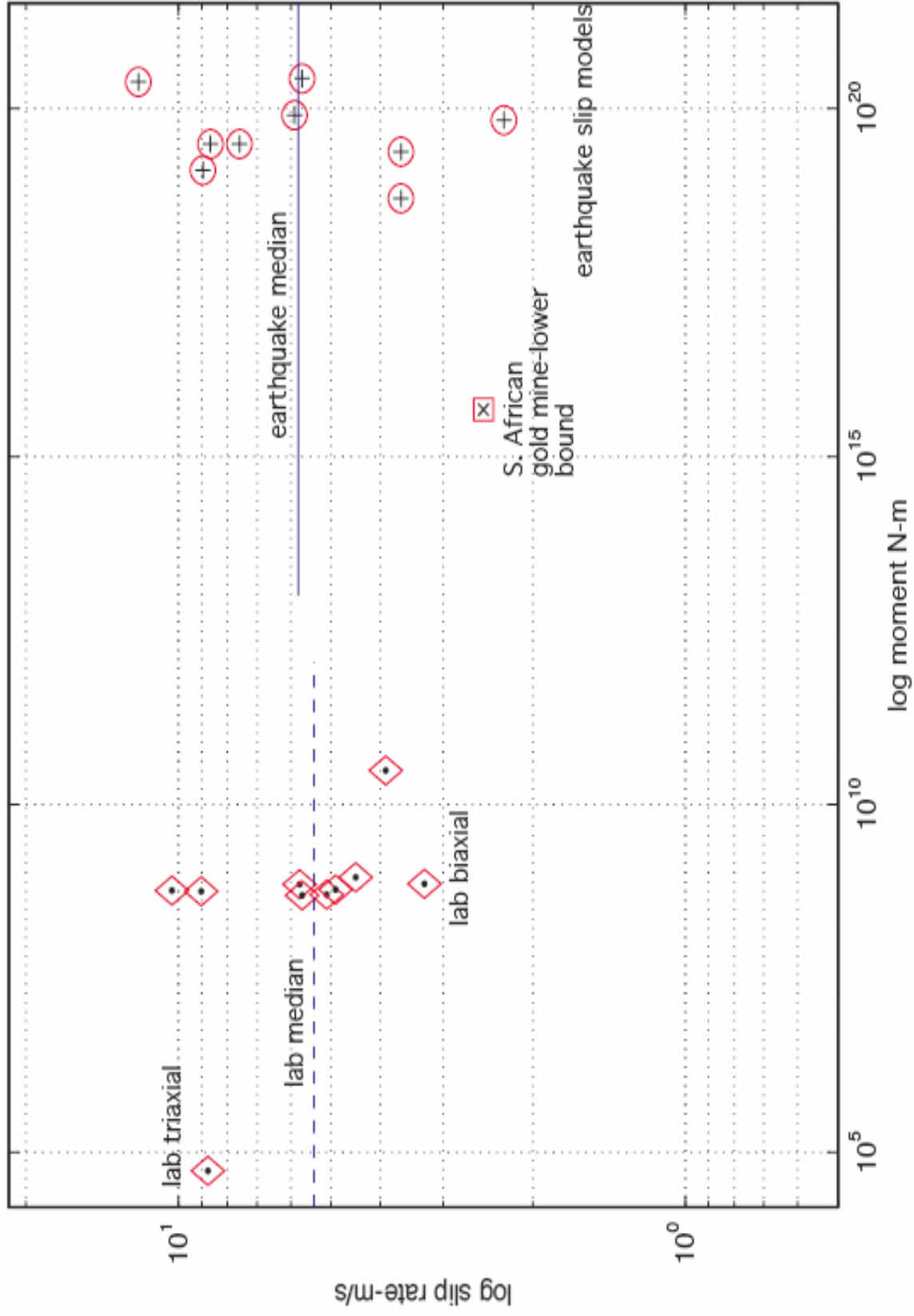
$$\tau_a = 0.233 \Delta\sigma \quad (13)$$



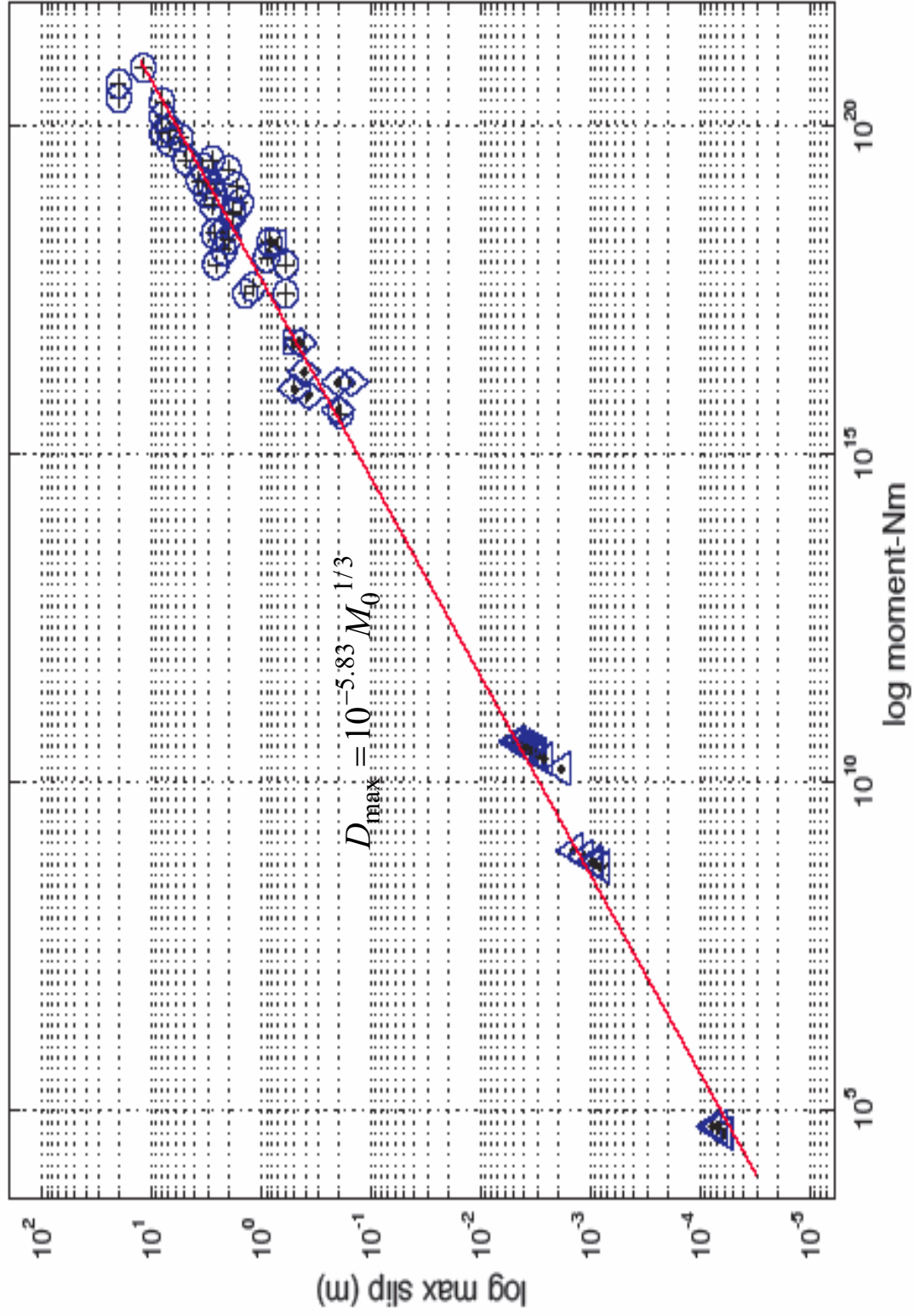
Laboratory adjustments to simulate earthquakes

- Loading stress factor: Effective normal stress at 6.8 km depth at KTB site/lab normal stress (108.2 MPa/lab normal stress)
- Stiffness adjustment: Replace lab fault surface with buried circular shear crack with same stiffness.
- For triaxial experiments, multiply by 2/3 to simulate more realistic biaxial tests.

Scaling of Maximum Slip Rate



Maximum Slip versus Seismic Moment-Continental Earthquakes and lab -slope of fit: 0.33



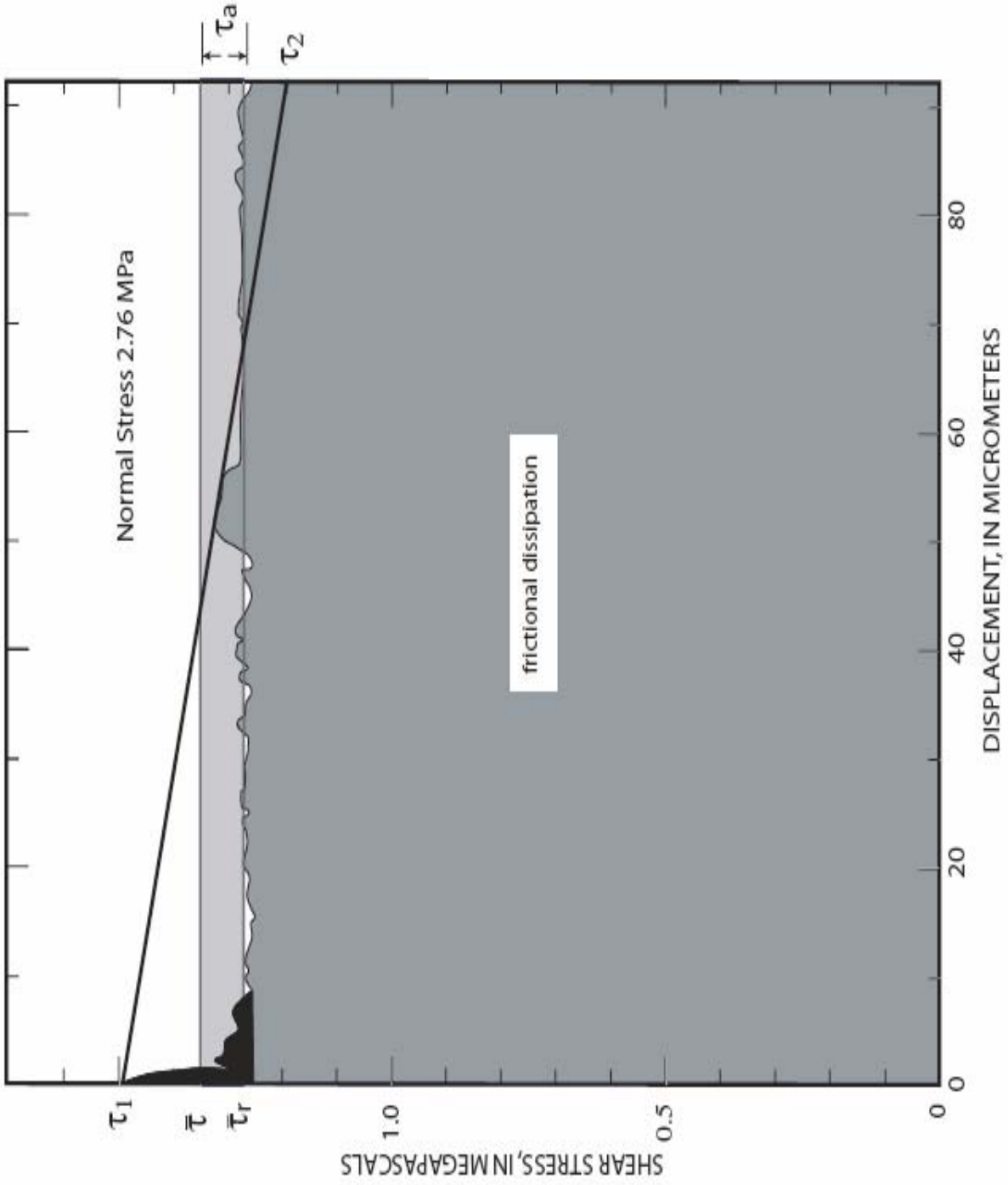


Table. Laboratory Stress Data, from Lockner and Okubo (1983)

Event	σ_n , MPa	$\Delta\sigma$, MPa	τ_n , MPa	$\Delta\sigma(ad)$, MPa	$\tau_a(ad)$, MPa	$\tau_a/\Delta\sigma$
5	1.66	0.2	0.04	13.0	2.61	0.20
6	1.66	0.23	0.01	15.0	0.65	0.04
7	2.21	0.24	0.06	11.8	2.94	0.25
8	2.21	0.28	0.05	13.7	2.45	0.18
9	2.76	0.31	0.08	12.2	3.14	0.26
10	2.76	0.32	0.07	12.5	2.74	0.22
11	3.31	0.48	0.07	15.7	2.29	0.15
12	3.31	0.42	0.10	13.7	3.27	0.24
13	4.41	0.42	0.17	10.3	4.17	0.40
14	4.41	0.47	0.15	11.5	3.68	0.32
15	4.41	0.39	0.09	9.6	2.21	0.23
16	4.41	0.44	0.09	10.8	2.21	0.20
17	4.41	0.24	0.11	5.9	2.70	0.46
18	4.41	0.35	0.12	8.6	2.94	0.34
19	3.45	0.42	0.07	13.2	2.20	0.17

Adjustment factor = $108.2/\sigma_n$ (KTB, 6.8 km depth)

med $\tau_a(ad)$ = 2.7 MPa

med $\Delta\sigma(ad)$ = 12.2 MPa

med $\tau_a/\Delta\sigma$ = 0.23

Table. Italian earthquake stress results; from Cocco and Rovelli (JGR, 1989)

Earthquake	$\Delta\sigma$, MPa	τ_a , MPa	$\tau_a/\Delta\sigma$
Valnerina	10.0	3.0	0.30
Ipinia	10.3	3.8	0.37
Ipinia	30.9	2.8	0.09
Umbria	17.2	3.4	0.20
Lazio Abruzzo	11.1	4.2	0.38
Lazio Abruzzo	14.3	3.3	0.23
Friuli	78.0	20.0	0.26
Friuli	35.3	6.0	0.17
Friuli	24.2	6.0	0.25
Friuli	32.5	9.5	0.29
Friuli	40.6	10.7	0.26
Friuli	43.0	6.2	0.14
Friuli	38.0	6.0	0.16
Montenegro	93.2	21.2	0.23

Med $\tau_a/\Delta\sigma = 0.24$

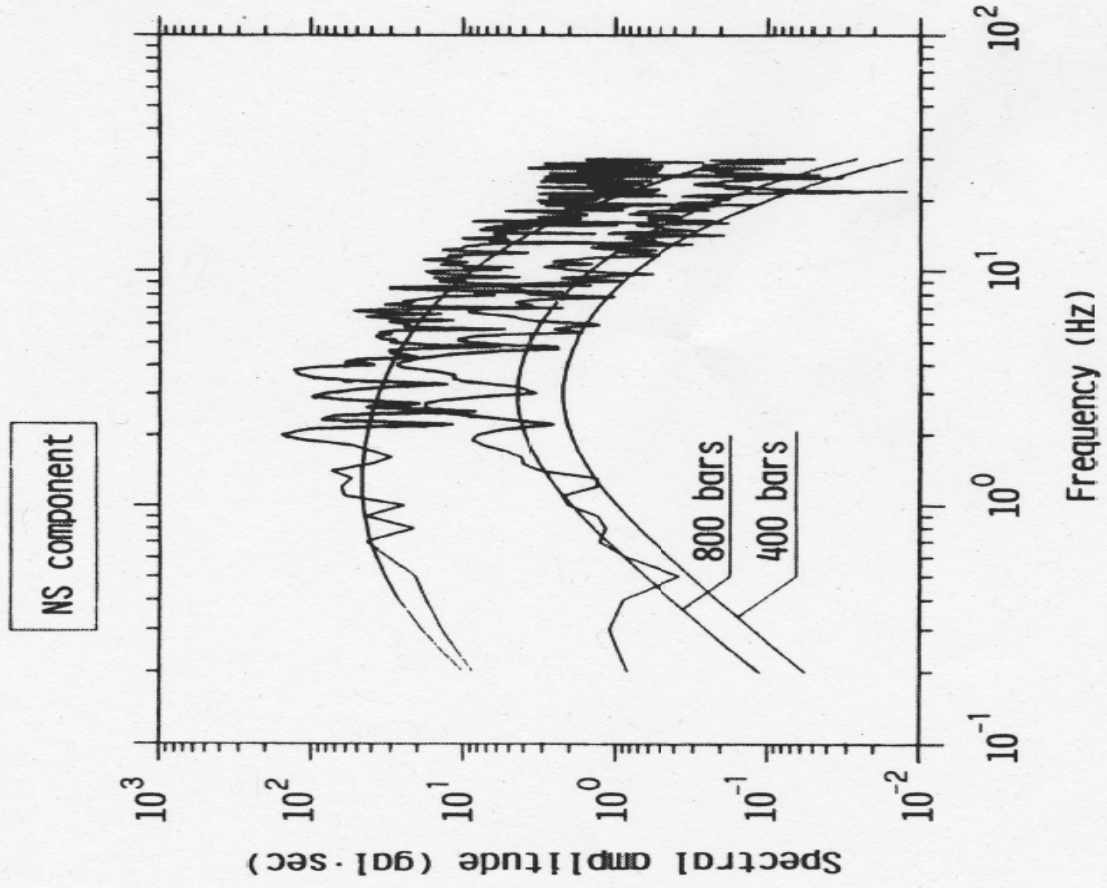
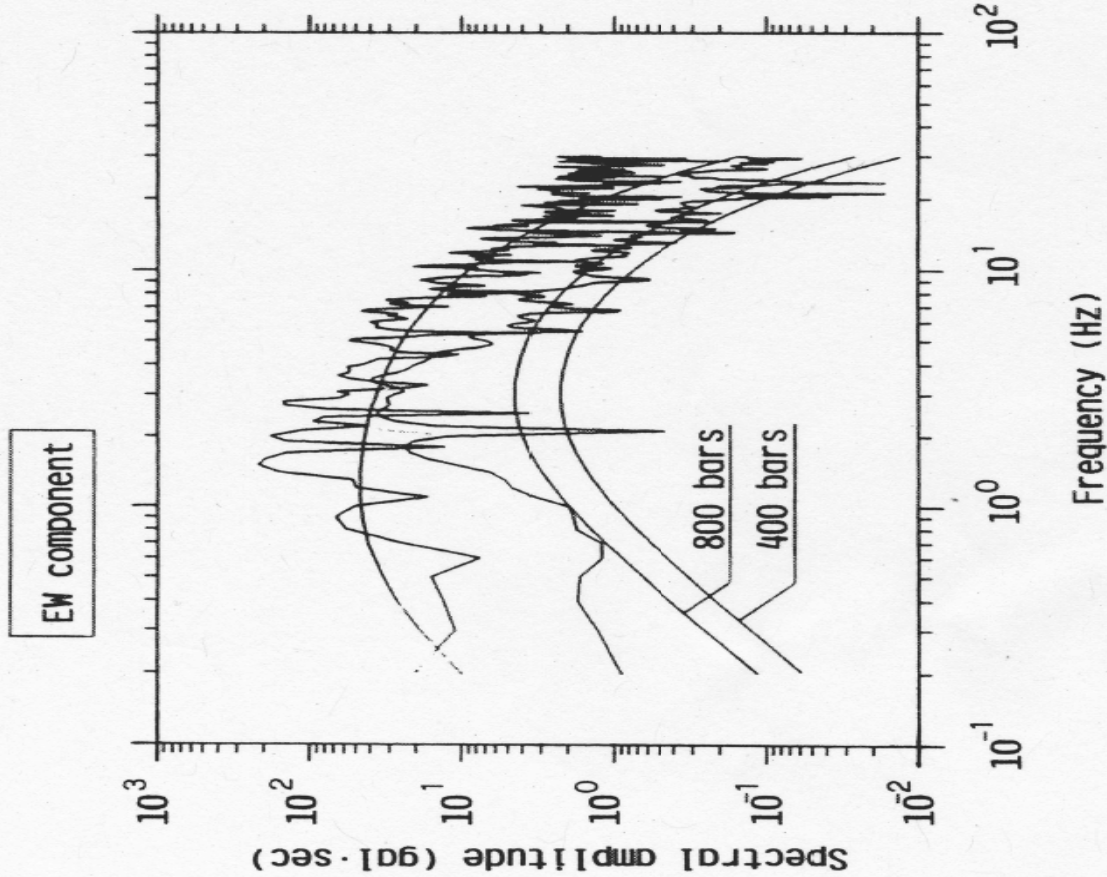


Fig. 8. Comparison between the theoretical spectral shape estimated from equation (1a) and data observed at Tolmezzo for the main shock and for the foreshock of the Friuli sequence. The theoretical spectrum of the foreshock has been drawn relative to two Brune stress drop values: 400 and 800 bars, respectively.

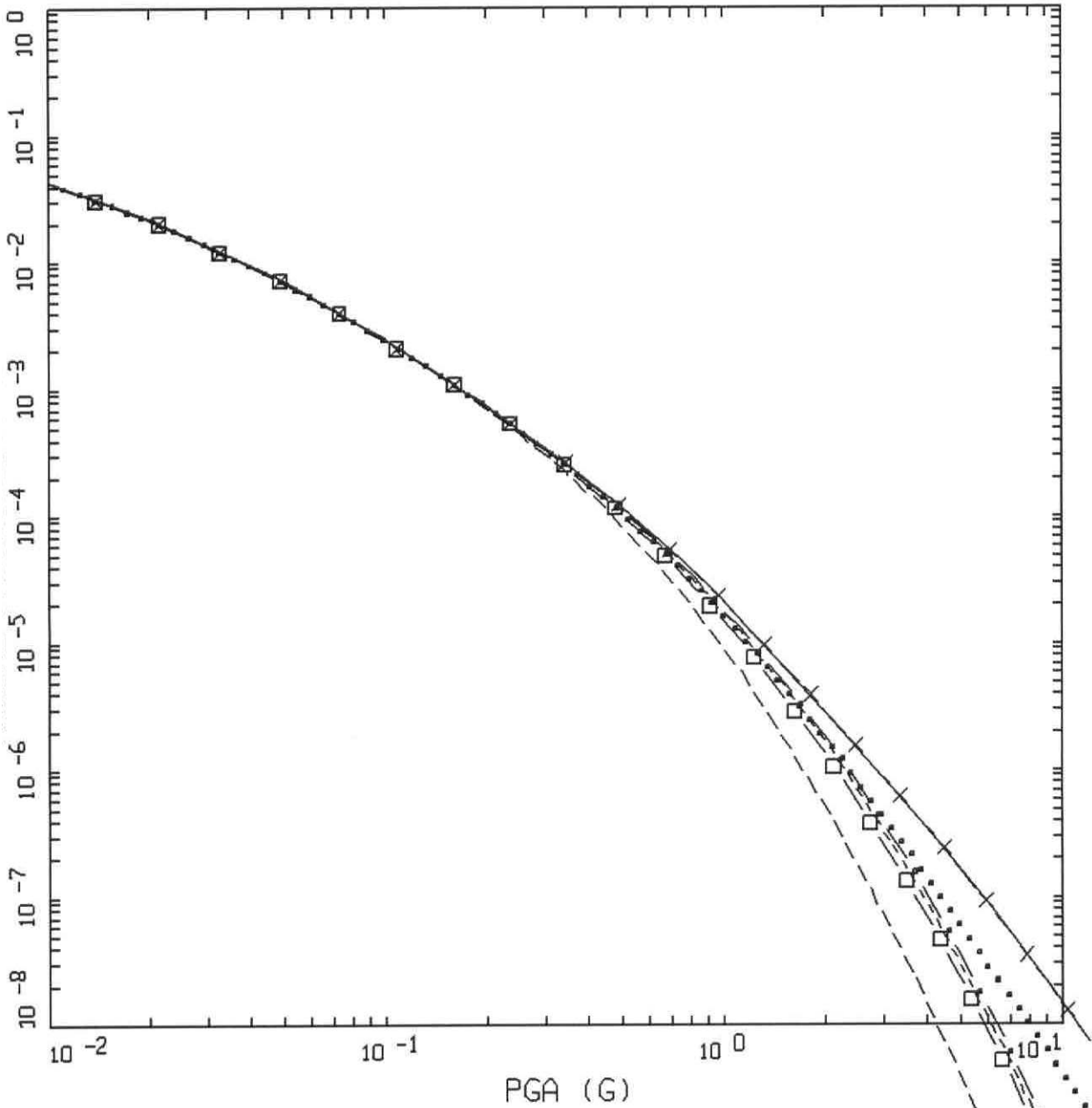
Acknowledgments. The authors wish to thank Jack Boatwright and Hiroo Kanamori for their helpful discussions and suggestions. We thank Jack Boatwright and Art McGarr for reviewing the manuscript and for helpful comments and Enzo Boschi for his encouragement to do research in this direction. Criticism and comments from Ornella Bonamassa, Dave Boore, Vladimir Keilis-Borok, Shri Singh; Aldo Zollo, Mustapha Megrhaoui, Maurizio Bonafede, Leonard Seeber, and Renato Funciello were very helpful throughout the development of this paper. Appreciation is expressed for Daniela Riposati's work in constructing many of the figures.

conclusions

- 1) Both lab results and point-source stochastic model suggest that apparent stress/stress drop = 0.23
- 2) Lab results and earthquake observations indicate that apparent stress depends on loading stresses but is independent of magnitude.

Stress Parameter - Feedback March 8th, 2007

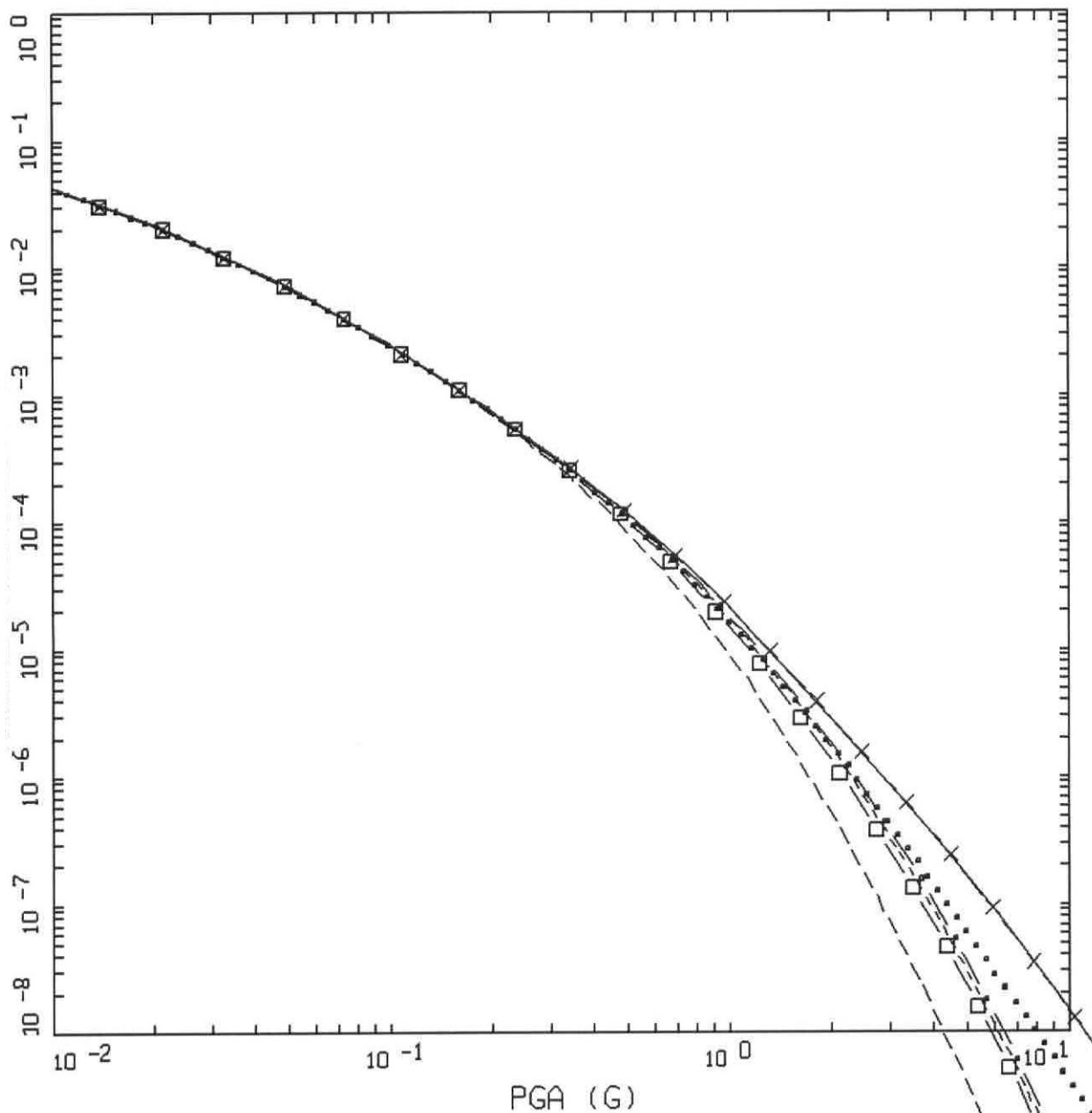
- W. Silva, R. Lee



YUCCA.06: HAZARD CURVE CONDT.
 STRESS DROP:PGA, COMBINED CASES

LEGEND

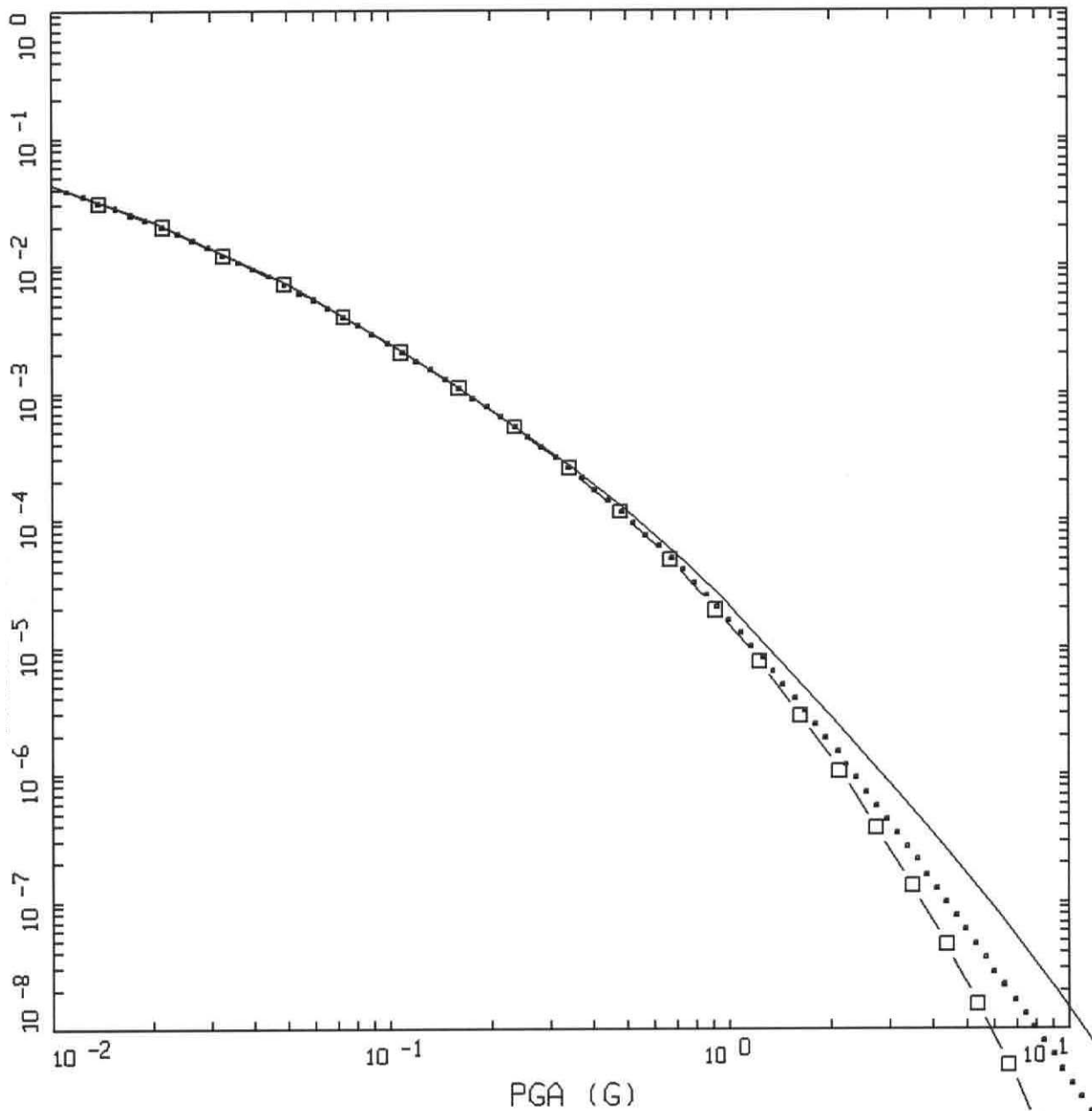
- INPUT MEAN HAZARD CURVE
- STRESS DROP CONDITIONED COMBINED MEAN HAZARD CURVE (EXPERTS 1-4)
- □ — STRESS DROP CONDITIONED COMBINED MEAN HAZARD CURVE (EXPERTS 1-3)
- STRESS DROP CONDITIONED MEAN HAZARD CURVE, EXPERT 1
- STRESS DROP CONDITIONED MEAN HAZARD CURVE, EXPERT 2
- • — STRESS DROP CONDITIONED MEAN HAZARD CURVE, EXPERT 3
- × — STRESS DROP CONDITIONED MEAN HAZARD CURVE, EXPERT 4



YUCCA.06: HAZARD CURVE CONDT.
 STRESS DROP:PGA, COMBINED CASES

LEGEND

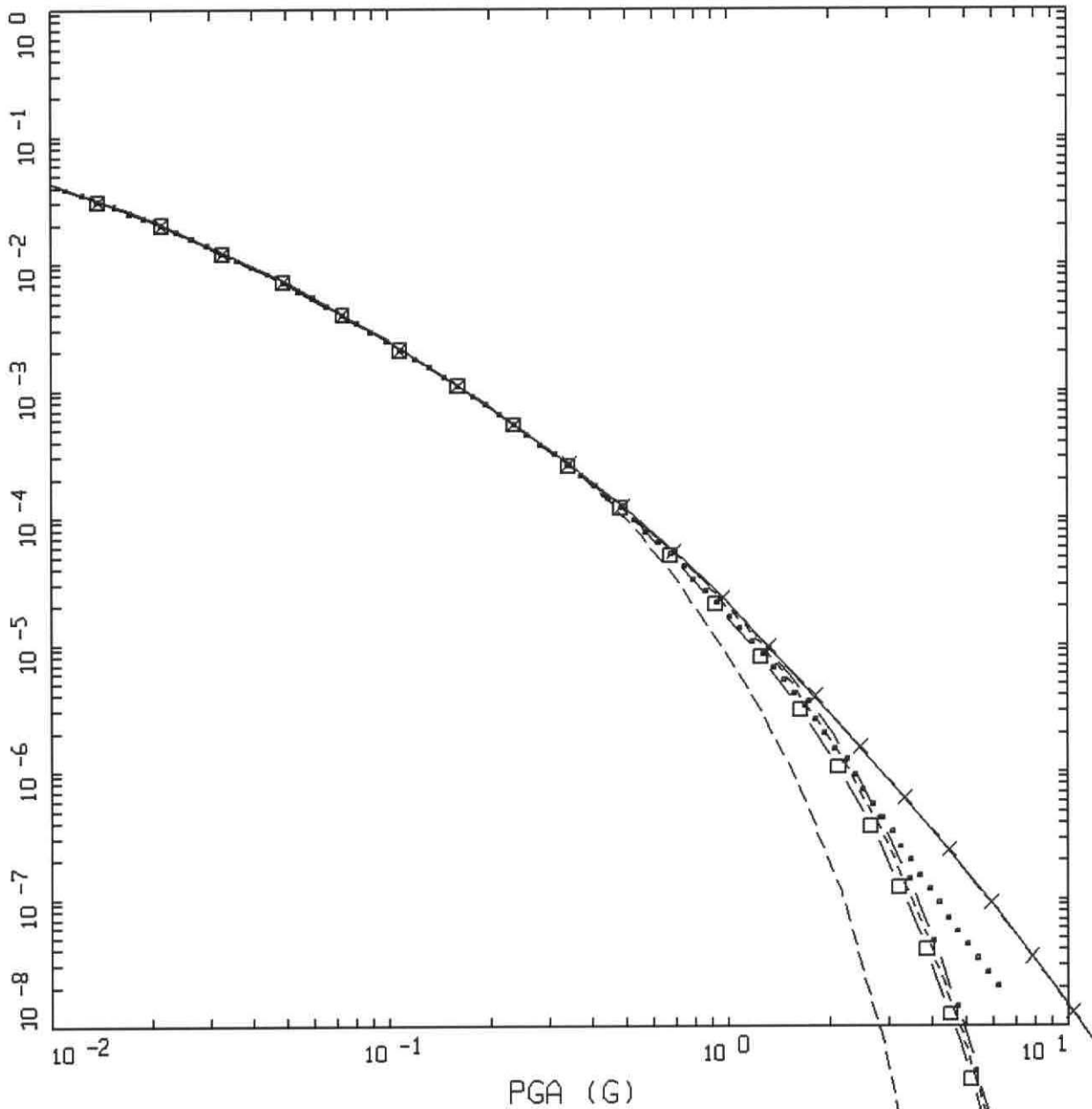
- INPUT MEAN HAZARD CURVE
- STRESS DROP CONDITIONED COMBINED MEAN HAZARD CURVE (EXPERTS 1-4)
- □ — STRESS DROP CONDITIONED COMBINED MEAN HAZARD CURVE (EXPERTS 1-3)
- STRESS DROP CONDITIONED MEAN HAZARD CURVE, EXPERT 1
- . - . STRESS DROP CONDITIONED MEAN HAZARD CURVE, EXPERT 2
- • — STRESS DROP CONDITIONED MEAN HAZARD CURVE, EXPERT 3
- × — STRESS DROP CONDITIONED MEAN HAZARD CURVE, EXPERT 4



YUCCA.06: HAZARD CURVE CONDT.
 STRESS DROP:PGA, COMBINED CASES

LEGEND

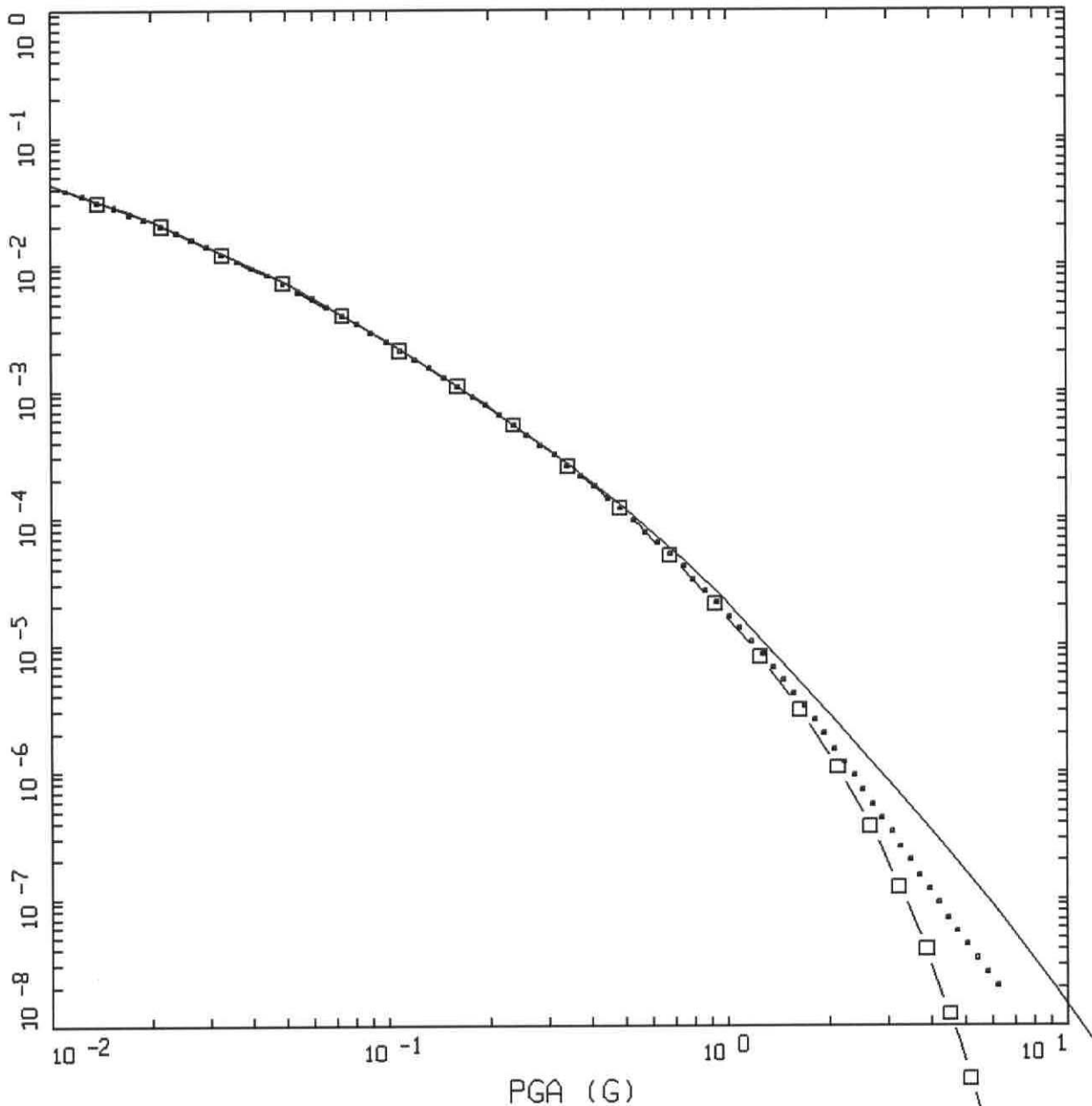
- INPUT MEAN HAZARD CURVE
- STRESS DROP CONDITIONED COMBINED MEAN HAZARD CURVE (EXPERTS 1-4)
- □ - STRESS DROP CONDITIONED COMBINED MEAN HAZARD CURVE (EXPERTS 1-3)



YUCCA.06: HAZARD CURVE CONDT.
 STRESS DROP:PGA, COMB, SIGMA=0.3

LEGEND

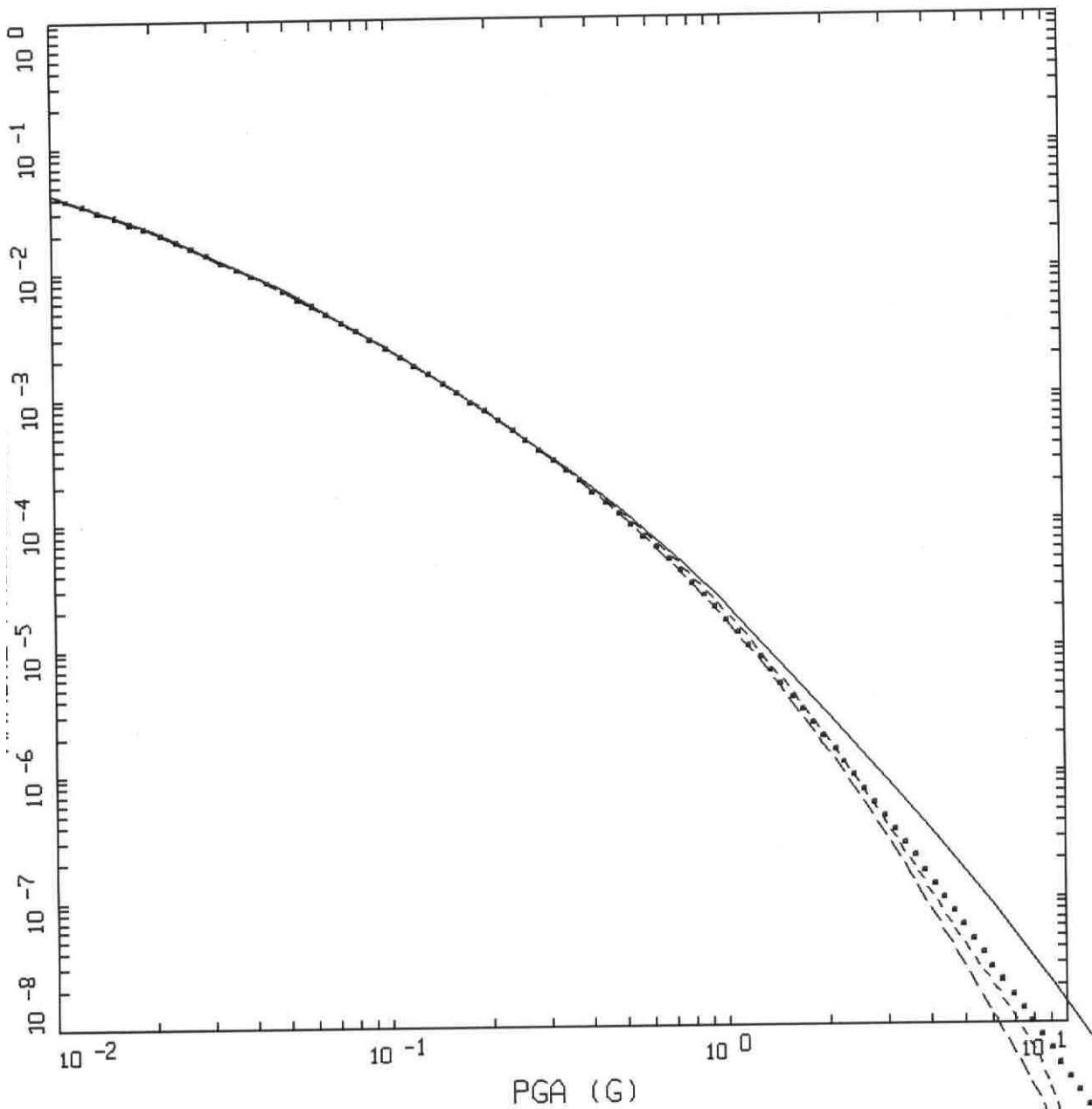
- INPUT MEAN HAZARD CURVE
- STRESS DROP CONDITIONED COMBINED MEAN HAZARD CURVE (EXPERTS 1-4)
- STRESS DROP CONDITIONED COMBINED MEAN HAZARD CURVE (EXPERTS 1-3)
- STRESS DROP CONDITIONED MEAN HAZARD CURVE, EXPERT 1
- STRESS DROP CONDITIONED MEAN HAZARD CURVE, EXPERT 2
- . - - STRESS DROP CONDITIONED MEAN HAZARD CURVE, EXPERT 3
- x - - STRESS DROP CONDITIONED MEAN HAZARD CURVE, EXPERT 4



YUCCA.06: HAZARD CURVE CONDT.
 STRESS DROP:PGA, COMB, SIGMA=0.3

LEGEND

- INPUT MEAN HAZARD CURVE
- STRESS DROP CONDITIONED COMBINED MEAN HAZARD CURVE (EXPERTS 1-4)
- □ - STRESS DROP CONDITIONED COMBINED MEAN HAZARD CURVE (EXPERTS 1-3)



YUCCA.06: HAZARD CURVE CONDT.
 STRESS+STRAIN:PGA, COMBINED

LEGEND

- INPUT MEAN HAZARD CURVE
- STRESS DROP CONDITIONED MEAN HAZARD CURVE
- STRAIN CONDITIONED MEAN HAZARD CURVE
- . - . - STRES DROP + STRAIN CONDITIONED MEAN HAZARD CURVE

Issues

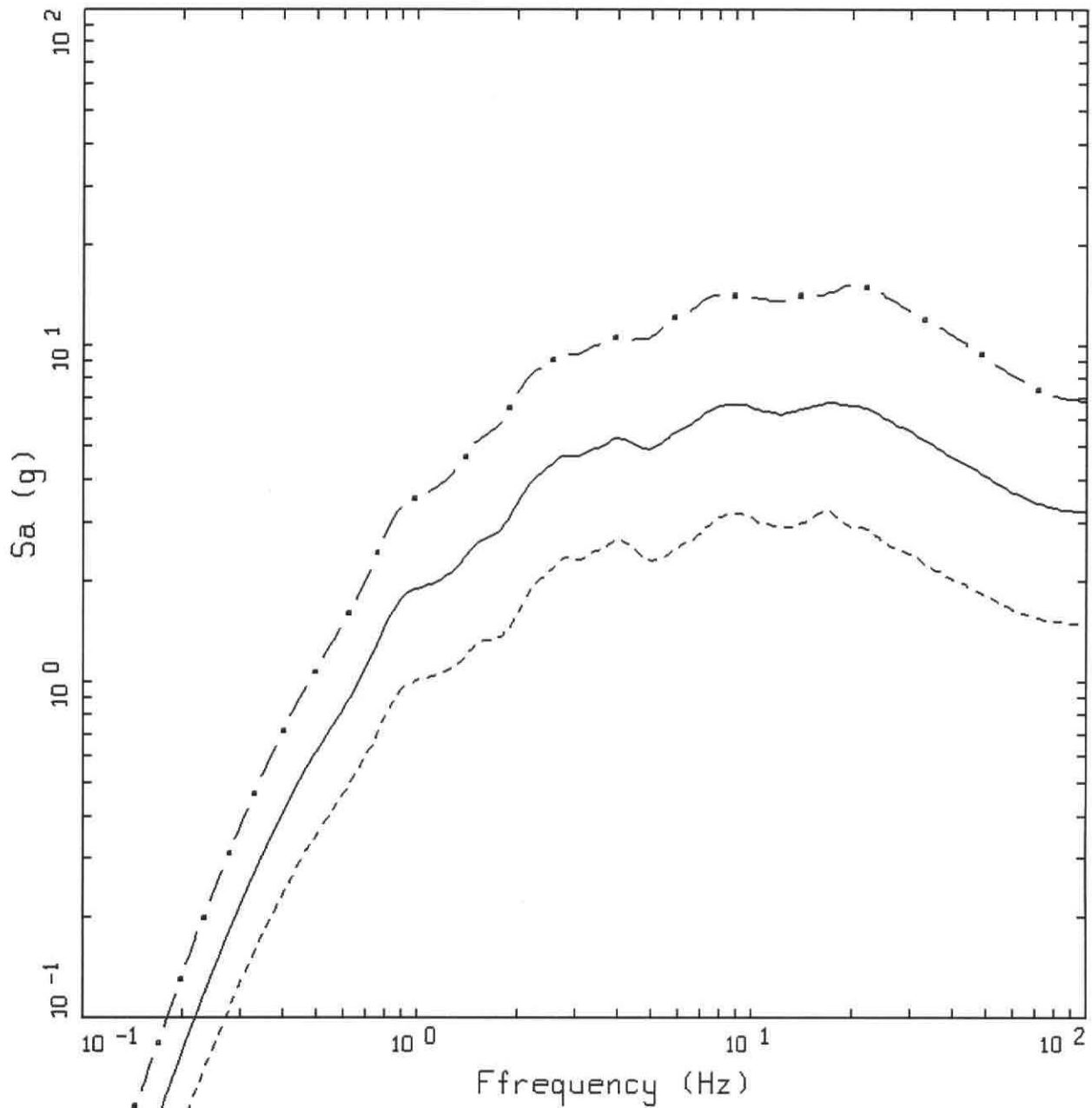
- Pt. A limiting stress parameter pga distribution

Impact of varying $\Delta\sigma$, depth, κ , profile

$$\sigma_{In} = 0.76$$

Impact of varying depth only (3-20 km)

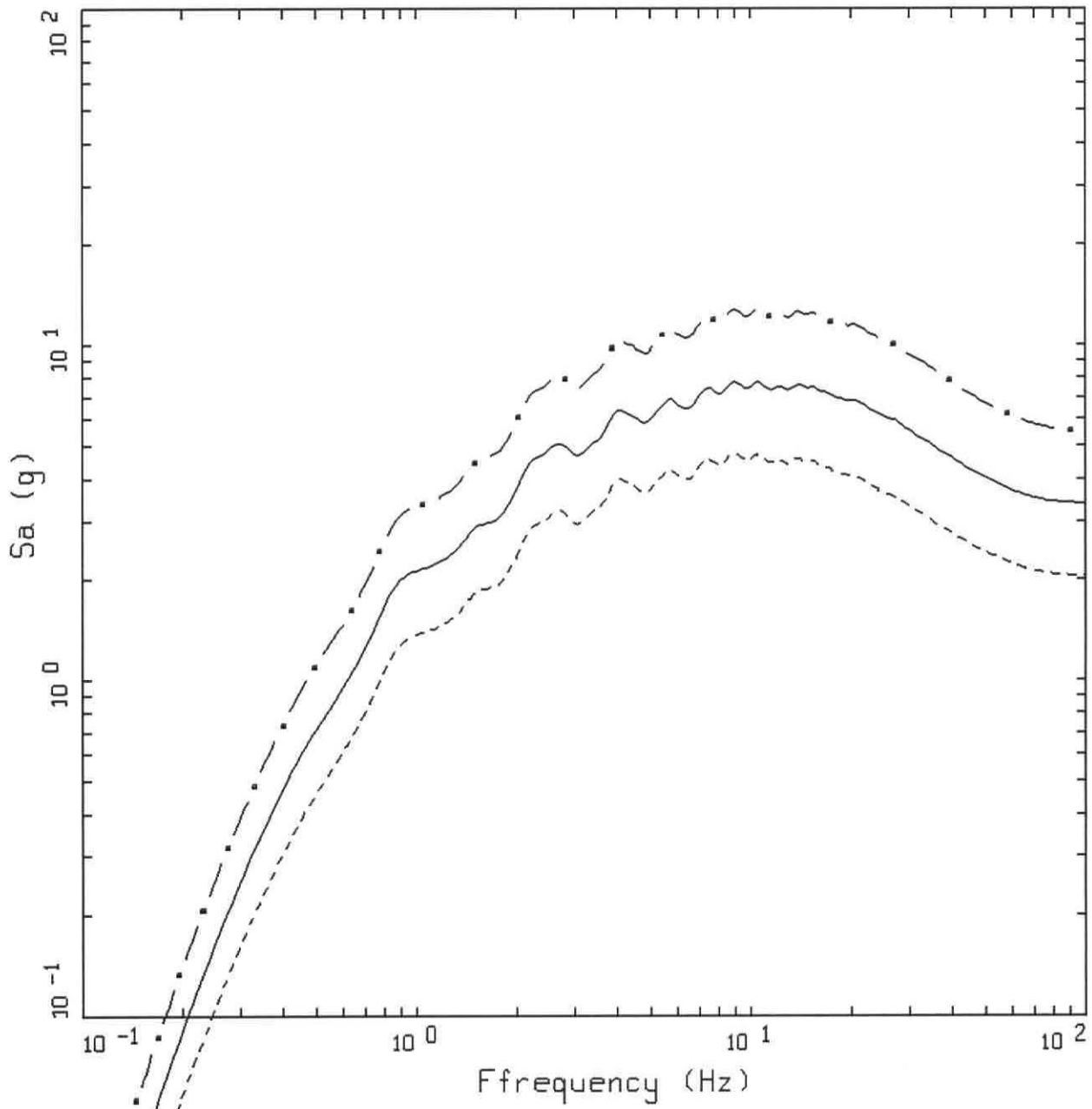
Basis for $\sigma_{In} = 0.?$



M = 6.5, D = 1 KM, SDRP = 1000 BARS
 DEPTH = 8 KM

LEGEND

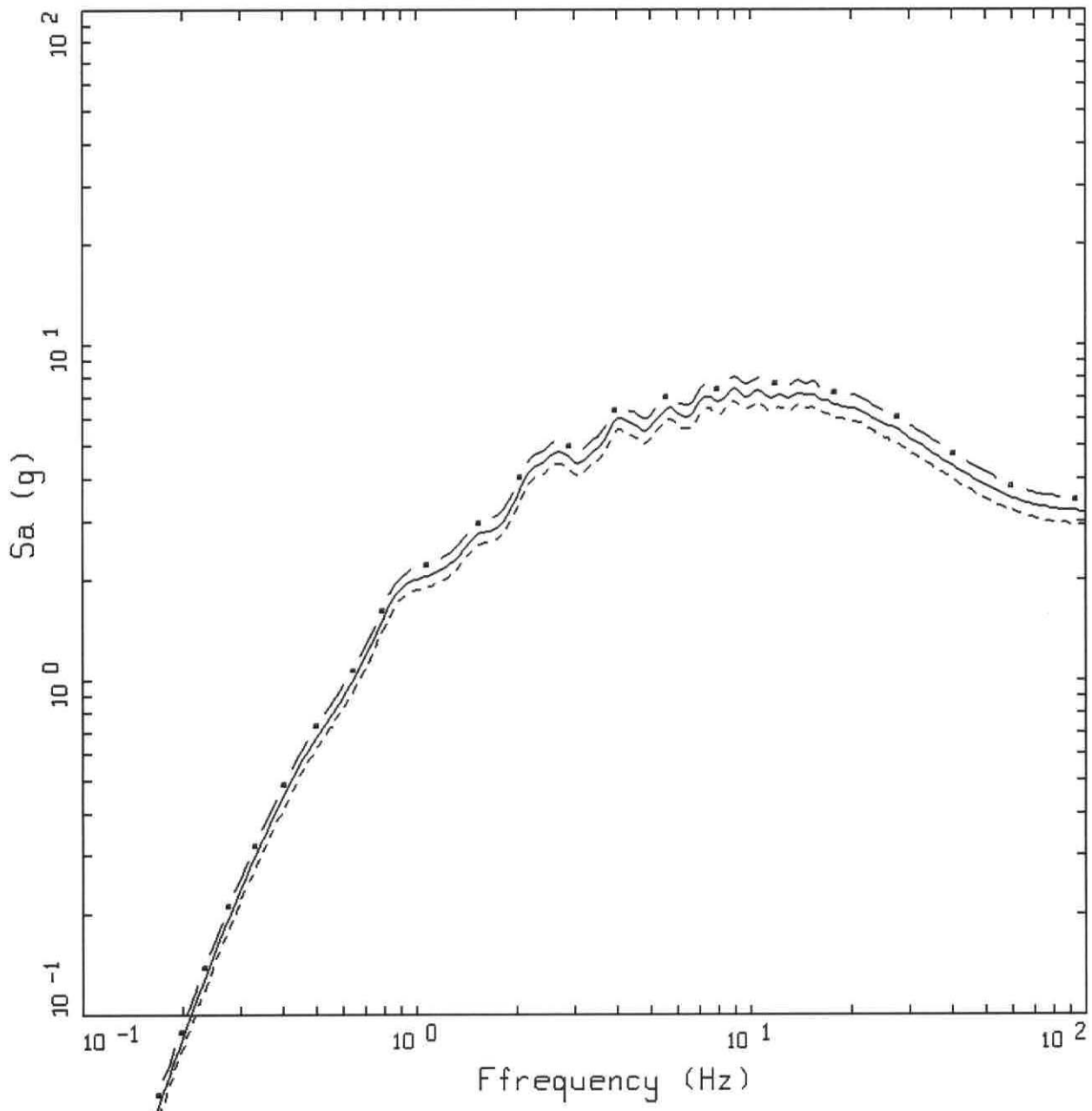
- - - 84TH PERCENTILE, PARAMETRIC UNCERTAINTY; PGA = 6.828 G
- 50TH PERCENTILE, PARAMETRIC UNCERTAINTY; PGA = 3.183 G
- - - 16TH PERCENTILE, PARAMETRIC UNCERTAINTY; PGA = 1.484 G



M = 6.5, D = 1 KM, SDROP = 1000 BARS
 DEPTH = 8 KM, DEPTH RANDOMIZATION ONLY

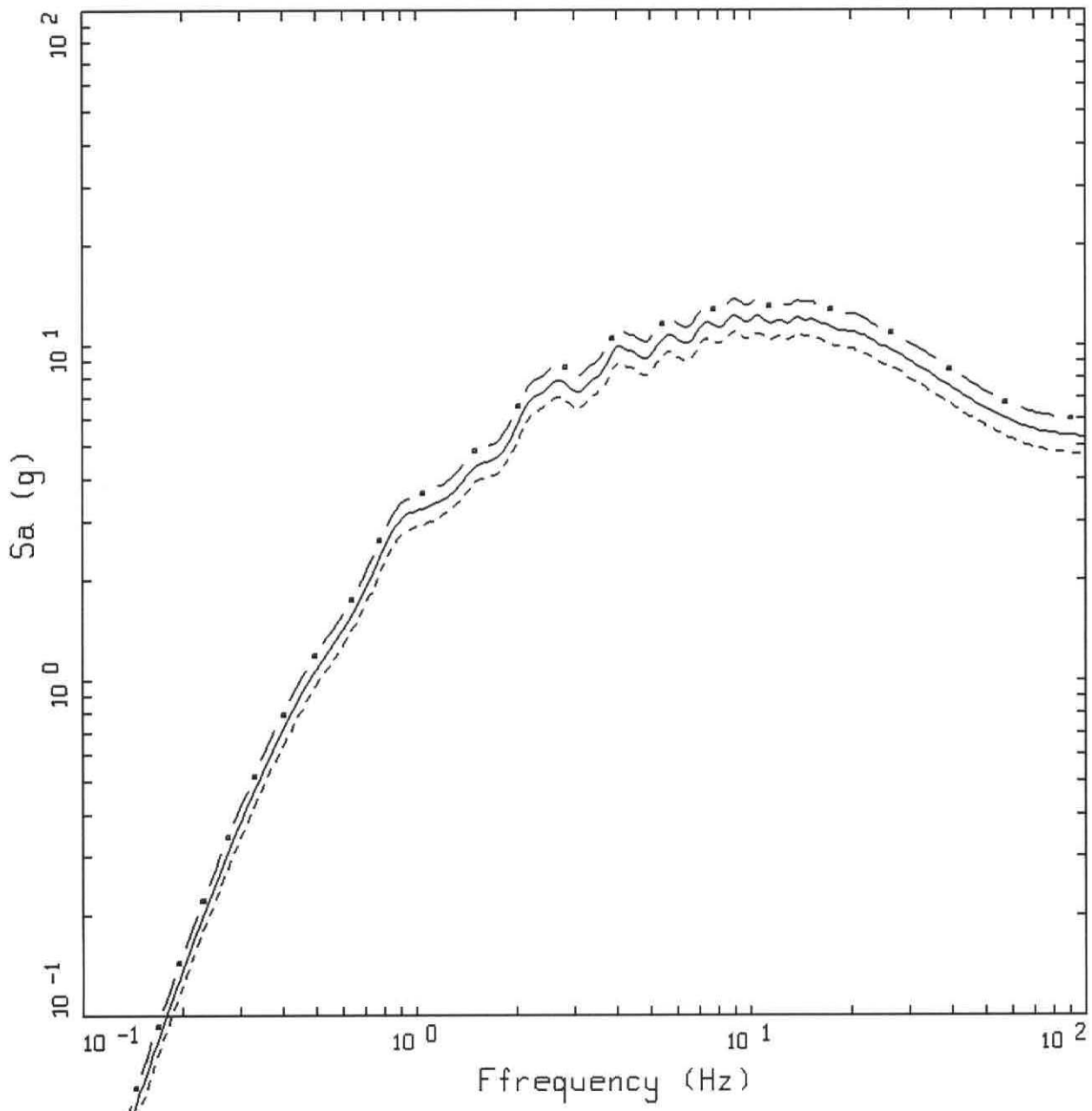
LEGEND

- - - 84TH PERCENTILE, PARAMETRIC UNCERTAINTY; PGA = 5.515 G
- 50TH PERCENTILE, PARAMETRIC UNCERTAINTY; PGA = 3.353 G
- - - 16TH PERCENTILE, PARAMETRIC UNCERTAINTY; PGA = 2.038 G



M = 6.5, D = 1 KM, SDROP = 1000 BARS
 DEPTH = 8 KM, 1 KM VARIATION

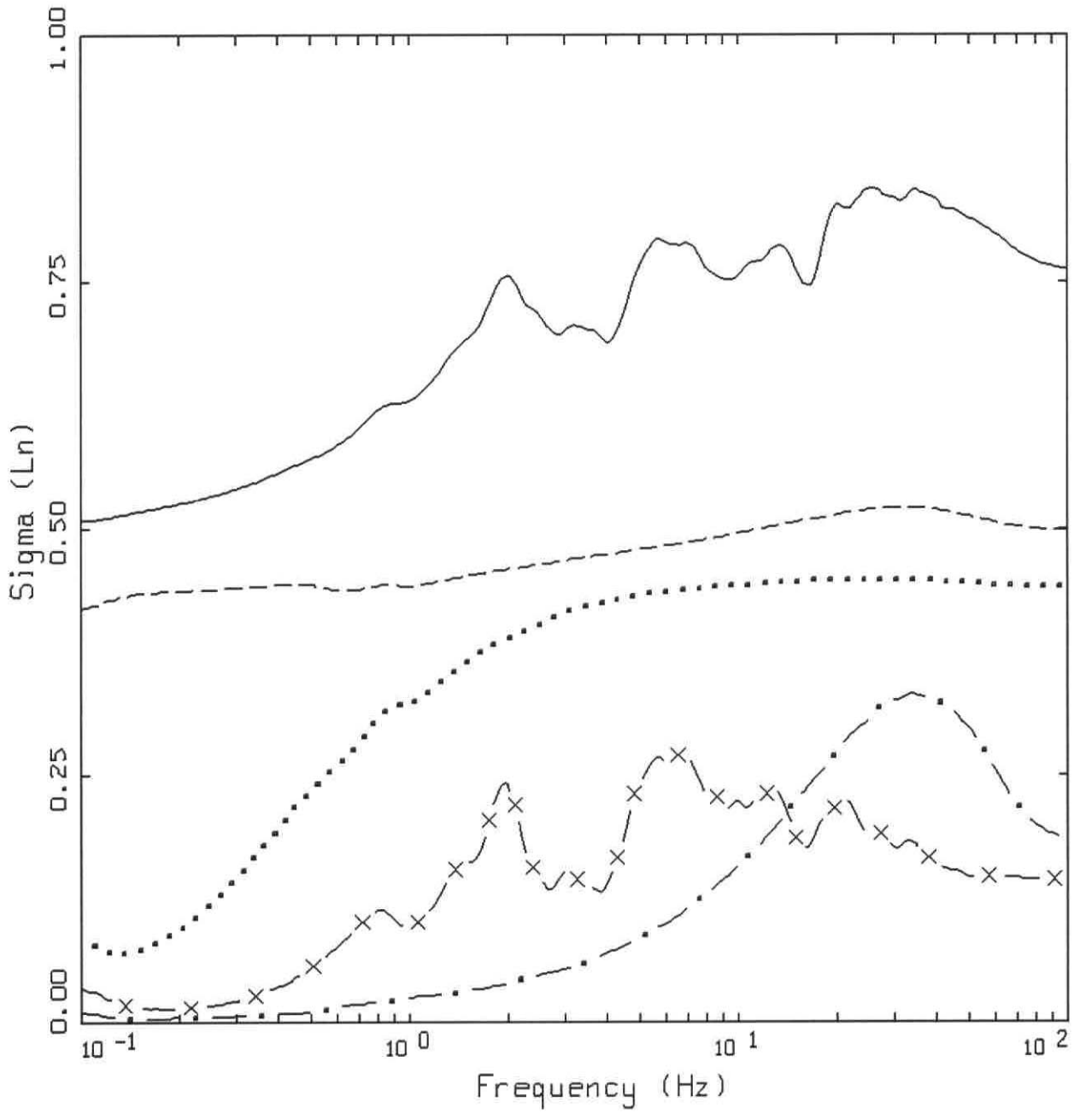
- LEGEND
- • — 84TH PERCENTILE, PARAMETRIC UNCERTAINTY; PGA = 3.457 G
 - 50TH PERCENTILE, PARAMETRIC UNCERTAINTY; PGA = 3.171 G
 - - - 16TH PERCENTILE, PARAMETRIC UNCERTAINTY; PGA = 2.909 G



M = 6.5, D = 1 KM, SDROP = 1000 BARS
 DEPTH = 5 KM, VARIATION 1 KM

LEGEND

- • — 84TH PERCENTILE, PARAMETRIC UNCERTAINTY; PGA = 5.980 G
- 50TH PERCENTILE, PARAMETRIC UNCERTAINTY; PGA = 5.318 G
- - - 16TH PERCENTILE, PARAMETRIC UNCERTAINTY; PGA = 4.729 G



- LEGEND
- VARIATION OF ALL
 - VARIATION OF STRESS DROP, SIGMA(LN) = 0.5
 - - - VARIATION OF SOURCE DEPTH, SIGMA(LN) = 0.5
 - . - VARIATION OF KAPPA, SIGMA(LN) = 0.3
 - x - VARIATION OF PROFILE

Revised 3/8/07

Maximum Stress Parameters from Adjusted Laboratory Results

The results from 15 stick-slip friction experiments are listed in the Table 1. The static stress drops $\Delta\sigma$ and the apparent stresses τ_a have been adjusted to the loading stresses measured at a depth of 6.8 km at the KTB site, Germany where the normal stress acting on optimally-oriented fault planes is 108.2 MPa. That is, the stress adjustment factor is $108.2 \text{ MPa}/\sigma_n$. This adjustment to midcrustal stress conditions yields stress drops and apparent stresses that are fairly typical for earthquakes, as seen in the Table. These adjusted stresses are conservative inasmuch as the loading stresses at 8 km depth in the extensional stress regime below Yucca Mountain are much less according to lab-based crustal strength estimates (e.g., Brace and Kohlstedt, 1980); in fact, the effective normal stress acting on a fault optimally oriented for failure below Yucca Mountain is approximately 54 MPa, for a typical coefficient of friction of 0.75. If the coefficient of friction is 0.6 then the effective normal stress would be 65 MPa. For any likely coefficient of friction, the crustal strength at 8 km below Yucca Mountain is much less than at the KTB site at depth 6.8 km.

Table 1. Laboratory Stress Data, from Lockner and Okubo (1983)

Event	σ_n MPa	$\Delta\sigma$ MPa	τ_a MPa	$\Delta\sigma(\text{ad})$ MPa	$\tau_a(\text{ad})$ MPa	$\tau_a/\Delta\sigma$
5	1.66	0.2	0.04	13.0	2.61	0.20
6	1.66	0.23	0.01	15.0	0.65	0.04
7	2.21	0.24	0.06	11.8	2.94	0.25
8	2.21	0.28	0.05	13.7	2.45	0.18
9	2.76	0.31	0.08	12.2	3.14	0.26
10	2.76	0.32	0.07	12.5	2.74	0.22
11	3.31	0.48	0.07	15.7	2.29	0.15
12	3.31	0.42	0.10	13.7	3.27	0.24
13	4.41	0.42	0.17	10.3	4.17	0.40
14	4.41	0.47	0.15	11.5	3.68	0.32
15	4.41	0.39	0.09	9.6	2.21	0.23
16	4.41	0.44	0.09	10.8	2.21	0.20
17	4.41	0.24	0.11	5.9	2.70	0.46
18	4.41	0.35	0.12	8.6	2.94	0.34
19	3.45	0.42	0.07	13.2	2.20	0.17

For these results, the median value of $\Delta\sigma(\text{ad})$ is 12.2 MPa. The arithmetic average for $\Delta\sigma(\text{ad})$ is 11.8 MPa with a standard deviation of 2.5 MPa. The distribution of $\log\Delta\sigma$ (base 10) has a mean of 1.06 with a standard deviation of 0.11. That is, the geometric mean is 11.5 MPa. I consider this lognormal distribution to be the most realistic for purposes of estimating the likelihood of a given value being exceeded.

To calculate likely upper limits for the stress parameter based on the laboratory results I have considered the geometric mean + 1σ , geometric mean + 2σ and the geometric mean + 5σ , which are 14.8, 19.1, and 40.7 MPa, respectively. The assigned weights for these three possibilities are 0.2, 0.5, and 0.3, respectively.

I have two reasons for assuming that the laboratory stress drops listed in the Table 1 are equivalent to stress parameters. First, as formulated from the so-called Brune spectrum, the stress parameter should be the same as the static stress drop. Second, these laboratory stresses show exactly the same behavior as those derived from the acceleration spectra given in Boore (1983). That is, from this spectrum, Singh and Ordaz (1994) showed that $\tau_a/\Delta\sigma=0.23$, which is in perfect agreement with the median of the same ratios listed in the Table 1.

Laboratory results (Table 2) for eight stick-slip events whose rupture surfaces were contained in the central portion of the fault (Lockner et al., 1982) provide some confirmation of those listed in Table 1.

Table 2. Laboratory stress data from Lockner et al. (1982)

Event	σ_n MPa	$\Delta\sigma$ MPa	$\Delta\sigma(\text{ad})$ MPa
1	0.63	0.063	10.8
2	1.32	0.11	9.0
3	2.76	0.25	9.8
4	3.45	0.29	9.1
5	3.6	0.32	9.6
6	3.45	0.4	12.5
7	3.5	0.39	12.1
8	4.1	0.45	11.9

For the results in Table 2, the median value of $\Delta\sigma$ (ad) is 10.3 MPa. The arithmetic mean is 10.6 MPa with a standard deviation of 1.4. The mean of $\log\Delta\sigma$ (ad) is 1.02 with a standard deviation of 0.06; that is, the geometric mean is 10.5 MPa. Thus, the results listed in Table 2 give nearly the same average values for the adjusted stress parameter as those in Table 1.

More details on relating laboratory results to their earthquake counterparts can be found in McGarr and Fletcher (2003).

References.

Boore, D. M. (1983). Stochastic simulation of high-frequency ground motions based on seismological models of the radiated spectra, *Bull. Seismol. Soc. Am.*, **73**, 1865-1894.

Brace, W. F. and D. L. Kohlstedt (1980). Limits on lithospheric stress imposed by laboratory experiments, *J. Geophys. Res.*, **85**, 6248-6252.

Lockner, D. A. and P. G. Okubo (1983). Measurements of frictional heating in granite, *J. Geophys. Res.*, **88**, 4313-4320.

Lockner, D. A., P. G. Okubo, and J. H. Dieterich (1982). Containment of stick-slip failures on a simulated fault by pore fluid injection, *Geophys. Res. Lett.*, **9**, 801-804.

McGarr, A. and J. B. Fletcher (2003). Maximum slip in earthquake fault zones, apparent stress, and stick-slip friction, *Bull. Seismol. Soc. Am.*, **93**, 2355-2362.

Singh, S. K. and M. Ordaz (1994). Seismic energy release in Mexican subduction zone earthquakes, *Bull. Seismol. Soc. Am.*, **84**, 1533-1550.

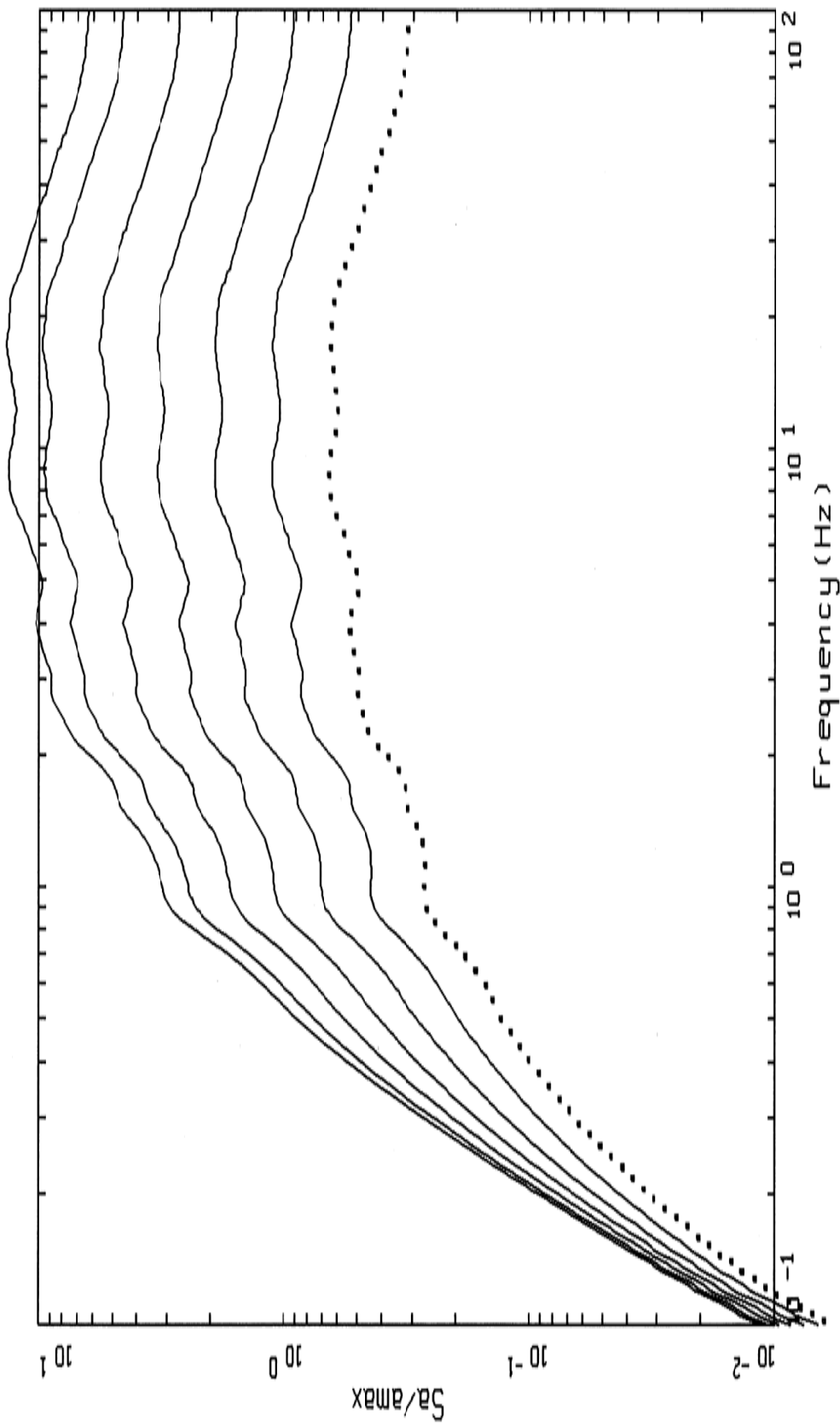
Art McGarr

Meeting 4/4/07

- Presentation by W. Silva

April 2, 2007

Expert	Current $\Delta\sigma_{\max}^{\text{HF}}$, Weights				
	Weights	$\Delta\sigma_{\max}^{\text{HF}}$ (bars)	mean $\Delta\sigma_{\max}^{\text{HF}}$ (bars)	Weights	Class Weights
1	0.25	333		0.2	0.2 (0.8)
		500	517	0.6	0.2 (0.8)
		750		0.2	0.2 (0.8)
		667		0.2	0.8 (0.2)
		1000	1033	0.6	0.8 (0.2)
	1500	930 (620)	0.2	0.8 (0.2)	
2					
	0.25	150		0.2	
		190	247	0.5	
			0.3		
3					
	0.25	800 (667)		0.2	
		1000	1060 (1033)	0.6	
			0.2		
			746		
4					
	0.25		50, $\sigma_{\text{in}} = 0.5$		



HORIZONTAL SPECTRA, POINT A
M=6.5, D=01 KM, SD = VARY

LEGEND			
.....	5 %	SD = 50 BARS,	PGA = 0.309 G, PGV = 25.32 CM/SEC
_____	5 %	SD = 100 BARS,	PGA = 0.534 G, PGV = 40.21 CM/SEC
_____	5 %	SD = 200 BARS,	PGA = 0.918 G, PGV = 63.19 CM/SEC
_____	5 %	SD = 400 BARS,	PGA = 1.570 G, PGV = 98.93 CM/SEC
_____	5 %	SD = 800 BARS,	PGA = 2.673 G, PGV = 151.52 CM/SEC
_____	5 %	SD = 1600 BARS,	PGA = 4.524 G, PGV = 231.15 CM/SEC
_____	5 %	SD = 2500 BARS,	PGA = 6.326 G, PGV = 301.73 CM/SEC

April 3, 2007

**POINT A
UHS**

APE	PGA(g)	PGV(cm/sec)	APE	$\gamma\%$
10^{-4}	0.53	48.0	10^{-4}	0.02
10^{-5}	1.20	127.0	10^{-5}	0.06
10^{-6}	2.86	301.0	10^{-6}	0.21
10^{-7}	5.84	655.0	10^{-7}	0.61

M 6.5, **D** = 1 km, **H** = 8 km, $\kappa \approx 0.02$ sec, 6,000 ft/sec outcrop

$\Delta\sigma$ (bars)	PGA(g)	PGV(cm/sec)	$\gamma\%$	$N \sigma_{in} (0.5)$
50	0.31	25.32	0.008	1.0
100	0.53	40.21	0.013	1.4
200	0.92	63.19	0.021	2.8
400	1.57	98.33	0.034	4.2
800	2.67	151.52	0.054	5.5
1600	4.52	231.15	0.084	6.9
2500	6.33	301.73	0.110	7.8
5000	10.59	452.42	0.160	9.2

Joe Andrews Modeling

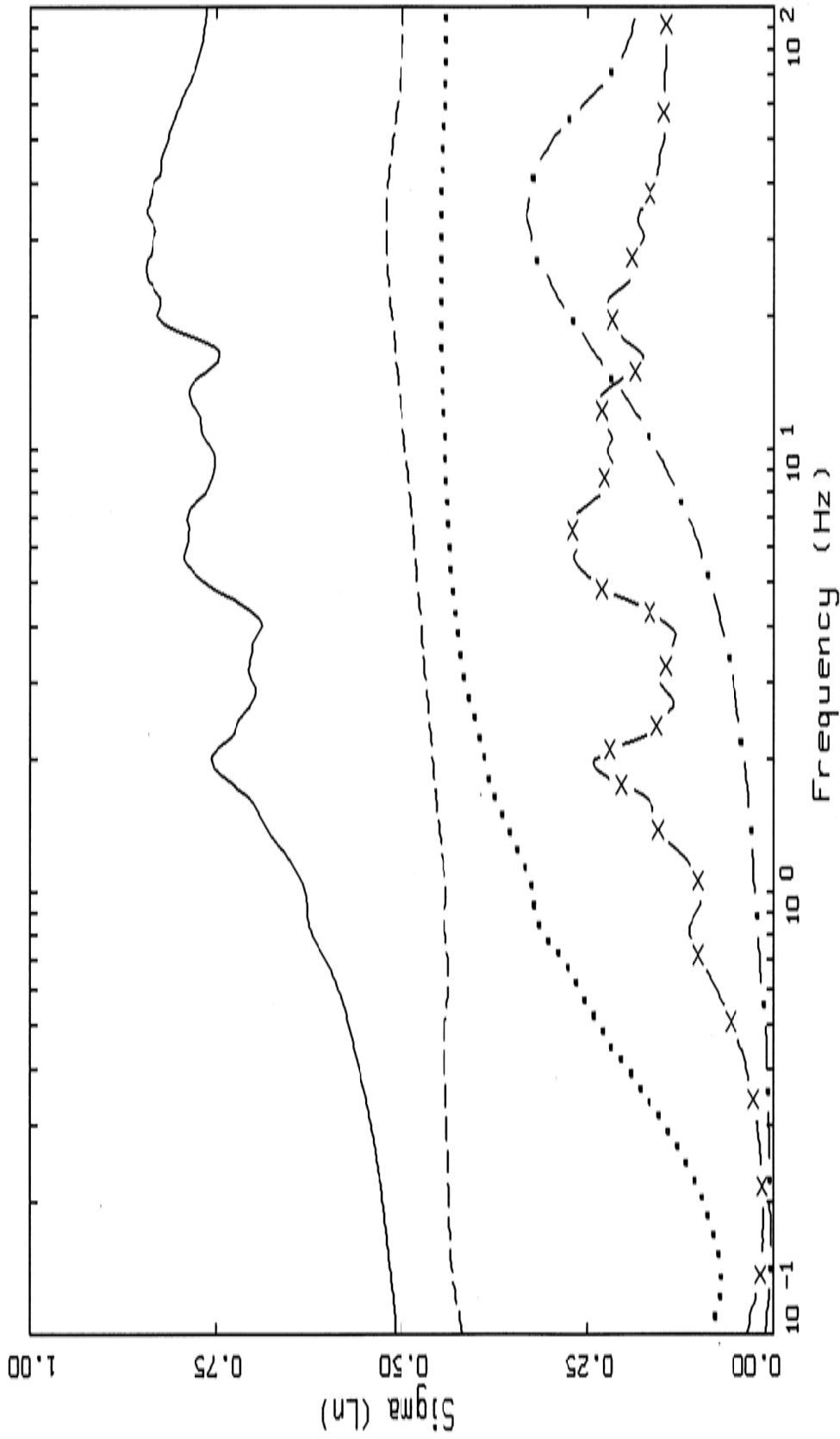
Max PGV (cm/sec), Salitario Canyon Fault: L = 18 km, W = 14 km, slip = 20m, **M** = 7.4,
 $\Delta\sigma$ (static) = 921 bars

H = 577,359*
V = 771,572*

Note: finite source modeling, slip = 5.26m, M = 6.4, $\Delta\sigma$ (static) = 27 bars

PGA = 0.31g, PGV = 28.4 cm/sec shallow slip
PGA = 0.64g, PGV = 40.7 cm/sec deep slip

* Includes nonlinearity (source?). Note model and nonlinearity not validated.



LEGEND
 VARIATION OF ALL
 VARIATION OF STRESS DROP, SIGMA(LN) = 0.5
 VARIATION OF SOURCE DEPTH, SIGMA(LN) = 0.5
 VARIATION OF KAPPA, SIGMA(LN) = 0.3
 VARIATION OF PROFILE

April 2, 2007

Single $\Delta\sigma_{\max}^{\text{HF}}$ Distribution

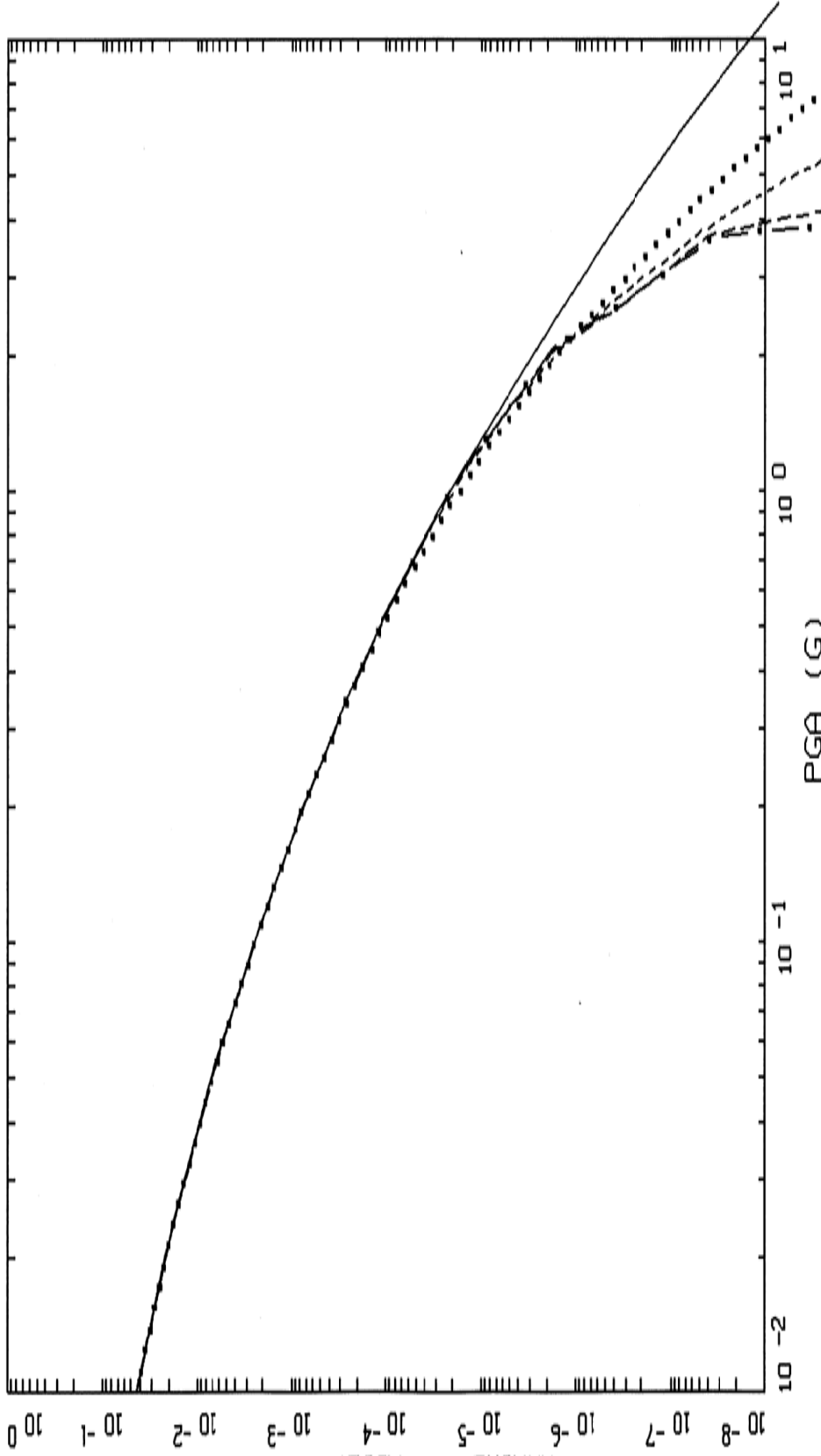
$\Delta\sigma_{\max}^{\text{HF}}$ (bars) range: 150 – 1,500, mean = 825

$\Delta\sigma_{\max}^{\text{HF}}$ (bars) expert means: 247, 620, 1033

Single Distribution

$\Delta\sigma_{\max}^{\text{HF}}$ (bars) **Weights**

300	0.2
600	0.6
1200	0.2



YUCCA.06: HAZARD CURVE CONDT.
 STRESS DROP:PGA, EXPERT 5

- LEGEND
- INPUT MEAN HAZARD CURVE
 - STRESS DROP CONDITIONED MEAN HAZARD CURVE, EXPERT 5, SIGMA=0.30
 - STRESS DROP CONDITIONED MEAN HAZARD CURVE, EXPERT 5, SIGMA=0.10
 - . - . STRESS DROP CONDITIONED MEAN HAZARD CURVE, EXPERT 5, SIGMA=0.05

April 2, 2007

Italy, Montenegro $\Delta\sigma_{HF}$

Inversions	Reverse M 4.4 – 6.6, \bar{M} = 5.5, N = 8 $\Delta\sigma_{HF}$ (bars), σ_{in} 438.2, 0.45	Normal M 5.5 – 6.8, \bar{M} = 5.6, N = 9 $\Delta\sigma_{HF}$ (bars), σ_{in} 181.6, 0.31	Reverse median Normal $\Delta\sigma_{HF}$ ratios
Published			2.41
1995*	118.5, 0.45	72.2, 0.57	1.64
2007**	59.4, 0.47	35.1, 0.54	1.69
2007***	70.2, 0.51	42.6, 0.59	1.65

*Original (1995) inversions, not all earthquakes/sites as published inversions, old GAB, GCD transfer functions. Geometrical attenuation R^{-1} ($R^{-1/2} > 60$ km)

**Updated inversion (initial), all earthquakes/most sites (2 rejected, noisy data) as published inversions, new GAB, GCD transfer functions, and M dependent geometrical attenuation $R^{-(A-B(M-6.5))}$ $A = 0.9$, $B = 0.078$.

***Same as ** but with R^{-1} ($R^{-1/2} > 60$ km).

WNA

Stress Parameters

Set	Stress Drop (bars)	σ_{In}
All	46.9	0.47
Shallow Slip	30.6	0.37
Deep Slip	56.6	0.38
	$\Delta\sigma$ (bars)	
	WUS	CEUS
M		
5.5	80	160
6.5	65	120
7.5	45	90
8.5	35	70
6.5		
	NS SS OB RV	
	50 60 70 80	

1. Maximum stress parameter limit:

$$P[x > x']^c = P[x_m > x' | \Delta\sigma_m] P[x > x']$$

where:

$P[x > x']^c$ is the conditioned (bound) hazard curve for Point A and ground motion x ;

$P[x_m > x' | \Delta\sigma_m]$ is the CCDF of motion limits (x_m) at Point A via a point-source and site response model with random parameters, conditional on stress parameter limit $\Delta\sigma_m$;

and

$P[x > x']$ is the unconditioned (original) Point A hazard curve for motion x .

2. Maximum strain limit (includes aleatory variability of shear strains conditional on Point A motion x):

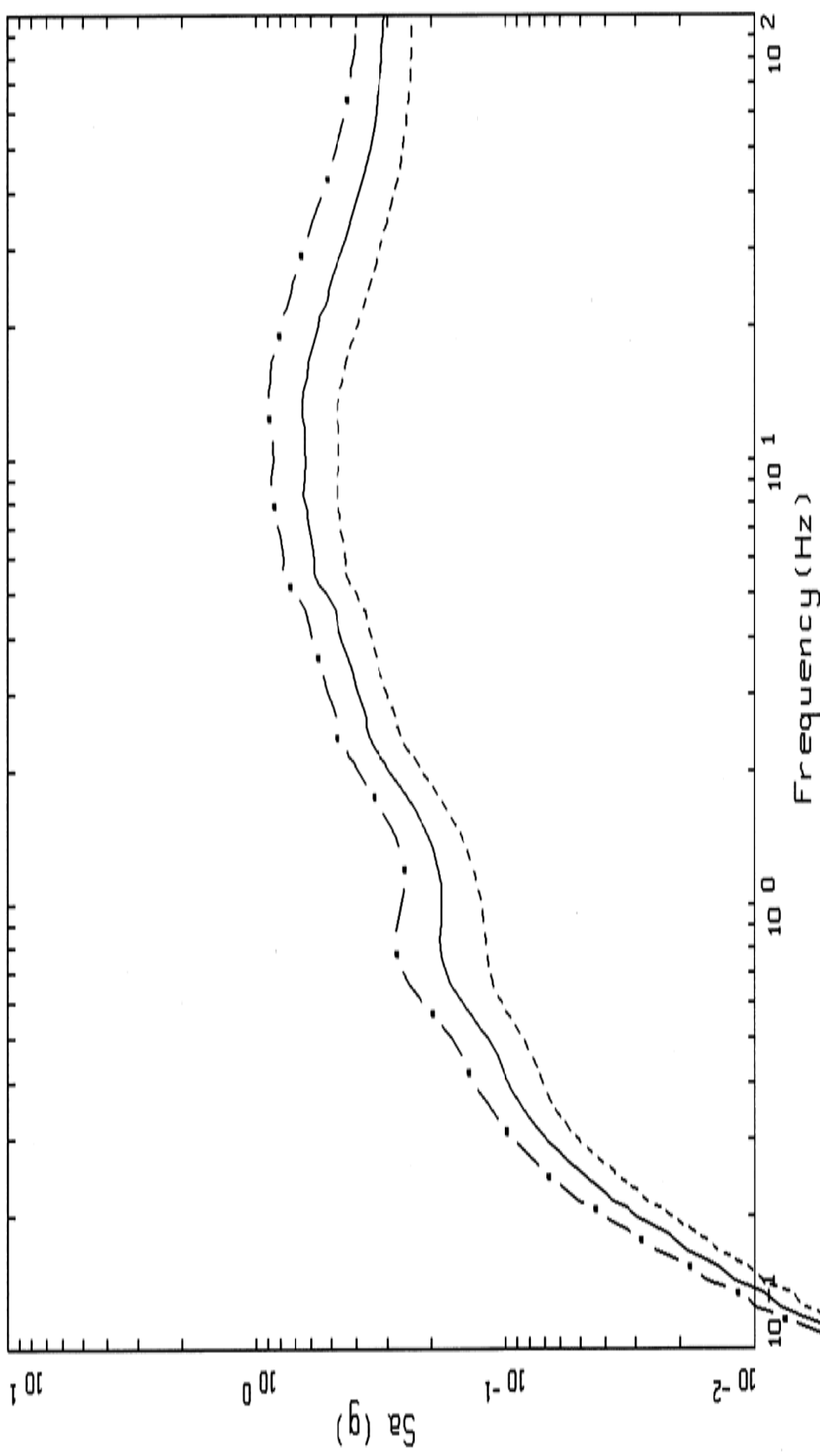
$$P[x > x']^c = \sum_i P[\gamma_m > \gamma | x_i] P[x_i]$$

where:

$P[x > x']^c$ is the conditioned (bound) hazard curve for Point A and ground motion x ;

$P[\gamma_m > \gamma | x_i]$ is the CCDF for strains at Point B conditional on ground motion x_i at Point A with γ_m the maximum shear strain;

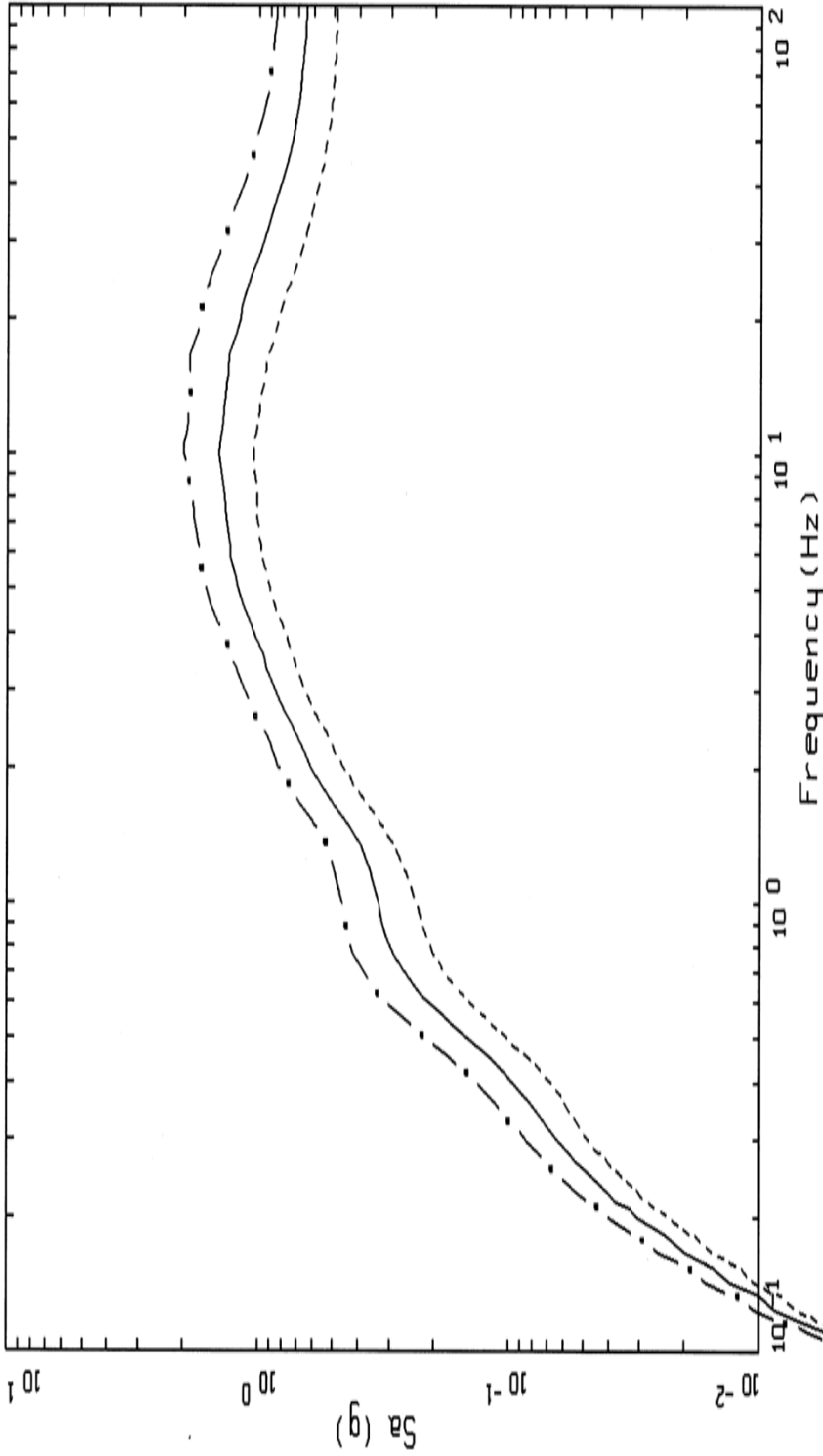
$P[x_i]$ is the probability of Point A motion x_i and the integration is over x_i greater than x' .



YUCCA MTN, M 6.4 FINITE SOURCE, RAKE 90, W=14 KM, SITE 1
 VARIATION OF ALL, SHALLOW SLIP, 5000 REALIZATIONS

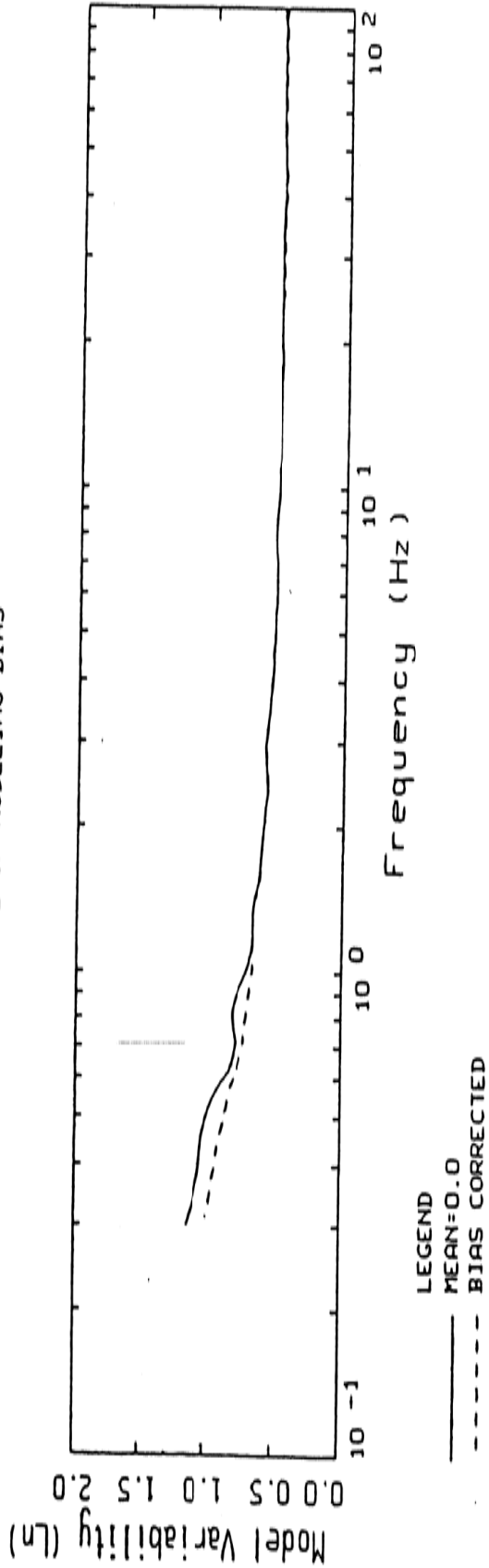
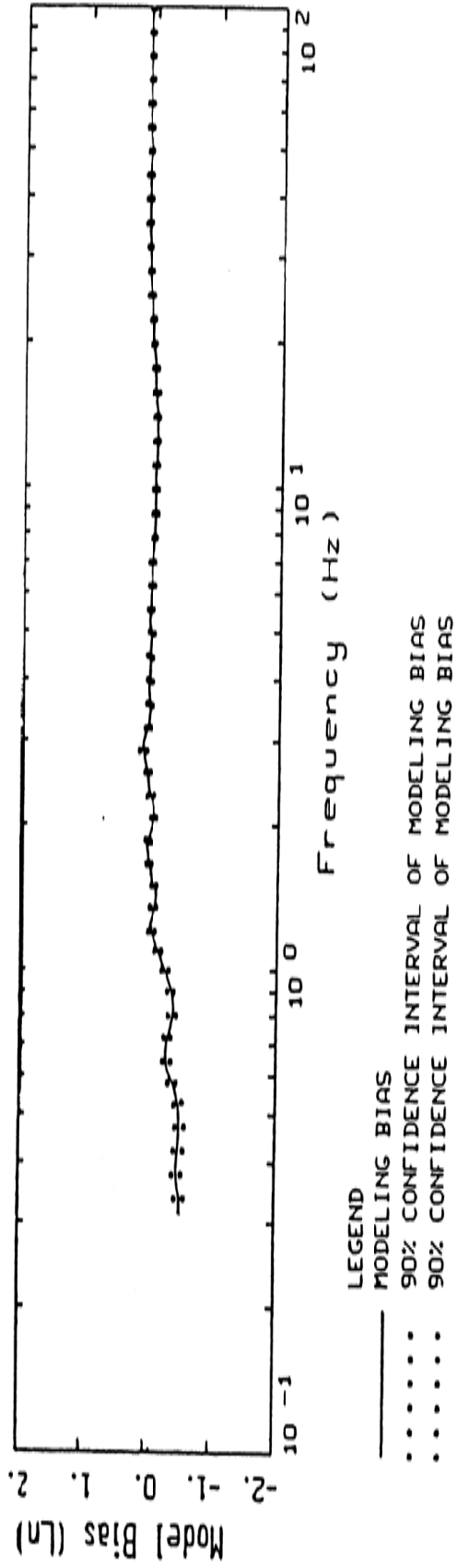
LEGEND

- • — 84TH PERCENTILE, PARAMETRIC UNCERTAINTY; PGA = 0.395 G, PGV = 34.324 CM/SEC
- 50TH PERCENTILE, PARAMETRIC UNCERTAINTY; PGA = 0.307 G, PGV = 28.410 CM/SEC
- - - 16TH PERCENTILE, PARAMETRIC UNCERTAINTY; PGA = 0.238 G, PGV = 23.514 CM/SEC



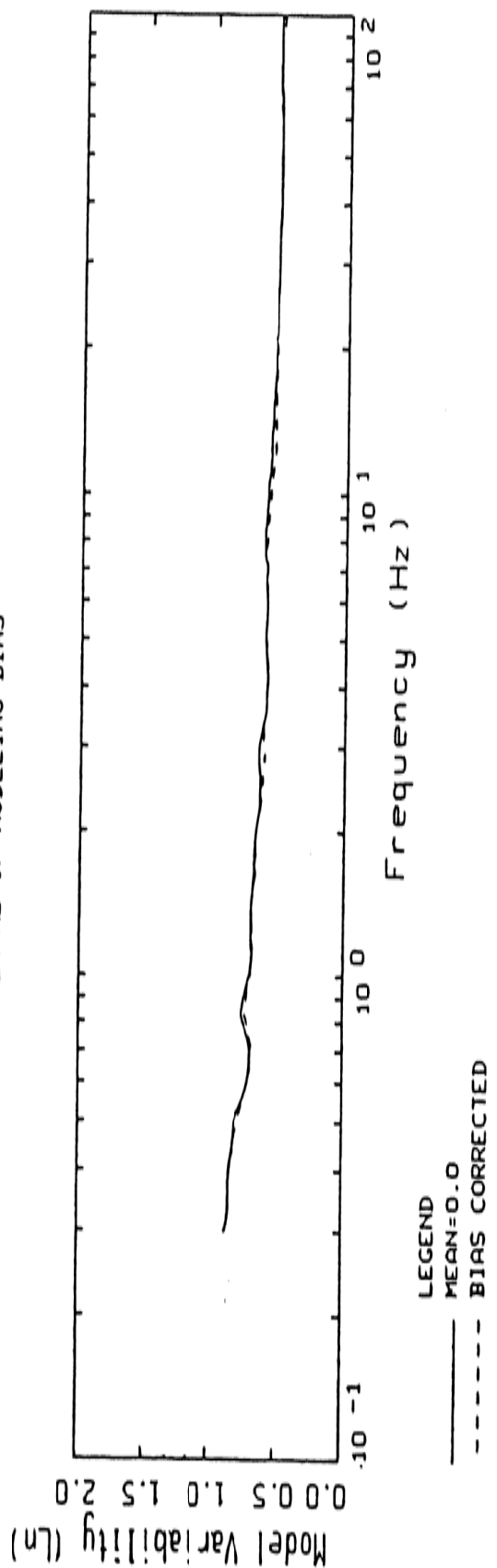
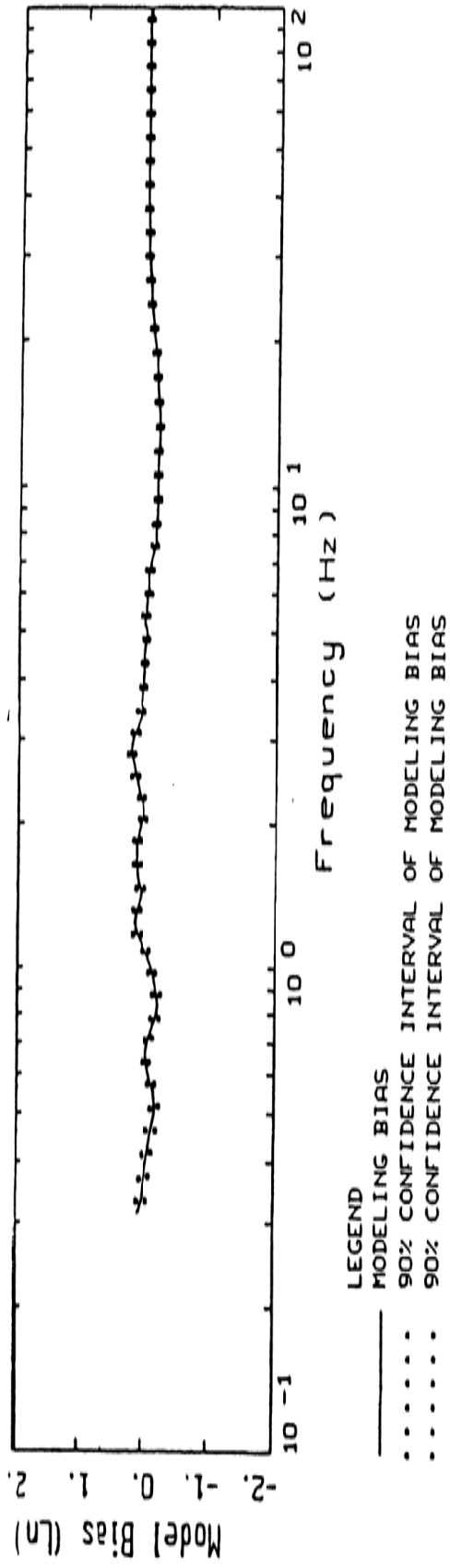
MSG5 YUCCA MTN, M 6.4 FINITE SOURCE, RAKE 90, W=14 KM, SITE 1
 VARIATION OF SLIP AND FOCUS, DEEP SLIP, 5000 REALIZATIONS

LEGEND
 - · - 84TH PERCENTILE, PARAMETRIC UNCERTAINTY; PGA = 0.848 G, PGV = 49.753 CM/SEC
 - - - 50TH PERCENTILE, PARAMETRIC UNCERTAINTY; PGA = 0.644 G, PGV = 40.724 CM/SEC
 - · - 16TH PERCENTILE, PARAMETRIC UNCERTAINTY; PGA = 0.489 G, PGV = 33.334 CM/SEC



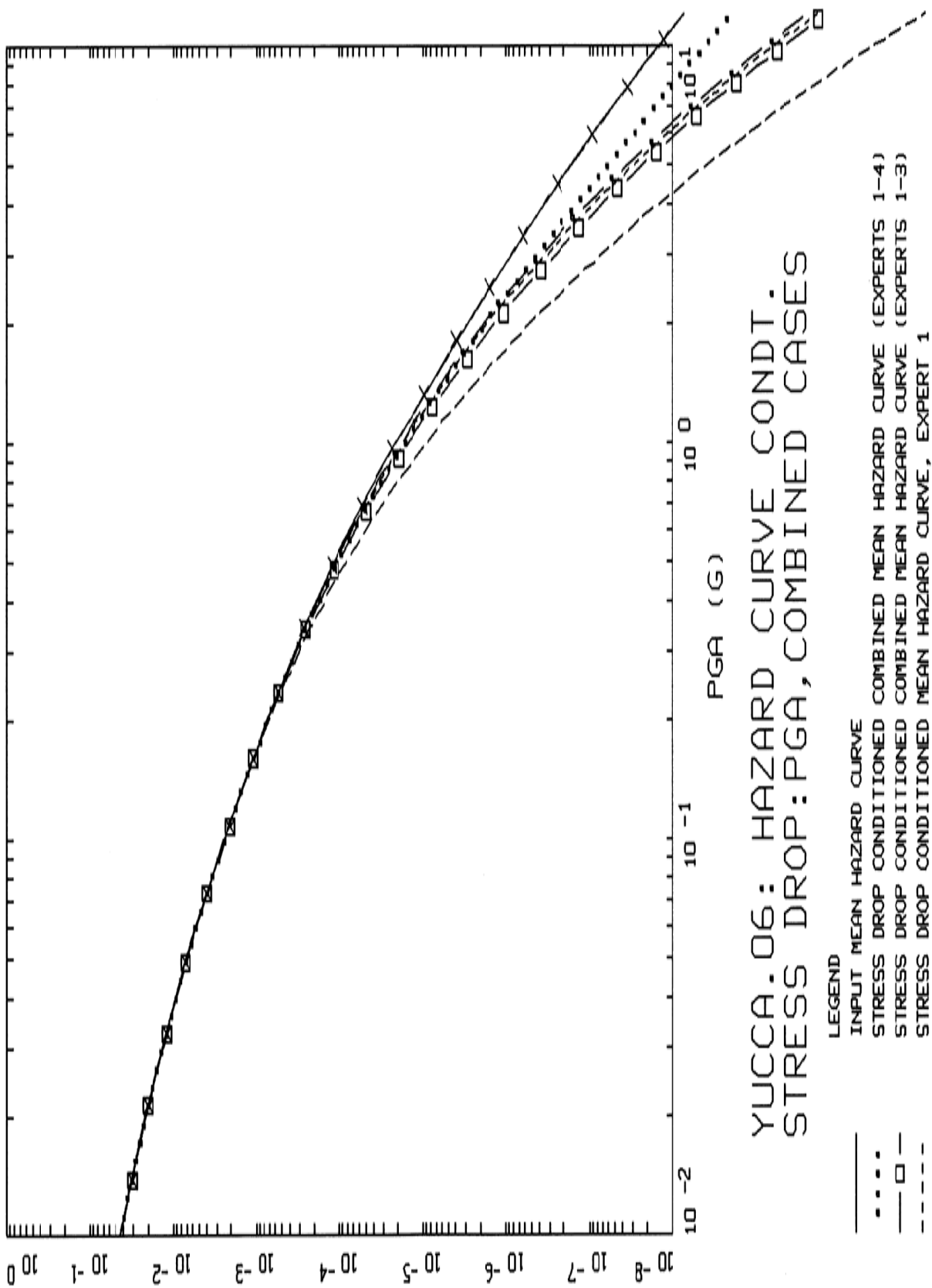
16 EARTHQUAKES POINT-SOURCE
NONLINEAR, ALL 503 SITES

Figure A1. Model bias and variability estimates for all earthquakes computed over all 503 sites for the point-source model.

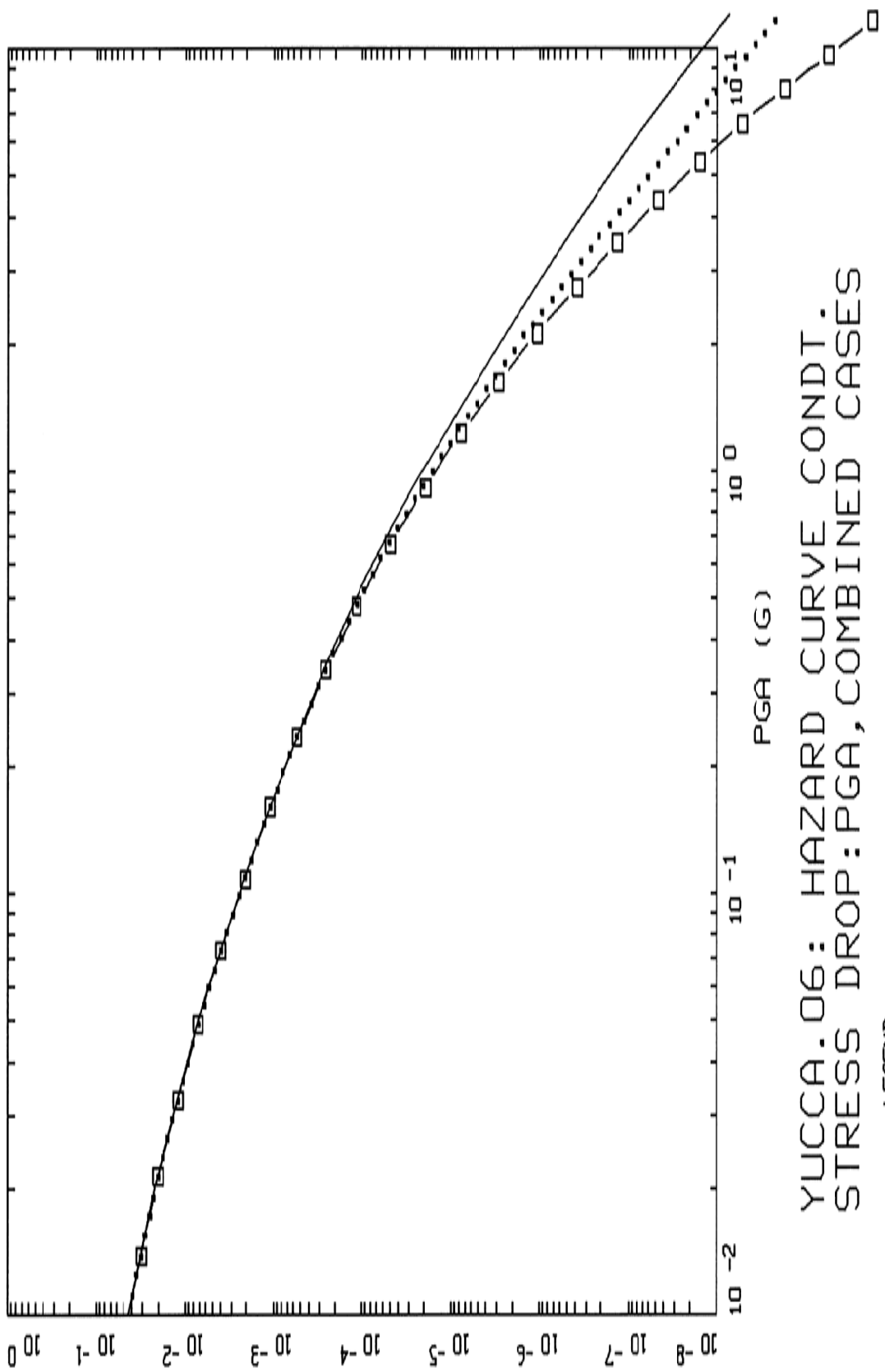


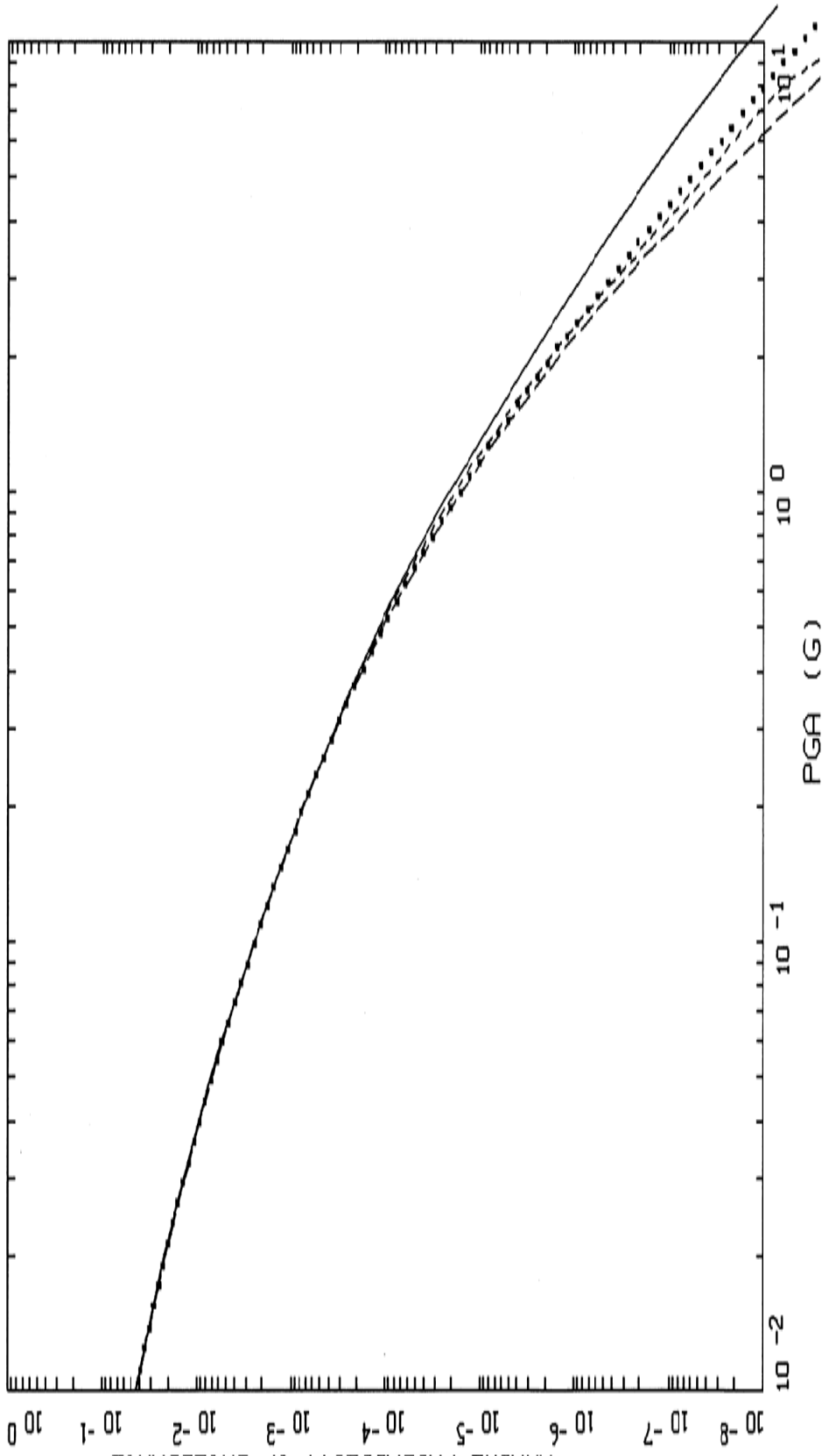
15 EARTHQUAKES FINITE-SOURCE
 NONLINEAR, ALL 487 SITES

Figure A2. Model bias and variability estimates for all earthquakes computed over all 487 sites for the finite-source model.



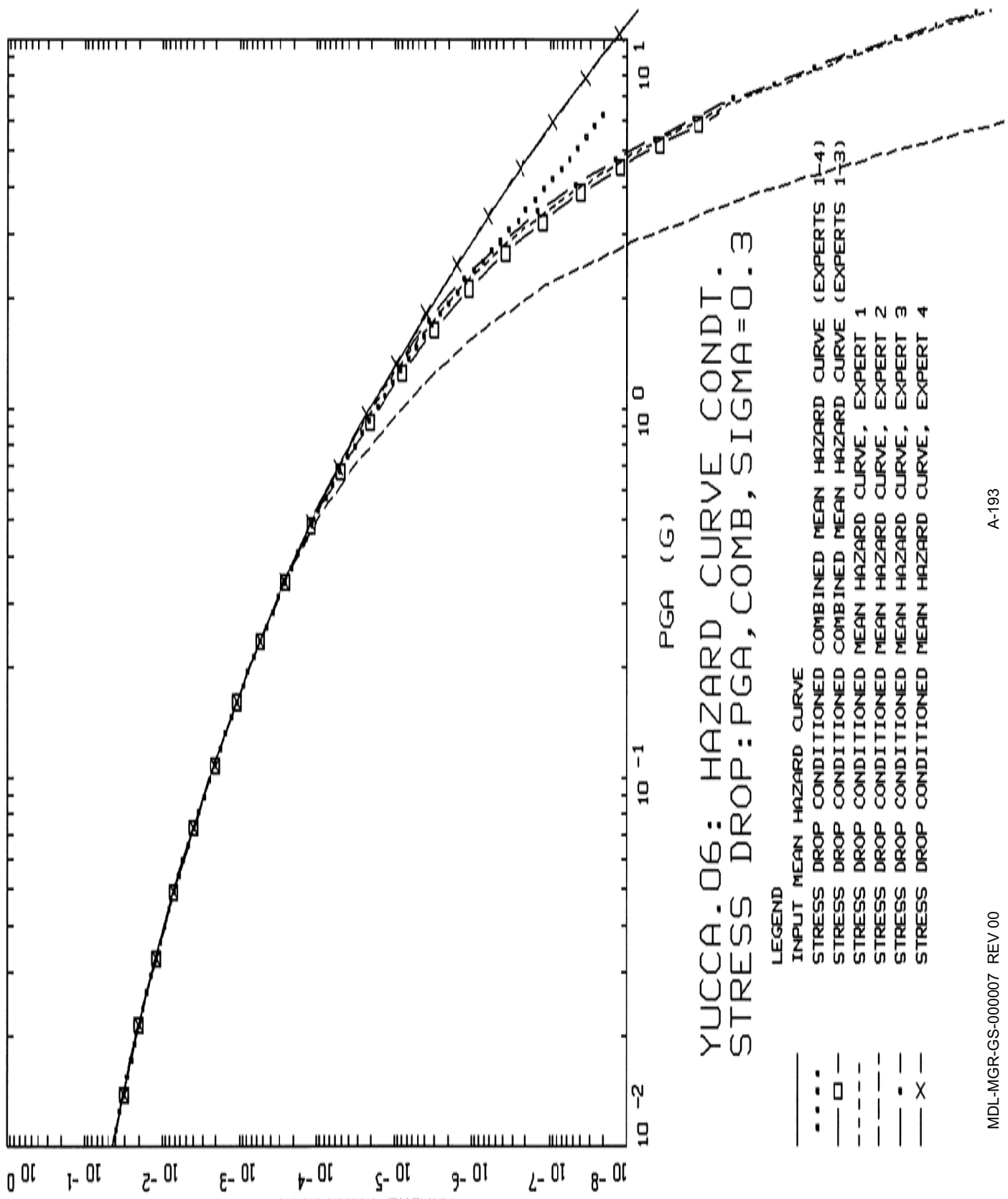
- LEGEND
- INPUT MEAN HAZARD CURVE
 - COMBINED MEAN HAZARD CURVE (EXPERTS 1-4)
 - COMBINED MEAN HAZARD CURVE (EXPERTS 1-3)
 - MEAN HAZARD CURVE, EXPERT 1
 - MEAN HAZARD CURVE, EXPERT 2
 - MEAN HAZARD CURVE, EXPERT 3
 - MEAN HAZARD CURVE, EXPERT 4

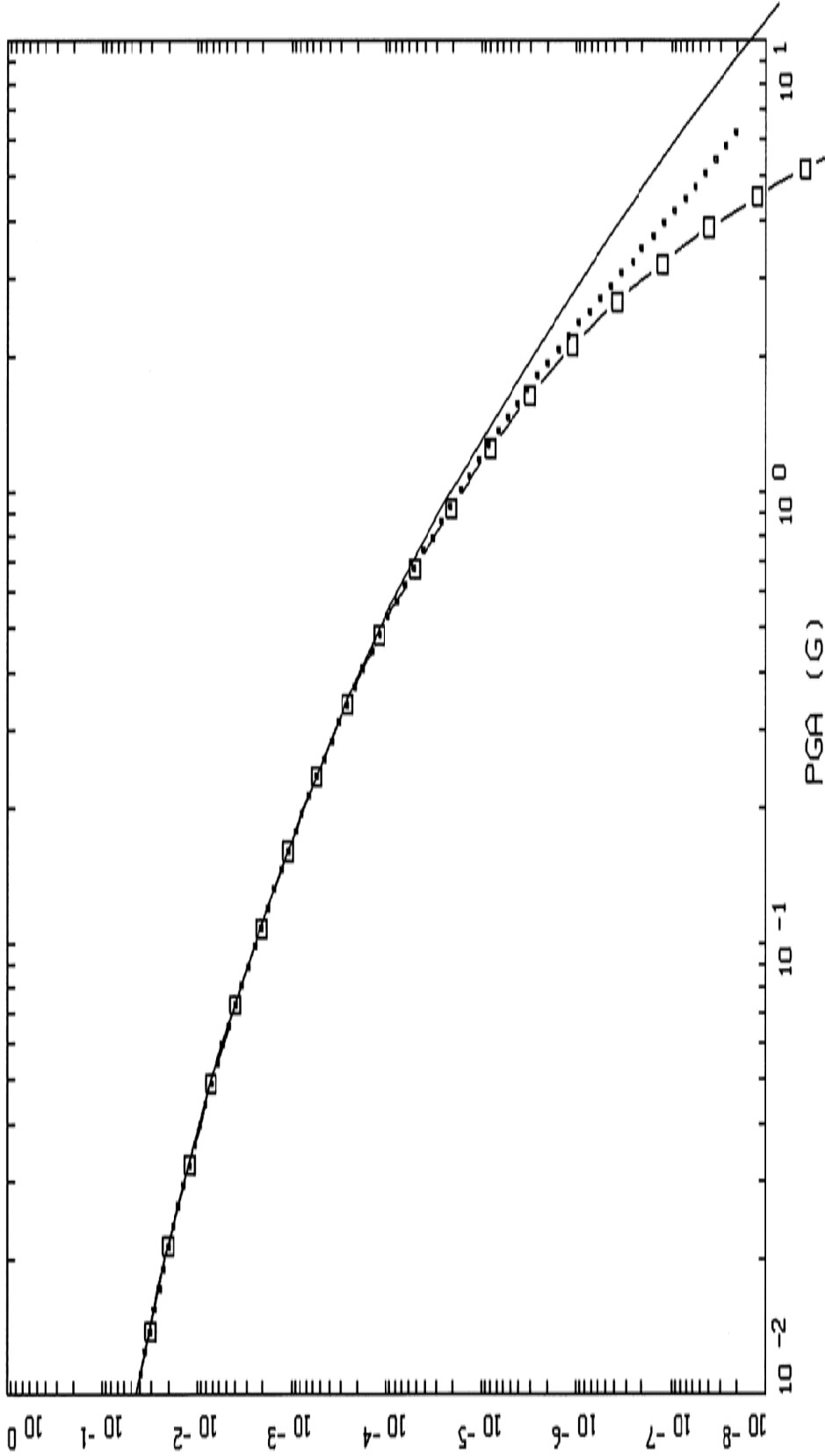




YUCCA.06: HAZARD CURVE CONDT.
STRESS+STRAIN:PGA, COMBINED

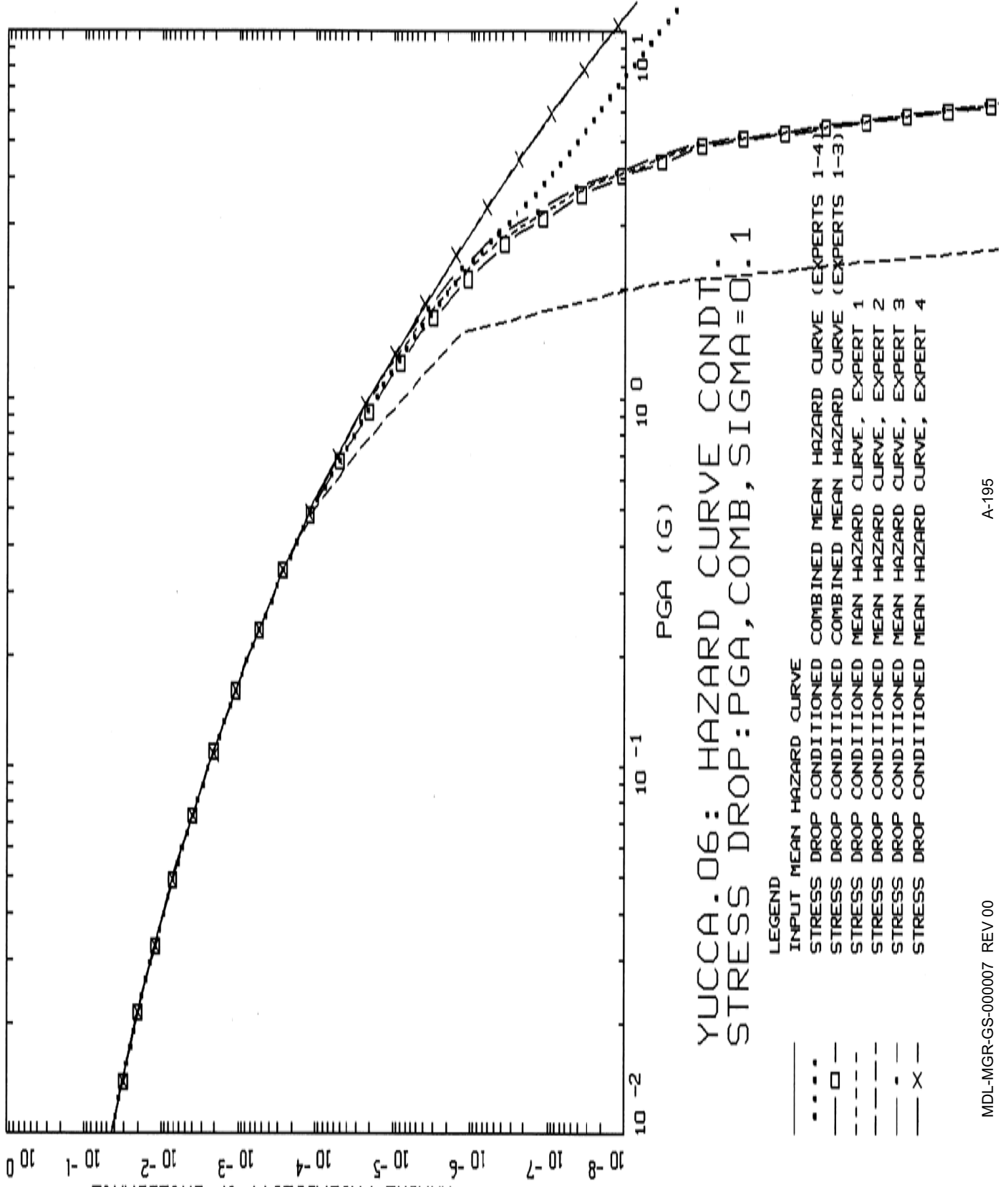
LEGEND
 _____ INPUT MEAN HAZARD CURVE
 STRESS DROP CONDITIONED MEAN HAZARD CURVE
 - - - - STRAIN CONDITIONED MEAN HAZARD CURVE
 - . - . STRESS DROP + STRAIN CONDITIONED MEAN HAZARD CURVE





YUCCA.06: HAZARD CURVE CONDT.
 STRESS DROP:PGA, COMB, SIGMA=0.3

LEGEND
 — INPUT MEAN HAZARD CURVE
 STRESS DROP CONDITIONED MEAN HAZARD CURVE (EXPERTS 1-4)
 - - - - STRESS DROP CONDITIONED MEAN HAZARD CURVE (EXPERTS 1-3)



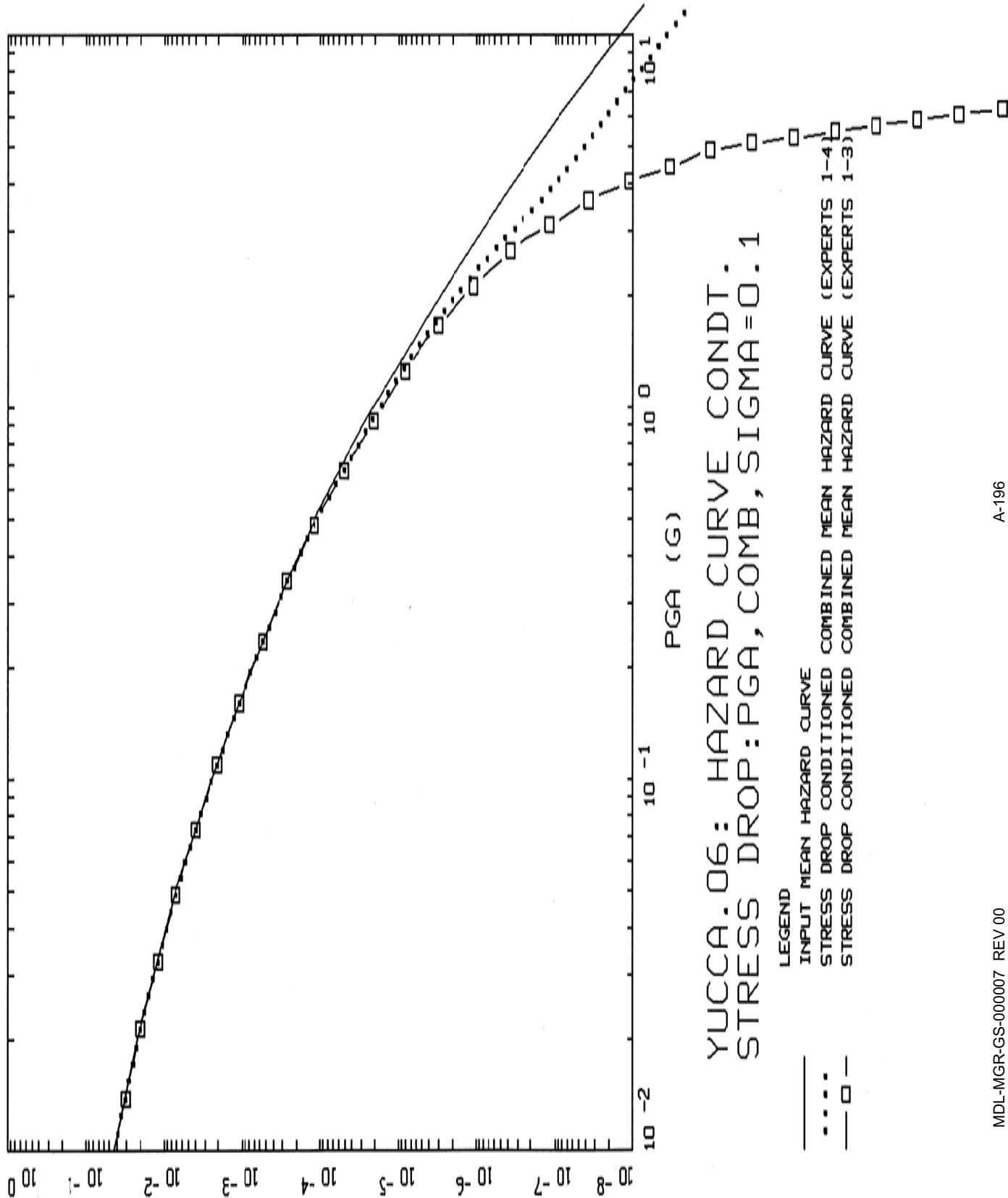


Table 6-2. Mean Shear-strain Increments Determined from Numerical Simulation of the Mechanical Behavior of Lithophysal Rock

Depth for In Situ Conditions (m)	Simulation Approach	Failure Criterion = Peak Stress		Failure Criterion = Yield Stress	
		Shear Strain Increment ^c (%) (mean \pm standard deviation)	0.15 \pm 0.02	0.13 \pm 0.03	Shear Strain Increment (%) (mean \pm standard deviation)
250	PFC2D+Circles ^a	0.15 \pm 0.02		0.11 \pm 0.04	
	PFC2D+Actual ^b	0.13 \pm 0.03		0.09 \pm 0.03	
400	UDEC+Circles	0.11 \pm 0.02		0.15 \pm 0.02	
	PFC2D+Circles	0.16 \pm 0.02		0.12 \pm 0.05	
	PFC2D+Actual	0.15 \pm 0.03		0.10 \pm 0.03	
	UDEC+Circles	0.12 \pm 0.02			

^a Lithophysae are represented in model as circular holes.

^b Lithophysae are represented in model as actual complex shapes traced from geologic field maps.

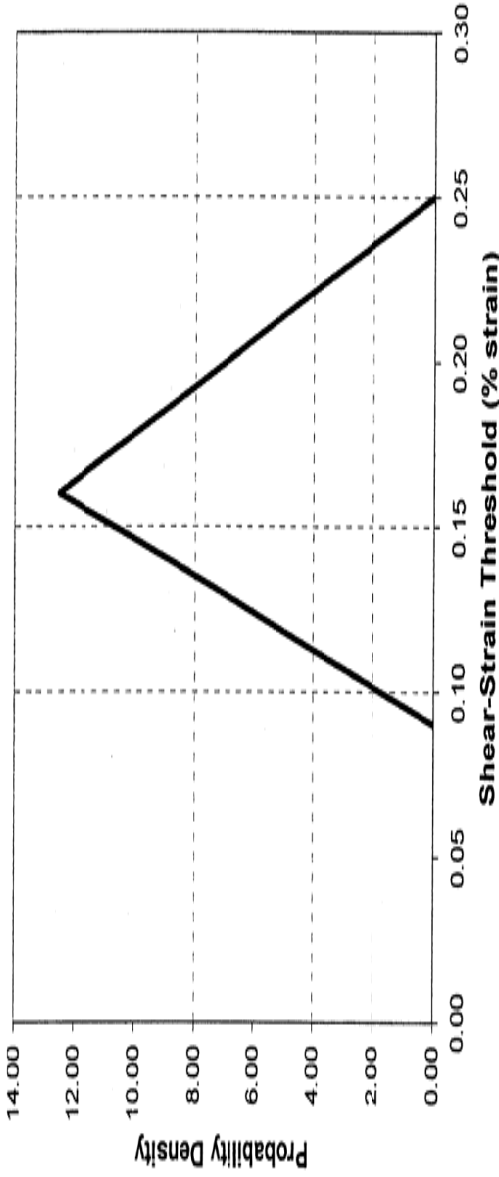
^c Shear strain increment is the increment in shear strain from the in situ stress state to the failure criterion. Failure criterion based on either a peak failure stress or yield stress condition.

Source: Appendix D, *Limiting Strains-Numerical Sims.xls*

Although the UDEC and PFC2D models were calibrated to the same laboratory results, the shear strain increment calculated from the UDEC results is systematically smaller than the shear strain increment calculated from the PFC2D results. One reason for this is that the UDEC synthetic sample is calibrated in such a way that its strength is slightly less than the strength of the PFC2D sample; at the same time, stiffness of the UDEC sample is larger than the stiffness of the PFC2D sample, resulting in the smaller strain increment calculated based on UDEC results. The other reason is that shear strain increment based on the PFC2D results is calculated assuming a friction angle of 30° (Section 5, Assumption 2). The shear strain increment based on the UDEC results is calculated using friction angles determined from the UDEC results, which generally are larger than 30°. In this case, smaller friction angles result in larger shear strain increments.

6.4.3 Assessment of Threshold Shear Strain Probability Distribution

Given the laboratory test data and the numerical simulations discussed in Sections 6.4.1 and 6.4.2, an assessment is made of the shear strain level at which geologically-observable damage would occur. This level is termed the "threshold shear strain" level for this analysis. As discussed previously in Section 6.4, the damage state associated with the peak stress is selected as the damage state for this analysis. Modeling studies described in Appendix B examined the evolution of axial stress, volumetric strain and the onset of systematic fracturing as functions of axial strain. The differences between strains at peak stress, at the point of volumetric strain reversal, and at the onset of systematic fracturing are relatively small (See Appendix B, Section B2.1, Figure B-3). These results justify use of shear strain increments determined for the state at peak stress as a reasonable threshold shear strain.



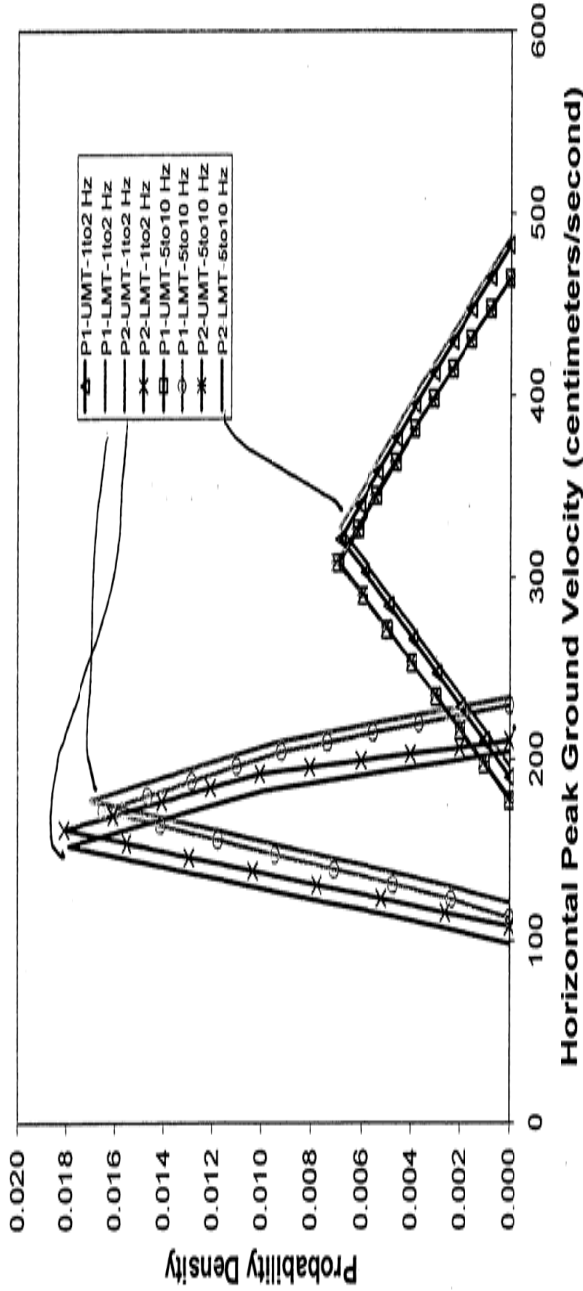
Source: Appendix D, *Probability Distributions.xls*.

Figure 6-7. Assessed Probability Distribution of Threshold Shear Strain for Topopah Spring Lithophysal Rock

Epistemic uncertainty in the assessment of the threshold shear strain is represented by the triangular probability distribution in Figure 6-7. The mode of the distribution is 0.16% strain, which is the mean of the testing data for the 288-mm-diameter samples with ratio $H/D > 1.5$ (Table 6-1). This value also is consistent with the mean estimates based on the PFC2D numerical simulations, which range from about 0.13% to 0.18% (Table 6-2). The lower limit of the triangular distribution lies at 0.09% strain, which bounds the shear strain increments for the 288-mm diameter laboratory test data (Figure 6-5). The upper limit of the distribution lies at 0.25%, which bounds most of the shear strain limits from the laboratory tests (Figure 6-5). As shown in Figure 6-5, two of the laboratory determinations of shear strain increment (for samples with H/D less than or equal to 1.5) fall outside the assessed distribution. This is justified because the focus of the assessment is on the shear-strain threshold for the weaker rock at Yucca Mountain, which would show pervasive inter-lithophysal fracturing at lower ground motions. The laboratory results for samples with H/D less than or equal to 1.5 would likely overestimate the shear strain threshold. The numerical simulations suggest the upper value of shear-strain threshold is closer to 0.20%. Calculation of the probability density for the triangular distribution is documented in Microsoft® Excel workbook *Probability Distributions.xls* on worksheet *Shear-Strain Threshold* (Appendix D).

6.5 GROUND MOTION CALCULATION

This section summarizes the analysis of ground motions for the threshold shear strain distribution assessed in Section 6.4.3. The analysis is given in Appendix C and results in the horizontal peak ground velocity (PGV) associated with threshold shear strains for the repository



Source: Appendix D, *Probability Distributions.xls*.

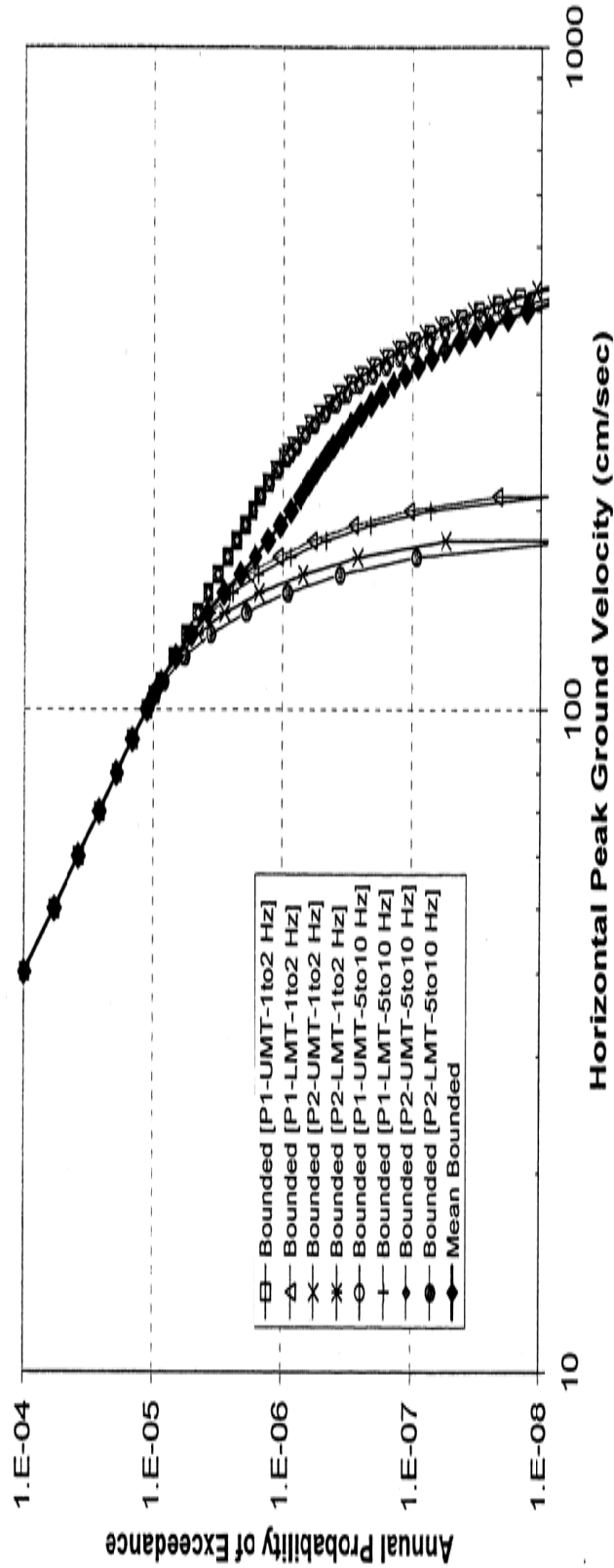
NOTE: In the legend, the notations refer to the various combinations of repository block velocity profile (P1, P2), dynamic material property curves (Upper Mean Tuff (UMT) and Lower Mean Tuff (LMT)), and response spectrum frequency range (1to 2 Hz and 5 to 10 Hz).

Figure 6-8. Probability Distribution of Bounding Horizontal PGV

6.7 BOUND TO EXTREME GROUND MOTION AT YUCCA MOUNTAIN

As discussed in Section 1, the characterizations of epistemic uncertainty and aleatory variability in the seismic hazard calculations show that, when extended to lower and lower annual frequencies of being exceeded, the ground motion level increases without bound, eventually reaching levels that are not credible and are physically unrealistic. In Section 6.6, an assessment is made of the bound to horizontal PGV experienced at the waste emplacement level at Yucca Mountain. Because the rocks at the emplacement level do *not* show evidence that this level of horizontal PGV has ever been achieved during the past 12.8 million years, the PGV probability distributions given in Section 6.6 are taken as a reasonable bound for use in TSPA. 10 CFR 63.102(j) [DIRS 156605] provides that "...events (event classes or scenario classes) that are very unlikely (less than one chance in 10,000 over 10,000 years) can be excluded from the analysis." It is recognized that there are not sufficient data to *prove* that the bounding ground motions given in Section 6.6 have less than one chance in 10,000 of occurrence over 10,000 years, such that they can be excluded from the TSPA per § 63.102(j) [DIRS 156605]. However, during the 12.8 million years since deposition of the rocks at Yucca Mountain, there have been numerous opportunities for ground motions to exceed levels that would lead to rock

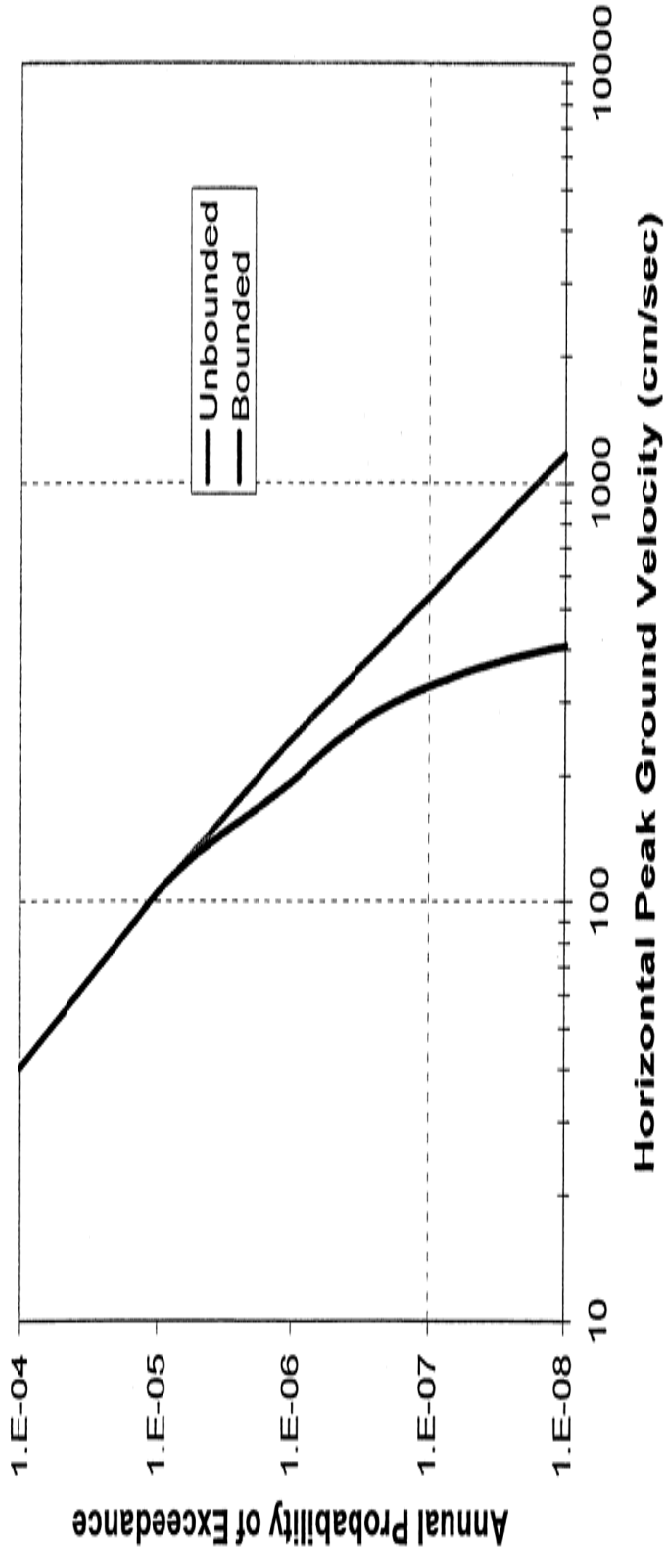
unbounded analysis is greater than x . Mathematically, the annual frequency (hazard) that the composite PGV value is greater than a given value, x , is defined by the product of the probability that the bounding value for PGV has a value greater than x and the annual frequency that the original unbounded motion has a PGV value greater than x . This calculation methodology is implemented on worksheet *Hazard Calcs* in Microsoft® Excel workbook *Probability Distributions.xls* (Appendix D). The process involves two steps. First, each of the 8 bounding horizontal PGV distributions is combined individually with the unbounded hazard curve for the waste emplacement level to produce eight modified mean hazard curves. Then for each value of horizontal PGV, the probabilities of the eight modified curves are averaged (arithmetic mean) to determine points on the final modified mean hazard curve (Figure 6-9). Equal weighting of the hazard curves is used to reflect the current assessment that the underlying cases representing epistemic uncertainty in site conditions are equally likely to represent actual conditions at Yucca Mountain. The unbounded hazard curve and the composite mean hazard curve reflecting the bound to horizontal PGV are shown in Figure 6-10.



Source: Appendix D, *Probability Distributions.xls*.

NOTE: The eight hazard curves result from combining the unbounded hazard curve with the eight "triangular" bounds to horizontal PGV. The eight "triangular" bounds represent epistemic uncertainty in the site-response modeling. The Mean Bounded curve represents the average of the other eight curves.

Figure 6-9. Individual and Average Bounded PGV Hazard Curves for the Waste Emplacement Level



Source: Appendix D, *Probability Distributions.xls*.

Figure 6-10. Comparison of Horizontal PGV Hazard Curves for Bounded and Unbounded Ground Motion at the Waste Emplacement Level

Rationale on stress parameter limits – Gail Atkinson, April 4, 2007

Considering the maximum stress parameter that should be applied in the calculation of ground motions at Yucca Mountain, my opinion based on the materials, data and experience available to me suggest that the stress parameter is a lognormally-distributed random variable, with an effective median of 80 bars, and a standard deviation of 0.2 log (10) units. This opinion, and some considerations in its interpretation, is based on the following rationale.

There is almost certainly an upper limit to the stress parameter, perhaps imposed by the strength of the seismogenic crust. We cannot determine this limit statistically based on available data (as an absolute truncation) or any known physical rationale. We can, however, place useful probabilistic bounds on the problem. Relevant information is provided by McGarr's report of 8 March 2007. The laboratory static stress drops listed in McGarr's report show behavior similar to that expected for earthquake stress parameters; however, there is epistemic uncertainty associated with assuming these two types of stress drops are exact counterparts.

The laboratory stress drops reported by McGarr (adjusted) show less variability than earthquake stress parameters because measurements in the lab tend to be much better controlled than corresponding earthquake estimates. They are less subject to the interpretation errors that may affect seismological measurements of stress, due to the wide range of methods and observation distances employed in seismological studies. The laboratory stress drops provide a reasonable justification to reduce the aleatory uncertainty of the stress parameter.

The best median stress parameter, on the basis of both laboratory and earthquake data, is in the range from 50 to 100 bars. I adopt a value of 80 bars as my best estimate of the median based on a broad experience database and evaluation of information presented during the Elicitation Process. Stress is characterized by a lognormal distribution. For $\log(\Delta\sigma)$, the mean is 1.9 (for $\Delta\sigma$ in bars) and the standard deviation is about 0.2 log (10) units. The standard deviation is assessed by taking both the earthquake and the more narrowly-distributed lab data into account. In essence, the actual standard deviation is considered to be intermediate to that suggested by laboratory data and that suggested by seismological data.

We cannot rule out any arbitrarily-high stress parameter, but, based on the available data and what we know, we can assign appropriately-low probabilities to exceptionally high values. This concept can be used to screen out stress drop values that fall outside the range of interest based on their having an unreasonably low probability. For example, if the occurrence of events that have a lower probability than $1E-8$ (1/10,000 in 10,000 years) are not of interest in the regulatory framework of Yucca Mountain, then we can exclude from consideration any events with a stress drop greater than 5.6 standard deviations above the median, as being less likely than $1E-8$. Furthermore, the range of interest in stress drops may be further restricted by considering the conditional probability of having a high stress drop in combination with a rare scenario event. If the

scenario event of interest has a probability of $1E-4$ p.a., for example, then the range of interest for the stress drop parameter would be values that have probabilities of $1E-4$ and greater (to give a compound probability of $1E-8$); this stress value (the 1/10,000 stress value) would correspond to 3.7 sigma on the normal probability distribution. For my preferred stress distribution of $\log \Delta\sigma = 1.9 \pm 0.2$, the 5.6 sigma cut-off in stress corresponds to a value of approximately 1000 bars, while the 3.7 sigma cut-off in stress corresponds to a value of approximately 440 bars. The normal distribution in stress can thus be used as a screening tool to remove stress drops that fall below the probability level of interest in the project.

Rationale for stress parameter limits proposed by Art McGarr, 6 April 2007

In my report of 8 March 2007, I listed laboratory measurements of static stress drop over a range of normal stresses. I also listed these stress drops as adjusted to the stress loading conditions observed at a depth of 6.8 km at the KTB site, Germany. The 15 adjusted stress drops range from 59 bars up to 157 bars. $\text{Log}_{10}\Delta\sigma$ has a mean of 1.06 with a standard deviation of 0.11.

I also argued that these laboratory stress drops show the behavior expected for the stress parameter (e.g., Hanks and McGuire, 1981; Boore, 1983; Singh and Ordaz, 1994). Taking into consideration that the loading stresses at seismogenic depths beneath Yucca Mountain, in an extensional tectonic environment are substantially less than those from the KTB site used to adjust the laboratory results, I decided that a reasonable distribution of limiting values is given by the geometric mean plus one, two, and five standard deviations (e.g., 14.8, 19.1, and 40.7 MPa) with weights of 0.2, 0.5 and 0.3, respectively.

On a related topic, apparent stresses in continental settings appear to have an upper bound of approximately 10 MPa, although a few higher values have been reported. For instance, Figure 1 of McGarr and Fletcher (2003), a compilation of apparent stresses from many studies covering quite a broad range of seismic moment, shows one apparent stress that is significantly greater than 10 MPa. Similarly, Table 1 of Imanishi and Ellsworth (2006), which is attached, lists three earthquakes whose apparent stresses are close to 20 MPa. Thus, although one can find a few exceptions, an upper bound of 10 MPa appears to be the general rule over the entire magnitude range of recorded earthquakes. Apparent stresses measured in the laboratory and adjusted in the same way as for the static stress drops are also consistent with an upper bound of about 10 MPa for earthquakes in continental settings. The adjusted apparent stresses listed in Table 1 of my report of 3/8/07 (also attached) range up to 4.17 MPa.

References.

Boore, D. M. (1983). Stochastic simulation of high-frequency ground motions based on seismological models of the radiated spectra, *Bull. Seismol. Soc. Am.*, **73**, 1865-1894.

Hanks, T. C. and R. K. McGuire (1981). The character of high frequency strong ground motion, *Bull. Seism. Soc. Am.*, **71**, 2071-2095.

McGarr, A. and J. B. Fletcher (2003). Maximum slip in earthquake fault zones, apparent stress, and stick-slip friction, *Bull. Seismol. Soc. Am.*, **93**, 2355-2362.

Singh, S. K. and M. Ordaz (1994). Seismic energy release in Mexican subduction zone earthquakes, *Bull. Seismol. Soc. Am.*, **84**, 1533-1550.

APPENDIX B
PREPARATION OF MODULUS AND DAMPING-RATIO DEGRADATION CURVES
FROM MODEL-PRODUCED DATA AT HIGH STRAIN AMPLITUDE FOR UNITS OF
THE REPOSITORY HORIZON



an HC|ITASCA company

Technical Memorandum

Date: August 24, 2007
To: Richard Quittmeyer, YMP
From: Terje Brandshaug, Branko Damjanac, Zorica Radaković-Guzina
Re: *Preparation of Modulus and Damping-Ratio Degradation Curves from Model-Produced Data at High Strain Amplitude for Units of the Repository Horizon*
Ref: ICG06-2133-38-46-TMR

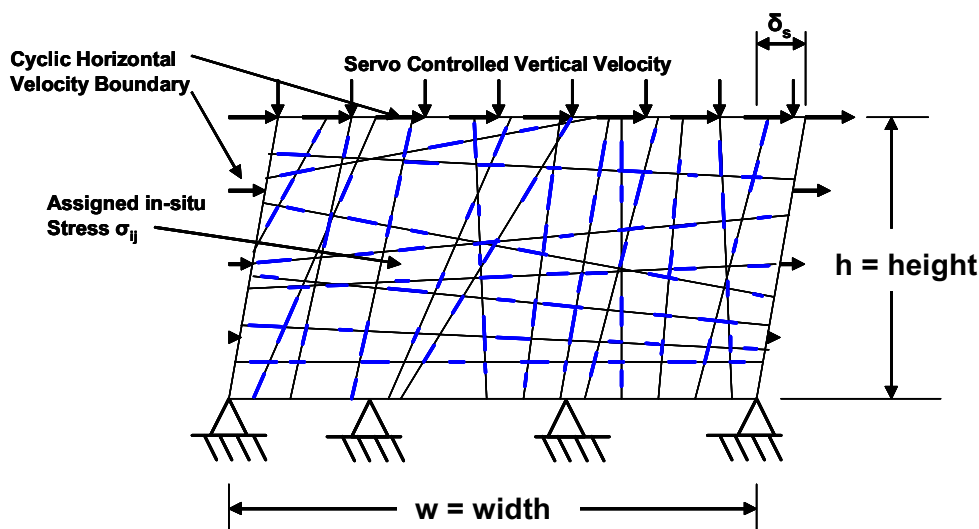
B1.0 BACKGROUND

The following is a brief description of numerical analyses using UDEC Version 3.14 (STN 10173-3.14-00) [DIRS 172322], Itasca's two-dimensional discontinuum code, to produce shear-modulus and damping-ratio degradation curves at high shear-strain amplitudes for lithologic units of the Topopah Spring Tuff formation (i.e., Yucca Mountain repository horizon). The units included are Tptpul, Tptpmn, Tptpll and Tptpln. Previous analyses using the same UDEC model were done to produce degradation curves for four of the major units (Calico Hills Formation, Prow Pass Tuff, Bullfrog Tuff and Tram Tuff) below the repository horizon (Brandshaug et al. 2004 [DIRS 171300]).

The degradation curves are extracted from a number of cyclic shear tests conducted numerically for each lithologic unit. The premise for using a numerical model in the current context is that it is impossible to conduct cyclic shear-strain experiments on physical specimens on a rock-mass scale (tens of meters). In this work, UDEC provides the mechanistic basis for producing the degradation curves because it integrates the effects of the rock mass components such as joint structure, joint and intact rock response and *in situ* stress environment.

B2.0 CONCEPTUAL MODEL

Figure B-1 illustrates the conceptual UDEC model in this work. The horizontal velocity boundaries impose a number of shear cycles upon the model, where each cycle reaches a maximum shear strain of $\varepsilon_s^{\max} = \pm \delta_s/h$, as shown in Figure B-1. The model was subjected to maximum shear strains of 0.0005, 0.001, 0.002, 0.003 and 0.005 in separate tests. The upper-horizontal model boundary also was assigned vertical velocities that were servo-controlled to maintain a constant average vertical stress equal to the specified *in situ* vertical stress in each lithologic unit. The controlled vertical velocity of the top horizontal boundary also was applied in relative proportion along the two lateral boundaries from 1 at the top to 0 at the bottom. Hence, the boundary conditions closely match a free body subjected to a free-field shear-motion effect.



Source: Schematic illustration

Figure B-1 Conceptual UDEC Model Showing Boundary Conditions and Example Jointing with Rock Bridges (blue)

The joint structure (i.e., spatial frequency and orientation) was taken directly from 3D joint structure data generated by FRACMAN (BSC 2004 [DIRS 162711], Appendix A) for a rock volume 100-m x 100-m x 100-m cube oriented N-S. Fracture orientation data for the Tptpul and Tptpln units were taken from the supporting Excel files “Tptpul-Fracman Generated Fracture Data.xls” and “Tptpln-Fracman Generated Fracture Data.xls”, respectively (DTN: MO0306MWDDDMIO.001 [DIRS 165791]). The DTN from which these data are taken has been superseded so modeling results described here for the Tptpul and Tptpln are unqualified and are only considered as corroborative information. Fracture orientation data for the Tptpll unit were taken from the supporting Excel file “Tptpll_TPO2.xls” (DTN: MO0408MWDDDMIO.002 [DIRS 171483]). Fracture orientation data for the Tptpmn unit were taken from supporting Excel files “VPPLONG_TPO.xls”, “S1shtA_TPO.xls”, “S1shtB_TPO.xls”, “s2sht_TPO.xls” and “s3sht_TPO.xls” (DTN: MO0408MWDDDMIO.002 [DIRS 171483]). Modeling results for the Tptpmn and Tptpll are qualified.

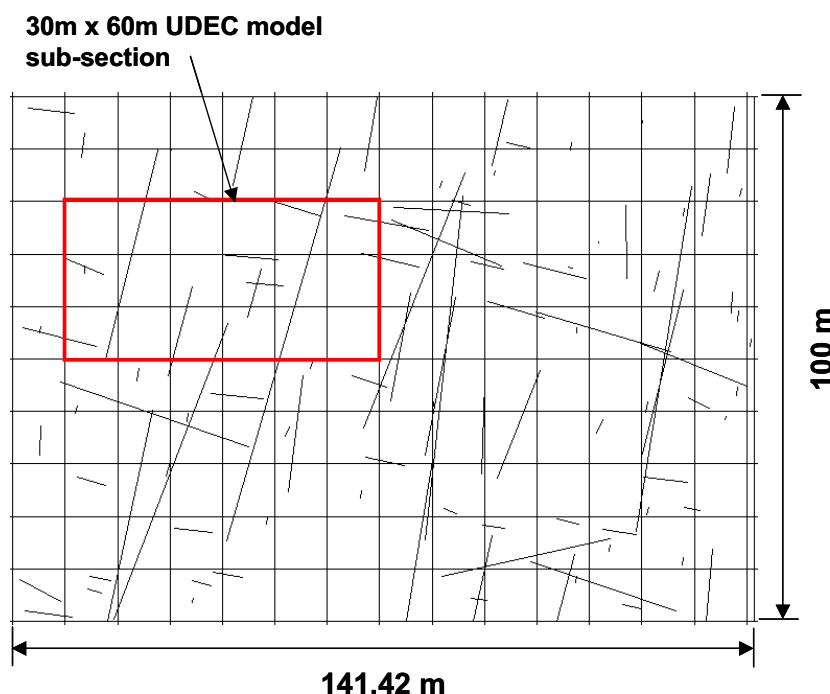
The joint structure was differentiated by dip angle into three sets with dips in the range 70° to 90° designated as “sub-vertical” cooling joints, 0° to 30° as “sub-horizontal” vapor-phase partings, and 30° to 70° as “random” joints. This differentiation is reasonably consistent with the range of joint dips provided in BSC (2000 [DIRS 152286]), BSC (2004 [DIRS 168550]) and BSC (2004 [DIRS 166107]).

Because UDEC is a 2D code, it is necessary to project the 3D joint structure onto the plane of the UDEC model. The plane of the UDEC model is assumed to be vertical, with the plane-normal oriented in the NW-SE direction (i.e., dip direction of 315°). The line of intersection between the 3D joint planes and the model plane defines each joint location in the UDEC model. Any 3D joint from the FRACMAN data with a dip direction in the ranges 45° ± 45° and 225° ± 45° that intersects the

model plane and belongs to the sub-vertical or random joint sets is represented as a joint in the UDEC model. All sub-horizontal joints that intersect the model plane, regardless of dip direction, are represented as joints in the UDEC model.

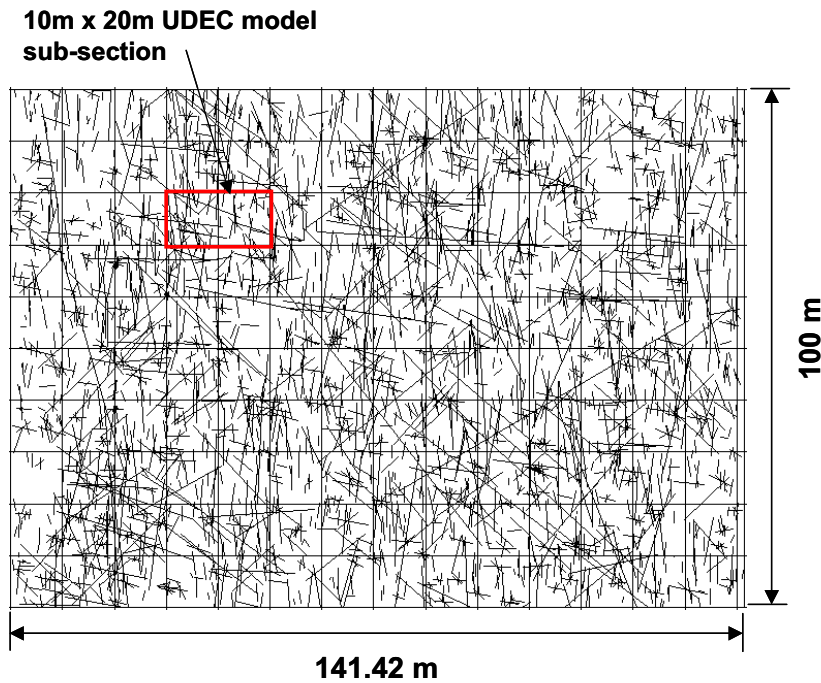
Figures B-2 to B-5 show the lines of intersection between the 3D FRACMAN joints and the plane of the UDEC model for the different units. These lines define the joints in the UDEC models. Note that the orthogonal grid shown in Figures B-2 to B-5 is not part of the joints. Their purpose is simply to provide a dimensional perspective, as the gridlines are 10-m apart. Note that the height and width of the UDEC model includes a sub-section of the joints. These sub-sections also are shown in Figures B-2 to B-5. With the exception of the Tptpmn unit, the UDEC model is 30-m high and 60-m wide. For the Tptpmn unit, the UDEC model is 10-m high and 20-m wide.

A Monte Carlo approach was used in these analyses. Hence, five separate model sub-sections were selected from the joint space shown in Figures B-2 to B-5 for each shear-strain amplitude investigated. This provides some sense of the variability of joint structure on the estimated model response.



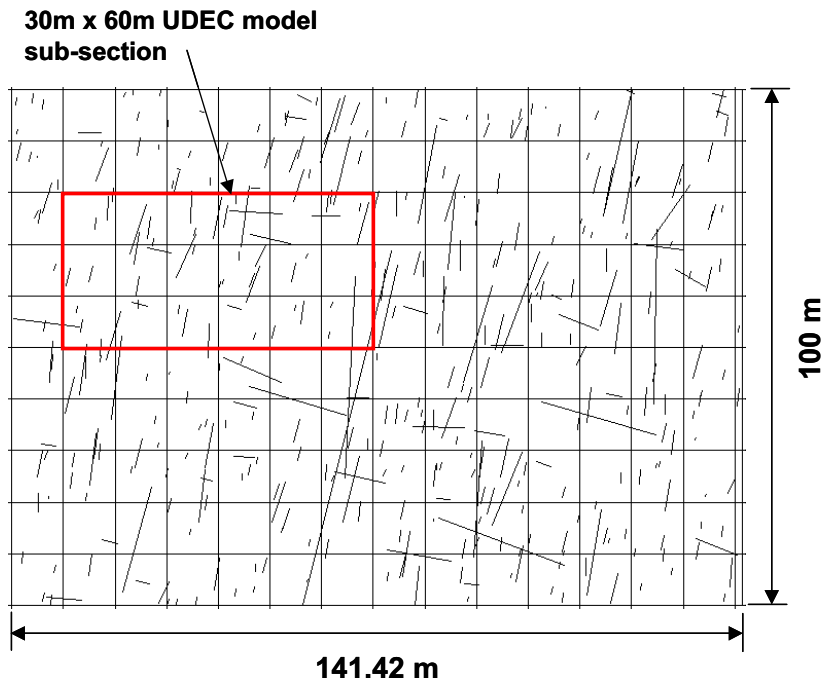
Source: icg06-2133-38-46-tmr_udec_figs.ppt

Figure B-2 *Lines of Intersection between 3D FRACMAN Joints and the UDEC Model Plane for the Tptpul Unit*



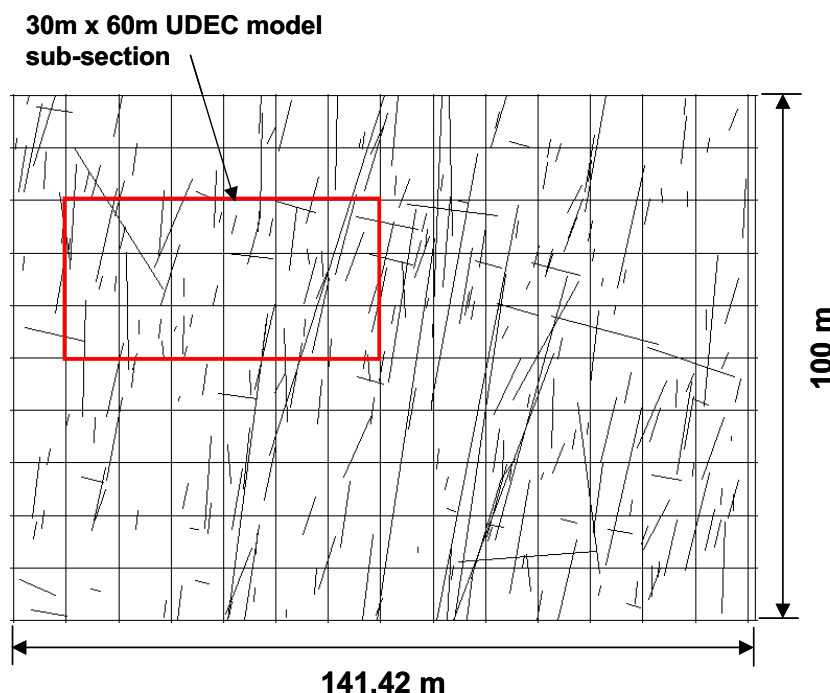
Source: icg06-2133-38-46-tmr_udec_figs.ppt

Figure B-3 Lines of Intersection between 3D FRACMAN Joints and the UDEC Model Plane for the Tptpmn Unit



Source: icg06-2133-38-46-tmr_udec_figs.ppt

Figure B-4 Lines of Intersection between 3D FRACMAN Joints and the UDEC Model Plane for the Tptpll Unit



Source: icg06-2133-38-46-tmr_udec_figs.ppt

Figure B-5 *Lines of Intersection between 3D FRACMAN Joints and the UDEC Model Plane for the Tptpln Unit*

Because the joints have finite length, they may not extend to the UDEC model boundaries. If a joint does not reach the model boundaries, it is extended to the boundaries. Note that the extended portions of the joint are given strength similar to that of intact rock (represented by the blue-colored joint segments in Figure B-1).

Along with existing geological data from the Yucca Mountain site, the UDEC model provides, at least, an initial understanding and first-order approximation of the characteristic shear modulus and damping-ratio degradation in the rocks of the repository horizon for the shear-strain amplitudes studied (0.0005 to 0.005 strain).

The joint mechanical response in the model is elastic/plastic, characterized by stiffness, cohesion, friction angle and dilation angle. The mechanical response of the matrix (or intact rock) is elasto-plastic using a Mohr-Coulomb material model and non-associated plasticity (zero dilation angle). Thus, in these models, energy dissipation may occur through both sliding on joints and yielding of the intact rock material. Note that tensile softening was used for the rock matrix. This reflects a loss of tensile strength (isotropically) of the intact rock if tensile failure occurs.

Table B-1 lists the properties and model parameters used for the four lithologic units evaluated in this study. The vertical stress, σ_V , in Table B-1 was determined from an average of the idealized zone geologic column of the Southern, Eastern and Northwestern “soft zones”. These are the same zones that have been used to develop base-case shear wave velocities and average lithologic unit

shear-wave velocities for the repository block. Input and output files, and workbooks containing other calculations, are included in an electronic attachment to this appendix.

Table B- 1 Parameters used in the UDEC Model to Produce Modulus Reduction and Damping-Ratio Degradation Curves

Property/Condition	Tptpul		Tptpmn		Tptpll		Tptpln	
	Avg.	St. Dev.	Avg.	St. Dev.	Avg.	St. Dev.	Avg.	St. Dev.
⁽¹⁾ Saturation	0.8		0.8		0.8		0.8	
⁽¹⁾ Porosity	0.2		0.2		0.2		0.2	
⁽²⁾ Dry Density kg/m ³	1834		2148		1979		2211	
⁽²⁾ Density kg/m ³	1994		2308		2139		2371	
⁽³⁾ σ_V (MPa)	5.2		6.5		8.0		9.3	
⁽⁴⁾ σ_H (MPa)	2.6		3.25		4.0		4.65	
Stiffness Scaling-Factor ⁽⁹⁾	0.48		0.90		0.85		0.51	
Young's Modulus (GPa)	Note ⁽⁵⁾		30.2 ⁽⁶⁾		Note ⁽⁵⁾		17.1 ⁽⁸⁾	
Poisson's Ratio	Note ⁽⁵⁾		0.20 ⁽⁷⁾		Note ⁽⁵⁾		0.20 ⁽⁷⁾	
Intact Coh (MPa)	Note ⁽⁵⁾		36 ⁽¹⁰⁾	11.1% ⁽¹⁰⁾	Note ⁽⁵⁾		36 ⁽¹⁰⁾	11.1% ⁽¹⁰⁾
Intact Friction (°)	Note ⁽⁵⁾		48.5 ⁽¹⁰⁾	15.5% ⁽¹⁰⁾	Note ⁽⁵⁾		48.5 ⁽¹⁰⁾	15.5% ⁽¹⁰⁾
Intact Ten Str (MPa)	Note ⁽⁵⁾		8.3 ⁽¹¹⁾		Note ⁽⁵⁾		8.3 ⁽¹¹⁾	
⁽¹²⁾ Joint Coh (MPa) ///	0 ⁽¹⁶⁾		0 ⁽¹⁵⁾		0 ⁽¹⁶⁾		0 ⁽¹⁵⁾	
Joint Fri (°) ///	33 ⁽¹⁶⁾		33 ⁽¹⁵⁾		33 ⁽¹⁶⁾		33 ⁽¹⁵⁾	
⁽¹⁷⁾ Joint Dilatation (°) ///	0		0		0		0	
⁽¹⁷⁾ Joint Ten (MPa) ///	0		0		0		0	
Joint kn (GPa/m) ///	10.6 ⁽¹⁹⁾		19.8 ⁽¹⁹⁾		19.0 ⁽¹⁹⁾		11.2 ⁽¹⁹⁾	
Joint ks (GPa/m) ///	5.3 ⁽²⁰⁾		9.9 ⁽¹⁸⁾		9.4 ⁽²⁰⁾		5.6 ⁽²⁰⁾	
⁽¹³⁾ Joint Coh (MPa) =	0.7 ⁽¹⁶⁾	0.1 MPa	0.7 ⁽¹⁵⁾	0.1 MPa ⁽¹⁵⁾	0.7 ⁽¹⁶⁾	0.1 MPa	0.7 ⁽¹⁵⁾	0.1 MPa
Joint Fri (°) =	44 ⁽¹⁶⁾	2°	44 ⁽¹⁵⁾	2° ⁽¹⁵⁾	44 ⁽¹⁶⁾	2°	44 ⁽¹⁵⁾	2° ⁽¹⁵⁾
⁽¹⁷⁾ Joint Dilatation (°) =	0		0		0		0	
Joint Ten (MPa) =	0.7 ⁽²²⁾		0.7 ⁽²²⁾		0.7 ⁽²²⁾		0.7 ⁽²²⁾	
Joint kn (GPa/m) =	12.4 ⁽¹⁹⁾		23.4 ⁽¹⁹⁾		22.2 ⁽¹⁹⁾		13.2 ⁽¹⁹⁾	
Joint ks (GPa/m) =	6.2 ⁽²⁰⁾		11.7 ⁽¹⁸⁾		11.1 ⁽²⁰⁾		6.6 ⁽²⁰⁾	
⁽¹⁴⁾ Joint Coh (MPa) #	0 ⁽¹⁶⁾		0 ⁽¹⁵⁾		0 ⁽¹⁶⁾		0 ⁽¹⁵⁾	
Joint Fri (°) #	33 ⁽¹⁶⁾		33 ⁽¹⁵⁾		33 ⁽¹⁶⁾		33 ⁽¹⁵⁾	
⁽¹⁷⁾ Joint Dilatation (°) #	0		0		0		0	
⁽¹⁷⁾ Joint Ten (MPa) #	0		0		0		0	
Joint kn (GPa/m) #	10.6 ⁽¹⁹⁾		19.8 ⁽¹⁹⁾		19.0 ⁽¹⁹⁾		11.2 ⁽¹⁹⁾	
Joint ks (GPa/m) #	5.3 ⁽²⁰⁾		9.9 ⁽¹⁸⁾		9.4 ⁽²⁰⁾		5.6 ⁽²⁰⁾	

- (1) Assumed values of porosity and saturation are used to determine density. Note, however, that because these are quasi-static calculations with no gravity acting (only initial stress), the value used for density is irrelevant — i.e., it does not affect the model results. Hence, this assumption has no effect on the results of these analyses. Section (Section 5.2)
- (2) Density = dry density + saturation*porosity*(water density). Dry density taken from ANL-EBS-MD-000027 REV 03 (BSC 2004 [DIRS 166107], Table E-1).
- (3) Determined from average depth of the idealized zone geologic column used to determine the shear-wave velocity profile of the Southern, Eastern and Northwestern "soft zones" and Table E-1, pg. E-2 of ANL-EBS-

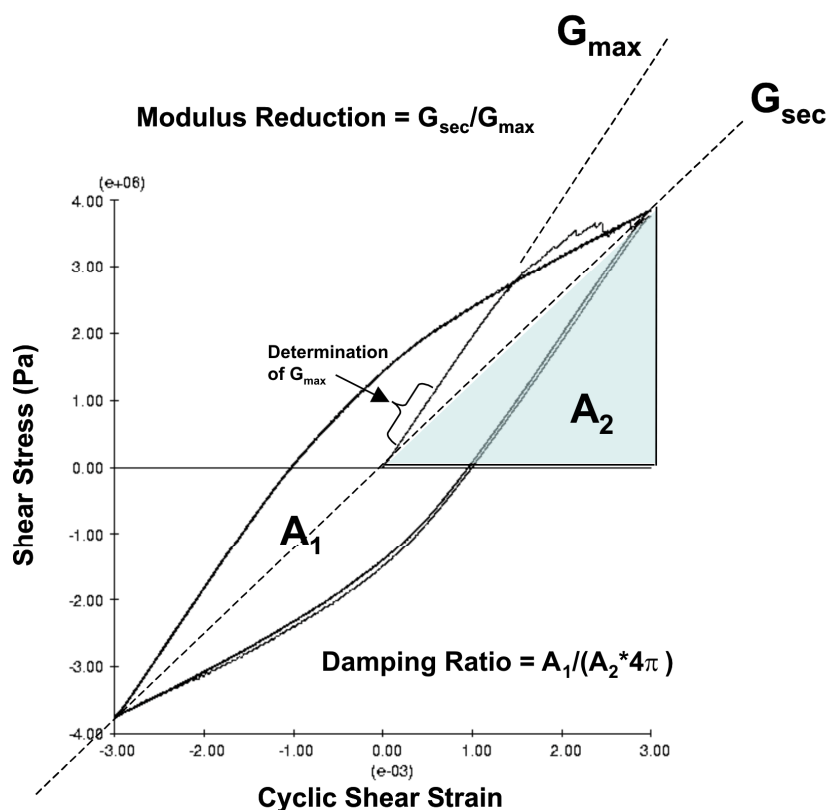
MD-000027 REV 03 (BSC 2004 [DIRS 166107]). See Attachment B, Workbook "icg06-2133-38-46-tmr_udec_sigv.xls"

- (4) $0.5 \times \sigma_v$
- (5) Matrix mechanical properties reflect the rock mass categories 1 to 5 given in Table E-10 of ANL-EBS-MD-000027 REV 03 (BSC 2004 [DIRS 166107]), as a function of the distribution of lithophysal porosity given in Figure E-10 of ANL-EBS-MD-000027 REV 03 (BSC 2004 [DIRS 166107]). See Attachment A.
- (6) From ANL-EBS-MD-000027 REV 03 (BSC 2004 [DIRS 166107]) Table E-6 pg. E-10 and using a scaling factor of 0.90.
- (7) From ANL-EBS-MD-000027 REV 03 (BSC 2004 [DIRS 166107]) Table E-6 pg. E-10.
- (8) From ANL-EBS-MD-000027 REV 03 (BSC 2004 [DIRS 166107]) Table E-6 pg. E-10 and using a scaling factor of 0.51.
- (9) Stiffness scaling-factors used to obtain similar shear wave velocity as field measured.
- (10) From ANL-EBS-MD-000027 REV 03 (BSC 2004 [DIRS 166107]) Fig E-2 pg. E-16.
- (11) From ANL-EBS-MD-000027 REV 03 (BSC 2004 [DIRS 166107]) Table E-7 pg. E-10 to E-12.
- (12) The // symbol identifies sub-vertical joints (i.e., cooling joints).
- (13) The = symbol identifies sub-horizontal joints (i.e., vapor phase partings).
- (14) The # symbol identifies random joints.
- (15) From ANL-EBS-MD-000027 REV 03 (BSC 2004 [DIRS 166107]) Table E-5 pg. E-7.
- (16) Assumed same value as for Tptpmn. These units are similar in many respects to the middle non-lithophysal unit of the Topopah Spring Tuff (the Tptpmn). Hence, the Topopah Spring Tuff should be a reasonable analog for the fracturing in these units as they are mineralogically similar, of similar thickness, were laid down and cooled in a similar manner, and have much the same tectonic history. (Section 5.3)
- (17) **Joint Dilation Angle** is assumed zero for all joints. Defining the dilation angle of a joint as the ratio of normal displacement to plastic shear displacement, during joint shearing, the dilation angle generally is not constant. It increases from zero to a maximum value with increasing shear displacement, and then tends to decrease again to zero with further shearing (as damage of the joint wall material accumulates). Its value also depends significantly on the amount of normal stress supported by the joint. During initial shearing, damage of the joint wall material occurs (e.g., asperities are sheared or crushed/ground), which reduces the dilation angle. Although some recovery of the dilation angle may occur upon shear reversal, subsequent cycles also cause damage accumulation that further reduces the dilation angle. Because the current analysis attempts to determine steady-state damping effects in a rock mass from repeated shear cycles, it is reasonable to assume that sufficient joint damage has occurred that the joint dilation angle is zero. Joint dilation has the effect of very slightly increasing the confinement (or mean stress) in the rock mass. This would have little to no effect on the results of the current analyses. (Section 5.3)
Joint Tensile Strength is assumed zero for vertical to sub-vertical joints in all units, as well as any random joints. These are generally cooling joints and tectonically generated joints, which are rough to smooth, unaltered, unfilled joints. They represent discontinuities, which, by definition, have no tensile strength. This assumption is consistent with common rock-mechanics practice that most joints have very low to zero tensile strength. (Section 5.3)
- (18) From ANL-EBS-MD-000027 REV 03 (BSC 2004 [DIRS 166107]) Table E-5 pg. E-7 and using a scaling-factor of 0.90.
- (19) Assumed normal joint stiffness twice the joint shear stiffness. Joint normal stiffness is typically nonlinear and increases with increasing normal stress. The pre-peak strength joint shear stiffness is typically linear but tends to become nonlinear (decrease) as peak strength is approached. The relative magnitude of the joint normal and shear stiffness are typically within one order of magnitude. For the purpose of these calculations, the normal stiffness is taken as constant and twice the shear stiffness value. In practice, these parameters often are also given the same value. Typically, results are not sensitive to this parameter value unless it is varied by several orders of magnitude. (Section 5.3)
- (20) Assumed same value as Tptpmn (see sub-note (16)) but using a scaling-factor consistent with the specific lithologic unit. (Section 5.3)
- (21) From ANL-EBS-MD-000027 REV 03 (BSC 2004 [DIRS 166107]) Table E-5 pg. E-7.
- (22) Consistent joint tensile strength = (cohesion/(tan(friction angle))).

Table B- 2 Average Initial Shear Stiffness in UDEC Model for the Different Lithologic Units

Lithologic Unit	Initial Shear Modulus (GPa)
Tptpul	3.30
Tptpmn	4.38
Tptpll	4.06
Tptpln	4.52

While simulating the cyclic shear test, the UDEC model automatically records the maximum (i.e., initial) shear modulus, G_{\max} , from the lower portion of the initial loading of the first shear cycle, as shown in Figure B-6. Termination of the test is determined automatically by two convergence criteria: (1) less than 5% difference in the area of the hysteresis loops between consecutive shear cycles, and (2) less than 5% difference in the secant shear modulus, G_{sec} , between consecutive cycles. Both criteria must be satisfied for termination to occur. Definitions of the modulus reduction and damping ratio are also shown in Figure B-6, where A_1 and A_2 are the area of the hysteresis loop and shaded triangle, respectively.



Source: Schematic illustration

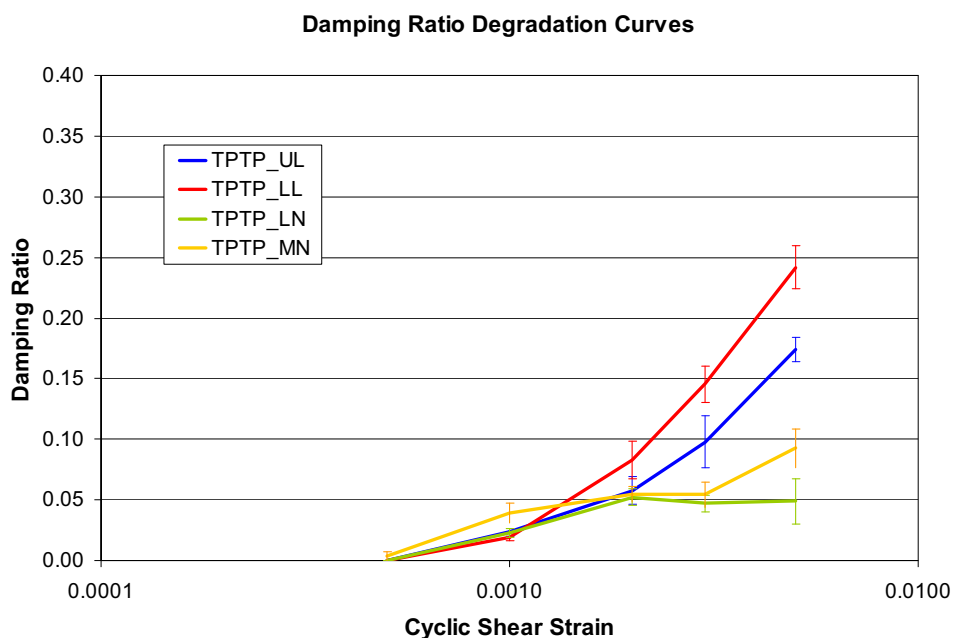
Figure B-6 Definition of Modulus Reduction and Damping Ratio

Conceptually, the model is able to make use of all available geological and mechanical site-data and *in situ* stress information. Although the model is difficult to validate directly (due to the large scale being represented), it is based on simple mechanisms and well-known component behavior.

B3.0 RESULTS

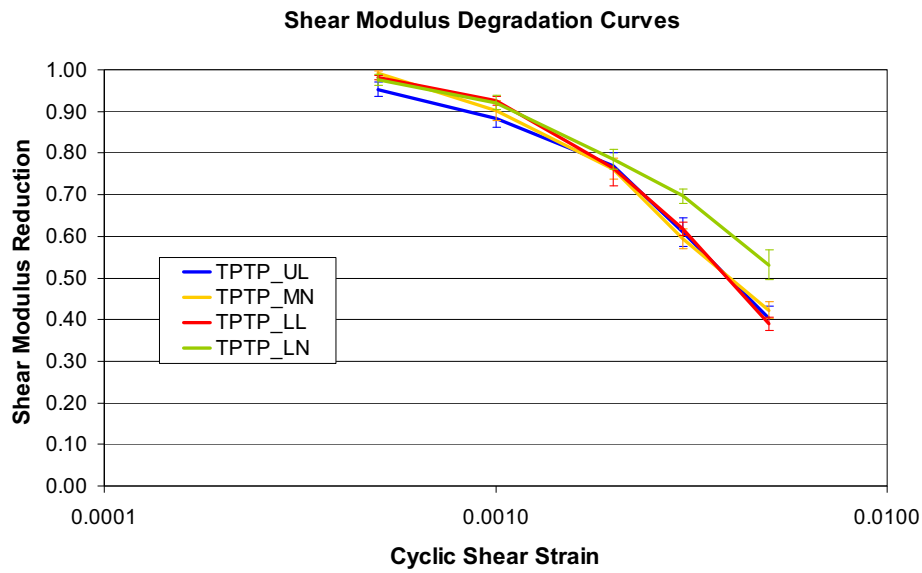
The damping-ratio and modulus degradation curves obtained from these analyses are shown in Figures B-7 and B-8, respectively, for the different lithologic units evaluated. Each curve in these figures shows the mean response from five models of different joint realization. The error bars indicate a dispersion of \pm one standard deviation from the mean. In Figure B-7, it is noticed that the damping-ratio for the lithophysal units (Tptpll and Tptpul) are somewhat higher beyond a shear strain amplitude of about 0.0015, while the modulus reduction shown in Figure B-8 appears to be somewhat similar for all the units.

Figure B-9 shows the general cyclic stress-strain response obtained during the simulations of the Tptpmn and Tptpll units for a strain amplitude of 0.003, while Figure B-10 shows the general trend of the displacements and plasticity indicators at the end of these tests. Much more plastic yielding of the intact rock takes place in the Tptpll unit during the test, and accounts for much of the dissipated energy suggested by the hysteresis loops for this unit — hence, also, the difference in damping-ratio shown in Figure B-7 between the lithophysal and non-lithophysal units.



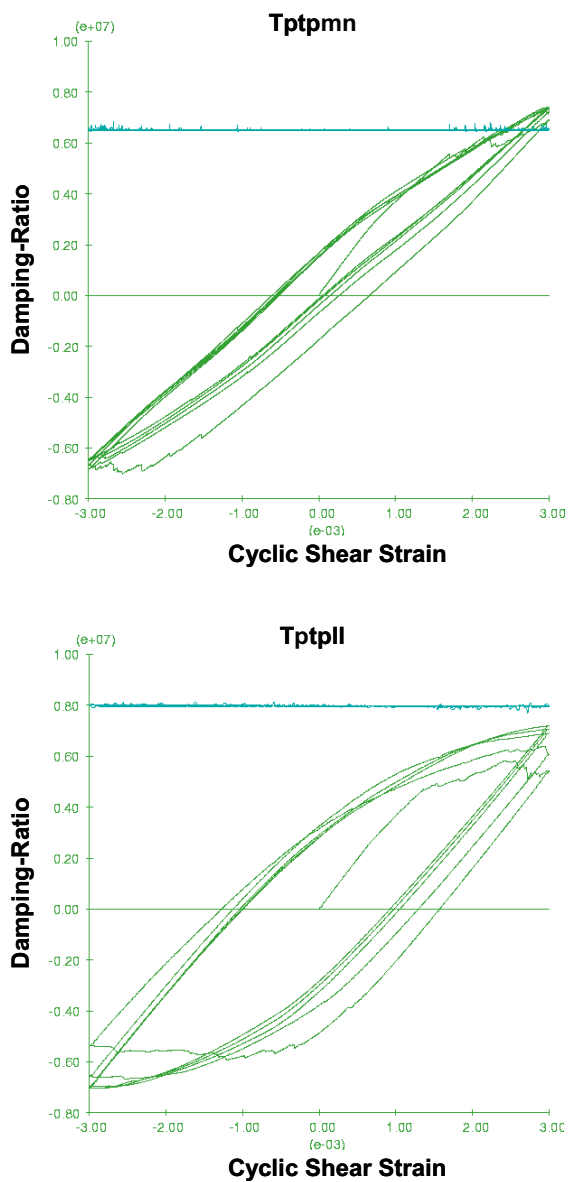
Source: Attachment B, icg06-2133-38-46-tmr_uddec_output.xls, worksheet "Damping Ratio LOG"

Figure B-7 Predicted Damping-Ratio Degradation Curves for Repository Units Tptpul, Tptpmn, Tptpll and Tptpln



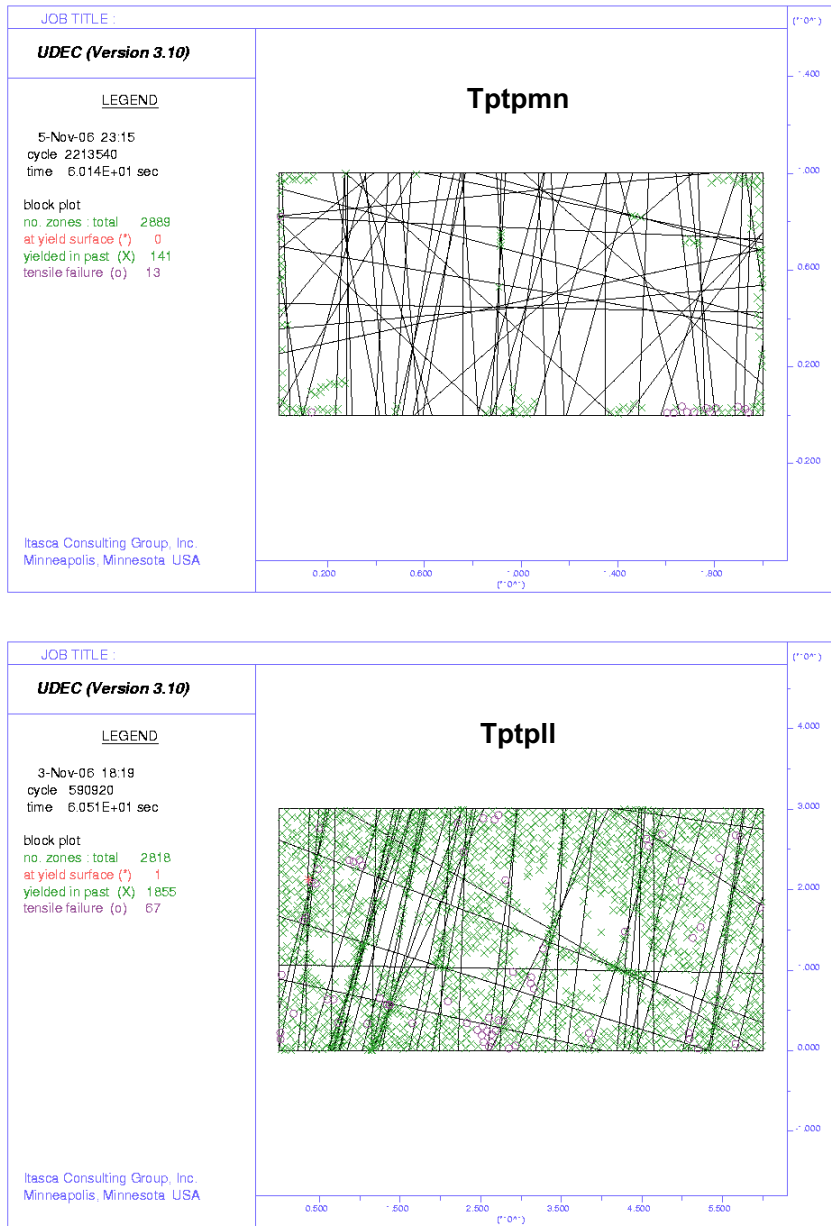
Source: Attachment B, icg06-2133-38-46-tmr_uddec_output.xls, worksheet "Modulus Reduction LOG"

Figure B-8 Predicted Shear Modulus Degradation Curves for Repository Units *Tptpul, Tptpmn, Tptpll and Tptpln*



Source: icg06-2133-38-46-tmr_udec_figs.ppt

Figure B-9 *Stress-Strain Curves from Simulated Cyclic Shear Tests on Tptpmn (top) and Tptpll Units*



Source: icg06-2133-38-46-tmr_uddec_figs.ppt

Figure B-10 Predicted Yielding of Intact Rock During Cyclic Shear Test on Tptpmn (top) and Tptpll Units

ATTACHMENT A

Stiffness and Strength Properties Used For the Lithophysal Units Ttppll and Ttppl

The cohesion values used for the intact rock in the cyclic shear test for Ttppll and Ttppl units were taken from the table below, reproduced from BSC (2004 [DIRS 166107], Table E-10), using a friction angle of 40° . The bulk and shear moduli and cohesion were assigned randomly to zones in the UDEC model bases on the distribution shown in the following figure.

Drift Degradation Analysis

Table E-10. Suggested Range of Mechanical Properties Developed from 11.5-in. Core Testing, Selected for Base-Case Design and Performance Analyses

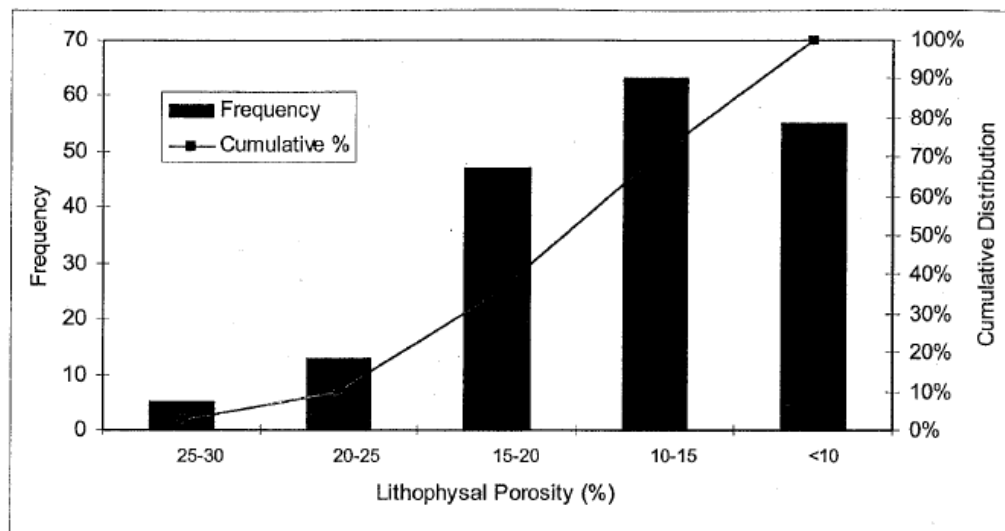
Rock Mass Category	Unconfined Compressive Strength (MPa)	Estimated Young's Modulus ^a (GPa)	Cohesion ^c (MPa)			Bulk Modulus ^c , K (GPa)	Shear Modulus ^c , G (GPa)	Approximate Lithophysal Porosity From Laboratory Tests ^b (%)
			$\phi=50$	$\phi=45$	$\phi=40$			
1	10	1.9	1.82	2.07	2.33	1.07	0.80	35 ± 8
2	15	6.4	2.73	3.11	3.50	3.54	2.65	28 ± 6
3	20	10.8	3.64	4.14	4.66	6.01	4.51	21 ± 4
4	25	15.3	4.55	5.18	5.83	8.48	6.36	13 ± 5
5	30	19.7	5.46	6.21	7.00	10.95	8.21	7 ± 7

Source: DTNs provided in Table E-9.

^a Young's Modulus estimated from linear fit to 11.5-in. core data given in Figure E-8.

^b Approximated lithophysal porosity and ranges are from BSC 2004 [DIRS 168970], Table 6.6-1.

^c Cohesion is calculated using Equation E-8. Bulk and shear modulus values are calculated based on Equations E-2 and E-3.



NOTE: Lithophysal porosity data are from ECRB Cross-Drift station 14+44 to 23+26 (Appendix O, Section O6.6; see Microsoft Excel file, *Drift Deg AMR AF T-A-P Fit.xls*, worksheet "Volume Percent - Stats", which can be accessed through the TDMS using DTN: MO0408MWDDDMIO.002).

Figure E-10. Distribution of Lithophysal Porosity Abundance (Frequency) for the Tptpl in the Enhanced Characterization of the Repository Block Cross-Drift

~~E4.1.4 Investigation of Impact of Lithophysal Variability on Rock Mass Properties~~

~~The Tptpl rock mass is characterized by lithophysal porosity that varies with position in the rock mass. The Topopah Spring unit was laid down rapidly in thin, but laterally-extensive sheets. The formation of lithophysae, which is a phenomenon resulting from movement of vapor within the rock mass during the cooling process, results in a similar layering effect of lithophysal porosity. The mapping presented in Appendix O and analysis of spatial variability presented in Appendix T shows that the lithophysal porosity occurs in thin, laterally-extensive sheets with variability occurring primarily within the plane perpendicular to dip of the units. The approach to assessment of drift stability described in Section 6.4.2 uses parametric analyses based on the consideration of a homogenous rock mass characterized by constant rock properties. To represent the inherent variability of the rock mass, a series of discrete constant property levels, linked to lithophysal porosity, are used to represent (approximately) the lowest, highest and median in situ conditions. The likelihood of occurrence of these particular conditions is based on the percentage of a given strength category to exist in the Tptpl. This simplistic approach (as opposed to attempting to model spatial variability directly) was taken to facilitate modeling.~~

~~The rock mass porosity is, in reality, spatially-variable over a relatively small length scale (on the order of meters – see Appendix O). Therefore, the rock mass rarely consists of uniformly weak or strong material, but consists of small regions of varying strength and modulus. Appendix T presents a model that produces a synthetic representation of the spatial variability of the lithophysal porosity in the Tptpl, based on field mapping as described in Appendix O. Therefore, the consideration of a homogenous rock mass will tend to over predict the failure~~

ATTACHMENT B

Input, Output, Calculation, and Display Files

Input, output, calculation, and display files are contained in an electronic (compact disk) attachment to this report (Attachment B). The “readme.doc” file contained on the compact disk is duplicated below:

Description of directories and content:

The files in these directories represent input and output from numerical model cyclic shear strain tests using UDEC Version 3.14 (STN 10173-3.14-00) to produce shear-modulus and damping-ratio degradation curves at high shear strain amplitudes for lithologic units of the Topopah Spring member (tptpll, tptpln, tptpmn, tptpul). The analysis was conducted by Itasca Consulting Group, Inc, and first reported in Itasca technical memorandum ICG06-2133-38-46-TMR.

Five shear strain levels are considered; 0.0005, 0.001, 0.002, 0.003, and 0.005, hence, There is five sub-directories for each lithologic unit. The directory name is “iii_jjj”, where “iii” identifies the geologic unit, and “jjj” reflects the shears strain level of the cyclic shear test.

The Excel file “icg06-2133-38-46-tmr_udec_output.xls” in the current directory contains output of the entire study, i.e., the UDEC output for each lithologic unit and all strain levels as separate work sheets. It also contains as separate work sheets the modulus-reduction and damping ratio figures used in Itasca technical memorandum ICG06-2133-38-46-TMR.

All other figures are provided in the PowerPoint file “icg06-2133-38-46-tmr_udec_figs.ppt”.

The file Excel file “icg06-2133-38-46-tmr_udec_sigv.xls” was used to determine the vertical stress levels in the four different units for the purpose of the UDEC model.

The directories starting with “Unscaled_” for each lithologic unit contain output (stress-strain curve) of first loading (to 0.001 strain) to determine unscaled maximum shear modulus from the model. In these directories, ASCII files “iii_001.dat” are found, which give max shear modulus of five model realizations. These ASCII files are used in the Excel file “icg06-2133-38-46-tmr_udec_scale_fac.xls” to determine stiffness-scaling factors for the UDECmodel.

The “Joint_gen” directory contains a fish function used to obtain joint traces on a 2D vertical plane from a synthetic 3D joint structure (disk shaped joints in 3D). A readme file is provided in the directory that explains the different files.

APPENDIX C
DEVELOPMENT OF VELOCITY PROFILES FOR YUCCA MOUNTAIN SITE-
RESPONSE MODELING

APPENDIX C

Development of Base Case Vs and Vp profiles for Yucca Mountain calculations.

Base Case Vs and Vp profiles were developed for the RB and SFA using the data and approach described in Section 6.4.2. This Appendix contains the files that show the details of the calculations performed to develop the base case profiles. Where not self explanatory, a “README” sheet has been added to the excel file that explains the data contained and the calculations performed in that excel file.

LIST OF DTNs

The DTNs for the data used in the analyses are summarized below. Note that of the data listed below, the USGS data (1) and the 2004-2005 SASW data (2) are the additional data that were acquired for this study. The remaining data (3, 4 and 5) were acquired, checked, qualified and documented as per the previous study (BSC, 2004). The data acquired, checked and qualified as part of 2004 study were used directly as inputs for this study.

- 1) To estimate the Vs and Vp profiles for the deeper units (Calico Hills Tuff, Prow Pass Tuff and Bullfrog Tuff), the sonic velocity data collected by USGS (Nelson, 1991) was used. The DTNs for the individual boreholes is listed below:
 - GS990908314213_001_S99491_001.zip: Geophysical log and core measurements data from UE25 a#1
 - GS990908314213_001_S99491_006.zip: Geophysical log and core measurements data from UE25 b#1
 - GS990908314213_001_S99491_007.zip: Geophysical log and core measurements data from UE25 c#1
 - GS990908314213_001_S99491_008.zip: Geophysical log and core measurements data from UE25 c#2
 - GS990908314213_001_S99491_009.zip: Geophysical log and core measurements data from UE25 c#3
 - GS960708312132_002_S99394_026.zip: Geophysical log and core measurements data from USW G-1
 - GS960708312132_002_S99394_027.zip: Geophysical log and core measurements data from USW G-2
 - GS960708312132_002_S99394_028.zip: Geophysical log and core measurements data from USW G-3 and GU-3
 - GS960708312132_002_S99394_029.zip: Geophysical log and core measurements data from USW G-4
 - GS960708312132_002_S99394_030.zip: Geophysical log and core measurements data from USW H-1
 - GS960708312132_002_S99394_031.zip: Geophysical log and core measurements data from USW H-3
 - GS960708312132_002_S99394_032.zip: Geophysical log and core measurements data from USW H-4

- GS960708312132_002_S99394_033.zip: Geophysical log and core measurements data from USW H-5
 - GS960708312132_002_S99394_034.zip: Geophysical log and core measurements data from USW H-6
 - GS960708312132_002_S99394_035.zip: Geophysical log and core measurements data from USW P-1
 - GS990908314213_001_S99491_020.zip: Geophysical log and core measurements data from UE25 J-13
- 2) The SASW data collected in 2004-2005 at the RB, SFA, ECRB and ESF:
- MO0609SASWSTDC.003 for the RB (YM surveys) and SFA (NPF surveys).
 - MO0609SASWUTDC.004 for ECRB and ESF
- 3) 2000-2001 SASW data
- MO0110SASWWHBS.000 for the SFA
 - MO0110SASWVDYM.000 for the RB
- 4) 2000-2001 Downhole Data
- MO0110DVBBOREH.000_zz_sep299846 for RF#17
 - MO0111DVDWHBSC.001_zz_sep299529 for RF#14, RF#15, RF#16, RF#18, RF#19, RF#20, RF#21, RF#22, RF#23, RF#24, RF#25, RF#26, RF#28, RF#29.
 - MO0111DVDWHBSC.001_s01165_001 and 002 for RF#13
- 5) 2000-2001 Suspension Data
- The source-to-receiver data was used (BSC, 2004).
 - MO0204SEISSDWHB_001_S02094_001 (RF#13)
 - MO0204SEPBSWHB_001_S02084_017 (RF#14)
 - MO0204SEPBSWHB_001_S02084_018 (RF#15)
 - MO0204SEPBSWHB_001_S02084_019 (RF#16)
 - MO0204SEPBSWHB_001_S02084_020 (RF#17)
 - MO0204SEPBSWHB_001_S02084_021 (RF#18)
 - MO0204SEPBSWHB_001_S02084_022 (RF#19)
 - MO0204SEPBSWHB_001_S02084_023 (RF#20)
 - MO0204SEPBSWHB_001_S02084_024 (RF#21)
 - MO0204SEPBSWHB_001_S02084_025 (RF#22)
 - MO0204SEPBSWHB_001_S02084_026 (RF#23)
 - MO0204SEPBSWHB_001_S02084_027 (RF#24)
 - MO0204SEPBSWHB_001_S02084_028 (RF#25)
 - MO0204SEPBSWHB_001_S02084_029 (RF#26)
 - MO0204SEPBSWHB_001_S02084_030 (RF#28)
 - MO0204SEPBSWHB_001_S02084_031 (RF#29)

Note that as part of the 2004 study (BSC 2004, Section 6.2.3.2.3), the raw suspension data collected in the field (and in the TDMS files listed above) were smoothed "by eye". The smooth profiles were then used in the analyses.

The "smoothing" process has been documented in the scientific notebook SN-M&O-SCI-037-V1 and the data is contained in Supplemental Records (SR) 17 of the same. The smooth profiles obtained from the raw data (BSC, 2004) were used in this analysis as well. Therefore, the suspension data on the spreadsheets need to be checked against the data in SR17.

REPORT FIGURES

Table C-1 lists the paths in the CD data files in which the data shown on the figures in Section 6.4.2 can be found.

Explanation of Data Digitization Method

The raw V_s data obtained from TDMS were digitized in 5 feet intervals. As a result, the reported value on the spreadsheets could be up to 5 feet offset from the actual depth at which the transition in V_s values was observed. In addition, continuing with the convention used in the 2004 study (BSC, 2004), the jump was assumed to occur just below the depth reported in the TDMS data. As an example, if the V_s value changed from 500 feet/sec to 1000 feet/sec at 25 feet depth, the new value (1000 feet/sec) was assumed to occur at 25.01 feet depth. Therefore, on the spreadsheets, the V_s value at 25 feet would be 500 feet/sec and at 30 feet would be 1000 feet/sec.

In the site response analyses performed for the project, the average profiles calculated on the spreadsheets in Appendix C were smoothed "by eye" and the smooth profiles were run as base case velocity profiles. Therefore, the offset caused due to our digitizing scheme gets averaged out in the final base case profiles that were run and does not impact the results.

APPENDIX D
SURFACE FACILITY AREA AND REPOSITORY BLOCK GROUND MOTION
CALCULATIONS

APPENDIX D

Yucca Mountain calculations using Approach 3.

Previous calculations of ground motion were carried out at Yucca Mountain using approach 2B. (See report Development of Earthquake Ground Motion Input for Preclosure Seismic Design and Postclosure Performance Assessment of a Geological Repository at Yucca Mountain, NV; MDL-MGR-GS-000003 REV 00, BSC 2004; [DIRS 166274]) Currently we are using Approach 3 (NUREG/CR-6769; [DIRS 163799]) with updated velocity profiles and nonlinear dynamic material models.

Design ground motions at Yucca Mountain are being developed at two locations, the Surface Facilities Area (SFA), also known as Point D and formerly referred to as the Waste Handling Building (WHB), and the Repository Block, or Point B (Figure 1-1).

REPORT FIGURES

Table D-1 lists the paths in the DVD data files in which the data shown on figures in sections 6.4 and 6.5 can be found.

TABLE D-1		
List of Data Files Used in Report Figures		
6.4.1-17	All	Y06.D\EXCEL\SiteA_RefEq_scale.xls
6.5.1-1	Original Point A	Y07.SAT\EXTHCSVR.MD2\PSHA.F09\HPGV.FRA
	Base Case	Y07.SAT\EXTHCSVR.MD2\FRACTILE.PGV\FRACTILE.OUT
	Sigma = 0.1	Y07.SAT\EXTHCSVR.MD2\FRACTILE.PGV\FRACT10.OUT
	Sigma = 0.2	Y07.SAT\EXTHCSVR.MD2\FRACTILE.PGV\FRACT20.OUT
	Sigma = 0.4	Y07.SAT\EXTHCSVR.MD2\FRACTILE.PGV\FRACT40.OUT
6.5.1-2	Original Point A	Y07.SAT\EXTHCSVR.MD2\PSHA.F09\H1000.FRA
	Base Case	Y07.SAT\EXTHCSVR.MD2\FRACTILE.PGA\FRACTILE.OUT
	Sigma = 0.1	Y07.SAT\EXTHCSVR.MD2\FRACTILE.PGA\FRACT10.OUT
	Sigma = 0.2	Y07.SAT\EXTHCSVR.MD2\FRACTILE.PGA\FRACT20.OUT
	Sigma = 0.4	Y07.SAT\EXTHCSVR.MD2\FRACTILE.PGA\FRACT40.OUT
6.5.1-3	Original Point A	Y07.SAT\EXTHCSVR.MD2\PSHA.F09\H0010.FRA
	Base Case	Y07.SAT\EXTHCSVR.MD2\FRACTILE.010\FRACTILE.OUT
	Sigma = 0.1	Y07.SAT\EXTHCSVR.MD2\FRACTILE.010\FRACT10.OUT
	Sigma = 0.2	Y07.SAT\EXTHCSVR.MD2\FRACTILE.010\FRACT20.OUT
	Sigma = 0.4	Y07.SAT\EXTHCSVR.MD2\FRACTILE.010\FRACT40.OUT
6.5.1-4	Original Point A	Y07.SAT\EXTHCSVR.MD1\PSHA.F09\HPGV.FRA
	Base Case	Y07.SAT\EXTHCSVR.MD1\FRACTILE.PGA\SCALE\FINDIT\FDH1000.DAT
	Sigma = 0.1	Y07.SAT\EXTHCSVR.MD1\FRACTILE.PGA\SCALE.S10\FINDIT\FDH1000.DAT
	Sigma = 0.2	Y07.SAT\EXTHCSVR.MD1\FRACTILE.PGA\SCALE.S20\FINDIT\FDH1000.DAT
	Sigma = 0.4	Y07.SAT\EXTHCSVR.MD1\FRACTILE.PGA\SCALE.S40\FINDIT\FDH1000.DAT
6.5.1-5	Original Point A	Y07.SAT\EXTHCSVR.MD1\PSHA.F09\H1000.FRA
	Base Case	Y07.SAT\EXTHCSVR.MD1\FRACTILE.PGA\SCALE\FINDIT\FDH1000.DAT
	Sigma = 0.1	Y07.SAT\EXTHCSVR.MD1\FRACTILE.PGA\SCALE.S10\FINDIT\FDH1000.DAT
	Sigma = 0.2	Y07.SAT\EXTHCSVR.MD1\FRACTILE.PGA\SCALE.S20\FINDIT\FDH1000.DAT
	Sigma = 0.4	Y07.SAT\EXTHCSVR.MD1\FRACTILE.PGA\SCALE.S40\FINDIT\FDH1000.DAT

TABLE D-1		
List of Data Files Used in Report Figures		
6.5.1-6	Original Point A	Y07.SAT\EXTHCSVR.MD1\PSHA.F09\H0010.FRA
	Base Case	Y07.SAT\EXTHCSVR.MD1\FRACTILE.PGA\SCALE\FINDIT\FDH0010.DAT
	Sigma = 0.1	Y07.SAT\EXTHCSVR.MD1\FRACTILE.PGA\SCALE.S10\FINDIT\FDH0010.DAT
	Sigma = 0.2	Y07.SAT\EXTHCSVR.MD1\FRACTILE.PGA\SCALE.S20\FINDIT\FDH0010.DAT
	Sigma = 0.4	Y07.SAT\EXTHCSVR.MD1\FRACTILE.PGA\SCALE.S40\FINDIT\FDH0010.DAT
6.5.1-7	Original Point A	Y07.SAT\EXTHCSVR.M12\PSHA.F09\HPGV.FRA
	Base Case	Y07.SAT\EXTHCSVR.M12\FRACTILE.PGV\FRACTILE.OUT
6.5.1-8	Original Point A	Y07.SAT\EXTHCSVR.M12\PSHA.F09\H1000.FRA
	Base Case	Y07.SAT\EXTHCSVR.M12\FRACTILE.PGA\FRACTILE.OUT
6.5.1-9	Original Point A	Y07.SAT\EXTHCSVR.M12\PSHA.F09\H0010.FRA
	Base Case	Y07.SAT\EXTHCSVR.M12\FRACTILE.010\FRACTILE.OUT
6.5.1-10	Unconditioned	Y06.D\EHCS15E2.MD1\PSHA.F09\HAZUHS\HUHSMN.OUT
	Conditioned	Y06.D\EHCS15E3.M12\HAZUHS.10G\HUHSMN.OUT
6.5.1-11	Unconditioned	Y06.D\EHCS15E2.MD1\PSHA.F09\HAZUHS\HUHSMN.OUT
	Conditioned	Y06.D\EHCS15E3.M12\HAZUHS.10G\HUHSMN.OUT
6.5.1-12	Unconditioned	Y06.D\EHCS15E2.MD1\PSHA.F09\HAZUHS\HUHSMN.OUT
	Conditioned	Y06.D\EHCS15E3.M12\HAZUHS.10G\HUHSMN.OUT
6.5.1-13	Unconditioned	Y06.D\EHCS15E2.MD1\PSHA.F09\HAZUHS\HUHSMN.OUT
	Conditioned	Y06.D\EHCS1532.M12\HAZUHS.10G\HUHSMN.OUT
6.5.1-14	Unconditioned	Y06.D\EHCS15E2.MD1\PSHA.F09\HAZUHS\HUHSMN.OUT
	Conditioned	Y06.D\EHCS15E3.M12\HAZUHS.10G\HUHSMN.OUT
6.5.1-15	Unconditioned	Y06.D\EHCS15E2.MD1\PSHA.F09\HAZUHS\HUHSMN.OUT
	Conditioned	Y06.D\EHCS15E3.M12\HAZUHS.10G\HUHSMN.OUT
6.5.2-1a	0.01G	Y06.D\RASCALS\AMPS.01\AM1P02D1.D2\G001\LOGN\AMPMED.LOG
	0.05G	Y06.D\RASCALS\AMPS.01\AM1P02D1.D2\G005\LOGN\AMPMED.LOG
	0.10G	Y06.D\RASCALS\AMPS.01\AM1P02D1.D2\G010\LOGN\AMPMED.LOG
	0.20G	Y06.D\RASCALS\AMPS.01\AM1P02D1.D2\G020\LOGN\AMPMED.LOG
	0.30G	Y06.D\RASCALS\AMPS.01\AM1P02D1.D2\G030\LOGN\AMPMED.LOG
	0.40G	Y06.D\RASCALS\AMPS.01\AM1P02D1.D2\G040\LOGN\AMPMED.LOG
6.5.2-1b	0.50G	Y06.D\RASCALS\AMPS.01\AM1P02D1.D2\G050\LOGN\AMPMED.LOG
	0.75G	Y06.D\RASCALS\AMPS.01\AM1P02D1.D2\G075\LOGN\AMPMED.LOG
	1.00G	Y06.D\RASCALS\AMPS.01\AM1P02D1.D2\G100\LOGN\AMPMED.LOG
	1.25G	Y06.D\RASCALS\AMPS.01\AM1P02D1.D2\G125\LOGN\AMPMED.LOG
	1.50G	Y06.D\RASCALS\AMPS.01\AM1P02D1.D2\G150\LOGN\AMPMED.LOG
	2.00G	Y06.D\RASCALS\AMPS.01\AM1P02D1.D2\G200\LOGN\AMPMED.LOG
6.5.2-1c	2.50G	Y06.D\RASCALS\AMPS.01\AM1P02D1.D2\G250\LOGN\AMPMED.LOG
	3.00G	Y06.D\RASCALS\AMPS.01\AM1P02D1.D2\G300\LOGN\AMPMED.LOG
	4.00G	Y06.D\RASCALS\AMPS.01\AM1P02D1.D2\G400\LOGN\AMPMED.LOG
	5.00G	Y06.D\RASCALS\AMPS.01\AM1P02D1.D2\G500\LOGN\AMPMED.LOG
	6.00G	Y06.D\RASCALS\AMPS.01\AM1P02D1.D2\G600\LOGN\AMPMED.LOG
	7.00G	Y06.D\RASCALS\AMPS.01\AM1P02D1.D2\G700\LOGN\AMPMED.LOG
6.5.2-1d	8.00G	Y06.D\RASCALS\AMPS.01\AM1P02D1.D2\G800\LOGN\AMPMED.LOG
	9.00G	Y06.D\RASCALS\AMPS.01\AM1P02D1.D2\G900\LOGN\AMPMED.LOG
	10.00G	Y06.D\RASCALS\AMPS.01\AM1P02D1.D2\G1000\LOGN\AMPMED.LOG

TABLE D-1		
List of Data Files Used in Report Figures		
6.5.2-2a	0.01G	Y06.D\RASCALS\AMPS.01\AM1P02D5.D2\G001\LOGN\AMPMED.LOG
	0.05G	Y06.D\RASCALS\AMPS.01\AM1P02D5.D2\G005\LOGN\AMPMED.LOG
	0.10G	Y06.D\RASCALS\AMPS.01\AM1P02D5.D2\G010\LOGN\AMPMED.LOG
	0.20G	Y06.D\RASCALS\AMPS.01\AM1P02D5.D2\G020\LOGN\AMPMED.LOG
	0.30G	Y06.D\RASCALS\AMPS.01\AM1P02D5.D2\G030\LOGN\AMPMED.LOG
	0.40G	Y06.D\RASCALS\AMPS.01\AM1P02D5.D2\G040\LOGN\AMPMED.LOG
6.5.2-2b	0.50G	Y06.D\RASCALS\AMPS.01\AM1P02D5.D2\G050\LOGN\AMPMED.LOG
	0.75G	Y06.D\RASCALS\AMPS.01\AM1P02D5.D2\G075\LOGN\AMPMED.LOG
	1.00G	Y06.D\RASCALS\AMPS.01\AM1P02D5.D2\G100\LOGN\AMPMED.LOG
	1.25G	Y06.D\RASCALS\AMPS.01\AM1P02D5.D2\G125\LOGN\AMPMED.LOG
	1.50G	Y06.D\RASCALS\AMPS.01\AM1P02D5.D2\G150\LOGN\AMPMED.LOG
	2.00G	Y06.D\RASCALS\AMPS.01\AM1P02D5.D2\G200\LOGN\AMPMED.LOG
6.5.2-2c	2.50G	Y06.D\RASCALS\AMPS.01\AM1P02D5.D2\G250\LOGN\AMPMED.LOG
	3.00G	Y06.D\RASCALS\AMPS.01\AM1P02D5.D2\G300\LOGN\AMPMED.LOG
	4.00G	Y06.D\RASCALS\AMPS.01\AM1P02D5.D2\G400\LOGN\AMPMED.LOG
	5.00G	Y06.D\RASCALS\AMPS.01\AM1P02D5.D2\G500\LOGN\AMPMED.LOG
	6.00G	Y06.D\RASCALS\AMPS.01\AM1P02D5.D2\G600\LOGN\AMPMED.LOG
	7.00G	Y06.D\RASCALS\AMPS.01\AM1P02D5.D2\G700\LOGN\AMPMED.LOG
6.5.2-2d	8.00G	Y06.D\RASCALS\AMPS.01\AM1P02D5.D2\G800\LOGN\AMPMED.LOG
	9.00G	Y06.D\RASCALS\AMPS.01\AM1P02D5.D2\G900\LOGN\AMPMED.LOG
	10.00G	Y06.D\RASCALS\AMPS.01\AM1P02D5.D2\G1000\LOGN\AMPMED.LOG
6.5.2-3a	0.01G	Y06.D\RASCALS\AMPS.02\AM1P02P7.D2\G001\LOGN\AMPMED.LOG
	0.05G	Y06.D\RASCALS\AMPS.02\AM1P02P7.D2\G005\LOGN\AMPMED.LOG
	0.10G	Y06.D\RASCALS\AMPS.02\AM1P02P7.D2\G010\LOGN\AMPMED.LOG
	0.20G	Y06.D\RASCALS\AMPS.02\AM1P02P7.D2\G020\LOGN\AMPMED.LOG
	0.30G	Y06.D\RASCALS\AMPS.02\AM1P02P7.D2\G030\LOGN\AMPMED.LOG
	0.40G	Y06.D\RASCALS\AMPS.02\AM1P02P7.D2\G040\LOGN\AMPMED.LOG
6.5.2-3b	0.50G	Y06.D\RASCALS\AMPS.02\AM1P02P7.D2\G050\LOGN\AMPMED.LOG
	0.75G	Y06.D\RASCALS\AMPS.02\AM1P02P7.D2\G075\LOGN\AMPMED.LOG
	1.00G	Y06.D\RASCALS\AMPS.02\AM1P02P7.D2\G100\LOGN\AMPMED.LOG
	1.25G	Y06.D\RASCALS\AMPS.02\AM1P02P7.D2\G125\LOGN\AMPMED.LOG
	1.50G	Y06.D\RASCALS\AMPS.02\AM1P02P7.D2\G150\LOGN\AMPMED.LOG
	2.00G	Y06.D\RASCALS\AMPS.02\AM1P02P7.D2\G200\LOGN\AMPMED.LOG
6.5.2-3c	2.50G	Y06.D\RASCALS\AMPS.02\AM1P02P7.D2\G250\LOGN\AMPMED.LOG
	3.00G	Y06.D\RASCALS\AMPS.02\AM1P02P7.D2\G300\LOGN\AMPMED.LOG
	4.00G	Y06.D\RASCALS\AMPS.02\AM1P02P7.D2\G400\LOGN\AMPMED.LOG
	5.00G	Y06.D\RASCALS\AMPS.02\AM1P02P7.D2\G500\LOGN\AMPMED.LOG
	6.00G	Y06.D\RASCALS\AMPS.02\AM1P02P7.D2\G600\LOGN\AMPMED.LOG
	7.00G	Y06.D\RASCALS\AMPS.02\AM1P02P7.D2\G700\LOGN\AMPMED.LOG
6.5.2-3d	8.00G	Y06.D\RASCALS\AMPS.02\AM1P02P7.D2\G800\LOGN\AMPMED.LOG
	9.00G	Y06.D\RASCALS\AMPS.02\AM1P02P7.D2\G900\LOGN\AMPMED.LOG
	10.00G	Y06.D\RASCALS\AMPS.02\AM1P02P7.D2\G1000\LOGN\AMPMED.LOG
6.5.2-4	All	Y06.D\Excel\empiricalCamp.xls!VHm6
6.5.2-5	All	Y06.D\Excel\empiricalCamp.xls!VHm6
6.5.2-6	0.01G	Y06.D\RASCALS\AMPS.02\AM1P02P6.D2\G001\LOGN\V_H.LOG

TABLE D-1		
List of Data Files Used in Report Figures		
	0.05G	Y06.D\RASCALS\AMPS.02\AM1P02P6.D2\G005\LOGN\V_H.LOG
	0.10G	Y06.D\RASCALS\AMPS.02\AM1P02P6.D2\G010\LOGN\V_H.LOG
	0.20G	Y06.D\RASCALS\AMPS.02\AM1P02P6.D2\G020\LOGN\V_H.LOG
	0.30G	Y06.D\RASCALS\AMPS.02\AM1P02P6.D2\G030\LOGN\V_H.LOG
6.5.2-7	Horizontal	Y06.D\10GHAZ.01R\FCTP03D1.CMB\HAZUHS\HUMN.OUT
	Vertical	Y06.D\10GHAZ.01R\VFTP03D1.CMB\HAZUHS\HUMN.OUT
6.5.2-8	Horizontal	Y06.D\10GHAZ.01R\FCTP03D1.CMB\HAZUHS\HUMN.OUT
	Vertical	Y06.D\10GHAZ.01R\VFTP03D1.CMB\HAZUHS\HUMN.OUT
6.5.2-9	Horizontal	Y06.D\10GHAZ.01R\FCTP03D1.CMB\HAZUHS\HUMN.OUT
	Vertical	Y06.D\10GHAZ.01R\VFTP03D1.CMB\HAZUHS\HUMN.OUT
6.5.2-10	Horizontal	Y06.D\10GHAZ.01R\FCTP04D1.CMB\HAZUHS\HUMN.OUT
	Vertical	Y06.D\10GHAZ.01R\VFTP04D1.CMB\HAZUHS\HUMN.OUT
6.5.2-11	Horizontal	Y06.D\10GHAZ.01R\FCTP04D1.CMB\HAZUHS\HUMN.OUT
	Vertical	Y06.D\10GHAZ.01R\VFTP04D1.CMB\HAZUHS\HUMN.OUT
6.5.2-12	Horizontal	Y06.D\10GHAZ.01R\FCTP04D1.CMB\HAZUHS\HUMN.OUT
	Vertical	Y06.D\10GHAZ.01R\VFTP04D1.CMB\HAZUHS\HUMN.OUT
6.5.2-13	Horizontal	Y06.D\10GHAZ.01R\FCTP02D1.CMB\HAZUHS\HUMN.OUT
	Vertical	Y06.D\10GHAZ.01R\VFTP02D1.CMB\HAZUHS\HUMN.OUT
6.5.2-14	Horizontal	Y06.D\10GHAZ.01R\FCTP02D1.CMB\HAZUHS\HUMN.OUT
	Vertical	Y06.D\10GHAZ.01R\VFTP02D1.CMB\HAZUHS\HUMN.OUT
6.5.2-15	Horizontal	Y06.D\10GHAZ.01R\FCTP02D1.CMB\HAZUHS\HUMN.OUT
	Vertical	Y06.D\10GHAZ.01R\VFTP02D1.CMB\HAZUHS\HUMN.OUT
6.5.2-16	Horizontal	Y06.D\10GHAZ.01R\FCTP01D1.CMB\HAZUHS\HUMN.OUT
	Vertical	Y06.D\10GHAZ.01R\VFTP01D1.CMB\HAZUHS\HUMN.OUT
6.5.2-17	Horizontal	Y06.D\10GHAZ.01R\FCTP01D1.CMB\HAZUHS\HUMN.OUT
	Vertical	Y06.D\10GHAZ.01R\VFTP01D1.CMB\HAZUHS\HUMN.OUT
6.5.2-18	Horizontal	Y06.D\10GHAZ.01R\FCTP01D1.CMB\HAZUHS\HUMN.OUT
	Vertical	Y06.D\10GHAZ.01R\VFTP01D1.CMB\HAZUHS\HUMN.OUT
6.5.2-19	Horizontal	Y06.D\10GHAZ.01R\FCTP03DS.CM1\HAZUHS\HUMN.OUT
	Vertical	Y06.D\10GHAZ.01R\VFTP03DS.CMB\HAZUHS\HUMN.OUT
6.5.2-20	Horizontal	Y06.D\10GHAZ.01R\FCTP03DS.CM1\HAZUHS\HUMN.OUT
	Vertical	Y06.D\10GHAZ.01R\VFTP03DS.CMB\HAZUHS\HUMN.OUT
6.5.2-21	Horizontal	Y06.D\10GHAZ.01R\FCTP03DS.CM1\HAZUHS\HUMN.OUT
	Vertical	Y06.D\10GHAZ.01R\VFTP03DS.CMB\HAZUHS\HUMN.OUT
6.5.2-22	Horizontal	Y06.D\10GHAZ.01R\FCTP04DS.CM1\HAZUHS\HUMN.OUT
	Vertical	Y06.D\10GHAZ.01R\VFTP04DS.CMB\HAZUHS\HUMN.OUT
6.5.2-23	Horizontal	Y06.D\10GHAZ.01R\FCTP04DS.CM1\HAZUHS\HUMN.OUT
	Vertical	Y06.D\10GHAZ.01R\VFTP04DS.CMB\HAZUHS\HUMN.OUT
6.5.2-24	Horizontal	Y06.D\10GHAZ.01R\FCTP04DS.CM1\HAZUHS\HUMN.OUT
	Vertical	Y06.D\10GHAZ.01R\VFTP04DS.CMB\HAZUHS\HUMN.OUT
6.5.2-25	Horizontal	Y06.D\10GHAZ.01R\FCTP02DS.CM1\HAZUHS\HUMN.OUT
	Vertical	Y06.D\10GHAZ.01R\VFTP02DS.CMB\HAZUHS\HUMN.OUT
6.5.2-26	Horizontal	Y06.D\10GHAZ.01R\FCTP02DS.CM1\HAZUHS\HUMN.OUT
	Vertical	Y06.D\10GHAZ.01R\VFTP02DS.CMB\HAZUHS\HUMN.OUT
6.5.2-27	Horizontal	Y06.D\10GHAZ.01R\FCTP02DS.CM1\HAZUHS\HUMN.OUT

TABLE D-1		
List of Data Files Used in Report Figures		
	Vertical	Y06.D\10GHAZ.01R\VFTP02DS.CMB\HAZUHS\HUMN.OUT
6.5.2-28	Horizontal	Y06.D\10GHAZ.01R\FCTPEND1.ENV\HAZUHS\HUMN.OUT
	Vertical	Y06.D\10GHAZ.01R\VFTPEND1.ENV\HAZUHS\HUMN.OUT
6.5.2-29	Horizontal	Y06.D\10GHAZ.01R\FCTPEND1.ENV\HAZUHS\HUMN.OUT
	Vertical	Y06.D\10GHAZ.01R\VFTPEND1.ENV\HAZUHS\HUMN.OUT
6.5.2-30	Horizontal	Y06.D\10GHAZ.01R\FCTPEND1.ENV\HAZUHS\HUMN.OUT
	Vertical	Y06.D\10GHAZ.01R\VFTPEND1.ENV\HAZUHS\HUMN.OUT
6.5.2-31	Horizontal	Y06.D\10GHAZ.01R\FCTPENDS.EN1\HAZUHS\HUMN.OUT
	Vertical	Y06.D\10GHAZ.01R\VFTPENDS.ENV\HAZUHS\HUMN.OUT
6.5.2-32	Horizontal	Y06.D\10GHAZ.01R\FCTPENDS.EN1\HAZUHS\HUMN.OUT
	Vertical	Y06.D\10GHAZ.01R\VFTPENDS.ENV\HAZUHS\HUMN.OUT
6.5.2-33	Horizontal	Y06.D\10GHAZ.01R\FCTPENDS.EN1\HAZUHS\HUMN.OUT
	Vertical	Y06.D\10GHAZ.01R\VFTPENDS.ENV\HAZUHS\HUMN.OUT
6.5.2-34	Horizontal	Y06.D\10GHAZ.01R\FCTALL.EN1\HAZUHS\HUMN.OUT
	Vertical	Y06.D\10GHAZ.01R\VFTALL.ENV\HAZUHS\HUMN.OUT
6.5.2-35	Horizontal	Y06.D\10GHAZ.01R\FCTALL.EN1\HAZUHS\HUMN.OUT
	Vertical	Y06.D\10GHAZ.01R\VFTALL.ENV\HAZUHS\HUMN.OUT
6.5.2-36	Horizontal	Y06.D\10GHAZ.01R\FCTALL.EN1\HAZUHS\HUMN.OUT
	Vertical	Y06.D\10GHAZ.01R\VFTALL.ENV\HAZUHS\HUMN.OUT
6.5.2-37	Horizontal	Y06.D\10GHAZ.01R\FCTALL.EN1\HAZUHS\HUMN.OUT
	Vertical	Y06.D\10GHAZ.01R\VFTALL.ENV\HAZUHS\HUMN.OUT
6.5.2-38	Horizontal	Y06.D\10GHAZ.01R\FCTALL.EN1\HAZUHS\HUMN.OUT
	Vertical	Y06.D\10GHAZ.01R\VFTALL.ENV\HAZUHS\HUMN.OUT
6.5.2-39	Horizontal	Y06.D\10GHAZ.01R\FCTALL.EN1\HAZUHS\HUMN.OUT
	Vertical	Y06.D\10GHAZ.01R\VFTALL.ENV\HAZUHS\HUMN.OUT
6.5.2-40	Horizontal	Y06.D\10GHAZ.01R\FCTALL.EN1\HAZUHS\HUMN.OUT
	Vertical	Y06.D\10GHAZ.01R\VFTALL.ENV\HAZUHS\HUMN.OUT
6.5.2-41	Horizontal	Y06.D\10GHAZ.01R\FCTALL.EN1\HAZUHS\HUMN.OUT
	Vertical	Y06.D\10GHAZ.01R\VFTALL.ENV\HAZUHS\HUMN.OUT
6.5.2-42	All	Y06.D\10GHAZ.01R\FCTALL.EN1\FPGVMN.OUT
6.5.2-43	Horizontal	Y06.D\10GHAZ.01R\FCTALL.EN1\HAZUHS\HUMN.OUT
	Vertical	Y06.D\10GHAZ.01R\VFTALL.ENV\HAZUHS\HUMN.OUT
6.5.2-44	Horizontal	Y06.D\10GHAZ.01R\FCTALL.EN1\HAZUHS\HUMN.OUT
	Vertical	Y06.D\10GHAZ.01R\VFTALL.ENV\HAZUHS\HUMN.OUT
6.5.2-45	Horizontal	Y06.D\10GHAZ.01R\FCTALL.EN1\HAZUHS\HUMN.OUT
	Vertical	Y06.D\10GHAZ.01R\VFTALL.ENV\HAZUHS\HUMN.OUT
6.5.2-46	Horizontal	Y06.D\10GHAZ.01R\FCTALL.EN1\HAZUHS\HUMN.OUT
	Vertical	Y06.D\10GHAZ.01R\VFTALL.ENV\HAZUHS\HUMN.OUT
6.5.2-47	Horizontal	Y06.D\10GHAZ.01R\FCTALL.EN1\HAZUHS\HUMN.OUT
	Vertical	Y06.D\10GHAZ.01R\VFTALL.ENV\HAZUHS\HUMN.OUT
6.5.2-48	Horizontal	Y06.D\10GHAZ.01R\FCTALL.EN1\HAZUHS\HUMN.OUT
	Vertical	Y06.D\10GHAZ.01R\VFTALL.ENV\HAZUHS\HUMN.OUT
6.5.2-49	Horizontal	Y06.D\10GHAZ.01R\FCTALL.EN1\HAZUHS\HUMN.OUT
	Vertical	Y06.D\10GHAZ.01R\VFTALL.ENV\HAZUHS\HUMN.OUT
6.5.2-50	Horizontal (2007)	Y06.D\MATCH.FNL\10-3\TARGET\H\TARGETI.DAT

TABLE D-1		
List of Data Files Used in Report Figures		
	Horizontal (2004)	MO0410SDSDE103.002 [DIRS 172236]
6.5.2-51	Horizontal (2007)	Y06.D\MATCH.FNL\5E-4\TARGET\H\TARGETI.DAT
	Horizontal (2004)	MO0410SDSTMHIS.005 [DIRS 172237]
6.5.2-52	Horizontal (2007)	Y06.D\MATCH.FNL\10-4\TARGET\H\TARGETI.DAT
	Horizontal (2004)	MO0410WHBDF104.002 [DIRS 172238]
6.5.2-53	Vertical (2007)	Y06.D\MATCH.FNL\10-3\TARGET\V\TARGETI.DAT
	Vertical (2004)	MO0410SDSDE103.002 [DIRS 172236]
6.5.2-54	Vertical (2007)	Y06.D\MATCH.FNL\5E-4\TARGET\V\TARGETI.DAT
	Vertical (2004)	MO0410SDSTMHIS.005 [DIRS 172237]
6.5.2-55	Vertical (2007)	Y06.D\MATCH.FNL\10-4\TARGET\V\TARGETI.DAT
	Vertical (2004)	MO0410WHBDF104.002 [DIRS 172238]
6.5.2-56	3-Oct	Y06.D\MATCH.FNL\10-3\TARGET\H\TARGETI.DAT
	5.00E-04	Y06.D\MATCH.FNL\5E-4\TARGET\H\TARGETI.DAT
	4-Oct	Y06.D\MATCH.FNL\10-4\TARGET\H\TARGETI.DAT
6.5.2-57	3-Oct	Y06.D\MATCH.FNL\10-3\TARGET\V\TARGETI.DAT
	5.00E-04	Y06.D\MATCH.FNL\5E-4\TARGET\V\TARGETI.DAT
	4-Oct	Y06.D\MATCH.FNL\10-4\TARGET\V\TARGETI.DAT
6.5.2-58	All	Y06.D\EXCEL\DAMPED SPECTRA 2007\HORIZONTAL.xls
6.5.2-59	All	Y06.D\EXCEL\DAMPED SPECTRA 2007\HORIZONTAL.xls
6.5.2-60	All	Y06.D\EXCEL\DAMPED SPECTRA 2007\HORIZONTAL.xls
6.5.2-61	All	Y06.D\EXCEL\DAMPED SPECTRA 2007\HORIZONTAL.xls
6.5.2-62	All	Y06.D\EXCEL\DAMPED SPECTRA 2007\HORIZONTAL.xls
6.5.2-63	All	Y06.D\EXCEL\DAMPED SPECTRA 2007\VERTICAL.xls
6.5.2-64	All	Y06.D\EXCEL\DAMPED SPECTRA 2007\VERTICAL.xls
6.5.2-65	All	Y06.D\EXCEL\DAMPED SPECTRA 2007\VERTICAL.xls
6.5.2-66	200 FT	Y06.D\10GHAZ.01R\FCTP01D1.CMB\HAZUHS\HUMN.OUT
	100 FT	Y06.D\10GHAZ.01R\FCTP02D1.CMB\HAZUHS\HUMN.OUT
	70 FT	Y06.D\10GHAZ.01R\FCTP04D1.CMB\HAZUHS\HUMN.OUT
	30 FT	Y06.D\10GHAZ.01R\FCTP03D1.CMB\HAZUHS\HUMN.OUT
6.5.2-67	200 FT	Y06.D\10GHAZ.01R\FCTP01D1.CMB\HAZUHS\HUMN.OUT
	100 FT	Y06.D\10GHAZ.01R\FCTP02D1.CMB\HAZUHS\HUMN.OUT
	70 FT	Y06.D\10GHAZ.01R\FCTP04D1.CMB\HAZUHS\HUMN.OUT
	30 FT	Y06.D\10GHAZ.01R\FCTP03D1.CMB\HAZUHS\HUMN.OUT
6.5.2-68	200 FT	Y06.D\10GHAZ.01R\FCTP01D1.CMB\HAZUHS\HUMN.OUT
	100 FT	Y06.D\10GHAZ.01R\FCTP02D1.CMB\HAZUHS\HUMN.OUT
	70 FT	Y06.D\10GHAZ.01R\FCTP04D1.CMB\HAZUHS\HUMN.OUT
	30 FT	Y06.D\10GHAZ.01R\FCTP03D1.CMB\HAZUHS\HUMN.OUT
6.5.2-69	200 FT	Y06.D\10GHAZ.01R\FCTP01D1.CMB\HAZUHS\HUMN.OUT
	100 FT	Y06.D\10GHAZ.01R\FCTP02D1.CMB\HAZUHS\HUMN.OUT
	70 FT	Y06.D\10GHAZ.01R\FCTP04D1.CMB\HAZUHS\HUMN.OUT
	30 FT	Y06.D\10GHAZ.01R\FCTP03D1.CMB\HAZUHS\HUMN.OUT
6.5.2-70	200 FT	Y06.D\10GHAZ.01R\FCTP01D1.CMB\HAZUHS\HUMN.OUT
	100 FT	Y06.D\10GHAZ.01R\FCTP02D1.CMB\HAZUHS\HUMN.OUT
	70 FT	Y06.D\10GHAZ.01R\FCTP04D1.CMB\HAZUHS\HUMN.OUT
	30 FT	Y06.D\10GHAZ.01R\FCTP03D1.CMB\HAZUHS\HUMN.OUT

TABLE D-1		
List of Data Files Used in Report Figures		
6.5.2-71	North East	Y06.D\10GHAZ.01R\FCTPEND1.ENV\HAZUHS\HUMN.OUT
	South Case A	Y06.D\10GHAZ.01R\FCTPEND2.ENV\HAZUHS\HUMN.OUT
	South Case B	Y06.D\10GHAZ.01R\FCTPEND3.ENV\HAZUHS\HUMN.OUT
	South Case C	Y06.D\10GHAZ.01R\FCTPEND4.ENV\HAZUHS\HUMN.OUT
6.5.2-72	North East	Y06.D\10GHAZ.01R\FCTPEND1.ENV\HAZUHS\HUMN.OUT
	South Case A	Y06.D\10GHAZ.01R\FCTPEND2.ENV\HAZUHS\HUMN.OUT
	South Case B	Y06.D\10GHAZ.01R\FCTPEND3.ENV\HAZUHS\HUMN.OUT
	South Case C	Y06.D\10GHAZ.01R\FCTPEND4.ENV\HAZUHS\HUMN.OUT
6.5.2-73	North East	Y06.D\10GHAZ.01R\FCTPEND1.ENV\HAZUHS\HUMN.OUT
	South Case A	Y06.D\10GHAZ.01R\FCTPEND2.ENV\HAZUHS\HUMN.OUT
	South Case B	Y06.D\10GHAZ.01R\FCTPEND3.ENV\HAZUHS\HUMN.OUT
	South Case C	Y06.D\10GHAZ.01R\FCTPEND4.ENV\HAZUHS\HUMN.OUT
6.5.2-74	North East	Y06.D\10GHAZ.01R\FCTPEND1.ENV\HAZUHS\HUMN.OUT
	South Case A	Y06.D\10GHAZ.01R\FCTPEND2.ENV\HAZUHS\HUMN.OUT
	South Case B	Y06.D\10GHAZ.01R\FCTPEND3.ENV\HAZUHS\HUMN.OUT
	South Case C	Y06.D\10GHAZ.01R\FCTPEND4.ENV\HAZUHS\HUMN.OUT
6.5.2-75	North East	Y06.D\10GHAZ.01R\FCTPEND1.ENV\HAZUHS\HUMN.OUT
	South Case A	Y06.D\10GHAZ.01R\FCTPEND2.ENV\HAZUHS\HUMN.OUT
	South Case B	Y06.D\10GHAZ.01R\FCTPEND3.ENV\HAZUHS\HUMN.OUT
	South Case C	Y06.D\10GHAZ.01R\FCTPEND4.ENV\HAZUHS\HUMN.OUT
6.5.2-76	UMT, UMA	Y06.D\10GHAZ.01R\FCTPEN.M1\HAZUHS\HUMN.OUT
	UMT, LMA	Y06.D\10GHAZ.01R\FCTPEN.M2\HAZUHS\HUMN.OUT
	LMT, UMA	Y06.D\10GHAZ.01R\FCTPEN.M3\HAZUHS\HUMN.OUT
	LMT, LMA	Y06.D\10GHAZ.01R\FCTPEN.M4\HAZUHS\HUMN.OUT
6.5.2-77	UMT, UMA	Y06.D\10GHAZ.01R\FCTPEN.M1\HAZUHS\HUMN.OUT
	UMT, LMA	Y06.D\10GHAZ.01R\FCTPEN.M2\HAZUHS\HUMN.OUT
	LMT, UMA	Y06.D\10GHAZ.01R\FCTPEN.M3\HAZUHS\HUMN.OUT
	LMT, LMA	Y06.D\10GHAZ.01R\FCTPEN.M4\HAZUHS\HUMN.OUT
6.5.2-78	UMT, UMA	Y06.D\10GHAZ.01R\FCTPEN.M1\HAZUHS\HUMN.OUT
	UMT, LMA	Y06.D\10GHAZ.01R\FCTPEN.M2\HAZUHS\HUMN.OUT
	LMT, UMA	Y06.D\10GHAZ.01R\FCTPEN.M3\HAZUHS\HUMN.OUT
	LMT, LMA	Y06.D\10GHAZ.01R\FCTPEN.M4\HAZUHS\HUMN.OUT
6.5.2-79	UMT, UMA	Y06.D\10GHAZ.01R\FCTPEN.M1\HAZUHS\HUMN.OUT
	UMT, LMA	Y06.D\10GHAZ.01R\FCTPEN.M2\HAZUHS\HUMN.OUT
	LMT, UMA	Y06.D\10GHAZ.01R\FCTPEN.M3\HAZUHS\HUMN.OUT
	LMT, LMA	Y06.D\10GHAZ.01R\FCTPEN.M4\HAZUHS\HUMN.OUT
6.5.2-80	UMT, UMA	Y06.D\10GHAZ.01R\FCTPEN.M1\HAZUHS\HUMN.OUT
	UMT, LMA	Y06.D\10GHAZ.01R\FCTPEN.M2\HAZUHS\HUMN.OUT
	LMT, UMA	Y06.D\10GHAZ.01R\FCTPEN.M3\HAZUHS\HUMN.OUT
	LMT, LMA	Y06.D\10GHAZ.01R\FCTPEN.M4\HAZUHS\HUMN.OUT
6.5.2-81	Base Case	Y06.D\HAZUHSI.SEN\FCTP05D2.M2\HAZUHS\HUMN.OUT
	Case 1	Y06.D\HAZUHSI.SEN\FCTP12D2.M2\HAZUHS\HUMN.OUT
	Case 3	Y06.D\HAZUHSI.SEN\FCTP32D2.M2\HAZUHS\HUMN.OUT
	Case 4	Y06.D\HAZUHSI.SEN\FCTP42D2.M2\HAZUHS\HUMN.OUT
	Case 5	Y06.D\HAZUHSI.SEN\FCTP52D2.M2\HAZUHS\HUMN.OUT

TABLE D-1		
List of Data Files Used in Report Figures		
	Case 6	Y06.D\HAZUHSI.SEN\FCTP62D2.M2\HAZUHS\HUMN.OUT
	Case 7	Y06.D\HAZUHSI.SEN\FCTP72D2.M2\HAZUHS\HUMN.OUT
6.5.2-82	Base Case	Y06.D\HAZUHSI.SEN\FCTP05D2.M2\HAZUHS\HUMN.OUT
	Case 1	Y06.D\HAZUHSI.SEN\FCTP12D2.M2\HAZUHS\HUMN.OUT
	Case 3	Y06.D\HAZUHSI.SEN\FCTP32D2.M2\HAZUHS\HUMN.OUT
	Case 4	Y06.D\HAZUHSI.SEN\FCTP42D2.M2\HAZUHS\HUMN.OUT
	Case 5	Y06.D\HAZUHSI.SEN\FCTP52D2.M2\HAZUHS\HUMN.OUT
	Case 6	Y06.D\HAZUHSI.SEN\FCTP62D2.M2\HAZUHS\HUMN.OUT
	Case 7	Y06.D\HAZUHSI.SEN\FCTP72D2.M2\HAZUHS\HUMN.OUT
6.5.2-83	Base Case	Y06.D\HAZUHSI.SEN\FCTP05D2.M2\HAZUHS\HUMN.OUT
	Case 1	Y06.D\HAZUHSI.SEN\FCTP12D2.M2\HAZUHS\HUMN.OUT
	Case 3	Y06.D\HAZUHSI.SEN\FCTP32D2.M2\HAZUHS\HUMN.OUT
	Case 4	Y06.D\HAZUHSI.SEN\FCTP42D2.M2\HAZUHS\HUMN.OUT
	Case 5	Y06.D\HAZUHSI.SEN\FCTP52D2.M2\HAZUHS\HUMN.OUT
	Case 6	Y06.D\HAZUHSI.SEN\FCTP62D2.M2\HAZUHS\HUMN.OUT
	Case 7	Y06.D\HAZUHSI.SEN\FCTP72D2.M2\HAZUHS\HUMN.OUT
6.5.2-84	Base Case	Y06.D\HAZUHSI.SEN\FCTP05D2.M2\HAZUHS\HUMN.OUT
	Case 1	Y06.D\HAZUHSI.SEN\FCTP12D2.M2\HAZUHS\HUMN.OUT
	Case 3	Y06.D\HAZUHSI.SEN\FCTP32D2.M2\HAZUHS\HUMN.OUT
	Case 4	Y06.D\HAZUHSI.SEN\FCTP42D2.M2\HAZUHS\HUMN.OUT
	Case 5	Y06.D\HAZUHSI.SEN\FCTP52D2.M2\HAZUHS\HUMN.OUT
	Case 6	Y06.D\HAZUHSI.SEN\FCTP62D2.M2\HAZUHS\HUMN.OUT
	Case 7	Y06.D\HAZUHSI.SEN\FCTP72D2.M2\HAZUHS\HUMN.OUT
6.5.2-85	Base Case	Y06.D\HAZUHSI.SEN\FCTP05D2.M2\HAZUHS\HUMN.OUT
	Case 1	Y06.D\HAZUHSI.SEN\FCTP12D2.M2\HAZUHS\HUMN.OUT
	Case 3	Y06.D\HAZUHSI.SEN\FCTP32D2.M2\HAZUHS\HUMN.OUT
	Case 4	Y06.D\HAZUHSI.SEN\FCTP42D2.M2\HAZUHS\HUMN.OUT
	Case 5	Y06.D\HAZUHSI.SEN\FCTP52D2.M2\HAZUHS\HUMN.OUT
	Case 6	Y06.D\HAZUHSI.SEN\FCTP62D2.M2\HAZUHS\HUMN.OUT
	Case 7	Y06.D\HAZUHSI.SEN\FCTP72D2.M2\HAZUHS\HUMN.OUT
6.5.2-86	Horizontal 1	Y06.D\MATCH.FNL\ATH\NRCWUS.CD\ROCK\M65D050.100\WWJ090.AT2
	Horizontal 2	Y06.D\MATCH.FNL\ATH\NRCWUS.CD\ROCK\M65D050.100\WWJ180.AT2
	Vertical	Y06.D\MATCH.FNL\ATH\NRCWUS.CD\ROCK\M65D050.100\WWJ-UP.AT2
6.5.2-87	Horizontal 1	Y06.D\MATCH.FNL\ATH\NRCWUS.CD\ROCK\M65D050.100\CUC090.AT2
	Horizontal 2	Y06.D\MATCH.FNL\ATH\NRCWUS.CD\ROCK\M65D050.100\CUC180.AT2
	Vertical	Y06.D\MATCH.FNL\ATH\NRCWUS.CD\ROCK\M65D050.100\CUC-UP.AT2
6.5.2-88	Horizontal 1	Y06.D\MATCH.FNL\ATH\CEUS.CD\ROCK\M65D050.100\a-vir200.ATH
	Horizontal 2	Y06.D\MATCH.FNL\ATH\CEUS.CD\ROCK\M65D050.100\a-vir290.ATH
	Vertical	Y06.D\MATCH.FNL\ATH\CEUS.CD\ROCK\M65D050.100\a-vir-up.ATH
6.5.2-89	Horizontal 1	Y06.D\MATCH.FNL\ATH\NRCWUS.CD\SOIL\M55D000.050\a-ccb270.at2
	Horizontal 2	Y06.D\MATCH.FNL\ATH\NRCWUS.CD\SOIL\M55D000.050\a-ccb360.at2
	Vertical	Y06.D\MATCH.FNL\ATH\NRCWUS.CD\SOIL\M55D000.050\a-ccb-up.at2
6.5.2-90	Horizontal 1	Y06.D\MATCH.FNL\ATH\NRCWUS.CD\ROCK\M75D050.100\tap036-n.at2
	Horizontal 2	Y06.D\MATCH.FNL\ATH\NRCWUS.CD\ROCK\M75D050.100\tap036-w.at2
	Vertical	Y06.D\MATCH.FNL\ATH\NRCWUS.CD\ROCK\M75D050.100\tap036-v.at2

TABLE D-1		
List of Data Files Used in Report Figures		
6.5.2-91	Horizontal 1	Y06.D\MATCH.FNL\ATH\NRCWUS.CD\ROCK\M75D010.050\izn090.at2
	Horizontal 2	Y06.D\MATCH.FNL\ATH\NRCWUS.CD\ROCK\M75D010.050\izn180.at2
	Vertical	Y06.D\MATCH.FNL\ATH\NRCWUS.CD\ROCK\M75D010.050\izn-up.at2
6.5.2-92	Horizontal 1	Y06.D\MATCH.FNL\ATH\CEUS.CD\ROCK\M75D010.050\29p\avd\29p000.ATH
	Horizontal 2	Y06.D\MATCH.FNL\ATH\CEUS.CD\ROCK\M75D010.050\29p\avd\29p090.ATH
	Vertical	Y06.D\MATCH.FNL\ATH\CEUS.CD\ROCK\M75D010.050\29p\avd\29p-up.ATH
6.5.2-93	Horizontal 1	Y06.D\MATCH.FNL\ATH\CEUS.CD\ROCK\M75D010.050\sh\avd\sh1000.ATH
	Horizontal 2	Y06.D\MATCH.FNL\ATH\CEUS.CD\ROCK\M75D010.050\sh\avd\sh1090.ATH
	Vertical	Y06.D\MATCH.FNL\ATH\CEUS.CD\ROCK\M75D010.050\sh\avd\sh1-up.ATH
6.5.2-94	Horizontal 1	Y06.D\MATCH.FNL\ATH\NRCWUS.CD\ROCK\M75D050.100\sil000.at2
	Horizontal 2	Y06.D\MATCH.FNL\ATH\NRCWUS.CD\ROCK\M75D050.100\sil090.at2
	Vertical	Y06.D\MATCH.FNL\ATH\NRCWUS.CD\ROCK\M75D050.100\sil-up.at2
6.5.2-95	Horizontal 1	Y06.D\MATCH.FNL\ATH\CEUS.CD\ROCK\M75D050.100\mcd\avd\mcd090.ATH
	Horizontal 2	Y06.D\MATCH.FNL\ATH\CEUS.CD\ROCK\M75D050.100\mcd\avd\mcd000.ATH
	Vertical	Y06.D\MATCH.FNL\ATH\CEUS.CD\ROCK\M75D050.100\mcd\avd\mcd--v.ATH
6.5.2-96	Target Spectrum	Y06.D\MATCH.FNL\10-3\SWS1H.1\UHS\TARGET11.DAT
	Spectral Match	Y06.D\MATCH.FNL\10-3\SWS1H.1\UHS\BASE4\SPC\MATCH.050
6.5.2-97	Ratio	Y06.D\MATCH.FNL\10-3\SWS1H.1\UHS\BASE4\SPC\MATCH.RAT
6.5.2-98	Acceleration	Y06.D\MATCH.FNL\10-3\SWS1H.1\UHS\BASE4\MATCH.ATH
	Velocity	Y06.D\MATCH.FNL\10-3\SWS1H.1\UHS\BASE4\MATCH.VTH
	Displacement	Y06.D\MATCH.FNL\10-3\SWS1H.1\UHS\BASE4\MATCH.DTH
6.5.2-99	Target Spectrum	Y06.D\MATCH.FNL\10-3\SWS1H.2\UHS\TARGET11.DAT
	Spectral Match	Y06.D\MATCH.FNL\10-3\SWS1H.2\UHS\BASE4\SPC\MATCH.050
6.5.2-100	Ratio	Y06.D\MATCH.FNL\10-3\SWS1H.2\UHS\BASE4\SPC\MATCH.RAT
6.5.2-101	Acceleration	Y06.D\MATCH.FNL\10-3\SWS1H.2\UHS\BASE4\MATCH.ATH
	Velocity	Y06.D\MATCH.FNL\10-3\SWS1H.2\UHS\BASE4\MATCH.VTH
	Displacement	Y06.D\MATCH.FNL\10-3\SWS1H.2\UHS\BASE4\MATCH.DTH
6.5.2-102	Target Spectrum	Y06.D\MATCH.FNL\10-3\SWS1V5\UHS\TARGET11.DAT
	Spectral Match	Y06.D\MATCH.FNL\10-3\SWS1V5\UHS\BASE4\SPC\MATCH.050
6.5.2-103	Ratio	Y06.D\MATCH.FNL\10-3\SWS1V5\UHS\BASE4\SPC\MATCH.RAT
6.5.2-104	Acceleration	Y06.D\MATCH.FNL\10-3\SWS1V5\UHS\BASE4\MATCH.ATH
	Velocity	Y06.D\MATCH.FNL\10-3\SWS1V5\UHS\BASE4\MATCH.VTH
	Displacement	Y06.D\MATCH.FNL\10-3\SWS1V5\UHS\BASE4\MATCH.DTH
6.5.2-105	Target Spectrum	Y06.D\MATCH.FNL\10-3\SWS2H.1\UHS\TARGET11.DAT
	Spectral Match	Y06.D\MATCH.FNL\10-3\SWS2H.1\UHS\BASE4\SPC\MATCH.050
6.5.2-106	Ratio	Y06.D\MATCH.FNL\10-3\SWS2H.1\UHS\BASE4\SPC\MATCH.RAT
6.5.2-107	Acceleration	Y06.D\MATCH.FNL\10-3\SWS2H.1\UHS\BASE4\MATCH.ATH
	Velocity	Y06.D\MATCH.FNL\10-3\SWS2H.1\UHS\BASE4\MATCH.VTH

TABLE D-1		
List of Data Files Used in Report Figures		
	Displacement	Y06.D\MATCH.FNL\10-3\SWS2H.1\UHS\BASE4\MATCH.DTH
6.5.2-108	Target Spectrum	Y06.D\MATCH.FNL\10-3\SWS2H.2\UHS\TARGETI1.DAT
	Spectral Match	Y06.D\MATCH.FNL\10-3\SWS2H.2\UHS\BASE4\SPC\MATCH.050
6.5.2-109	Ratio	Y06.D\MATCH.FNL\10-3\SWS2H.2\UHS\BASE4\SPC\MATCH.RAT
6.5.2-110	Acceleration	Y06.D\MATCH.FNL\10-3\SWS2H.2\UHS\BASE4\MATCH.ATH
	Velocity	Y06.D\MATCH.FNL\10-3\SWS2H.2\UHS\BASE4\MATCH.VTH
	Displacement	Y06.D\MATCH.FNL\10-3\SWS2H.2\UHS\BASE4\MATCH.DTH
6.5.2-111	Target Spectrum	Y06.D\MATCH.FNL\10-3\SWS2V5\UHS\TARGETI1.DAT
	Spectral Match	Y06.D\MATCH.FNL\10-3\SWS2V5\UHS\BASE4\SPC\MATCH.050
6.5.2-112	Ratio	Y06.D\MATCH.FNL\10-3\SWS2V5\UHS\BASE4\SPC\MATCH.RAT
6.5.2-113	Acceleration	Y06.D\MATCH.FNL\10-3\SWS2V5\UHS\BASE4\MATCH.ATH
	Velocity	Y06.D\MATCH.FNL\10-3\SWS2V5\UHS\BASE4\MATCH.VTH
	Displacement	Y06.D\MATCH.FNL\10-3\SWS2V5\UHS\BASE4\MATCH.DTH
6.5.2-114	Target Spectrum	Y06.D\MATCH.FNL\10-3\SWS3H.1\UHS\TARGETI1.DAT
	Spectral Match	Y06.D\MATCH.FNL\10-3\SWS3H.1\UHS\BASE4\SPC\MATCH.050
6.5.2-115	Ratio	Y06.D\MATCH.FNL\10-3\SWS3H.1\UHS\BASE4\SPC\MATCH.RAT
6.5.2-116	Acceleration	Y06.D\MATCH.FNL\10-3\SWS3H.1\UHS\BASE4\MATCH.ATH
	Velocity	Y06.D\MATCH.FNL\10-3\SWS3H.1\UHS\BASE4\MATCH.VTH
	Displacement	Y06.D\MATCH.FNL\10-3\SWS3H.1\UHS\BASE4\MATCH.DTH
6.5.2-117	Target Spectrum	Y06.D\MATCH.FNL\10-3\SWS3H.2\UHS\TARGETI1.DAT
	Spectral Match	Y06.D\MATCH.FNL\10-3\SWS3H.2\UHS\BASE4\SPC\MATCH.050
6.5.2-118	Ratio	Y06.D\MATCH.FNL\10-3\SWS3H.2\UHS\BASE4\SPC\MATCH.RAT
6.5.2-119	Acceleration	Y06.D\MATCH.FNL\10-3\SWS3H.2\UHS\BASE4\MATCH.ATH
	Velocity	Y06.D\MATCH.FNL\10-3\SWS3H.2\UHS\BASE4\MATCH.VTH
	Displacement	Y06.D\MATCH.FNL\10-3\SWS3H.2\UHS\BASE4\MATCH.DTH
6.5.2-120	Target Spectrum	Y06.D\MATCH.FNL\10-3\SWS3V5\UHS\TARGETI1.DAT
	Spectral Match	Y06.D\MATCH.FNL\10-3\SWS3V5\UHS\BASE4\SPC\MATCH.050
6.5.2-121	Ratio	Y06.D\MATCH.FNL\10-3\SWS3V5\UHS\BASE4\SPC\MATCH.RAT
6.5.2-122	Acceleration	Y06.D\MATCH.FNL\10-3\SWS3V5\UHS\BASE4\MATCH.ATH
	Velocity	Y06.D\MATCH.FNL\10-3\SWS3V5\UHS\BASE4\MATCH.VTH
	Displacement	Y06.D\MATCH.FNL\10-3\SWS3V5\UHS\BASE4\MATCH.DTH

TABLE D-1		
List of Data Files Used in Report Figures		
6.5.2-123	Target Spectrum	Y06.D\MATCH.FNL\10-3\SWS4H.1\UHS\TARGET11.DAT
	Spectral Match	Y06.D\MATCH.FNL\10-3\SWS4H.1\UHS\BASE4\SPC\MATCH.050
6.5.2-124	Ratio	Y06.D\MATCH.FNL\10-3\SWS4H.1\UHS\BASE4\SPC\MATCH.RAT
6.5.2-125	Acceleration	Y06.D\MATCH.FNL\10-3\SWS4H.1\UHS\BASE4\MATCH.ATH
	Velocity	Y06.D\MATCH.FNL\10-3\SWS4H.1\UHS\BASE4\MATCH.VTH
	Displacement	Y06.D\MATCH.FNL\10-3\SWS4H.1\UHS\BASE4\MATCH.DTH
6.5.2-126	Target Spectrum	Y06.D\MATCH.FNL\10-3\SWS4H.2\UHS\TARGET11.DAT
	Spectral Match	Y06.D\MATCH.FNL\10-3\SWS4H.2\UHS\BASE4\SPC\MATCH.050
6.5.2-127	Ratio	Y06.D\MATCH.FNL\10-3\SWS4H.2\UHS\BASE4\SPC\MATCH.RAT
6.5.2-128	Acceleration	Y06.D\MATCH.FNL\10-3\SWS4H.2\UHS\BASE4\MATCH.ATH
	Velocity	Y06.D\MATCH.FNL\10-3\SWS4H.2\UHS\BASE4\MATCH.VTH
	Displacement	Y06.D\MATCH.FNL\10-3\SWS4H.2\UHS\BASE4\MATCH.DTH
6.5.2-129	Target Spectrum	Y06.D\MATCH.FNL\10-3\SWS4V5\UHS\TARGET11.DAT
	Spectral Match	Y06.D\MATCH.FNL\10-3\SWS4V5\UHS\BASE4\SPC\MATCH.050
6.5.2-130	Ratio	Y06.D\MATCH.FNL\10-3\SWS4V5\UHS\BASE4\SPC\MATCH.RAT
6.5.2-131	Acceleration	Y06.D\MATCH.FNL\10-3\SWS4V5\UHS\BASE4\MATCH.ATH
	Velocity	Y06.D\MATCH.FNL\10-3\SWS4V5\UHS\BASE4\MATCH.VTH
	Displacement	Y06.D\MATCH.FNL\10-3\SWS4V5\UHS\BASE4\MATCH.DTH
6.5.2-132	Target Spectrum	Y06.D\MATCH.FNL\10-3\SWS5H.1\UHS\TARGET11.DAT
	Spectral Match	Y06.D\MATCH.FNL\10-3\SWS5H.1\UHS\BASE4\SPC\MATCH.050
6.5.2-133	Ratio	Y06.D\MATCH.FNL\10-3\SWS5H.1\UHS\BASE4\SPC\MATCH.RAT
6.5.2-134	Acceleration	Y06.D\MATCH.FNL\10-3\SWS5H.1\UHS\BASE4\MATCH.ATH
	Velocity	Y06.D\MATCH.FNL\10-3\SWS5H.1\UHS\BASE4\MATCH.VTH
	Displacement	Y06.D\MATCH.FNL\10-3\SWS5H.1\UHS\BASE4\MATCH.DTH
6.5.2-135	Target Spectrum	Y06.D\MATCH.FNL\10-3\SWS5H.2\UHS\TARGET11.DAT
	Spectral Match	Y06.D\MATCH.FNL\10-3\SWS5H.2\UHS\BASE4\SPC\MATCH.050
6.5.2-136	Ratio	Y06.D\MATCH.FNL\10-3\SWS5H.2\UHS\BASE4\SPC\MATCH.RAT
6.5.2-137	Acceleration	Y06.D\MATCH.FNL\10-3\SWS5H.2\UHS\BASE4\MATCH.ATH
	Velocity	Y06.D\MATCH.FNL\10-3\SWS5H.2\UHS\BASE4\MATCH.VTH
	Displacement	Y06.D\MATCH.FNL\10-3\SWS5H.2\UHS\BASE4\MATCH.DTH

TABLE D-1		
List of Data Files Used in Report Figures		
6.5.2-138	Target Spectrum	Y06.D\MATCH.FNL\10-3\SWS5V5\UHS\TARGETI1.DAT
	Spectral Match	Y06.D\MATCH.FNL\10-3\SWS5V5\UHS\BASE4\SPC\MATCH.050
6.5.2-139	Ratio	Y06.D\MATCH.FNL\10-3\SWS5V5\UHS\BASE4\SPC\MATCH.RAT
	Acceleration	Y06.D\MATCH.FNL\10-3\SWS5V5\UHS\BASE4\MATCH.ATH
6.5.2-140	Velocity	Y06.D\MATCH.FNL\10-3\SWS5V5\UHS\BASE4\MATCH.VTH
	Displacement	Y06.D\MATCH.FNL\10-3\SWS5V5\UHS\BASE4\MATCH.DTH
6.5.2-141	Target Spectrum	Y06.D\MATCH.FNL\5E-4\SWS1H.1\UHS\TARGETI1.DAT
	Spectral Match	Y06.D\MATCH.FNL\5E-4\SWS1H.1\UHS\BASE4\SPC\MATCH.050
6.5.2-142	Ratio	Y06.D\MATCH.FNL\5E-4\SWS1H.1\UHS\BASE4\SPC\MATCH.RAT
	Acceleration	Y06.D\MATCH.FNL\5E-4\SWS1H.1\UHS\BASE4\MATCH.ATH
6.5.2-143	Velocity	Y06.D\MATCH.FNL\5E-4\SWS1H.1\UHS\BASE4\MATCH.VTH
	Displacement	Y06.D\MATCH.FNL\5E-4\SWS1H.1\UHS\BASE4\MATCH.DTH
6.5.2-144	Target Spectrum	Y06.D\MATCH.FNL\5E-4\SWS1H.2\UHS\TARGETI1.DAT
	Spectral Match	Y06.D\MATCH.FNL\5E-4\SWS1H.2\UHS\BASE4\SPC\MATCH.050
6.5.2-145	Ratio	Y06.D\MATCH.FNL\5E-4\SWS1H.2\UHS\BASE4\SPC\MATCH.RAT
	Acceleration	Y06.D\MATCH.FNL\5E-4\SWS1H.2\UHS\BASE4\MATCH.ATH
6.5.2-146	Velocity	Y06.D\MATCH.FNL\5E-4\SWS1H.2\UHS\BASE4\MATCH.VTH
	Displacement	Y06.D\MATCH.FNL\5E-4\SWS1H.2\UHS\BASE4\MATCH.DTH
6.5.2-147	Target Spectrum	Y06.D\MATCH.FNL\5E-4\SWS1V5\UHS\TARGETI1.DAT
	Spectral Match	Y06.D\MATCH.FNL\5E-4\SWS1V5\UHS\BASE4\SPC\MATCH.050
6.5.2-148	Ratio	Y06.D\MATCH.FNL\5E-4\SWS1V5\UHS\BASE4\SPC\MATCH.RAT
	Acceleration	Y06.D\MATCH.FNL\5E-4\SWS1V5\UHS\BASE4\MATCH.ATH
6.5.2-149	Velocity	Y06.D\MATCH.FNL\5E-4\SWS1V5\UHS\BASE4\MATCH.VTH
	Displacement	Y06.D\MATCH.FNL\5E-4\SWS1V5\UHS\BASE4\MATCH.DTH
6.5.2-150	Target Spectrum	Y06.D\MATCH.FNL\5E-4\SWS2H.1\UHS\TARGETI1.DAT
	Spectral Match	Y06.D\MATCH.FNL\5E-4\SWS2H.1\UHS\BASE4\SPC\MATCH.050
6.5.2-151	Ratio	Y06.D\MATCH.FNL\5E-4\SWS2H.1\UHS\BASE4\SPC\MATCH.RAT
	Acceleration	Y06.D\MATCH.FNL\5E-4\SWS2H.1\UHS\BASE4\MATCH.ATH
6.5.2-152	Velocity	Y06.D\MATCH.FNL\5E-4\SWS2H.1\UHS\BASE4\MATCH.VTH
	Displacement	Y06.D\MATCH.FNL\5E-4\SWS2H.1\UHS\BASE4\MATCH.DTH

TABLE D-1		
List of Data Files Used in Report Figures		
6.5.2-153	Target Spectrum	Y06.D\MATCH.FNL\5E-4\SWS2H.2\UHS\TARGETI1.DAT
	Spectral Match	Y06.D\MATCH.FNL\5E-4\SWS2H.2\UHS\BASE4\SPC\MATCH.050
6.5.2-154	Ratio	Y06.D\MATCH.FNL\5E-4\SWS2H.2\UHS\BASE4\SPC\MATCH.RAT
6.5.2-155	Acceleration	Y06.D\MATCH.FNL\5E-4\SWS2H.2\UHS\BASE4\MATCH.ATH
	Velocity	Y06.D\MATCH.FNL\5E-4\SWS2H.2\UHS\BASE4\MATCH.VTH
	Displacement	Y06.D\MATCH.FNL\5E-4\SWS2H.2\UHS\BASE4\MATCH.DTH
6.5.2-156	Target Spectrum	Y06.D\MATCH.FNL\5E-4\SWS2V5\UHS\TARGETI1.DAT
	Spectral Match	Y06.D\MATCH.FNL\5E-4\SWS2V5\UHS\BASE4\SPC\MATCH.050
6.5.2-157	Ratio	Y06.D\MATCH.FNL\5E-4\SWS2V5\UHS\BASE4\SPC\MATCH.RAT
6.5.2-158	Acceleration	Y06.D\MATCH.FNL\5E-4\SWS2V5\UHS\BASE4\MATCH.ATH
	Velocity	Y06.D\MATCH.FNL\5E-4\SWS2V5\UHS\BASE4\MATCH.VTH
	Displacement	Y06.D\MATCH.FNL\5E-4\SWS2V5\UHS\BASE4\MATCH.DTH
6.5.2-159	Target Spectrum	Y06.D\MATCH.FNL\5E-4\SWS3H.1\UHS\TARGETI1.DAT
	Spectral Match	Y06.D\MATCH.FNL\5E-4\SWS3H.1\UHS\BASE4\SPC\MATCH.050
6.5.2-160	Ratio	Y06.D\MATCH.FNL\5E-4\SWS3H.1\UHS\BASE4\SPC\MATCH.RAT
6.5.2-161	Acceleration	Y06.D\MATCH.FNL\5E-4\SWS3H.1\UHS\BASE4\MATCH.ATH
	Velocity	Y06.D\MATCH.FNL\5E-4\SWS3H.1\UHS\BASE4\MATCH.VTH
	Displacement	Y06.D\MATCH.FNL\5E-4\SWS3H.1\UHS\BASE4\MATCH.DTH
6.5.2-162	Target Spectrum	Y06.D\MATCH.FNL\5E-4\SWS3H.2\UHS\TARGETI1.DAT
	Spectral Match	Y06.D\MATCH.FNL\5E-4\SWS3H.2\UHS\BASE4\SPC\MATCH.050
6.5.2-163	Ratio	Y06.D\MATCH.FNL\5E-4\SWS3H.2\UHS\BASE4\SPC\MATCH.RAT
6.5.2-164	Acceleration	Y06.D\MATCH.FNL\5E-4\SWS3H.2\UHS\BASE4\MATCH.ATH
	Velocity	Y06.D\MATCH.FNL\5E-4\SWS3H.2\UHS\BASE4\MATCH.VTH
	Displacement	Y06.D\MATCH.FNL\5E-4\SWS3H.2\UHS\BASE4\MATCH.DTH
6.5.2-165	Target Spectrum	Y06.D\MATCH.FNL\5E-4\SWS3V5\UHS\TARGETI1.DAT
	Spectral Match	Y06.D\MATCH.FNL\5E-4\SWS3V5\UHS\BASE4\SPC\MATCH.050
6.5.2-166	Ratio	Y06.D\MATCH.FNL\5E-4\SWS3V5\UHS\BASE4\SPC\MATCH.RAT
6.5.2-167	Acceleration	Y06.D\MATCH.FNL\5E-4\SWS3V5\UHS\BASE4\MATCH.ATH
	Velocity	Y06.D\MATCH.FNL\5E-4\SWS3V5\UHS\BASE4\MATCH.VTH
	Displacement	Y06.D\MATCH.FNL\5E-4\SWS3V5\UHS\BASE4\MATCH.DTH
6.5.2-168	Target Spectrum	Y06.D\MATCH.FNL\5E-4\SWS4H.1\UHS\TARGETI1.DAT
	Spectral Match	Y06.D\MATCH.FNL\5E-4\SWS4H.1\UHS\BASE4\SPC\MATCH.050
6.5.2-169	Ratio	Y06.D\MATCH.FNL\5E-4\SWS4H.1\UHS\BASE4\SPC\MATCH.RAT
6.5.2-170	Acceleration	Y06.D\MATCH.FNL\5E-4\SWS4H.1\UHS\BASE4\MATCH.ATH
	Velocity	Y06.D\MATCH.FNL\5E-4\SWS4H.1\UHS\BASE4\MATCH.VTH
	Displacement	Y06.D\MATCH.FNL\5E-4\SWS4H.1\UHS\BASE4\MATCH.DTH
6.5.2-171	Target Spectrum	Y06.D\MATCH.FNL\5E-4\SWS4H.2\UHS\TARGETI1.DAT
	Spectral Match	Y06.D\MATCH.FNL\5E-4\SWS4H.2\UHS\BASE4\SPC\MATCH.050

TABLE D-1		
List of Data Files Used in Report Figures		
6.5.2-172	Ratio	Y06.D\MATCH.FNL\5E-4\SWS4H.2\UHS\BASE4\SPC\MATCH.RAT
6.5.2-173	Acceleration	Y06.D\MATCH.FNL\5E-4\SWS4H.2\UHS\BASE4\MATCH.ATH
	Velocity	Y06.D\MATCH.FNL\5E-4\SWS4H.2\UHS\BASE4\MATCH.VTH
	Displacement	Y06.D\MATCH.FNL\5E-4\SWS4H.2\UHS\BASE4\MATCH.DTH
6.5.2-174	Target Spectrum	Y06.D\MATCH.FNL\5E-4\SWS4V5\UHS\TARGETI1.DAT
	Spectral Match	Y06.D\MATCH.FNL\5E-4\SWS4V5\UHS\BASE4\SPC\MATCH.050
6.5.2-175	Ratio	Y06.D\MATCH.FNL\5E-4\SWS4V5\UHS\BASE4\SPC\MATCH.RAT
6.5.2-176	Acceleration	Y06.D\MATCH.FNL\5E-4\SWS4V5\UHS\BASE4\MATCH.ATH
	Velocity	Y06.D\MATCH.FNL\5E-4\SWS4V5\UHS\BASE4\MATCH.VTH
	Displacement	Y06.D\MATCH.FNL\5E-4\SWS4V5\UHS\BASE4\MATCH.DTH
6.5.2-177	Target Spectrum	Y06.D\MATCH.FNL\5E-4\SWS5H.1\UHS\TARGETI1.DAT
	Spectral Match	Y06.D\MATCH.FNL\5E-4\SWS5H.1\UHS\BASE4\SPC\MATCH.050
6.5.2-178	Ratio	Y06.D\MATCH.FNL\5E-4\SWS5H.1\UHS\BASE4\SPC\MATCH.RAT
6.5.2-179	Acceleration	Y06.D\MATCH.FNL\5E-4\SWS5H.1\UHS\BASE4\MATCH.ATH
	Velocity	Y06.D\MATCH.FNL\5E-4\SWS5H.1\UHS\BASE4\MATCH.VTH
	Displacement	Y06.D\MATCH.FNL\5E-4\SWS5H.1\UHS\BASE4\MATCH.DTH
6.5.2-180	Target Spectrum	Y06.D\MATCH.FNL\5E-4\SWS5H.2\UHS\TARGETI1.DAT
	Spectral Match	Y06.D\MATCH.FNL\5E-4\SWS5H.2\UHS\BASE4\SPC\MATCH.050
6.5.2-181	Ratio	Y06.D\MATCH.FNL\5E-4\SWS5H.2\UHS\BASE4\SPC\MATCH.RAT
6.5.2-182	Acceleration	Y06.D\MATCH.FNL\5E-4\SWS5H.2\UHS\BASE4\MATCH.ATH
	Velocity	Y06.D\MATCH.FNL\5E-4\SWS5H.2\UHS\BASE4\MATCH.VTH
	Displacement	Y06.D\MATCH.FNL\5E-4\SWS5H.2\UHS\BASE4\MATCH.DTH
6.5.2-183	Target Spectrum	Y06.D\MATCH.FNL\5E-4\SWS5V5\UHS\TARGETI1.DAT
	Spectral Match	Y06.D\MATCH.FNL\5E-4\SWS5V5\UHS\BASE4\SPC\MATCH.050
6.5.2-184	Ratio	Y06.D\MATCH.FNL\5E-4\SWS5V5\UHS\BASE4\SPC\MATCH.RAT
6.5.2-185	Acceleration	Y06.D\MATCH.FNL\5E-4\SWS5V5\UHS\BASE4\MATCH.ATH
	Velocity	Y06.D\MATCH.FNL\5E-4\SWS5V5\UHS\BASE4\MATCH.VTH
	Displacement	Y06.D\MATCH.FNL\5E-4\SWS5V5\UHS\BASE4\MATCH.DTH
6.5.2-186	Target Spectrum	Y06.D\MATCH.FNL\10-4\SWS1H.1\UHS\TARGETI1.DAT
	Spectral Match	Y06.D\MATCH.FNL\10-4\SWS1H.1\UHS\BASE4\SPC\MATCH.050
6.5.2-187	Ratio	Y06.D\MATCH.FNL\10-4\SWS1H.1\UHS\BASE4\SPC\MATCH.RAT
6.5.2-188	Acceleration	Y06.D\MATCH.FNL\10-4\SWS1H.1\UHS\BASE4\MATCH.ATH
	Velocity	Y06.D\MATCH.FNL\10-4\SWS1H.1\UHS\BASE4\MATCH.VTH
	Displacement	Y06.D\MATCH.FNL\10-4\SWS1H.1\UHS\BASE4\MATCH.DTH
6.5.2-189	Target Spectrum	Y06.D\MATCH.FNL\10-4\SWS1H.2\UHS\TARGETI1.DAT
	Spectral Match	Y06.D\MATCH.FNL\10-4\SWS1H.2\UHS\BASE4\SPC\MATCH.050
6.5.2-190	Ratio	Y06.D\MATCH.FNL\10-4\SWS1H.2\UHS\BASE4\SPC\MATCH.RAT
6.5.2-191	Acceleration	Y06.D\MATCH.FNL\10-4\SWS1H.2\UHS\BASE4\MATCH.ATH
	Velocity	Y06.D\MATCH.FNL\10-4\SWS1H.2\UHS\BASE4\MATCH.VTH
	Displacement	Y06.D\MATCH.FNL\10-4\SWS1H.2\UHS\BASE4\MATCH.DTH
6.5.2-192	Target Spectrum	Y06.D\MATCH.FNL\10-4\SWS1V5\UHS\TARGETI1.DAT
	Spectral Match	Y06.D\MATCH.FNL\10-4\SWS1V5\UHS\BASE4\SPC\MATCH.050
6.5.2-193	Ratio	Y06.D\MATCH.FNL\10-4\SWS1V5\UHS\BASE4\SPC\MATCH.RAT
6.5.2-194	Acceleration	Y06.D\MATCH.FNL\10-4\SWS1V5\UHS\BASE4\MATCH.ATH
	Velocity	Y06.D\MATCH.FNL\10-4\SWS1V5\UHS\BASE4\MATCH.VTH

TABLE D-1		
List of Data Files Used in Report Figures		
	Displacement	Y06.D\MATCH.FNL\10-4\SWS1V5\UHS\BASE4\MATCH.DTH
6.5.2-195	Target Spectrum	Y06.D\MATCH.FNL\10-4\SWS2H.1\UHS\TARGET11.DAT
	Spectral Match	Y06.D\MATCH.FNL\10-4\SWS2H.1\UHS\BASE4\SPC\MATCH.050
6.5.2-196	Ratio	Y06.D\MATCH.FNL\10-4\SWS2H.1\UHS\BASE4\SPC\MATCH.RAT
6.5.2-197	Acceleration	Y06.D\MATCH.FNL\10-4\SWS2H.1\UHS\BASE4\MATCH.ATH
	Velocity	Y06.D\MATCH.FNL\10-4\SWS2H.1\UHS\BASE4\MATCH.VTH
	Displacement	Y06.D\MATCH.FNL\10-4\SWS2H.1\UHS\BASE4\MATCH.DTH
6.5.2-198	Target Spectrum	Y06.D\MATCH.FNL\10-4\SWS2H.2\UHS\TARGET11.DAT
	Spectral Match	Y06.D\MATCH.FNL\10-4\SWS2H.2\UHS\BASE4\SPC\MATCH.050
6.5.2-199	Ratio	Y06.D\MATCH.FNL\10-4\SWS2H.2\UHS\BASE4\SPC\MATCH.RAT
6.5.2-200	Acceleration	Y06.D\MATCH.FNL\10-4\SWS2H.2\UHS\BASE4\MATCH.ATH
	Velocity	Y06.D\MATCH.FNL\10-4\SWS2H.2\UHS\BASE4\MATCH.VTH
	Displacement	Y06.D\MATCH.FNL\10-4\SWS2H.2\UHS\BASE4\MATCH.DTH
6.5.2-201	Target Spectrum	Y06.D\MATCH.FNL\10-4\SWS2V5\UHS\TARGET11.DAT
	Spectral Match	Y06.D\MATCH.FNL\10-4\SWS2V5\UHS\BASE4\SPC\MATCH.050
6.5.2-202	Ratio	Y06.D\MATCH.FNL\10-4\SWS2V5\UHS\BASE4\SPC\MATCH.RAT
6.5.2-203	Acceleration	Y06.D\MATCH.FNL\10-4\SWS2V5\UHS\BASE4\MATCH.ATH
	Velocity	Y06.D\MATCH.FNL\10-4\SWS2V5\UHS\BASE4\MATCH.VTH
	Displacement	Y06.D\MATCH.FNL\10-4\SWS2V5\UHS\BASE4\MATCH.DTH
6.5.2-204	Target Spectrum	Y06.D\MATCH.FNL\10-4\SWS3H.1\UHS\TARGET11.DAT
	Spectral Match	Y06.D\MATCH.FNL\10-4\SWS3H.1\UHS\BASE4\SPC\MATCH.050
6.5.2-205	Ratio	Y06.D\MATCH.FNL\10-4\SWS3H.1\UHS\BASE4\SPC\MATCH.RAT
6.5.2-206	Acceleration	Y06.D\MATCH.FNL\10-4\SWS3H.1\UHS\BASE4\MATCH.ATH
	Velocity	Y06.D\MATCH.FNL\10-4\SWS3H.1\UHS\BASE4\MATCH.VTH
	Displacement	Y06.D\MATCH.FNL\10-4\SWS3H.1\UHS\BASE4\MATCH.DTH
6.5.2-207	Target Spectrum	Y06.D\MATCH.FNL\10-4\SWS3H.2\UHS\TARGET11.DAT
	Spectral Match	Y06.D\MATCH.FNL\10-4\SWS3H.2\UHS\BASE4\SPC\MATCH.050
6.5.2-208	Ratio	Y06.D\MATCH.FNL\10-4\SWS3H.2\UHS\BASE4\SPC\MATCH.RAT
6.5.2-209	Acceleration	Y06.D\MATCH.FNL\10-4\SWS3H.2\UHS\BASE4\MATCH.ATH
	Velocity	Y06.D\MATCH.FNL\10-4\SWS3H.2\UHS\BASE4\MATCH.VTH
	Displacement	Y06.D\MATCH.FNL\10-4\SWS3H.2\UHS\BASE4\MATCH.DTH
6.5.2-210	Target Spectrum	Y06.D\MATCH.FNL\10-4\SWS3V5\UHS\TARGET11.DAT
	Spectral Match	Y06.D\MATCH.FNL\10-4\SWS3V5\UHS\BASE4\SPC\MATCH.050
6.5.2-211	Ratio	Y06.D\MATCH.FNL\10-4\SWS3V5\UHS\BASE4\SPC\MATCH.RAT
6.5.2-212	Acceleration	Y06.D\MATCH.FNL\10-4\SWS3V5\UHS\BASE4\MATCH.ATH
	Velocity	Y06.D\MATCH.FNL\10-4\SWS3V5\UHS\BASE4\MATCH.VTH
	Displacement	Y06.D\MATCH.FNL\10-4\SWS3V5\UHS\BASE4\MATCH.DTH
6.5.2-213	Target Spectrum	Y06.D\MATCH.FNL\10-4\SWS4H.1\UHS\TARGET11.DAT
	Spectral Match	Y06.D\MATCH.FNL\10-4\SWS4H.1\UHS\BASE4\SPC\MATCH.050
6.5.2-214	Ratio	Y06.D\MATCH.FNL\10-4\SWS4H.1\UHS\BASE4\SPC\MATCH.RAT
6.5.2-215	Acceleration	Y06.D\MATCH.FNL\10-4\SWS4H.1\UHS\BASE4\MATCH.ATH
	Velocity	Y06.D\MATCH.FNL\10-4\SWS4H.1\UHS\BASE4\MATCH.VTH
	Displacement	Y06.D\MATCH.FNL\10-4\SWS4H.1\UHS\BASE4\MATCH.DTH
6.5.2-216	Target Spectrum	Y06.D\MATCH.FNL\10-4\SWS4H.2\UHS\TARGET11.DAT
	Spectral Match	Y06.D\MATCH.FNL\10-4\SWS4H.2\UHS\BASE4\SPC\MATCH.050

TABLE D-1		
List of Data Files Used in Report Figures		
6.5.2-217	Ratio	Y06.D\MATCH.FNL\10-4\SWS4H.2\UHS\BASE4\SPC\MATCH.RAT
6.5.2-218	Acceleration	Y06.D\MATCH.FNL\10-4\SWS4H.2\UHS\BASE4\MATCH.ATH
	Velocity	Y06.D\MATCH.FNL\10-4\SWS4H.2\UHS\BASE4\MATCH.VTH
	Displacement	Y06.D\MATCH.FNL\10-4\SWS4H.2\UHS\BASE4\MATCH.DTH
6.5.2-219	Target Spectrum	Y06.D\MATCH.FNL\10-4\SWS4V5\UHS\TARGETI1.DAT
	Spectral Match	Y06.D\MATCH.FNL\10-4\SWS4V5\UHS\BASE4\SPC\MATCH.050
6.5.2-220	Ratio	Y06.D\MATCH.FNL\10-4\SWS4V5\UHS\BASE4\SPC\MATCH.RAT
6.5.2-221	Acceleration	Y06.D\MATCH.FNL\10-4\SWS4V5\UHS\BASE4\MATCH.ATH
	Velocity	Y06.D\MATCH.FNL\10-4\SWS4V5\UHS\BASE4\MATCH.VTH
	Displacement	Y06.D\MATCH.FNL\10-4\SWS4V5\UHS\BASE4\MATCH.DTH
6.5.2-222	Target Spectrum	Y06.D\MATCH.FNL\10-4\SWS5H.1\UHS\TARGETI1.DAT
	Spectral Match	Y06.D\MATCH.FNL\10-4\SWS5H.1\UHS\BASE4\SPC\MATCH.050
6.5.2-223	Ratio	Y06.D\MATCH.FNL\10-4\SWS5H.1\UHS\BASE4\SPC\MATCH.RAT
6.5.2-224	Acceleration	Y06.D\MATCH.FNL\10-4\SWS5H.1\UHS\BASE4\MATCH.ATH
	Velocity	Y06.D\MATCH.FNL\10-4\SWS5H.1\UHS\BASE4\MATCH.VTH
	Displacement	Y06.D\MATCH.FNL\10-4\SWS5H.1\UHS\BASE4\MATCH.DTH
6.5.2-225	Target Spectrum	Y06.D\MATCH.FNL\10-4\SWS5H.2\UHS\TARGETI1.DAT
	Spectral Match	Y06.D\MATCH.FNL\10-4\SWS5H.2\UHS\BASE4\SPC\MATCH.050
6.5.2-226	Ratio	Y06.D\MATCH.FNL\10-4\SWS5H.2\UHS\BASE4\SPC\MATCH.RAT
6.5.2-227	Acceleration	Y06.D\MATCH.FNL\10-4\SWS5H.2\UHS\BASE4\MATCH.ATH
	Velocity	Y06.D\MATCH.FNL\10-4\SWS5H.2\UHS\BASE4\MATCH.VTH
	Displacement	Y06.D\MATCH.FNL\10-4\SWS5H.2\UHS\BASE4\MATCH.DTH
6.5.2-228	Target Spectrum	Y06.D\MATCH.FNL\10-4\SWS5V5\UHS\TARGETI1.DAT
	Spectral Match	Y06.D\MATCH.FNL\10-4\SWS5V5\UHS\BASE4\SPC\MATCH.050
6.5.2-229	Ratio	Y06.D\MATCH.FNL\10-4\SWS5V5\UHS\BASE4\SPC\MATCH.RAT
6.5.2-230	Acceleration	Y06.D\MATCH.FNL\10-4\SWS5V5\UHS\BASE4\MATCH.ATH
	Velocity	Y06.D\MATCH.FNL\10-4\SWS5V5\UHS\BASE4\MATCH.VTH
	Displacement	Y06.D\MATCH.FNL\10-4\SWS5V5\UHS\BASE4\MATCH.DTH
6.5.2-231	All	Y06.D\RASCALS\AMPS.02\SIG10G45.ALL\NE.030\P-10001.OUT
6.5.2-232	All	Y06.D\RASCALS\AMPS.02\SIG10G45.ALL\NE.030\P-10001.OUT
6.5.2-233	All	Y06.D\RASCALS\AMPS.02\SIG10G45.ALL\NE.030\P-10001.OUT
6.5.2-234	All	Y06.D\RASCALS\AMPS.02\SIG10G45.ALL\NE.030\P-10001.OUT
6.5.2-235	All	Y06.D\RASCALS\AMPS.02\SIG10G45.ALL\NE.070\P-10001.OUT
6.5.2-236	All	Y06.D\RASCALS\AMPS.02\SIG10G45.ALL\NE.070\P-10001.OUT
6.5.2-237	All	Y06.D\RASCALS\AMPS.02\SIG10G45.ALL\NE.070\P-10001.OUT
6.5.2-238	All	Y06.D\RASCALS\AMPS.02\SIG10G45.ALL\NE.070\P-10001.OUT
6.5.2-239	All	Y06.D\RASCALS\AMPS.02\SIG10G45.ALL\NE.100\P-10001.OUT
6.5.2-240	All	Y06.D\RASCALS\AMPS.02\SIG10G45.ALL\NE.100\P-10001.OUT
6.5.2-241	All	Y06.D\RASCALS\AMPS.02\SIG10G45.ALL\NE.100\P-10001.OUT
6.5.2-242	All	Y06.D\RASCALS\AMPS.02\SIG10G45.ALL\NE.100\P-10001.OUT
6.5.2-243	All	Y06.D\RASCALS\AMPS.02\SIG10G45.ALL\NE.200\P-10001.OUT
6.5.2-244	All	Y06.D\RASCALS\AMPS.02\SIG10G45.ALL\NE.200\P-10001.OUT
6.5.2-245	All	Y06.D\RASCALS\AMPS.02\SIG10G45.ALL\NE.200\P-10001.OUT
6.5.2-246	All	Y06.D\RASCALS\AMPS.02\SIG10G45.ALL\NE.200\P-10001.OUT
6.5.2-247	All	Y06.D\RASCALS\AMPS.02\SIG10G45.ALL\SOUTH.030\P-10001.OUT

TABLE D-1		
List of Data Files Used in Report Figures		
6.5.2-248	All	Y06.D\RASCALS\AMPS.02\SIG10G45.ALL\SOUTH.030\P-10001.OUT
6.5.2-249	All	Y06.D\RASCALS\AMPS.02\SIG10G45.ALL\SOUTH.030\P-10001.OUT
6.5.2-250	All	Y06.D\RASCALS\AMPS.02\SIG10G45.ALL\SOUTH.030\P-10001.OUT
6.5.2-251	All	Y06.D\RASCALS\AMPS.02\SIG10G45.ALL\SOUTH.070\P-10001.OUT
6.5.2-252	All	Y06.D\RASCALS\AMPS.02\SIG10G45.ALL\SOUTH.070\P-10001.OUT
6.5.2-253	All	Y06.D\RASCALS\AMPS.02\SIG10G45.ALL\SOUTH.070\P-10001.OUT
6.5.2-254	All	Y06.D\RASCALS\AMPS.02\SIG10G45.ALL\SOUTH.070\P-10001.OUT
6.5.2-255	All	Y06.D\RASCALS\AMPS.02\SIG10G45.ALL\SOUTH.100\P-10001.OUT
6.5.2-256	All	Y06.D\RASCALS\AMPS.02\SIG10G45.ALL\SOUTH.100\P-10001.OUT
6.5.2-257	All	Y06.D\RASCALS\AMPS.02\SIG10G45.ALL\SOUTH.100\P-10001.OUT
6.5.2-258	All	Y06.D\RASCALS\AMPS.02\SIG10G45.ALL\SOUTH.100\P-10001.OUT
6.5.2-259	All	Y06.D\RASCALS\AMPS.02\SIG10G45.ALL\NE.030\P-10002.OUT
6.5.2-260	All	Y06.D\RASCALS\AMPS.02\SIG10G45.ALL\NE.030\P-10002.OUT
6.5.2-261	All	Y06.D\RASCALS\AMPS.02\SIG10G45.ALL\NE.030\P-10002.OUT
6.5.2-262	All	Y06.D\RASCALS\AMPS.02\SIG10G45.ALL\NE.030\P-10002.OUT
6.5.2-263	All	Y06.D\RASCALS\AMPS.02\SIG10G45.ALL\NE.070\P-10002.OUT
6.5.2-264	All	Y06.D\RASCALS\AMPS.02\SIG10G45.ALL\NE.070\P-10002.OUT
6.5.2-265	All	Y06.D\RASCALS\AMPS.02\SIG10G45.ALL\NE.070\P-10002.OUT
6.5.2-266	All	Y06.D\RASCALS\AMPS.02\SIG10G45.ALL\NE.070\P-10002.OUT
6.5.2-267	All	Y06.D\RASCALS\AMPS.02\SIG10G45.ALL\NE.100\P-10002.OUT
6.5.2-268	All	Y06.D\RASCALS\AMPS.02\SIG10G45.ALL\NE.100\P-10002.OUT
6.5.2-269	All	Y06.D\RASCALS\AMPS.02\SIG10G45.ALL\NE.100\P-10002.OUT
6.5.2-270	All	Y06.D\RASCALS\AMPS.02\SIG10G45.ALL\NE.100\P-10002.OUT
6.5.2-271	All	Y06.D\RASCALS\AMPS.02\SIG10G45.ALL\NE.200\P-10002.OUT
6.5.2-272	All	Y06.D\RASCALS\AMPS.02\SIG10G45.ALL\NE.200\P-10002.OUT
6.5.2-273	All	Y06.D\RASCALS\AMPS.02\SIG10G45.ALL\NE.200\P-10002.OUT
6.5.2-274	All	Y06.D\RASCALS\AMPS.02\SIG10G45.ALL\NE.200\P-10002.OUT
6.5.2-275	All	Y06.D\RASCALS\AMPS.02\SIG10G45.ALL\SOUTH.030\P-10002.OUT
6.5.2-276	All	Y06.D\RASCALS\AMPS.02\SIG10G45.ALL\SOUTH.030\P-10002.OUT
6.5.2-277	All	Y06.D\RASCALS\AMPS.02\SIG10G45.ALL\SOUTH.030\P-10002.OUT
6.5.2-278	All	Y06.D\RASCALS\AMPS.02\SIG10G45.ALL\SOUTH.030\P-10002.OUT
6.5.2-279	All	Y06.D\RASCALS\AMPS.02\SIG10G45.ALL\SOUTH.070\P-10002.OUT
6.5.2-280	All	Y06.D\RASCALS\AMPS.02\SIG10G45.ALL\SOUTH.070\P-10002.OUT
6.5.2-281	All	Y06.D\RASCALS\AMPS.02\SIG10G45.ALL\SOUTH.070\P-10002.OUT
6.5.2-282	All	Y06.D\RASCALS\AMPS.02\SIG10G45.ALL\SOUTH.070\P-10002.OUT
6.5.2-283	All	Y06.D\RASCALS\AMPS.02\SIG10G45.ALL\SOUTH.100\P-10002.OUT
6.5.2-284	All	Y06.D\RASCALS\AMPS.02\SIG10G45.ALL\SOUTH.100\P-10002.OUT
6.5.2-285	All	Y06.D\RASCALS\AMPS.02\SIG10G45.ALL\SOUTH.100\P-10002.OUT
6.5.2-286	All	Y06.D\RASCALS\AMPS.02\SIG10G45.ALL\SOUTH.100\P-10002.OUT
6.5.2-287	All	Y06.D\RASCALS\AMPS.02\SIG10G45.ALL\NE.030\P-10010.OUT
6.5.2-288	All	Y06.D\RASCALS\AMPS.02\SIG10G45.ALL\NE.030\P-10010.OUT
6.5.2-289	All	Y06.D\RASCALS\AMPS.02\SIG10G45.ALL\NE.030\P-10010.OUT
6.5.2-290	All	Y06.D\RASCALS\AMPS.02\SIG10G45.ALL\NE.030\P-10010.OUT
6.5.2-291	All	Y06.D\RASCALS\AMPS.02\SIG10G45.ALL\NE.070\P-10010.OUT
6.5.2-292	All	Y06.D\RASCALS\AMPS.02\SIG10G45.ALL\NE.070\P-10010.OUT

TABLE D-1		
List of Data Files Used in Report Figures		
6.5.2-293	All	Y06.D\RASCALS\AMPS.02\SIG10G45.ALL\NE.070\P-10010.OUT
6.5.2-294	All	Y06.D\RASCALS\AMPS.02\SIG10G45.ALL\NE.070\P-10010.OUT
6.5.2-295	All	Y06.D\RASCALS\AMPS.02\SIG10G45.ALL\NE.100\P-10010.OUT
6.5.2-296	All	Y06.D\RASCALS\AMPS.02\SIG10G45.ALL\NE.100\P-10010.OUT
6.5.2-297	All	Y06.D\RASCALS\AMPS.02\SIG10G45.ALL\NE.100\P-10010.OUT
6.5.2-298	All	Y06.D\RASCALS\AMPS.02\SIG10G45.ALL\NE.100\P-10010.OUT
6.5.2-299	All	Y06.D\RASCALS\AMPS.02\SIG10G45.ALL\NE.200\P-10010.OUT
6.5.2-300	All	Y06.D\RASCALS\AMPS.02\SIG10G45.ALL\NE.200\P-10010.OUT
6.5.2-301	All	Y06.D\RASCALS\AMPS.02\SIG10G45.ALL\NE.200\P-10010.OUT
6.5.2-302	All	Y06.D\RASCALS\AMPS.02\SIG10G45.ALL\NE.200\P-10010.OUT
6.5.2-303	All	Y06.D\RASCALS\AMPS.02\SIG10G45.ALL\SOUTH.030\P-10010.OUT
6.5.2-304	All	Y06.D\RASCALS\AMPS.02\SIG10G45.ALL\SOUTH.030\P-10010.OUT
6.5.2-305	All	Y06.D\RASCALS\AMPS.02\SIG10G45.ALL\SOUTH.030\P-10010.OUT
6.5.2-306	All	Y06.D\RASCALS\AMPS.02\SIG10G45.ALL\SOUTH.030\P-10010.OUT
6.5.2-307	All	Y06.D\RASCALS\AMPS.02\SIG10G45.ALL\SOUTH.070\P-10010.OUT
6.5.2-308	All	Y06.D\RASCALS\AMPS.02\SIG10G45.ALL\SOUTH.070\P-10010.OUT
6.5.2-309	All	Y06.D\RASCALS\AMPS.02\SIG10G45.ALL\SOUTH.070\P-10010.OUT
6.5.2-310	All	Y06.D\RASCALS\AMPS.02\SIG10G45.ALL\SOUTH.070\P-10010.OUT
6.5.2-311	All	Y06.D\RASCALS\AMPS.02\SIG10G45.ALL\SOUTH.100\P-10010.OUT
6.5.2-312	All	Y06.D\RASCALS\AMPS.02\SIG10G45.ALL\SOUTH.100\P-10010.OUT
6.5.2-313	All	Y06.D\RASCALS\AMPS.02\SIG10G45.ALL\SOUTH.100\P-10010.OUT
6.5.2-314	All	Y06.D\RASCALS\AMPS.02\SIG10G45.ALL\SOUTH.100\P-10010.OUT
6.5.3-1a	0.01G	Y06.D\RASCALS\AMPS.01\AM1P02D5.B1\G001\LOGN\AMPMED.LOG
	0.05G	Y06.D\RASCALS\AMPS.01\AM1P02D5.B1\G005\LOGN\AMPMED.LOG
	0.10G	Y06.D\RASCALS\AMPS.01\AM1P02D5.B1\G010\LOGN\AMPMED.LOG
	0.20G	Y06.D\RASCALS\AMPS.01\AM1P02D5.B1\G020\LOGN\AMPMED.LOG
	0.30G	Y06.D\RASCALS\AMPS.01\AM1P02D5.B1\G030\LOGN\AMPMED.LOG
	0.40G	Y06.D\RASCALS\AMPS.01\AM1P02D5.B1\G040\LOGN\AMPMED.LOG
6.5.3-1b	0.50G	Y06.D\RASCALS\AMPS.01\AM1P02D5.B1\G050\LOGN\AMPMED.LOG
	0.75G	Y06.D\RASCALS\AMPS.01\AM1P02D5.B1\G075\LOGN\AMPMED.LOG
	1.00G	Y06.D\RASCALS\AMPS.01\AM1P02D5.B1\G100\LOGN\AMPMED.LOG
	1.25G	Y06.D\RASCALS\AMPS.01\AM1P02D5.B1\G125\LOGN\AMPMED.LOG
	1.50G	Y06.D\RASCALS\AMPS.01\AM1P02D5.B1\G150\LOGN\AMPMED.LOG
	2.00G	Y06.D\RASCALS\AMPS.01\AM1P02D5.B1\G200\LOGN\AMPMED.LOG
6.5.3-1c	2.50G	Y06.D\RASCALS\AMPS.01\AM1P02D5.B1\G250\LOGN\AMPMED.LOG
	3.00G	Y06.D\RASCALS\AMPS.01\AM1P02D5.B1\G300\LOGN\AMPMED.LOG
	4.00G	Y06.D\RASCALS\AMPS.01\AM1P02D5.B1\G400\LOGN\AMPMED.LOG
	5.00G	Y06.D\RASCALS\AMPS.01\AM1P02D5.B1\G500\LOGN\AMPMED.LOG
	6.00G	Y06.D\RASCALS\AMPS.01\AM1P02D5.B1\G600\LOGN\AMPMED.LOG
	7.00G	Y06.D\RASCALS\AMPS.01\AM1P02D5.B1\G700\LOGN\AMPMED.LOG
6.5.3-1d	8.00G	Y06.D\RASCALS\AMPS.01\AM1P02D5.B1\G800\LOGN\AMPMED.LOG
	9.00G	Y06.D\RASCALS\AMPS.01\AM1P02D5.B1\G900\LOGN\AMPMED.LOG
	10.00G	Y06.D\RASCALS\AMPS.01\AM1P02D5.B1\G1000\LOGN\AMPMED.LOG

TABLE D-1		
List of Data Files Used in Report Figures		
6.5.3-2	0.01G	Y06.D\RASCALS\AMPS.02\AM1P02P6.B1\G001\LOGN\V_H.LOG
	0.05G	Y06.D\RASCALS\AMPS.02\AM1P02P6.B1\G005\LOGN\V_H.LOG
	0.10G	Y06.D\RASCALS\AMPS.02\AM1P02P6.B1\G010\LOGN\V_H.LOG
	0.20G	Y06.D\RASCALS\AMPS.02\AM1P02P6.B1\G020\LOGN\V_H.LOG
	0.30G	Y06.D\RASCALS\AMPS.02\AM1P02P6.B1\G030\LOGN\V_H.LOG
6.5.3-3	Horizontal	Y06.D\10GHAZ.03B\FCTP02B1.CMB\HAZUHS\HUMN.OUT
	Vertical	Y06.D\10GHAZ.03B\VFTP02B1.CMB\HAZUHS\HUMN.OUT
6.5.3-4	Horizontal	Y06.D\10GHAZ.03B\FCTP02B1.CMB\HAZUHS\HUMN.OUT
	Vertical	Y06.D\10GHAZ.03B\VFTP02B1.CMB\HAZUHS\HUMN.OUT
6.5.3-5	Horizontal	Y06.D\10GHAZ.03B\FCTP02B1.CMB\HAZUHS\HUMN.OUT
	Vertical	Y06.D\10GHAZ.03B\VFTP02B1.CMB\HAZUHS\HUMN.OUT
6.5.3-6	Horizontal	Y06.D\10GHAZ.03B\FCTP02B4.CMB\HAZUHS\HUMN.OUT
	Vertical	Y06.D\10GHAZ.03B\VFTP02B4.CMB\HAZUHS\HUMN.OUT
6.5.3-7	Horizontal	Y06.D\10GHAZ.03B\FCTP02B4.CMB\HAZUHS\HUMN.OUT
	Vertical	Y06.D\10GHAZ.03B\VFTP02B4.CMB\HAZUHS\HUMN.OUT
6.5.3-8	Horizontal	Y06.D\10GHAZ.03B\FCTP02B4.CMB\HAZUHS\HUMN.OUT
	Vertical	Y06.D\10GHAZ.03B\VFTP02B4.CMB\HAZUHS\HUMN.OUT
6.5.3-9	Horizontal	Y06.D\10GHAZ.03B\FCTPENB.ENV\HAZUHS\HUMN.OUT
	Vertical	Y06.D\10GHAZ.03B\VFTPENB.ENV\HAZUHS\HUMN.OUT
6.5.3-10	Horizontal	Y06.D\10GHAZ.03B\FCTPENB.ENV\HAZUHS\HUMN.OUT
	Vertical	Y06.D\10GHAZ.03B\VFTPENB.ENV\HAZUHS\HUMN.OUT
6.5.3-11	Horizontal	Y06.D\10GHAZ.03B\FCTPENB.ENV\HAZUHS\HUMN.OUT
	Vertical	Y06.D\10GHAZ.03B\VFTPENB.ENV\HAZUHS\HUMN.OUT
6.5.3-12	Horizontal	Y06.D\10GHAZ.03B\FCTPENB.ENV\HAZUHS\HUMN.OUT
	Vertical	Y06.D\10GHAZ.03B\VFTPENB.ENV\HAZUHS\HUMN.OUT
6.5.3-13	Horizontal	Y06.D\10GHAZ.03B\FCTPENB.ENV\HAZUHS\HUMN.OUT
	Vertical	Y06.D\10GHAZ.03B\VFTPENB.ENV\HAZUHS\HUMN.OUT
6.5.3-14	Horizontal	Y06.D\10GHAZ.03B\FCTPENB.ENV\HAZUHS\HUMN.OUT
	Vertical	Y06.D\10GHAZ.03B\VFTPENB.ENV\HAZUHS\HUMN.OUT
6.5.3-15	Horizontal	Y06.D\10GHAZ.03B\FCTPENB.ENV\HAZUHS\HUMN.OUT
	Vertical	Y06.D\10GHAZ.03B\VFTPENB.ENV\HAZUHS\HUMN.OUT
6.5.3-16	Horizontal	Y06.D\10GHAZ.03B\FCTPENB.ENV\HAZUHS\HUMN.OUT
	Vertical	Y06.D\10GHAZ.03B\VFTPENB.ENV\HAZUHS\HUMN.OUT
6.5.3-17a	Mean	Y06.D\10GHAZ.03B\FCTPENB.ENV\FPGVMN.OUT
	Median	Y06.D\10GHAZ.03B\FCTPENB.ENV\FPGVFE.OUT
	5 th	Y06.D\10GHAZ.03B\FCTPENB.ENV\FPGVFB.OUT
	15 th	Y06.D\10GHAZ.03B\FCTPENB.ENV\FPGVFC.OUT
	85 th	Y06.D\10GHAZ.03B\FCTPENB.ENV\FPGVFG.OUT
	95 th	Y06.D\10GHAZ.03B\FCTPENB.ENV\FPGVFH.OUT
6.5.3-17b	2005 Conditioned	DTN MO0501BPVELEMP.001 [DIRS 172682]
	2004 Unconditioned	DTNs MO0401SEPPGVRL.022 [DIRS 169099], MO0303DPGVB106.002 [DIRS 162712], MO0210PGVPB107.000 [DIRS 162713]
	2008 Conditioned	Y06.D\10GHAZ.03B\FCTPENB.ENV\FPGVMN.OUT
6.5.3-18	Mean	Y06.D\10GHAZ.03B\FCTPENB.ENV\FPGVMN.OUT
	Median	Y06.D\10GHAZ.03B\FCTPENB.ENV\FPGVFE.OUT

TABLE D-1		
List of Data Files Used in Report Figures		
	5 th	Y06.D\10GHAZ.03B\VFTPENB.ENV\FPGVFB.OUT
	15 th	Y06.D\10GHAZ.03B\VFTPENB.ENV\FPGVFC.OUT
	85 th	Y06.D\10GHAZ.03B\VFTPENB.ENV\FPGVFG.OUT
	95 th	Y06.D\10GHAZ.03B\VFTPENB.ENV\FPGVFH.OUT
6.5.3-19	Horizontal	Y06.D\10GHAZ.03B\FCTPENB.ENV\HAZUHS\HUMN.OUT
	Vertical	Y06.D\10GHAZ.03B\VFTPENB.ENV\HAZUHS\HUMN.OUT
6.5.3-20	Horizontal	Y06.D\10GHAZ.03B\FCTPENB.ENV\HAZUHS\HUMN.OUT
	Vertical	Y06.D\10GHAZ.03B\VFTPENB.ENV\HAZUHS\HUMN.OUT
6.5.3-21	Horizontal	Y06.D\10GHAZ.03B\FCTPENB.ENV\HAZUHS\HUMN.OUT
	Vertical	Y06.D\10GHAZ.03B\VFTPENB.ENV\HAZUHS\HUMN.OUT
6.5.3-22	Horizontal	Y06.D\10GHAZ.03B\FCTPENB.ENV\HAZUHS\HUMN.OUT
	Vertical	Y06.D\10GHAZ.03B\VFTPENB.ENV\HAZUHS\HUMN.OUT
6.5.3-23	Horizontal	Y06.D\10GHAZ.03B\FCTPENB.ENV\HAZUHS\HUMN.OUT
	Vertical	Y06.D\10GHAZ.03B\VFTPENB.ENV\HAZUHS\HUMN.OUT
6.5.3-24	Horizontal	Y06.D\10GHAZ.03B\FCTPENB.ENV\HAZUHS\HUMN.OUT
	Vertical	Y06.D\10GHAZ.03B\VFTPENB.ENV\HAZUHS\HUMN.OUT
6.5.3-25	Horizontal	Y06.D\10GHAZ.03B\FCTPENB.ENV\HAZUHS\HUMN.OUT
	Vertical	Y06.D\10GHAZ.03B\VFTPENB.ENV\HAZUHS\HUMN.OUT
6.5.3-26	Horizontal	Y06.D\MATCH.FNL\10-3\TARGET.REP\H\TARGETI.DAT
	Vertical	Y06.D\MATCH.FNL\10-3\TARGET.REP\V\TARGETI.DAT
6.5.3-27	Horizontal	Y06.D\MATCH.FNL\5E-4\TARGET.REP\H\TARGETI.DAT
	Vertical	Y06.D\MATCH.FNL\5E-4\TARGET.REP\V\TARGETI.DAT
6.5.3-28	Horizontal	Y06.D\MATCH.FNL\10-4\TARGET.REP\H\TARGETI.DAT
	Vertical	Y06.D\MATCH.FNL\10-4\TARGET.REP\V\TARGETI.DAT
6.5.3-29	2007 Horizontal	Y06.D\MATCH.FNL\10-3\TARGET.REP\H\TARGETI.DAT
	2004 Horizontal	MO0405SDSTPNTB.001 [DIRS 169851]
6.5.3-30	2007 Horizontal	Y06.D\MATCH.FNL\5E-4\TARGET.REP\H\TARGETI.DAT
	2004 Horizontal	MO0405SDSTPNTB.001 [DIRS 169851]
6.5.3-31	2007 Horizontal	Y06.D\MATCH.FNL\10-4\TARGET.REP\H\TARGETI.DAT
	2004 Horizontal	MO0407SDARS104.001 [DIRS 170683]
6.5.3-32	2007 Vertical	Y06.D\MATCH.FNL\10-3\TARGET.REP\V\TARGETI.DAT
	2004 Vertical	MO0407SDARS104.001 [DIRS 170683]
6.5.3-33	2007 Vertical	Y06.D\MATCH.FNL\5E-4\TARGET.REP\V\TARGETI.DAT
	2004 Vertical	MO0306SDSAVDTH.000 [DIRS 164033]
6.5.3-34	2007 Vertical	Y06.D\MATCH.FNL\10-4\TARGET.REP\V\TARGETI.DAT
	2004 Vertical	MO0306SDSAVDTH.000 [DIRS 164033]
6.5.3-35	Envelope	Y06.D\10GHAZ.03B\FCTPENB.ENV\HAZUHS\HUMN.OUT
	Soft Zone	Y06.D\10GHAZ.03B\FCTP02B1.CMB\HAZUHS\HUMN.OUT
	Stiff Zone	Y06.D\10GHAZ.03B\FCTP02B4.CMB\HAZUHS\HUMN.OUT
6.5.3-36	Envelope	Y06.D\10GHAZ.03B\FCTPENB.ENV\HAZUHS\HUMN.OUT
	Soft Zone	Y06.D\10GHAZ.03B\FCTP02B1.CMB\HAZUHS\HUMN.OUT
	Stiff Zone	Y06.D\10GHAZ.03B\FCTP02B4.CMB\HAZUHS\HUMN.OUT
6.5.3-37	Envelope	Y06.D\10GHAZ.03B\FCTPENB.ENV\HAZUHS\HUMN.OUT
	Soft Zone	Y06.D\10GHAZ.03B\FCTP02B1.CMB\HAZUHS\HUMN.OUT
	Stiff Zone	Y06.D\10GHAZ.03B\FCTP02B4.CMB\HAZUHS\HUMN.OUT

TABLE D-1		
List of Data Files Used in Report Figures		
6.5.3-38	Envelope	Y06.D\10GHAZ.03B\FCTPENB.ENV\HAZUHS\HUMN.OUT
	Soft Zone	Y06.D\10GHAZ.03B\FCTP02B1.CMB\HAZUHS\HUMN.OUT
	Stiff Zone	Y06.D\10GHAZ.03B\FCTP02B4.CMB\HAZUHS\HUMN.OUT
6.5.3-39	Envelope	Y06.D\10GHAZ.03B\FCTPENB.ENV\HAZUHS\HUMN.OUT
	Soft Zone	Y06.D\10GHAZ.03B\FCTP02B1.CMB\HAZUHS\HUMN.OUT
	Stiff Zone	Y06.D\10GHAZ.03B\FCTP02B4.CMB\HAZUHS\HUMN.OUT
6.5.3-40	Envelope	Y06.D\10GHAZ.03B\FCTPENB.ENV\HAZUHS\HUMN.OUT
	Soft Zone	Y06.D\10GHAZ.03B\FCTP02B1.CMB\HAZUHS\HUMN.OUT
	Stiff Zone	Y06.D\10GHAZ.03B\FCTP02B4.CMB\HAZUHS\HUMN.OUT
6.5.3-41	Envelope	Y06.D\10GHAZ.03B\FCTPENB.ENV\HAZUHS\HUMN.OUT
	Soft Zone	Y06.D\10GHAZ.03B\FCTP02B1.CMB\HAZUHS\HUMN.OUT
	Stiff Zone	Y06.D\10GHAZ.03B\FCTP02B4.CMB\HAZUHS\HUMN.OUT
6.5.3-42	UMT	Y06.D\10GHAZ.03B\FCTP02B1.M1\HAZUHS\HUMN.OUT
	LMT	Y06.D\10GHAZ.03B\FCTP02B1.M3\HAZUHS\HUMN.OUT
6.5.3-43	UMT	Y06.D\10GHAZ.03B\FCTP02B1.M1\HAZUHS\HUMN.OUT
	LMT	Y06.D\10GHAZ.03B\FCTP02B1.M3\HAZUHS\HUMN.OUT
6.5.3-44	UMT	Y06.D\10GHAZ.03B\FCTP02B1.M1\HAZUHS\HUMN.OUT
	LMT	Y06.D\10GHAZ.03B\FCTP02B1.M3\HAZUHS\HUMN.OUT
6.5.3-45	UMT	Y06.D\10GHAZ.03B\FCTP02B1.M1\HAZUHS\HUMN.OUT
	LMT	Y06.D\10GHAZ.03B\FCTP02B1.M3\HAZUHS\HUMN.OUT
6.5.3-46	UMT	Y06.D\10GHAZ.03B\FCTP02B1.M1\HAZUHS\HUMN.OUT
	LMT	Y06.D\10GHAZ.03B\FCTP02B1.M3\HAZUHS\HUMN.OUT
6.5.3-47	UMT	Y06.D\10GHAZ.03B\FCTP02B1.M1\HAZUHS\HUMN.OUT
	LMT	Y06.D\10GHAZ.03B\FCTP02B1.M3\HAZUHS\HUMN.OUT
6.5.3-48	UMT	Y06.D\10GHAZ.03B\FCTP02B1.M1\HAZUHS\HUMN.OUT
	LMT	Y06.D\10GHAZ.03B\FCTP02B1.M3\HAZUHS\HUMN.OUT
6.5.3-49	Horizontal 1	Y06.D\MATCH.FNL\ATH\NRCWUS.CD\ROCK\M65D050.100\MEL\H1.A02
	Horizontal 2	Y06.D\MATCH.FNL\ATH\NRCWUS.CD\ROCK\M65D050.100\MEL\H2.A02
	Vertical	Y06.D\MATCH.FNL\ATH\NRCWUS.CD\ROCK\M65D050.100\MEL\UP.A02
6.5.3-50	Horizontal 1	Y06.D\MATCH.FNL\ATH\NRCWUS.CD\ROCK\M75D010.050\TCU015-N.AT2
	Horizontal 2	Y06.D\MATCH.FNL\ATH\NRCWUS.CD\ROCK\M75D010.050\TCU015-W.AT2
	Vertical	Y06.D\MATCH.FNL\ATH\NRCWUS.CD\ROCK\M75D010.050\TCU015-V.AT2
6.5.3-51	Target Spectrum	Y06.D\MATCH.FNL\10-3\REP1H.1\UHS\TARGETI1.DAT
	Spectral Match	Y06.D\MATCH.FNL\10-3\REP1H.1\UHS\BASE4\SPC\MATCH.050
6.5.3-52	Ratio	Y06.D\MATCH.FNL\10-3\REP1H.1\UHS\BASE4\SPC\MATCH.RAT
6.5.3-53	Acceleration	Y06.D\MATCH.FNL\10-3\REP1H.1\UHS\BASE4\MATCH.ATH
	Velocity	Y06.D\MATCH.FNL\10-3\REP1H.1\UHS\BASE4\MATCH.VTH
	Displacement	Y06.D\MATCH.FNL\10-3\REP1H.1\UHS\BASE4\MATCH.DTH
6.5.3-54	Target Spectrum	Y06.D\MATCH.FNL\10-3\REP1H.2\UHS\TARGETI1.DAT
	Spectral Match	Y06.D\MATCH.FNL\10-3\REP1H.2\UHS\BASE4\SPC\MATCH.050
6.5.3-55	Ratio	Y06.D\MATCH.FNL\10-3\REP1H.2\UHS\BASE4\SPC\MATCH.RAT
6.5.3-56	Acceleration	Y06.D\MATCH.FNL\10-3\REP1H.2\UHS\BASE4\MATCH.ATH
	Velocity	Y06.D\MATCH.FNL\10-3\REP1H.2\UHS\BASE4\MATCH.VTH
	Displacement	Y06.D\MATCH.FNL\10-3\REP1H.2\UHS\BASE4\MATCH.DTH
6.5.3-57	Target Spectrum	Y06.D\MATCH.FNL\10-3\REP1V\UHS\TARGETI1.DAT

TABLE D-1		
List of Data Files Used in Report Figures		
	Spectral Match	Y06.D\MATCH.FNL\10-3\REP1V\UHS\BASE4\SPC\MATCH.050
6.5.3-58	Ratio	Y06.D\MATCH.FNL\10-3\REP1V\UHS\BASE4\SPC\MATCH.RAT
6.5.3-59	Acceleration	Y06.D\MATCH.FNL\10-3\REP1V\UHS\BASE4\MATCH.ATH
	Velocity	Y06.D\MATCH.FNL\10-3\REP1V\UHS\BASE4\MATCH.VTH
	Displacement	Y06.D\MATCH.FNL\10-3\REP1V\UHS\BASE4\MATCH.DTH
6.5.3-60	Target Spectrum	Y06.D\MATCH.FNL\5E-4\REP1H.1\UHS\TARGET11.DAT
	Spectral Match	Y06.D\MATCH.FNL\5E-4\REP1H.1\UHS\BASE4\SPC\MATCH.050
6.5.3-61	Ratio	Y06.D\MATCH.FNL\5E-4\REP1H.1\UHS\BASE4\SPC\MATCH.RAT
6.5.3-62	Acceleration	Y06.D\MATCH.FNL\5E-4\REP1H.1\UHS\BASE4\MATCH.ATH
	Velocity	Y06.D\MATCH.FNL\5E-4\REP1H.1\UHS\BASE4\MATCH.VTH
	Displacement	Y06.D\MATCH.FNL\5E-4\REP1H.1\UHS\BASE4\MATCH.DTH
6.5.3-63	Target Spectrum	Y06.D\MATCH.FNL\5E-4\REP1H.2\UHS\TARGET11.DAT
	Spectral Match	Y06.D\MATCH.FNL\5E-4\REP1H.2\UHS\BASE4\SPC\MATCH.050
6.5.3-64	Ratio	Y06.D\MATCH.FNL\5E-4\REP1H.2\UHS\BASE4\SPC\MATCH.RAT
6.5.3-65	Acceleration	Y06.D\MATCH.FNL\5E-4\REP1H.2\UHS\BASE4\MATCH.ATH
	Velocity	Y06.D\MATCH.FNL\5E-4\REP1H.2\UHS\BASE4\MATCH.VTH
	Displacement	Y06.D\MATCH.FNL\5E-4\REP1H.2\UHS\BASE4\MATCH.DTH
6.5.3-66	Target Spectrum	Y06.D\MATCH.FNL\5E-4\REP1V\UHS\TARGET11.DAT
	Spectral Match	Y06.D\MATCH.FNL\5E-4\REP1V\UHS\BASE4\SPC\MATCH.050
6.5.3-67	Ratio	Y06.D\MATCH.FNL\5E-4\REP1V\UHS\BASE4\SPC\MATCH.RAT
6.5.3-68	Acceleration	Y06.D\MATCH.FNL\5E-4\REP1V\UHS\BASE4\MATCH.ATH
	Velocity	Y06.D\MATCH.FNL\5E-4\REP1V\UHS\BASE4\MATCH.VTH
	Displacement	Y06.D\MATCH.FNL\5E-4\REP1V\UHS\BASE4\MATCH.DTH
6.5.3-69	Target Spectrum	Y06.D\MATCH.FNL\10-4\REP1H.1\UHS\TARGET11.DAT
	Spectral Match	Y06.D\MATCH.FNL\10-4\REP1H.1\UHS\BASE4\SPC\MATCH.050
6.5.3-70	Ratio	Y06.D\MATCH.FNL\10-4\REP1H.1\UHS\BASE4\SPC\MATCH.RAT
6.5.3-71	Acceleration	Y06.D\MATCH.FNL\10-4\REP1H.1\UHS\BASE4\MATCH.ATH
	Velocity	Y06.D\MATCH.FNL\10-4\REP1H.1\UHS\BASE4\MATCH.VTH
	Displacement	Y06.D\MATCH.FNL\10-4\REP1H.1\UHS\BASE4\MATCH.DTH
6.5.3-72	Target Spectrum	Y06.D\MATCH.FNL\10-4\REP1H.2\UHS\TARGET11.DAT
	Spectral Match	Y06.D\MATCH.FNL\10-4\REP1H.2\UHS\BASE4\SPC\MATCH.050
6.5.3-73	Ratio	Y06.D\MATCH.FNL\10-4\REP1H.2\UHS\BASE4\SPC\MATCH.RAT
6.5.3-74	Acceleration	Y06.D\MATCH.FNL\10-4\REP1H.2\UHS\BASE4\MATCH.ATH
	Velocity	Y06.D\MATCH.FNL\10-4\REP1H.2\UHS\BASE4\MATCH.VTH
	Displacement	Y06.D\MATCH.FNL\10-4\REP1H.2\UHS\BASE4\MATCH.DTH
6.5.3-75	Target Spectrum	Y06.D\MATCH.FNL\10-4\REP1V\UHS\TARGET11.DAT
	Spectral Match	Y06.D\MATCH.FNL\10-4\REP1V\UHS\BASE4\SPC\MATCH.050
6.5.3-76	Ratio	Y06.D\MATCH.FNL\10-4\REP1V\UHS\BASE4\SPC\MATCH.RAT
6.5.3-77	Acceleration	Y06.D\MATCH.FNL\10-4\REP1V\UHS\BASE4\MATCH.ATH
	Velocity	Y06.D\MATCH.FNL\10-4\REP1V\UHS\BASE4\MATCH.VTH
	Displacement	Y06.D\MATCH.FNL\10-4\REP1V\UHS\BASE4\MATCH.DTH
6.5.3-78	RB UHS	Y06.D\10GHAZ.03B\FCTPENB.ENV\HAZUHS\HUMN.OUT
	2004 Median, +/- 1 Sigma	BSC (2004 [DIRS 170027], Figure 6.3-145
6.5.3-79	RB UHS	Y06.D\10GHAZ.03B\FCTPENB.ENV\HAZUHS\HUMN.OUT

TABLE D-1		
List of Data Files Used in Report Figures		
	2004 Median, +/- 1 Sigma	BSC (2004 [DIRS 170027], Figure 6.3-133
6.5.3-80	RB UHS	Y06.D\10GHAZ.03B\FCTPENB.ENV\HAZUHS\HUMN.OUT
	2004 Median, +/- 1 Sigma	BSC (2004 [DIRS 170027], Figure 6.3-137

DATA FILES

All of the data files have been included as attachments on DVDs. The DVDs also include a Readme.txt file which describe the basic directory structure of the entire set of data and the inputs and outputs of each program at each step of the process.

INPUTS

The first step is to develop transfer functions, or amplification factors, between a reference rock outcrop site, known as Point A, and Point D (Surface Facilities Area (SFA)) and Point B (Repository Block (RB)).

The inputs into the calculations include a velocity profile (known as a PAR file), nonlinear dynamic material properties which include material damping and shear modulus reduction curves (known as a MAT file), correlation model, and control motions at Point A.

Material Model

The nonlinear dynamic material models are the shear modulus reduction (G/G_{max}) and material damping ratio curves, and were developed by URS. There are two upper mean tuff (UMT) curves, six lower mean tuff (LMT) curves, one upper mean alluvium (UMA) curve and three lower mean alluvium (LMA) curves (Table D-2). Also, upper and lower bounding curves were developed.

For the SFA, which includes alluvium, there are four variations that are run: UMT/UMA, UMT/LMA, LMT/UMA, LMT/LMA, for the appropriate depth. For the repository block the velocity profile does not include alluvium, thus only two material variations are used: UMT, LMT, for the appropriate depth.

**TABLE D-2
Material Models**

1	Unity
2	Upper Mean Tuff 0-500 Ft
3	Upper Mean Tuff 500- Ft
4	Lower Mean Tuff; 0 - 20 FT
5	Lower Mean Tuff; 21 - 50 FT
6	Lower Mean Tuff; 51 - 120 FT
7	Lower Mean Tuff; 121 - 250 FT.
8	Lower Mean Tuff;251 - 500 FT
9	Lower Mean Tuff;501 -1000 F
10	Granular Fill ; 0 - 20 FT
11	Upper Mean Alluvium ; 51 - 120 FT
12	Lower Mean Alluvium 0-50 FEET
13	Lower Mean Alluvium 50-100 FEET
14	Lower Mean Alluvium 100-200 FEET
15	AVERAGE OF LOWER MEAN AND UPPER MEAN ALLUVIUM MODULUS REDUCTION CURVE , Site D'

Currently models 1, 10, and 15 are not being used. These were developed for previous calculations.

The material models are found in the MAT folder and the files YUCCA3.MAT, with the upper and lower bounds in YUCCA3U.MAT and YUCCA3L.MAT respectively. Details on the development of the material models can be found in Section 6.4.4

Correlation Model

This is the same model used in previous calculations. There is one model for the SFA and one for the repository block. (see Section 6.4.2.8). The files are in the COV folder. WHB.DAT is the correlation for SFA, and REP.DAT for the repository block.

Control Motions

Point A Control Motion (RVT)

The horizontal control motions are based on the horizontal Reference Earthquake ((RE) sometimes previously referred to as Design Earthquake) spectra developed for Point A at frequencies of 1-2hz and 5-10hz.

We are using spectra previously developed for the project and described in section 6.4.1. Runs are made at 22 ground motion levels (0.01 g to 10.0 g). The RE spectra are scaled such that the PGA (100 Hz value) of the RE spectra match the appropriate ground motion level. The appropriate RE for each ground motion level is chosen by comparing the PGA level of interest to the PGA level of the RE spectrum. Since the spectral shapes of the RE change little with AFE, a minimum suite of RE was selected that adequately span the range of expected Point A motions (Table D-3, D-4). Information on the controlling magnitude and distance per AFE is found Table D-5.

TABLE D-3
PGA of Point A RE

AFE	1-2 Hz	5-10 Hz
1E-3	0.1 g	0.2 g
5E-4	0.2 g	0.3 g
1E-4	0.3 g	0.6 g
1E-5	0.8 g	1.4 g
1E-6	2.0 g	3.4 g
1E-7	4.0 g	7.2 g

TABLE D-4
AFE Used As Input To Control Motion

GM Level (Directory)	1-2 Hz	5-10 Hz
0.01 (G001)	5E-4	5E-4
0.05 (G005)	5E-4	5E-4
0.10 (G010)	5E-4	5E-4
0.20 (G020)	5E-4	5E-4
0.30 (G030)	1E-4	5E-4
0.40 (G040)	1E-4	5E-4
0.50 (G050)	1E-4	1E-4
0.75 (G075)	1E-5	1E-4
1.00 (G100)	1E-5	1E-4

GM Level (Directory)	1-2 Hz	5-10 Hz
1.25 (G125)	1E-5	1E-5
1.50 (G150)	1E-6	1E-5
1.75 (G175)	1E-6	1E-5
2.00 (G200)	1E-6	1E-5
2.50 (G250)	1E-6	1E-6
3.00 (G300)	1E-7	1E-6
4.00 (G400)	1E-7	1E-6
5.00 (G500)	1E-7	1E-6
6.00 (G600)	1E-7	1E-7
7.00 (G700)	1E-7	1E-7
8.00 (G800)	1E-7	1E-7
9.00 (G900)	1E-7	1E-7
10.00 (G1000)	1E-7	1E-7

TABLE D-5
RE Point A Magnitude and Distance

AFE	1-2 Hz	5-10 Hz
5E-4	M 7.0, 51 km	M 6.3, 5 km
1E-4	M 7.7, 52 km	M 6.3, 5 km
1E-5	M 7.7, 51 km	M 6.4, 4 km
1E-6	M 7.7, 51 km	M 6.5, 1 km
1E-7	M 7.7, 51 km	M 6.5, 1 km

The scaled spectra can be found in Excel\SiteA_RefEq_scale.xls

RASCALS v5.5 is run at each ground motion level. The inputs are the horizontal RE spectra scaled to the ground motion level and a time history (Coyote Lake 8/6/1979, Gilroy Array #1, component=230, M 5.7). The Point A magnitude is used in the RASCALS input files, as are the distance and source depth, which are varied to ensure a smooth FAS curve, the output of RASCALS. Also, the output response spectrum PGA value is checked, as it should match the target ground motion level.

An example directory structure is:

RASCALS\AMPS.01\MATCH.12\DES\Gmlevel (for 1-2hz)

RASCALS\AMPS.01\MATCH.510\DES\Gmlevel (for 5-10hz)

Gmlevel is G001 to G1000 (Table D-4)

In each directory RASCALS v5.5 is run with the input file MATCH.IN. The output files include MATCH.FAS, the Fourier spectra used for the site-specific RVT ground motion calculations; MATCH.OUT, the RASCALS output summary file; MATCH.R05, the calculated response spectrum.

Point A Control Motion (Point Source)

In order to develop vertical motions V/H ratios are developed. To develop the ratios RASCALS calculations are conducted using a stochastic point source calculation for horizontal ground motions (Section 6.3). Instead of 1-2hz and 5-10hz spectra, RASCALS v5.5 is run for magnitudes 5.0, 6.0 and 7.0 earthquakes, and only a basic response is calculated. This method

requires a velocity model, which is the model developed for the surface facilities, NE of Exhile Hill fault splay, material model 3 (UMT, 500- feet), with the Prow Pass layer as the top (outcrop) layer (for further details of the velocity model see below).

An example directory structure is:

RASCALS\AMPS.02\M50.A\Gmlevel (for magnitude 5.0)

RASCALS\AMPS.02\M60.A\Gmlevel (for magnitude 6.0)

RASCALS\AMPS.02\M70.A\Gmlevel (for magnitude 7.0)

Gmlevel is G001 to G1000 (Table D-4)

RASCALS v5.5 is run in a manner similar to the site-specific ground motions, which are described in detail later. In short, RANPAR v2.2 is run with a velocity profile, material models, and correlation model. The output is 30 randomized velocity profiles, material models, and RASCALS input files. RASCALS v5.5 is then run for the base case velocity profile and the 30 randomized models. The resulting 30 response spectra are averaged using LOGNORM v2.0. The depth of the source and epicentral distance to the point source in the RASCALS input file are varied until the 100 Hz value of the averaged response spectra is at the intended ground motion level. For example, in the directory G100 (i.e. 1.0g) the target ground motion level at 100 Hz is 1.0 g. The magnitude in the RASCALS input file is set to either 5.0, 6.0 or 7.0. Once the desired ground value is obtained the epicentral distance and source depth are the values used in the site-specific stochastic point-source calculations.

To obtain the vertical motions RASCALP v2.2 is run.

An example directory structure is:

RASCALP\AMPS.02\M50.A\Gmlevel (for magnitude 5.0)

RASCALP\AMPS.02\M60.A\Gmlevel (for magnitude 6.0)

RASCALP\AMPS.02\M70.A\Gmlevel (for magnitude 7.0)

Gmlevel is G001 to G1000

The same method used is the same as described above for RASCALS, except for the following: the velocity model includes the P-wave velocity values; no adjustment is made to the source depth and epicentral distance, the same values developed in RASCALS are used. RANPAR v2.2 and RASCALP v2.2 are run and the response spectra averaged using LOGNORM v2.0.

Velocity Profiles

Velocity profiles were developed for the SFA and repository block and are based on geophysical field data. The development process is documented in Section 6.4.2.

The velocity profiles were provided by URS. These are smoothed and then converted into a layer system parameter file, or PAR file. This file contains the layer thickness (m), velocity of layer (m/s), density, low strain damping, material model number, as well as information on wavetype, layer to input motion, layer to output motion, and type of output motion.

In developing the PAR files, layer thickness should not exceed $\frac{1}{4}$ wavelength (λ), where $\lambda = \text{Vel}/50 \text{ hz}$.

The velocity is determined from the plots provided by URS (Figures 6.4.2-37, 38, 60, 61, 62, 85 and 86). The densities were taken to be the same as previous calculations (1.8 g/cm^3 for

alluvium, 2.2 g/cm^3 for tuff), with a density of 2.4 g/cm^3 used for Calico, Prow Pass, Bull and Tram layers, see Section 6.4.3. The low strain damping is the value at 1×10^{-4} percent shear strain from the damping curves for the appropriate material model. The material model is the number of the model from the MAT file for that layer.

Surface Facilities Area

At the SFA profiles were developed for two sites, with one of the sites having several variations. These are northeast of the fault, south of the fault case A, south of the fault case B, and south of the fault case C. The fault is the Exhile Hill splay fault, which runs through the SFA. Case A and B are based on profiles using three geophysical techniques (downhole, SASW, and suspension), case C is based on profiles using two geophysical techniques (downhole and suspension). The difference between case A and case B are that case A continues from the bottom of the profile to the desired depth at the same velocity. Case B continues from the bottom of the profile to the desired depth increasing in velocity following the general trend of the upper part of the profile.

Variations in the depth of the alluvium, material models, and depth to the Calico geologic layer, the thickness of the Calico, and the velocity of the Calico leads to multiple PAR files for each site.

For the base case models the depth to the Calico is 1300 ft, with a thickness of 400 ft, and a velocity of 5600 ft/s. Below Calico are the following geologic layers with thickness and velocity, Prow Pass 500 ft, 6000 ft/s; Bull 500ft, 6500 ft/s; Tram 1000 ft, 6700 ft/s; followed by a crustal model.

The control motion is input at the bottom of the Calico layer, with the output motions calculated at the surface. The base case velocities are listed in Table D-6.

TABLE D-6
SFA Velocity Models

Site	Alluvial Depth (ft)	Material Model
NE of Fault	30	UMT/UMA
NE of Fault	30	UMT/LMA
NE of Fault	30	LMT/UMA
NE of Fault	30	LMT/LMA
NE of Fault	70	UMT/UMA
NE of Fault	70	UMT/LMA
NE of Fault	70	LMT/UMA
NE of Fault	70	LMT/LMA
NE of Fault	100	UMT/UMA
NE of Fault	100	UMT/LMA
NE of Fault	100	LMT/UMA
NE of Fault	100	LMT/LMA
NE of Fault	200	UMT/UMA
NE of Fault	200	UMT/LMA
NE of Fault	200	LMT/UMA

Site	Alluvial Depth (ft)	Material Model
NE of Fault	200	LMT/LMA
South of Fault Case A	30	UMT/UMA
South of Fault Case A	30	UMT/LMA
South of Fault Case A	30	LMT/UMA
South of Fault Case A	30	LMT/LMA
South of Fault Case A	70	UMT/UMA
South of Fault Case A	70	UMT/LMA
South of Fault Case A	70	LMT/UMA
South of Fault Case A	70	LMT/LMA
South of Fault Case A	100	UMT/UMA
South of Fault Case A	100	UMT/LMA
South of Fault Case A	100	LMT/UMA
South of Fault Case A	100	LMT/LMA
South of Fault Case B	30	UMT/UMA
South of Fault Case B	30	UMT/LMA
South of Fault Case B	30	LMT/UMA
South of Fault Case B	30	LMT/LMA
South of Fault Case B	70	UMT/UMA
South of Fault Case B	70	UMT/LMA
South of Fault Case B	70	LMT/UMA
South of Fault Case B	70	LMT/LMA
South of Fault Case B	100	UMT/UMA
South of Fault Case B	100	UMT/LMA
South of Fault Case B	100	LMT/UMA
South of Fault Case B	100	LMT/LMA
South of Fault Case C	30	UMT/UMA
South of Fault Case C	30	UMT/LMA
South of Fault Case C	30	LMT/UMA
South of Fault Case C	30	LMT/LMA
South of Fault Case C	70	UMT/UMA
South of Fault Case C	70	UMT/LMA
South of Fault Case C	70	LMT/UMA
South of Fault Case C	70	LMT/LMA
South of Fault Case C	100	UMT/UMA
South of Fault Case C	100	UMT/LMA
South of Fault Case C	100	LMT/UMA
South of Fault Case C	100	LMT/LMA

Repository Block

For the repository block, two base case profiles were developed, the mean of all three soft zones (north soft, central soft, south soft), and the mean of the central stiff zone.

For the base case models the depth to the Calico is 1100 ft, with a thickness of 400 ft, and a velocity of 5600 ft/s. Below Calico are the following geologic layers with thickness and

velocity, Prow Pass 500 ft, 6000 ft/s; Bull 500ft, 6500 ft/s; Tram 1000 ft, 6700 ft/s; followed by a crustal model. There is no alluvium in the profiles.

The control motion is input at the bottom of the Calico layer, with the output motions calculated at the top of the Calico layer. The base case velocities are listed in Table D-7.

**TABLE D-7
RB Velocity Models**

Site	Material Model
Mean of 3 Soft Zones	UMT
Mean of 3 Soft Zones	LMT
Central Stiff Zone	UMT
Central Stiff Zone	LMT

PAR Files

With the DOS operating system, files names are limited to eight characters with a three character extension. With so many PAR file variations, a naming convention has to be established.

The naming convention for PAR files is as follows:

12345678.PAR

- 1: M = Mountain (repository) S-Wave, F = SFA S-Wave, N=Mountain P-wave, P = SFA P-Wave
- 2: Base case profile. SFA 1 = NE of Fault, 2 = South of Fault Case A, 3 = South of Fault Case B, 4 = South of Fault Case C. Repository 1 = All 3 soft zones, 4 = Central Stiff Zone
- 3: Depth to Calico/Thickness of Calico. SFA 2 = 1300/400, Repository 2 = 1100/400
- 4: Alluvium Thickness. SFA. D=deep(200ft), I=intermediate(100ft), J=intermediate (70ft), S=shallow(30ft), N=no alluvium
- 5: Material Model for Tuff. U = Upper Mean, L = Lower Mean
- 6: Material Model for Alluvium. U = Upper Mean, L = Lower Mean, N = No alluvium
- 7: Type of Wave. S = Shear Waves (horizontal), P=P-wave (vertical)
- 8: blank=true base case (no randomization base.in), U=upper bound 10,000m/s, L=lower bound 0 m/s, B=base case used in randomization ras.in

Constraints of Point A Hazard Curves for Extreme Ground Motion

The first step in developing the constrained Point A hazard curves is to run RASCALS for a rock site at stress drops of 150, 400, 1100 bars and magnitudes 6.0 and 6.5.

An example directory is:

RASCALS\PT.A\EX.6\M60\D01H08\SD0150

M60 = M 6.0

M65 = M 6.5

SD0150 = 150 bar stress drop

SD0400 = 400 bar stress drop

SD1100 = 1100 bar stress drop

RASCALS v5.5 is run in a manner similar to the site-specific ground motions, which are described in detail in the calculations section. In short, RANPAR v2.2 is run with a velocity profile (PT.A\PAR\PROW2.PAR, which is the regional geology with the Prow Pass layer as the top layer), material models, and correlation model (for the repository model PT.A\COV\REP.DAT). The output is 60 randomized velocity profiles, material models, and RASCALS input files. RASCALS v5.5 is then run for the base case velocity profile and the 60 randomized models. The resulting 60 response spectra are averaged using LOGNORM v2.0 in the subfolder LOGN, input is SA.IN and output is SA.LOG.

The next step is to apply the stress drop constraints to the Point A hazard curves using the program EXTHC v1.0.

An example directory is:

EHCS15E2.MD1\EX.6\M60\D01H08\SD0150

With the same naming convention above for 2 magnitudes and 3 stress drops.

The input file is: H1000.in, which reads in the appropriate response spectra (SA.LOG), and the Point A PGA mean hazard curve, which was extrapolated to lower AFE (EHCS15E2.MD1\PSHA.F09\H1000.DAT). The extrapolation was done linearly in log amplitude-log AFE.

The output file is: H1000.DAT

FRACTILE v2.0 is run on the resulting hazard curves to get a combined PGA constrained hazard curve at 33 AFE levels. It is run in the directory:

EHCS15E2.MD1\FRACTILE.PGA\FRACTILE.IN

The hazard curves are weighted:

M6.0 0.5

M6.5 0.5

150 Bar Stress Drop 0.2

400 Bar Stress Drop 0.6

1100 Bar Stress Drop 0.2

The output file is: FRACTILE.OUT

FRACTILE v2.0 is also run on the original rock PGA hazard curve (\PSHA.F09\H1000.DAT) for 33 AFE levels. The input file is: FRACTORG.IN and the output file is: FRACTORG.OUT.

The ratio of the constrained mean hazard curves to the original rock hazard curve is calculated using SMRATIO v1.0 in the folder:

EHCS15E2.MD1\FRACTILE.PGA\SMRAT

The input file is SMRAT.in and the output file is H1000.RAT.

The Point A UHS, calculated using HAZUHS v1.0 (EHCS15E2.MD1\PSHA.F09\HAZUHS), input file: HUHSMN.IN, output: HUHSMN.OUT, are scaled using the values from the ratio (H1000.RAT) in the Excel file Scale.xls.

The scaled UHS are sorted by Frequency and AFE and written to the files

\EHCS15E2.MD1\FRACTILE.PGA\SCALE\FINDIT\

FDH0003.DAT (0.3 Hz)

FDH0005.DAT (0.5 Hz)

FDH0010.DAT (1.0 Hz)
FDH0020.DAT (2.0 Hz)
FDH0050.DAT (5.0 Hz)
FDH0100.DAT (10.0 Hz)
FDH0200.DAT (20.0 Hz)
FDH0500.DAT (50.0 Hz)
FDH1000.DAT (100.0 Hz/PGA)
FDHPGV.DAT (PGV)

The next step is to apply strain constraints to the adjusted hazard curves.

EXTHC v1.0 is run in the following directories

EHCS15E3.M12\MSTR10G.009\FREQ Strain of 0.09

EHCS15E3.M12\MSTR10G.025\FREQ Strain of 0.25

FREQ : 003 = 0.3 Hz, 005 = 0.5 Hz, 010 = 1.0 Hz, 020 = 2.0 Hz, 050 = 5.0 Hz, 100 = 10.0 Hz,
200 = 20.0 Hz, PGA = 100.0 Hz, PGV = PGV

The input files are:

AM1P02B1.IN = Repository Block, upper mean tuff, mean of all 3 soft zones

AM1P02B4.IN = Repository Block, upper mean tuff, central stiff zone

AM3P02B1.IN = Repository Block, lower mean tuff, mean of all 3 soft zones

AM3P02B4.IN = Repository Block, lower mean tuff, central stiff zone

The input files read in stress drop constrained scaled hazard curve for the appropriate frequency, and the response spectra from the appropriate repository RVT RASCALS calculations (SA.LOG), and the mean strain compatible properties (LOGMEAN.OUT) for ground motion levels 0.01g to 10.0g. The weighting of 1-2 Hz and 5-10 Hz can be found in Table D-8.

The strain constrained hazard curves are combined using FRACTILE v2.0.

The program is run in: EHCS15E3.M12\FRACT10G.###

Where ### is the frequency level using the convention above. The input file FRACTILE.IN reads in the EXTHC output files for the appropriate frequency from the strain levels of 0.09 and 0.25. The strain levels are equally weighted, the material model weights are in Table D-9. The Fractile output file is the final constrained Point A rock hazard curve for each frequency level that is used by SOILUHSI to develop the site-specific hazard curves.

SUMMARY OF SOFTWARE USED IN CALCULATIONS

RANPAR v2.2 (Rascal Set v1.0 STN:11232-1.0-00) Installed: 08-15-2007

RASCALS v5.5 (Rascal Set v1.0 STN:11232-1.0-00) Installed: 08-15-2007

RASCALP v2.2 (Rascal Set v1.0 STN:11232-1.0-00) Installed: 08-15-2007

SCP v1.0 (Rascal Set v1.1 STN:11232-1.1-00) Installed: 10-04-2007

LOGNORM v2.0 (Post Rascal v1.0 STN: 11231-1.0-00) Installed: 08-15-2007

SMRATIO v1.0 (Post Rascal v1.0 STN: 11231-1.0-00) Installed: 08-15-2007

SOILUHSI v1.0 (Soilhaz Set v1.0 STN: 11234-1.0-00) Installed: 12-12-2007

FRACTILE v2.0 (Soilhaz Set v1.0 STN: 11234-1.0-00) Installed: 12-12-2007

HCSCP v1.0 (Soilhaz Set v1.0 STN: 11234-1.0-00) Installed: 12-12-2007
SUHSINP v1.0 (Soilhaz Set v1.0 STN: 11234-1.0-00) Installed: 12-12-2007

HAZUHS v1.0 (STN: 11194-1.0-00) Installed: 08-15-2007
SIGCOMB v1.0 (STN:11233-1.1-00) Installed: 12-20-2007
EXTHC v1.0 (STN: 11242-1.0-00) Installed: 11-20-2007

BASE4 v4.0 (STN: 10940-4.0-00) Installed: 2002
CORBB v1.0 (STN: 10941-1.0-00) Installed: 2002
DUR v1.0 (STN: 10942-1.0-00) Installed: 2003
INTERPOL v1.0 (STN: 10944-1.0-00) Installed: 2002
MAXMIN v1.0 (STN: 10945-1.0-00) Installed: 2002
RELOT v1.0 (STN: 10949-1.0-00) Installed: 2003
SPCTLR v1.0 (STN: 10947-1.0-00) Installed: 2003

CALCULATIONS

Site response ground motion calculations are being carried out for horizontal motions using RASCALS v5.5 with Point A control motions as input (RVT-based equivalent-linear site response model (Section 6.2)), and for horizontal using RASCALS v5.5 and vertical using RASCALP v2.2 with the stochastic point source control motion (Section 6.3).

SFA Point A Control Motion (RVT)

Horizontal calculations are carried out for each reference earthquake, ground motion level (0.01 g – 10.0 g) and each velocity model (PAR file). For example: 1-2 hz, 0.10g, northeast of the fault, 100 ft of alluvium, with nonlinear dynamic curves upper mean tuff, upper mean alluvium.

The input for each calculation is a velocity profile, a material model file, a correlation model, and the corresponding Point A Fourier amplitude spectrum (FAS). First RANPAR v2.2 calculates 60 velocity profile and material model randomizations, and the necessary RASCALS input files. The inputs into RANPAR are the velocity model PAR file and material model files, with the upper and lower bounds, and the correlation model. RASCALS v5.5 is then run on the true base case profile and the 60 randomizations. (note: the true base case velocity profile for the example given has the top of the Calico at 1300 ft. The randomization is +/- 300 feet, so the velocity profile for the randomization has the top of the Calico at 1600 ft, because the depth to the Calico layer is randomized as well). The input into RASCALS is the appropriate velocity profile, material model, Point A FAS, and a frequency file, which denotes which frequency points to write the output spectra. The output is a RASCALS output file and a response spectra file, which includes PGA and PGV values, and the strain compatible properties. Then a transfer function is created by taking each of the 60 RASCALS output response spectra and dividing them by the appropriate Point A spectra using the program SMRATIO v1.0. The 60 transfer functions are then averaged using the program LOGNORM v2.0. This transfer function will be used to adjust the Point A hazard curves, which is described in the SOILUHSI section later in the appendix.

Transfer functions are also calculated for PGV by dividing the PGV value calculated by RASCALS, with the appropriate Point A PGV value, also calculated from the RASCALS run, then using LOGNORM to average the 60 PGV transfer functions.

Directory Structure:

Example: Rascals\amps.01\AM1P02D1.D1\G100

Rascals = Horizontal (vertically incident SH-waves)

amps.01 = Point A control motion input

AM1P02D1.D1 = profile

G100 = ground motion level (0.01g – 10.0 g)

profile: 12345678.90

1: A = amp runs

2-3: M1=UMT/UMA, M2=UMT/LMA, M3=LMT/UMA, M4=LMT/LMA

4-6: P01=200 ft alluvium, P02=100 ft alluvium, P03=30 ft alluvium, P04=70 ft Alluvium

7-8: D1=1-2Hz RE, D5=5-10Hz RE

9-0: D1=NE of Fault, D2=S of Fault Case A, D3=S of Fault Case B,

D4=S of Fault Case C

An example directory is:

rascals\amp.01\AM1P02D1.D1\G100

The RANPAR input file is FILEIN.DAT. Inputs for RANPAR are the material models YUCCA3.MAT, YUCCA3L.MAT and YUCCA3U.MAT (in the folder MAT), the correlation model WHB.DAT (in the folder COV) and the velocity model for randomization, SITE.PAR, and the velocity randomization limits, SITEU.PAR, SITEL.PAR ((in the folder PAR) note: the velocity profiles are renamed, to streamline the amount of editing needed for the calculations) The output of RANPAR is RANDOM.DAT a RANPAR summary file, 60 randomized material models, RAS#####.MAT, 60 randomized velocity profiles RAS#####.PAR, and 60 RASCALS input files, RAS#####.IN (##### = 0001 – 0060).

RASCALS v5.5 is run for the base case velocity model, the velocity model median randomized velocity model and the 60 randomizations. The input files for RASCALS are BASE.IN, RAS.IN and RAS#####.in, each file reads in a velocity PAR file and a material model, as well as the MATCH.FAS file from the corresponding Point A output (i.e. calculations being done for 1-2hz, 0.01g, read the MATCH.FAS from the Point A calculation at 1-2hz, 0.01g). Also, many of the input values, such as magnitude, epicentral distance, source depth, etc., for the RASCALS input files must match the RASCALS input file used in the corresponding Point A calculation. Kappa was set to 0.0 for the site-specific calculations, as the kappa for the site is represented in the input FAS.

Base.in is the RASCALS calculation for the base case model. Its inputs are the base case velocity profile, SITEB.PAR, the material model YUCCA3.MAT, and the Point A FAS.

RAS.IN is the RASCALS calculation for the median randomized velocity profile. Its inputs are the median velocity profile, SITE.PAR, the material model YUCCA3.MAT, and the Point A FAS. RAS0001.IN – RAS0060.IN are the randomized RASCALS calculation input files. The inputs are the corresponding randomized velocity profiles, material model and the Point A FAS.

The output of RASCALS is a output summary file, RAS####.out (as well as RAS.OUT and BASE.OUT, for the median and base case), a response spectra file, RAS####.R00, which includes the calculated PGV value, and the strain compatible properties (RAS####.scs) (#### = 0001 – 0060).

The next step is to calculate the transfer function, which is done in the subfolder SMRAT.MED. This is done using the program SMRATIO v1.0, which divides each of the 60 response spectra (RAS####.R00) by the response spectra from the corresponding Point A calculation. The input file is SMRAT.IN, the output are 60 transfer functions RAS####.RAT (#### = 0001 – 0060). The PGV transfer function is calculated in the subfolder SMRAT.PGV, using the program SMRATIO v1.0, which divides each of the 60 PGV values (RAS####.R00) by the PGV value from the corresponding Point A calculation. The input file is SMRAT.IN, the output are 60 transfer functions RAS####.RAT (#### = 0001 – 0060).

The 60 transfer functions are then averaged using LOGNORM v2.0, in the subfolder LOGN, with the input/output files being AMPMED.IN/AMPMED.LOG. The PGV transfer functions are averaged with the input/output files being AMPPGV.IN/AMPPGV.LOG, respectively. These calculations are completed in each of the ground motion level directories, for each velocity profile, and for 1-2 Hz and 5-10 Hz RE.

SFA Stochastic Point Source

The RASCALS calculations using the point source control motion are very similar to those described above using the Point A control motion. The main differences are that no Fourier spectrum is used as input, instead, a basic response spectrum is calculated by RASCALS, and only 30 randomizations are run. Also, vertical calculations are run using RASCALP v2.2. The Point Source method is used to develop V/H ratios to apply to the Horizontal hazard curves in order to obtain the vertical hazard curves (Section 6.5.2).

Calculations are carried out for each ground motion level (0.01 g – 10.0 g) and each velocity model (PAR file) for a magnitude of 5.0, 6.0, and 7.0. For example: magnitude 5.0, 0.10g, northeast of the fault, 100 ft of alluvium, with dynamic curves upper mean tuff, upper mean alluvium.

The input for each calculation is a velocity profile, a material model file, and a correlation model. Kappa was set to 0.02 for the site-specific calculations, but is reduced for the Point A calculations to account for attenuation in the velocity model.

First RANPAR v2.2 calculates 30 velocity profiles and material model randomizations, and the necessary input files. The inputs into RANPAR is the velocity model and material model files, with the upper and lower bounds, and the correlation model. RASCALS v5.5 or RASCALP v2.2 is then run on the true base case profile and the 30 randomizations. (note: the true base case velocity profile for the example given has the top of the Calico at 1300 ft. The randomization is +/- 300 feet, so the velocity profile for the randomization has the top of the Calico at 1600 ft, because we randomize not only the velocity, but the depth to the Calico layer as well). The input into RASCALS is the appropriate velocity profile, material model, and a frequency file, which denotes which frequency points to write the output spectra. The output is a RASCALS output file and a response spectra file, which includes PGA and PGV values, and the strain compatible

properties. The V/H ratio is calculated using SMRATIO v1.0, by dividing the 30 vertical response spectra by the corresponding horizontal response spectra. The ratios are then averaged using LOGNORM v2.0

Directory Structure:

Example: Rascals\amps.02\AM1P02P5.D1\G100

Rascals = Horizontal (vertically incident SH-waves),

Rascalp = Vertical (vertically incident P-waves)

amps.02 = Point source input

AM1P02P5.D1 = profile

G100 = ground motion level (0.01g – 10.0 g)

profile: 12345678.90

1: A = amp runs

2-3: M1=UMT/UMA, M2=UMT/LMA, M3=LMT/UMA, M4=LMT/LMA

4-6: P01=200 ft alluvium, P02=100 ft alluvium, P03=30 ft alluvium, P04=70 ft Alluvium

7-8: P5=magnitude 5.0, P6=magnitude 6.0, P7=magnitude 7.0

9-0: D1=NE of Fault, D2=S of Fault Case A, D3=S of Fault Case B,

D4=S of Fault Case C

An example directory is:

rascals\amp.02\AM1P02P5.D1\G100

The RANPAR input file is FILEIN.DAT. Inputs for RANPAR are the material models YUCCA3.MAT, YUCCA3L.MAT and YUCCA3U.MAT (in the folder MAT), the correlation model WHB.DAT (in the folder COV) and the velocity model for randomization, SITE.PAR, and the velocity randomization limits, SITEU.PAR, SILEL.PAR ((in the folder PAR) note: the velocity profiles are renamed, to streamline the amount of editing needed for the calculations)

The output of RANPAR is RANDOM.DAT a RANPAR summary file, 30 randomized material models, RAS####.MAT, 30 randomized velocity profiles RAS####.PAR, and 30 RASCALS input files, RAS####.IN, (#### = 0001 – 0030).

RASCALS v5.5 is run for the base case velocity model, the velocity model median randomized velocity model and the 30 randomizations. The input files for RASCALS are BASE.IN, RAS.IN and RAS####.in, each file reads in a velocity PAR file and a material model. The input values magnitude, epicentral distance, source depth for the RASCALS input files must match the RASCALS input file used in the corresponding Point A calculation (or RASCALP files for the vertical cases).

Base.in is the RASCALS calculation for the base case model. Its inputs are the base case velocity profile, SITEB.PAR, the material model YUCCA3.MAT. RAS.IN is the RASCALS calculation for the median randomized velocity profile. Its inputs are the median velocity profile, SITE.PAR, the material model YUCCA3.MAT. RAS0001.IN – RAS0030.IN are the randomized RASCALS calculation input files. The inputs are the corresponding randomized velocity profiles and material models.

The output of RASCALS is a output summary file, RAS####.out (as well as RAS.OUT and BASE.OUT, for the median and base case), a response spectra file, RAS####.R00, and the strain compatible properties RAS####.SCS (RAS####.SCP for RASCALP)

The next step is to calculate the V/H ratio, which is done in the subfolder SMRAT.V. This is done using the program SMRATIO v1.0, which divides each of the 30 response spectra (RAS####.R00) by the response spectra from the corresponding RASCALP response spectra. The input file is SMRAT.IN, the output are 30 ratios RAS####.RAT.

The 30 ratios are then averaged using LOGNORM v2.0, in the subfolder LOGN, with the input/output files being V_H.IN/V_H.LOG, (#### = 0001 – 0030).

For RASCALS point source calculation the median response spectra is calculated in the folder LOGN, LOGNORM v2.0 reads in the input file SA.IN, which reads in the 30 RASCALS calculated response spectra (*.R00 files). The output file is SA.LOG, and contains the median response spectra, and 16th and 84th percentiles.

The vertical ground motions are calculated in the exact same manner as described above. The only difference is that RASCALP v2.2 is used instead of RASCALS v5.5, and the velocity profile includes the P-wave profile (see Section 6.4.2.5.2). The V/H ratios are only calculated under the RASCALS\amps.02 subfolders. Again, the vertical ground motions are calculated under the RASCALP folder.

The calculations are completed in each of the ground motion level directories, for each velocity profile, and magnitudes 5, 6, and 7.

SFA Strain Compatible Properties

Strain compatible properties (Section 6.5.4.8) are written as an output of RASCALS and RASCALP in the point source calculations. The program SCP v1.0 reads the RASCALS and RASCALP output files of strain compatible properties and computes their statistics (median/mean and \pm one standard deviation, assuming both linear and lognormal statistics). HCSCP V1.0 interpolates the strain compatible properties for a given hazard curve or ground motion value. SIGCOMB V1.0 computes the weighted mean and combined standard deviation of strain compatible properties, combining the material model epistemic uncertainty and PGA and 1.0 sec SA values.

The program SCP v1.0 is run only under the RASCALS\AMPS.02\profile\GMlevel\SCP directories (profile as previously described, GMlevel G001 to G300) for each PAR profile file and ground motion level. The input file is SCP.IN and it reads in the 30 *.SCS files from RASCALS and the 30 *.SCP files from RASCALP of the equivalent directory. The output files are Linmean.out, Linmeanm.out, Linmeanp.out, Linsigma.out, Logmean.out, Logmeanm.out, Logmeanp.out, Logsigma.out, and 30 *.scm files.

The SCM files are the combination of the RASCALS and RASCALP strain compatible properties. Lin*.out assumes a normal distribution. Log*.out assumes a lognormal distribution. *.mean.out is the mean strain compatible properties, *sigma.out is the sigma values, *meanm.out is the mean minus one sigma values, *meanp.out is the mean plus one sigma values.

HCSCP v1.0 calculates the hazard consistent strain compatible properties. It is run in the directory RASCALS\AMPS.02\profile\HCSCP.10G profile = as described previously

The input files are for example: 100C0001.IN
100 = 1.0 Hz, PGA = 100.0 Hz
C= Sigma as multiplicative factor, S= Logsigma , M= Logmean
0001= 10⁻³ AFE, 0002= 5E-4 AFE, 0010= 10⁻⁴ AFE

The input file reads the PGA or 1.0 Hz value from the final SFA site-wide UHS, HAZSUHSI.01\FCTALL.ENV\HAZUHS\HUMN.OUT (described later in this Appendix), and the value from the SA for each ground motion level for a given PAR profile (SA is the Spectral Acceleration, it is calculated in the LOGN subdirectory of each RASCALS calculation. It is created with the LOGNORM v2.0 program and averages the 30 RASCALS calculated spectra. The output file is SA.LOG). It also reads the Logmean.out or Logsigma.out files for each ground motion level (0.01 g – 10.0 g) for a given PAR profile. The output files are simply *.out (i.e. 100M0001.OUT)

The strain compatible properties are combined for the various sites using SIGCOMB v1.0 SIGCOMB v1.0 is run in the directory Rascals\amps.02\SIG10G45.ALL With the following subdirectories:

NE.030 = NE of the Fault, 30 Feet of Alluvium
NE.070 = NE of the Fault, 70 Feet of Alluvium
NE.100 = NE of the Fault, 100 Feet of Alluvium
NE.200 = NE of the Fault, 200 Feet of Alluvium
SOUTH.030 = South of the Fault, 30 Feet of Alluvium
SOUTH.070 = South of the Fault, 70 Feet of Alluvium
SOUTH.100 = South of the Fault, 100 Feet of Alluvium

The input files are:

P-10001.IN combination of PGA and 1.0 Hz, 10⁻³ AFE
P-10002.IN combination of PGA and 1.0 Hz, 5E-4 AFE
P-10010.IN combination of PGA and 1.0 Hz, 10⁻⁴ AFE

The program reads in the PGAM0001.OUT, PGAS0001.OUT, 100M0001.OUT, and 100S0001.OUT (for 10⁻³ AFE), for all material model combinations for the given site/alluvial depth.

The weights used in SIGCOMB can be found in the Excel worksheet: Sigcomb.xls This data has been submitted to the TDMS (DTN: MO0801SCSPS1E3.003 [DIRS 184685], MO0801SCSPS5E4.003 [DIRS 184682], MO0801SCSPS1E4.003 [DIRS 184683])

SFA Horizontal SOILUHSI/HAZUHS

Once the transfer functions are developed, the next step is to apply them to the Point A hazard curves to obtain site-specific hazard curves and uniform hazard spectra (section 6.1.2).

The first step in this process is to run the program SUHSINP v1.0. This program creates input files for the SOILUHSI v1.0 program by reading the data from various files. SOILUHSI v1.0 is based on the methodology described in Bazzurro and Cornell (2004; [DIRS 177290]). It uses

full integration of the amplification factor over a range of rock amplitudes to calculate the hazard curve (Section 6.1.1.1). SUHSINP/SOILUHSI is run for each velocity profile PAR (i.e. SFA, NE of the fault, 100 ft of alluvium, UMT/UMA, 1-2 Hz), at eight frequencies (100.0 (PGA), 20.0, 10.0, 5.0, 2.0, 1.0, 0.5, 0.3) and PGV. For a given period (i.e. PGA) the program reads the Point A fractile curve, the Point A spectra for all ground motion levels (0.01 g – 10.0 g), and the transfer functions for all ground motion levels. The output is a modified hazard curve for the given period. The program FRACTILE v2.0 is then used to calculate the fractile curves about the modified hazard curve as well as to combine with weights (the material models, and south of the fault cases) and envelope the various location uncertainties (i.e. alluvial depths, NE of fault or south of fault). The final result is a suite of site-specific horizontal hazard curves for the site-wide SFA. Finally, HAZUHS v1.0 is used to calculate the UHS for a given AFE.

The SOILUHSI/HAZUHS set is calculated under the directory:

10GHAZ.01R\

In this folder the conditioned for extreme hazard Point A hazard curves are used and the V/H is constrained to a minimum value of 0.5.

The Point A hazard curves are in the folder PSHA.F09\

H0003.FRA = 0.3 Hz, H0005.FRA = 0.5 Hz, H0010.FRA = 1.0 Hz, H0020.FRA = 2.0 Hz, H0050.FRA = 5.0 Hz, H0100.FRA = 10.0 Hz, H0200.FRA = 20.0 Hz, H1000.FRA = 100.0 Hz (PGA), HPGV.FRA = PGV

Each includes the following fractile levels (MEAN, 0.005, 0.050, 0.150, 0.200, 0.500, 0.800, 0.850, 0.950, 0.995)

Note: Fractile curves with -9.9999 values should not be used. The software code could not calculate a value at the fractile level for the given amplitude. This is a known issue with the software. Fractile levels with -9.9999 values were not utilized in this study, and thus had no impact on the final results.

The conditioned for extreme hazard Point A hazard curves were calculated using EXTHC v1.0 and are in the folder EXTHC for the same frequencies described above and for the following fractile levels (0.05, 0.15, 0.50, 0.85, 0.95, MEAN)

Extreme Ground motions are described in Section 6.5.1 and Appendix A.

SUHSINP and SOILUHSI are run for each velocity profiles, and the directory naming convention is the same as the RASCALS calculations (i.e. AM1P01D1.D1 for UMT/UMA, 200ft of Alluvium, 1-2hz RE, NE of the Fault).

The subfolders are: SUHSI.###

= .003 = 0.3 Hz, .005 = 0.5 Hz, .010 = 1.0 Hz, .020 = 2.0 Hz, .050 = 5.0 Hz, .100 = 10.0 Hz, .200 = 20.0 Hz, .PGA = 100.0 Hz, .PGV = PGV

For each frequency SUHSINP and SOILUHSI are run for various conditioned Point A fractile curves. The SUHSINP input file is SIMN.IN for the mean curve, the output is MN.IN, the SOILUHSI input file.

SUHSINP reads in the Point A fractile curve for the given frequency. The response spectral value for the given frequency from the appropriate Point A RE (i.e. 1-2 hz or 5-10 hz) for all ground motion levels (0.01 to 10.0 g), the transfer function value for the given frequency from the appropriate PAR folder for all ground motion levels (0.01 to 10.0 g).

Weights were assigned to the RE based on the AFE, Table D-8.

TABLE D-8
Reference Earthquake Weights

Freq	1-2 Hz	5-10 Hz	AFE
0.3	1.0	0.0	10-3 - 10-8
0.5	1.0	0.0	10-3 - 10-8
1.0	1.0	0.0	10-3 - 10-4
	0.0	1.0	10-5 - 10-8
2.0	1.0	0.0	10-3
	0.0	1.0	10-4 - 10-8
5.0	0.0	1.0	10-3 - 10-8
10.0	0.0	1.0	10-3 - 10-8
20.0	0.0	1.0	10-3 - 10-8
100.0	0.0	1.0	10-3 - 10-8

Because the weights change with AFE for 1.0 and 2.0 Hz (Table D-8), the SUHSINP input file has to include both conditioned Point A RE response spectral values and transfer function values from 1-2 Hz and 5-10 Hz, of the appropriate RASCALS run. Weights are included in the 1.0 and 2.0 Hz SUHSINP input files, based on Table D-8, based on the AFE from the conditioned Point A fractile curves, which is also read by the SUHSINP input file.

The output from SUHSINP.IN is the input file, MN.IN, used by SOILUHSI v1.0. The output of SOILUHSI is MN.OUT, which is the modified mean hazard curve.

Next, FRACTILE v2.0 is run to calculate the fractile curves about the modified mean hazard curve. It is at this stage that the epistemic uncertainties are combined with weights, or are enveloped.

FRACTILE is run in the following subdirectories (still in the directory 10GHAZ.01R\):

FCTP01D1.CMB = NE of the Fault, 200 ft of alluvium, combination of material models and RE.

FCTP02D1.CMB = NE of the Fault, 100 ft of alluvium, combination of material models and RE.

FCTP03D1.CMB = NE of the Fault, 30 ft of alluvium, combination of material models and RE.

FCTP04D1.CMB = NE of the Fault, 70 ft of alluvium, combination of material models and RE.

FCTP02DS.CM1 = S of the Fault, 100 ft of alluvium, combination of South Case A, B and C, material models and RE.

FCTP03DS.CM1 = S of the Fault, 30 ft of alluvium, combination of South Case A, B and C, material models and RE.

FCTP04DS.CM1 = S of the Fault, 70 ft of alluvium, combination of South Case A, B and C, material models and RE.

FCTPEND1.ENV = NE of Fault, envelope of alluvial depths.

FCTPENDS.ENV = S of Fault, envelope of alluvial depths.

FCTALL.ENV = Envelope of NE of Fault and S of Fault, Final SFA Site-Wide hazard curves

The FRACTILE input files using the following naming convention: F0003MN.IN = 0.3 Hz, F0005MN.IN = 0.5 Hz, F0010MN.IN = 1.0 Hz, F0020MN.IN = 2.0 Hz, F0050MN.IN = 5.0 Hz, F0100MN.IN = 10.0 Hz, F0200MN.IN = 20.0 Hz, F1000MN.IN = 100.0 Hz

The output files are simply *.out

Weights have been assigned for the epistemic uncertainty in Tables D-9 to D-12 (Sections 6.4.2.7, 6.4.4.3)

TABLE D-9
Material Model Weights

Material Models	
UMA	0.55
LMA	0.45
UMT	0.70
LMT	0.30

TABLE D-10
South of the Fault Base Case Weights

South of Fault	
South A	0.47
South B	0.32
South C	0.21

TABLE D-11
Weights for NE of the Fault

NE Fault	
UMT/UMA	0.3850
UMT/LMA	0.3150
LMT/UMA	0.1650
LMT/LMA	0.1350

TABLE D-12
Weights for South of the Fault

	Case A	Case B	Case C
UMT/UMA	0.1810	0.1232	0.0809
UMT/LMA	0.1481	0.1008	0.0662
LMT/UMA	0.0776	0.0528	0.0347
LMT/LMA	0.0635	0.0432	0.0284

The input to each file when combining the epistemic uncertainty is the output from the SOILUHSI for the appropriate frequency and alluvial depth. The output (*.out) is the fractile hazard curves at the following levels: 0.05, 0.15, 0.50, 0.85, 0.95, MEAN. When enveloping the hazard curves, the input is the output from FRACTILE for the appropriate site (i.e., FCTP01D1.CMB), with the output being the enveloped mean hazard curve.

The final step is to calculate the uniform hazard spectra (UHS). This is done using the program HAZUHS v1.0. It is done in the folder 10GHAZ.01R\FCTALL.EN1\HAZUHS. This folder contains the final SFA site-wide hazard curves. The program HAZUHS simply reads in the mean hazard curves at each frequency and determines the value for a given AFE. The input file is HUMN.IN and the output file HUMN.OUT, which contains the UHS at the AFE of 10⁻³, 5E⁻⁴, 10⁻⁴, 10⁻⁵, 2E⁻⁶, 10⁻⁶, 10⁻⁷.

(Note: HAZUHS was also run on other hazard curves, i.e. Northeast of the Fault, 200 Ft of alluvium. This would then be done in the HAZUHS subfolder for FCTP01D1.CMB)

The final SFA Site-Wide hazard curves and UHS were submitted to the TDMS (DTN: MO0801HCUHSSFA.001 [DTN 184802]). Please note in the computation of the UHS from the hazard curves for all AFE the spectral value at 3.33 sec was inadvertently calculated at 3.0 sec. Thus, for periods greater than 2.0 sec, the SA amplitude is lower (has a higher AFE) than appropriate for the nominal UHS AFE. Please refer to Section 6.5.2.3.

Empirical

The vertical hazard curves were developed by calculating V/H ratios, then applying these ratios to the horizontal hazard curves using SOILUHSI. The V/H ratios were described in the SFA Point Source section above.

In addition to the model, empirical models were used. The attenuation models used were Abrahamson and Silva (1997 [DIRS 104205]) and Campbell and Bozorgnia (2003 [DIRS 183814]) for horizontal and vertical, rock and soil, with hanging wall or without hanging wall effects, for normal faulting (Abrahamson and Becker 1997 [DIRS 166530]), and all spectral values.

The calculations can be found in

EMPIRICAL.L\AMPS\MAG\Atten.site\GM

AMPS: AMPS.H = Horizontal AMPS.V = Vertical

MAG: M50 = M 5.0, M60 = M 6.0, M70 = M 7.0

Atten: AS1 = Abrahamson and Silva, hanging wall effect

AS0 = Abrahamson and Silva, no hanging wall effect

Camp1 = Campbell and Bozorgnia, hanging wall effect

Camp0 = Campbell and Bozorgnia, no hanging wall effect

Site: SOI = Soil, RCK = Rock

GM = ground motion level (9 levels); G010, G020, G030, G040, G050, G075, G100, G125, G150

The empirical calculations were conducted in the Excel tables Excel\EmpiricalAS.xls for Abrahamson and Silva and Excel\EmpiricalCamp.xls for Campbell and Bozorgnia. In the calculation of the vertical Abrahamson and Silva the values for the coefficient A1 differs from the published version for periods greater and equal to 0.2 sec. This results in V/H ratios that are high from approximately 0.2 sec to 1.0 sec, and lower from 1.0 sec to 5.0 sec. In the calculation of the horizontal Campbell and Bozorgnia values the coefficient value C5 at 0.05 sec is incorrect. This results in a lower values at period of 0.8 sec and less for the V/H ratio, especially at close distances. Please refer to Section 6.5.2.1.2. The horizontal results were pasted into the text files As.out and Camp03H.out. The V/H ratios are also calculated in the Excel tables, the period values converted to frequency and written to the text file EMP.INV. The program INTERPOL v1.0 is used to interpolate the values to 301 frequency values. The input file is INTERPOL.IN, and the output file is EMP.INT and INTERPOL.OUT, and program summary file.

SFA Vertical SOILUHSI/HAZUHS

The development of the vertical hazard curves and UHS are very similar to the method used to develop the horizontal. The main difference is for SOILUHSI (actually SUHSINP), the files read in the final SFA site-wide horizontal hazard curve, the empirical spectra, the RASCALS

model V/H ratios, and the empirical V/H ratios. Because of the combination of empirical and stochastic model, the combination and weighting of the multiple models gets quite complicated.

10GHAZ.01R\

In this folder the conditioned for extreme hazard Point A hazard curves are used and the V/H is constrained to a minimal value of 0.5.

SUHSINP and SOILUHSI are run for each velocity profile, and the directory naming convention is the same as the RASCALS point source calculations, with A replaced with V for vertical (i.e. VM1P01P6.D1 for UMT/UMA, 200ft of Alluvium, magnitude 6.0, NE of the Fault).

The subfolders are: VSI.###

= .003 = 0.3 Hz, .005 = 0.5 Hz, .010 = 1.0 Hz, .020 = 2.0 Hz, .050 = 5.0 Hz, .100 = 10.0 Hz, .200 = 20.0 Hz, .PGA = 100.0 Hz

For each frequency SUHSINP and SOILUHSI are run for various Point A fractile curves.

SIMNVH.IN is the SUHSINP input file.

SUHSINP reads in the SFA site-wide horizontal fractile curve for the given frequency, the Point A RASCALS calculated spectra, for the given magnitude, the empirical horizontal spectra for the given magnitude, the RASCALS calculated V/H ratios and empirical calculated V/H ratios for a given magnitude. The choice of ground motion level to use and the weights are determined from tables D-13 and D-14. The weights in table D-14 are based on the contributing earthquakes for each frequency in table D-13, such that the resulting magnitude is equal to the controlling magnitude at each frequency and AFE given in table D-14 (third column). When the controlling magnitude is greater than 7.0, one-hundred percent weight was given to a magnitude 7.0.

TABLE D-13
Development of Weights for V/H Ratios

Empirical Freq					Model D (km)			
	M	D (km)	G	Dir		G	Dir	AFE
0.3	7.0	31	0.05	G020	44	0.05	G005	10 ⁻³ to 10 ⁻⁷
0.5	7.0	31	0.05	G020	44	0.05	G005	10 ⁻³ to 10 ⁻⁷
1.0	7.0	31	0.05	G020	44	0.05	G005	10 ⁻³ to 10 ⁻⁴
	6.0	3	0.40	G100	2	0.20	G020	10 ⁻⁵
	6.0	1	0.44	G150	2	0.20	G020	10 ⁻⁶ to 10 ⁻⁷
2.0	7.0	31	0.05	G020	44	0.05	G005	10 ⁻³
	6.0	3	0.40	G100	2	0.20	G020	10 ⁻⁴ to 10 ⁻⁶
	6.0	1	0.44	G150	2	0.20	G020	10 ⁻⁷
5.0	5.0	8		G050	10	0.05	G005	10 ⁻³
	6.0	3	0.40	G100	2	0.20	G020	10 ⁻⁴ to 10 ⁻⁵
	6.0	1	0.44	G150	2	0.20	G020	10 ⁻⁶ to 10 ⁻⁷
10.0	5.0	8		G050	10	0.05	G005	10 ⁻³
	6.0	3	0.40	G100	2	0.20	G020	10 ⁻⁴ to 10 ⁻⁵

	6.0	1	0.44	G150		2	0.20	G020	10 ⁻⁶ to 10 ⁻⁷
20.0	5.0	8		G050		10	0.05	G005	10 ⁻³
	6.0	3	0.40	G100		2	0.20	G020	10 ⁻⁴ to 10 ⁻⁵
	6.0	1	0.44	G150		2	0.20	G020	10 ⁻⁶ to 10 ⁻⁷
100.0	5.0	8		G050		10	0.05	G005	10 ⁻³
(PGA)	6.0	3	0.40	G100		2	0.20	G020	10 ⁻⁴ to 10 ⁻⁵
	6.0	1	0.44	G150		2	0.20	G020	10 ⁻⁶ to 10 ⁻⁷

TABLE D-14
Weights Utilized in SFA V/H Ratios

Freq	AFE	Mw	R(km)	epsilon	M	weight	M	weight	M	weight	
0.3	1.00E-03	7.35	51.25	0.7	7.0	1.00					
0.3	1.00E-04	7.45	51.25	1.9	7.0	1.00					
0.3	1.00E-05	7.65	51.25	2.3	7.0	1.00					
0.3	1.00E-06	7.65	51.25	2.4	7.0	1.00					
0.3	1.00E-07	7.65	51.25	3.1	7.0	1.00					
0.5	1.00E-03	7.35	51.25	0.9	7.0	1.00					
0.5	1.00E-04	7.45	51.25	1.9	7.0	1.00					
0.5	1.00E-05	7.45	51.25	2.3	7.0	1.00					
0.5	1.00E-06	7.65	51.25	2.7	7.0	1.00					
0.5	1.00E-07	7.65	51.25	3.5	7.0	1.00					
1.0	1.00E-03	7.35	51.25	1.1	7.0	1.00					
1.0	1.00E-04	7.65	51.25	1.9	7.0	1.00					
1.0	1.00E-05	6.25	3.75	2.1	7.0	0.25	6.0	0.75			
1.0	1.00E-06	6.65	1.25	2.1	7.0	0.65	6.0	0.35			
1.0	1.00E-07	6.65	1.25	2.9	7.0	0.65	6.0	0.35			
2.0	1.00E-03	7.35	51.25	1.3	7.0	1.00					
2.0	1.00E-04	6.15	3.75	1.1	7.0	0.15	6.0	0.85			
2.0	1.00E-05	6.25	3.75	1.9	7.0	0.25	6.0	0.75			
2.0	1.00E-06	6.25	3.75	2.5	7.0	0.25	6.0	0.75			
2.0	1.00E-07	6.65	1.25	2.7	7.0	0.65	6.0	0.35			"P7"
5.0	1.00E-03	5.15	8.75	1.1	6.0	0.15	5.0	0.85	7.0	0.0	"P6"
5.0	1.00E-04	6.15	3.75	0.9	7.0	0.15	6.0	0.85			
5.0	1.00E-05	6.25	3.75	1.9	7.0	0.25	6.0	0.75			
5.0	1.00E-06	6.15	1.25	2.1	7.0	0.15	6.0	0.85			
5.0	1.00E-07	6.15	1.25	1.5	7.0	0.15	6.0	0.85			
10.0	1.00E-03	5.05	8.75	1.1	6.0	0.05	5.0	0.95	7.0	0.0	
10.0	1.00E-04	5.85	3.75	1.1	6.0	0.85	5.0	0.15			
10.0	1.00E-05	6.25	3.75	1.9	7.0	0.25	6.0	0.75			
10.0	1.00E-06	6.15	1.25	2.1	7.0	0.15	6.0	0.85			
10.0	1.00E-07	6.15	1.25	1.5	7.0	0.15	6.0	0.85			
20.0	1.00E-03	5.15	8.75	0.9	6.0	0.15	5.0	0.85	7.0	0.0	
20.0	1.00E-04	5.85	3.75	1.1	6.0	0.85	5.0	0.15	7.0	0.0	

20.0	1.00E-05	6.25	3.75	1.9	7.0	0.25	6.0	0.75			
20.0	1.00E-06	6.15	1.25	2.3	7.0	0.15	6.0	0.85			
20.0	1.00E-07	6.15	1.25	1.7	7.0	0.15	6.0	0.85			
100.0	1.00E-03	5.15	8.75	1.1	6.0	0.15	5.0	0.85	7.0	0.0	
100.0	1.00E-04	5.85	3.75	1.1	6.0	0.85	5.0	0.15	7.0	0.0	
100.0	1.00E-05	6.15	3.75	1.9	7.0	0.15	6.0	0.85			
100.0	1.00E-06	6.15	1.25	2.1	7.0	0.15	6.0	0.85			
100.0	1.00E-07	6.15	1.25	1.5	7.0	0.15	6.0	0.85			

Based on probability levels magnitude 7 is used for frequencies 0.3 Hz, 0.5 Hz, 1.0 Hz, and 2.0 Hz, and magnitude 6 is used for frequencies 5.0 Hz, 10.0 Hz, 20.0 Hz, and 100 Hz (PGA). Input files for SUHSINP/SOILUHSI exist for all frequencies for each magnitude, but only the ones described above are utilized.

The weights for the empirical models are listed in table D-15.

TABLE D-15
Weights for Empirical Models

Empirical	
Rock	0.8
Soil	0.2
AS	0.5
Hanging Wall	0.75
No Hanging Wall	0.25
CB	0.5
Hanging Wall	0.75
No Hanging Wall	0.25
Combined Weights	
AS	
Hanging Wall	0.1875
No Hanging Wall	0.0625
CB	
Hanging Wall	0.1875
No Hanging Wall	0.0625

AS=Abrahamson and Silva (1997 [DIRS 104205]); CB=Campbell and Bozorgnia (2003 [DIRS 183814])

The empirical model is given 0.5 weight, with the RASCALS model given 0.5 weight. Thus the final weights are listed in Table D-16.

TABLE D-16
Model Weights used for SFA Vertical SUHSINP

Rascals Model	0.5
Soil AS Hanging Wall	0.0375

	AS	No Hanging Wall	0.0125
	CB	Hanging Wall	0.0375
	CB	No Hanging Wall	0.0125
Rock	AS	Hanging Wall	0.15
	AS	No Hanging Wall	0.05
	CB	Hanging Wall	0.15
	CB	No Hanging Wall	0.05

For 0.3 Hz and 0.5 Hz, which use only one magnitude (M7.0, see Table D-14), the weighting used in the SUHSINP input file is straightforward. For the other frequencies, which involve multiple magnitude inputs with weights, a variable weighting must be used. The weights for magnitude are interpolated for AFE of the hazard curves. Similar to the UHS the value at 0.33 Hz was inadvertently read by SUHSINP, and not the 0.3 Hz value. This will impact the calculation of the 0.3 Hz hazard curve. SUHSINP v1.0 writes out the SOILUHSI v1.0 input file MNVH.IN, for the mean. SOILUHSI is run, and the output file MNVH.OUT is the adjust hazard curve.

The variable weighting was calculated in the folder:

\10GHAZ.01R\FCTALL.EN1\HAZUHS\VHWTS2

INTERPOL is used to interpolate the assigned weights for AFE to the Horizontal Hazard curve (HUMN.OUT). The weights are derived from table D-14. The INTERPOL input file is INTERMN.IN. The Interpolated weights are then combined with the model weights (Table D-16) in the Excel file WTSMN.XLS.

FRACTILE and HAZUHS are run exactly the same as the horizontal, the only difference is that the vertical adjusted hazard curves are read in. For horizontal the directories began with FCT, for vertical they begin with VFT. Again, based on probability levels magnitude 7 is used for frequencies 0.3 Hz, 0.5 Hz, 1.0 Hz, and 2.0 Hz, and magnitude 6 is used for frequencies 5.0 Hz, 10.0 Hz, 20.0 Hz, and 100 Hz (PGA). Otherwise, the naming convention, folder names, and process is all the same as the horizontal described above. As with the horizontal UHS, in the computation of the vertical UHS from the hazard curves for all AFE the spectral value at 3.33 sec was inadvertently calculated at 3.0 sec. Thus, for periods greater than 2.0 sec, the SA amplitude is lower (has a higher AFE) than appropriate for the nominal UHS AFE. Please refer to Section 6.5.2.3.

The final SFA Site-Wide hazard curves and UHS were submitted to the TDMS (DTN: MO0801HCUHSSFA.001 [DIRS 184802])

SFA Time Histories

Spectral compatible time histories are developed using RASCALS (Section 6.5.4.7). The targets are the UHS developed using HAZUHS for AFE of 10⁻³, 5E-4, and 10⁻⁴. Five sets of three-component time histories for each AFE were calculated. The UHS targets are interpolated to 298 points, RASCALS is used to match the target spectra using a seed time history to calculate a spectrum compatible time history. The time history is then baseline corrected, and the 5% damped response spectra of the baseline corrected time history calculated. Additionally, response spectra are calculated at dampings of 0.5%, 1%, 2%, 3%, 7%, 10%, 15%, and 20%.

Cross-correlation statistics between time history components are computed, as is Arias intensity versus duration for each component.

The seed time histories for the SFA are list in Table D-17.

TABLE D-17
Summary of SFA Seed Time Histories

AFE	Earthquake - Station	Time History M	Time History D	Time History Path
5E-4 Set 1	Northridge - Wrightwood Jackson Flat	6.7	68.4	nrcwus.cd\rock\m65d050.100\
5E-4 Set 2	Northridge - Rancho Cucamonga Deer Can	6.7	80.0	nrcwus.cd\rock\m65d050.100\
5E-4 Set 3	Whittier - Calabasas N. Las Virg	6.0	53.3	ceus.cd\rock\m65d050.100\
5E-4 Set 4	Whittier - Pasadena Calif Blvd	6.0	15.5	nrcwus.cd\soil\m55d000.050\
5E-4 Set 5	Chi Chi - TAP036	7.6	95.6	nrcwus.cd\rock\m75d050.100\
10-3 Set 1	Northridge - Wrightwood Jackson Flat	6.7	68.4	nrcwus.cd\rock\m65d050.100\
10-3 Set 2	Northridge - Rancho Cucamonga Deer Can	6.7	80.0	nrcwus.cd\rock\m65d050.100\
10-3 Set 3	Whittier - Calabasas N. Las Virg	6.0	53.3	ceus.cd\rock\m65d050.100\
10-3 Set 4	Whittier - Pasadena Calif Blvd	6.0	15.5	nrcwus.cd\soil\m55d000.050\
10-3 Set 5	Chi Chi - TAP036	7.6	95.6	nrcwus.cd\rock\m75d050.100\
10-4 Set 1	Kocaeli - Iznik	7.4	29.7	nrcwus.cd\rock\m75d010.050\
10-4 Set 2	Landers - TwentyNine Palms	7.3	42.2	ceus.cd\rock\m75d010.050\29p\avd\
10-4 Set 3	Cape Mendecino - Shelter Cove	7.1	33.8	ceus.cd\rock\m75d010.050\shl\avd\
10-4 Set 4	Landers - Silent Valley	7.3	51.7	nrcwus.cd\rock\m75d050.100\
10-4 Set 5	Kocaeli - Mecidiyekoy	7.4	62.3	ceus.cd\rock\m75d050.100\mcd\avd\

The time history matching must meet certain criteria. First, the time history dt needs to be 0.005 sec. If the time history does not have a dt of 0.005 sec, it is interpolated using INTERPOL v1.0. The FAS is visually checked to make sure it is smooth and does not contain large offsets. If necessary the source distance and depth values are adjusted in the RASCALS input file to obtain a smooth FAS. Between 0.2 and 50 Hz, the calculated spectrum cannot be more than 10% below or 30% above the target spectrum, no more than 9 points in a row can be below the target, the PGA value must be with 10% of the target, and the ratio of the average difference between the response spectrum and the target must be greater than 1.0.

The time histories are calculated in the folder match.fn\AFE

(AFE: 5E-4= 5×10^{-4} , 10-3 = 10^{-3} , 10-4= 10^{-4})

The target is interpolated to 298 points using INTERPOL v1.0 in the folder \target\h and target\v.

The interpolated target (TARGET11.DAT) is copied to the spectral matching folders.

If the vertical UHS was determined to be to peaked, it was smoothed by eye.

The matching is done in SWS1H.1\UHS, SWS1H.2\UHS, SWS1V5\UHS (Site-wide SFA, set 1, horizontal 1, horizontal 2, vertical, respectively (the V5 refers to a V/H ratio cutoff of 0.5. At one point during the calculations, V/H ratios with a cutoff of 0.5 or a cutoff of 0.67 were run, leading to two sets of vertical hazard curves and UHS. The V/H cutoff of 0.67 was abandoned). Five sets were calculated. The spectral matching is done using RASCALS v5.5. The input file is the target file TARGET11.DAT, the seed time history (the name of which varies), and the RASCALS input file, MATCH.IN. The output files are the FAS, MATCH.FAS, and the spectral compatible time history, MATCH.A08. In the subfolder the BASE4, the MATCH.A08

acceleration time history is baseline corrected using BASE4 v4.0. The input file is BASE.IN and the MATCH.A08. The output is the baseline correct acceleration velocity and displacement time histories, MATCH.ATH, MATCH.VTH, MATCH.DTH. MAXMIN v1.0 is used to determine the maximum value of the time histories. The input is MAXMIN.IN and the output MAXMIN.OUT. In the subfolder SPC, the response spectra at 9 dampings of the baseline corrected acceleration time history is calculated using the program SPCTLR v1.0. The input file is SPCTLR.IN and MATCH.ATH, and the output is MATCH.005, MATCH.010, MATCH.020, MATCH.030, MATCH.050, MATCH.070, MATCH.100, MATCH.150, MATCH.200 for dampings of 0.5%, 1%, 2%, 5%, 3%, 7%, 10%, 15%, and 20%, respectively.. SMRATIO v1.0 is used calculate the ratio between the response spectra and the target. This is used for checking to ensure the resulting match meets the criteria previously discussed. The input file is SMRAT.IN, which read in the files TARGETI1.DAT and MATCH.050. In the subfolder dur, the program DUR v1.0 is used to calculate Arias intensity versus duration. The input file is DUR.IN and MATCH.ATH, the output is MATCH.DUR and MATCH.OUT. The cross-correlations are calculated in the subfolder CORBB using the program CORBB v1.0. The cross-correlations are calculated between H1-H2, H1-V, and H2-V for acceleration, displacement and velocity.

The target spectra (design spectra) are submitted to the TDMS (DTN: MO0706DSDR5E4A.001 [DIRS 181422], MO0706DSDR1E4A.001 [DIRS 181421], MO0706DSDR1E3A.000 [DIRS 181423]).

The time histories are submitted to the TDMS (DTN: MO0706TH1E4APE.001 [DIRS 181960], MO0706TH1E3APE.001 [DIRS 182460], MO0706TH5E4APE.001 [DIRS 181961]).

SFA Damped Design Spectra

In addition to 5%-damped seismic design spectra, spectra at other damping values were calculated for the AFEs of 10^{-3} , 5×10^{-4} and 10^{-4} . Spectral ratios and damping coefficients as described below were computed and used to develop the suite of damped spectra. This methodology of estimating damped spectra at spectral damping ratios other than 5% is based on the approach developed by Idriss (1993); [DIRS 105524]. This approach provides two sets of relationships, one for damping ratios less than 5% and the other for damping ratios greater than 5%, which can be used to obtain the spectral ratios for a given damping value. These relationships, Equations D-1 and D-2, are shown below. Equations D-1 and D-2 represent the model for damping less than or equal to 5% and damping greater than 5% respectively. The 5%-damped spectral value when multiplied to this spectral ratio yields the spectral value at that damping ratio.

$$\text{Spectral Ratio (f,D)} = a1 - b1 \text{LN(D)} \quad (\text{f is frequency, D is damping and } D \leq 5\%) \quad (\text{D-1})$$

$$\text{Spectral Ratio (f,D)} = a2 - b2 \text{LN(D)} \quad (\text{f is frequency, D is damping and } D > 5\%) \quad (\text{D-2})$$

Spectra at damping values of 0.5%, 1%, 2%, 3%, 5%, 7%, 10%, 15% and 20% were generated using the computer program SPCTLRv1.0. This program uses an acceleration time history provided to it and generates response spectra at the damping value specified by the user. Spectra were generated using the five sets of spectrally-matched seismic design time histories (two horizontal and one vertical component) for each AFE. Therefore, for each AFE there were 90 horizontal (5 sets x 2 components x 9 damping values) and 45 vertical (5 sets x 1 component x 9

damping values) response spectra that were generated. Each of these spectra had spectral acceleration values, computed in units of g, at 298 frequency points. These spectra are calculated when spectrally matching time histories (MATCH.FNL). Details are included in the Time Histories section.

For each response spectra developed as described above, a ratio was calculated between the spectral acceleration value of that spectrum and the corresponding value for the corresponding 5%-damped spectrum. This ratio was termed as the Ratios (data). For each of the nine damping values listed above, the lognormal mean of the corresponding 30 horizontal (5 sets x 2 horizontal components x 3 return periods) and 15 vertical (5 sets x 1 vertical component x 3 return periods) ratios was computed. The calculations are shown in Excel files in the folder Excel\Yucca Damped Spectra 2007, with horizontal.xls being for horizontal spectra and vertical.xls being vertical spectra.

For each of the nine damping values, a best-fit curve was fitted through the average Ratios (data) using the trendline option in excel. A sample curve has been shown in Figure D-1.

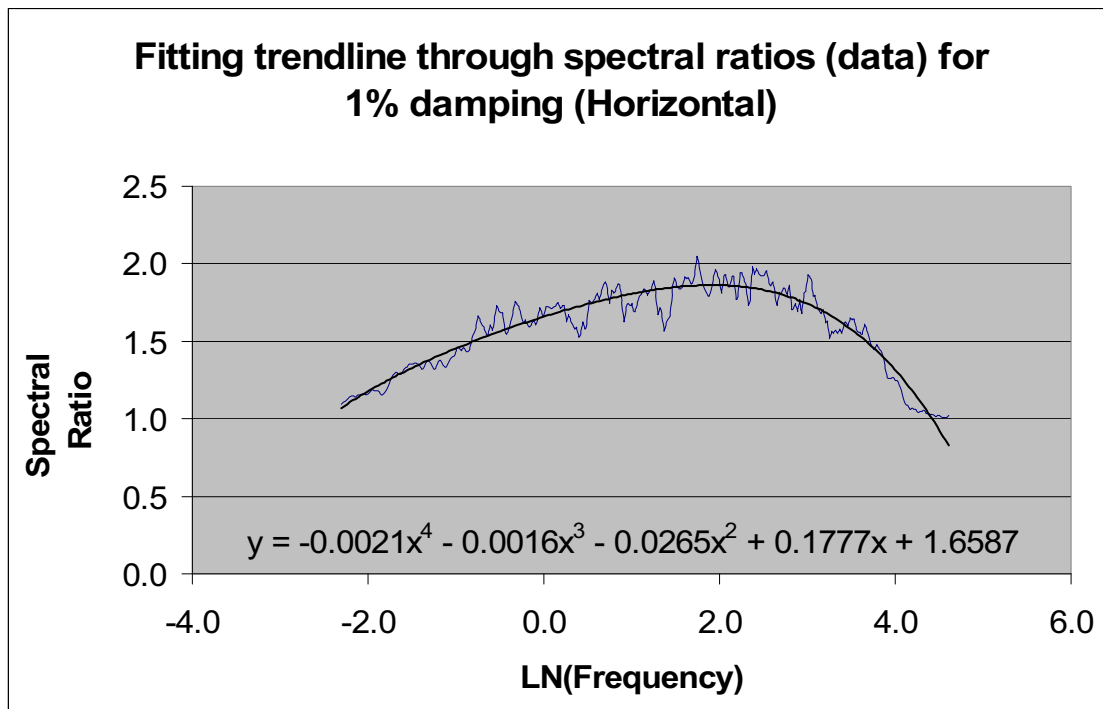


Figure D-1: A sample trendline used to compute smooth spectral ratios.

The equation of this trendline was used to calculate the spectral ratios (smooth) at 28 frequency points and these ratios (smooth) were used to develop the model. These 28 frequency points are considered to be a representative sample of the 298 frequency points at which the original spectra were developed.

Next, the spectral ratios (smooth) computed above were divided into two groups, one for damping less than 5% and the other for damping greater than 5%. For each group, at each of the 28 frequency points, another best-fit line was fitted through the set of spectral ratios (smooth) computed above and the corresponding damping values to get an equation similar in form to equation D-1 or D-2. This equation was used to obtain the coefficients a1, b1, a2 and b2 that are site-specific and therefore used to obtain the site-specific damped spectra for the project.

Figure D-2 shows an example of the best-fit line for spectral ratio (smooth) versus damping plot for the horizontal component, damping less than 5% and frequency 10Hz. The values of the coefficients a1 and b1 as obtained from the equation are 1.8744 and 0.6036 respectively.

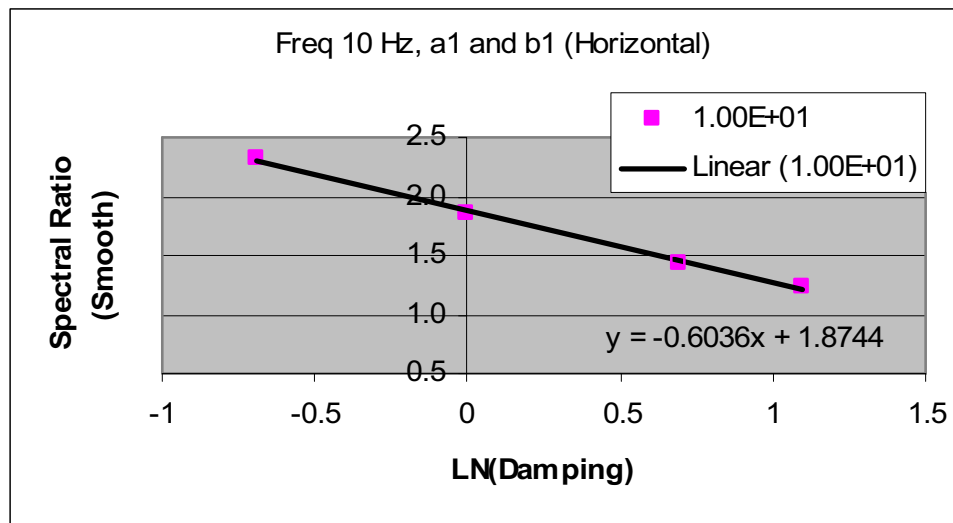


Figure D-2: An example of best-fit curve used to obtain the site-specific coefficients.

Tables D-18 and D-19 show the site-specific coefficients developed for the horizontal and the vertical cases using the above procedure.

TABLE D-18. HORIZONTAL COEFFICIENTS

Freq	a1	b1	a2	b2
0.1	1.0661	0.0237	1.2355	0.1371
0.2	1.2802	0.1348	1.4137	0.2576
0.298	1.3803	0.1927	1.4723	0.2982
0.404	1.4500	0.2384	1.5012	0.3191
0.498	1.4956	0.2667	1.5144	0.3292
0.6	1.5346	0.2938	1.5222	0.3356
0.706	1.5677	0.3176	1.5263	0.3395
0.793	1.5907	0.3346	1.5279	0.3415
0.89	1.6133	0.3517	1.5284	0.3427
1	1.6353	0.3688	1.5279	0.3434
2.01	1.7560	0.4689	1.5087	0.3369
2.98	1.8121	0.5201	1.4886	0.3271

Freq	a1	b1	a2	b2
4.04	1.8461	0.5539	1.4700	0.3173
4.98	1.8638	0.5734	1.4555	0.3093
5.99	1.8746	0.5873	1.4417	0.3014
7.05	1.8797	0.5963	1.4288	0.2938
8.11	1.8805	0.6013	1.4171	0.2867
9.11	1.8782	0.6034	1.4070	0.2804
10	1.8744	0.6036	1.3985	0.2751
20	1.8400	0.5518	1.3236	0.2243
30.5	1.6513	0.4693	1.2691	0.1844
40.4	1.6100	0.3727	1.2193	0.1465
49.8	1.3910	0.2862	1.1797	0.1156
59.9	1.2636	0.1943	1.1403	0.0845
70.5	1.1358	0.1012	1.1023	0.0542
81.1	1.0000	0.0000	1.0000	0.0000
91.1	1.0000	0.0000	1.0000	0.0000
100	1.0000	0.0000	1.0000	0.0000

TABLE D-19. VERTICAL COEFFICIENTS

Freq	a1	b1	a2	b2
0.1	1.0598	0.0169	1.1902	0.1112
0.2	1.2607	0.1267	1.3747	0.2335
0.298	1.3620	0.1867	1.4330	0.2747
0.404	1.4356	0.2331	1.4618	0.2963
0.498	1.4852	0.2658	1.4756	0.3074
0.6	1.5283	0.2952	1.4844	0.3151
0.706	1.5654	0.3213	1.4900	0.3205
0.793	1.5915	0.3400	1.4929	0.3236
0.89	1.6172	0.3588	1.4951	0.3262
1	1.6425	0.3777	1.4966	0.3284
2.01	1.7831	0.4890	1.4961	0.3341
2.98	1.8496	0.5467	1.4907	0.3333
4.04	1.8906	0.5850	1.4845	0.3306
4.98	1.9124	0.6074	1.4787	0.3276
5.99	1.9264	0.6236	1.4723	0.3239
7.05	1.9339	0.6345	1.4655	0.3198
8.11	1.9363	0.6410	1.4586	0.3155
9.11	1.9352	0.6442	1.4520	0.3112
10	1.9322	0.6451	1.4460	0.3073
20	1.8344	0.5965	1.3745	0.2601
30.5	1.7057	0.5132	1.3042	0.2137
40.4	1.5621	0.4145	1.2298	0.1649
49.8	1.4363	0.3257	1.1652	0.1228
59.9	1.3044	0.2311	1.0975	0.0788
70.5	1.1723	0.1352	1.0293	0.0348
81.1	1.0000	0.0000	1.0000	0.0000
91.1	1.0000	0.0000	1.0000	0.0000

100	1.0000	0.0000	1.0000	0.0000
-----	--------	--------	--------	--------

These coefficients were used to compute the spectral ratios for different damping values using equations D-1 and D-2. These ratios were termed as the Ratios (Model). These Ratios (Model) were multiplied with the 5% target spectra to obtain the spectra (termed as Spectra (Model)) at damping other than 5%. Figures 6.5.2-55 through 6.5.2-60 show the computed damped spectra (Spectra (Model)).

The data was submitted to the TDMS (DTN: MO0706DSDR5E4A.001 [DIRS 181422], MO0706DSDR1E4A.001 [DIRS 181421], MO0706DSDR1E3A.000 [DIRS 181423]).

Repository Block RASCALS Calculations

The calculations for the repository block (Section 6.5.5) are essentially the same as for the SFA. The only difference is the velocity profiles (section 6.4.2.6). The Point A inputs are the same, the material models for appropriate Tuff is the same (there is no alluvium for the repository block velocity profile). The directory paths and input/output files are the same. The one exception is the directory defining the velocity profile.

Example: Rascals\amps.02\AM1P02P5.B1\G100
 Rascals = Horizontal (vertically incident SH-wave),
 Rascalp = Vertical (vertically incident P-wave)
 Amps.01 = Point A RVT input , amps.02 = Point source input
 AM1P02P5.B1 = profile
 G100 = ground motion level (0.01g – 10.0 g)

profile: 12345678.90

1: A = amp runs

2-3: M1=UMT, M3=LMT

4-6: P02= Calico at 1100 ft with a thickness of 400 ft

7-8: D1=1-2Hz, D5=5-10Hz, P5=magnitude 5.0, P6=magnitude 6.0, P7=magnitude 7.0

9-0: B1=mean of all 3 soft zones, B4= Central Stiff zone

In all other respects the calculation of the transfer functions are exactly the same.

PGV V/H ratios are calculated for the Repository Block.

This is done in the folder SMRATV_H.PGV using the program SMRATIO. The PGV value, contained in the point-source RASCALS calculated file *.R00, divided by the PGV calculated by point-source RASCALP.

Likewise the calculation of the repository horizontal hazard curves was exactly the same as the SFA. The calculations were done in the folder 10GHAZ.03B

Repository SOILUHSI/HAZUHS

Again, this is very similar to the SFA described earlier. SUHSINP/SOILUHSI is run for each velocity profile (i.e. UMT, All 3 soft zones, 1-2 Hz) for eight frequencies (100.0 (PGA), 20.0, 10.0, 5.0, 2.0, 1.0, 0.5, 0.3) and PGV. For a given period (i.e. PGA) the program reads the Point A fractile curve, the Point A spectra for all ground motion levels (0.01 g – 10.0 g), and the

transfer functions for all ground motion levels. The output is a modified hazard curve for the given period. The program FRACTILE v2.0 is then used to calculate the fractile curves about the modified hazard curve as well as to combine with weights (the material models) and envelope the two locations. The final result is a suite of site-specific horizontal hazard curves for the repository block. Finally, HAZUHS v1.0 is used to calculate the UHS for a given AFE.

The SOILUHSI/HAZUHS set is calculated under the directory:

10GHAZ.03B\

In this folder the conditioned for extreme hazard Point A hazard curves are used and the V/H is constrained to a maximum value of 0.5.

The Point A hazard curves are in the folder PSHA.F09\

These are described in Section 6.4.1.

Each includes the following fractile levels (MEAN, 0.005, 0.050, 0.150, 0.200, 0.500, 0.800, 0.850, 0.950, 0.995)

The conditioned for extreme hazard Point A hazard curves were calculated using EXTHC v1.0 and are in the folder EXTHC for the frequencies 0.3 Hz, 0.5 Hz, 1.0 Hz, 2.0 Hz, 5.0 Hz, 10.0 Hz, 20.0 Hz, 100.0 Hz (PGA), and PGV and for the following fractile levels (0.05, 0.15, 0.50, 0.85, 0.95, MEAN)

Extreme Ground motions are described in Appendix A and Section 6.5.1.

SUHSINP and SOILUHSI are run for each velocity profiles, and the directory naming convention is the same as the RASCALS calculations (i.e. AM1P02D1.B1 for UMT, 1-2hz RE, all 3 soft zones).

The subfolders are: SUHSI.###

= .003 = 0.3 Hz, .005 = 0.5 Hz, .010 = 1.0 Hz, .020 = 2.0 Hz, .050 = 5.0 Hz, .100 = 10.0 Hz, .200 = 20.0 Hz, .PGA = 100.0 Hz, .PGV = PGV

For each frequency SUHSINP and SOILUHSI are run for various Point A fractile curves.

SIMN.IN is the SUHSINP input file for mean.

The weighting of the RE is the same.

The output from SUHSINP.IN is the input file, MN.IN, used by SOILUHSI v1.0. The output of SOILUHSI is MN.OUT, which is the modified mean hazard curve.

Next, FRACTILE v2.0 is run to calculate the fractile curves about the modified mean hazard curve. It is at this stage that the epistemic uncertainties are combined with weights, or are enveloped.

FRACTILE is run in the following subdirectories:

FCTP02B1.CMB = Mean of all 3 soft zones, combination of material models and RE.

FCTP02B4.CMB = Central Stiff Zone, combination of material models and RE.

FCTENB.ENV = Envelope of the two sites, Final Repository hazard curves

The FRACTILE input files using the following naming convention: F0003MN.IN = 0.3 Hz, F0005MN.IN = 0.5 Hz, F0010MN.IN = 1.0 Hz, F0020MN.IN = 2.0 Hz, F0050MN.IN = 5.0 Hz, F0100MN.IN = 10.0 Hz, F0200MN.IN = 20.0 Hz, F1000MN.IN = 100.0 Hz

The weights assigned for the epistemic uncertainty are listed in table D-20.

TABLE D-20
Weights for RB Material
Models

Material Models	
UMT	0.70
LMT	0.30

The input to each file when combining the epistemic uncertainty is the output from the SOILUHSI for the appropriate frequency and alluvial depth. The output is the fractile hazard curves at the following levels: 0.05, 0.15, 0.50, 0.85, 0.95, MEAN. In enveloping the input is the output from FRACTILE, with the output being the enveloped mean hazard curve.

The final step is to calculate the uniform hazard spectra (UHS). This is done using the program HAZUHS v1.0. It is done in the folder 10GHAZ.03B\FCTPENB.ENV\HAZUHS. This folder contains the final Repository hazard curves. The program HAZUHS simply reads in the mean hazard curves at each frequency and determines the value for a given AFE. The input file is HUMN.IN and the output file HUMN.OUT, which contains the UHS at the AFE of 10-3, 5E-4, 10-4, 10-5, 2E-6, 10-6, 10-7.

The envelope of the two sites hazard curves, which is the final repository hazard curves and UHS are submitted to the TDMS (DTN: MO0801HCUHSREB.001 [DIRS 184803])

Repository Vertical SOILUHSI/HAZUHS

The development of the vertical hazard curves and UHS are very similar to the method used to develop the horizontal and similar to development of the vertical for SFA. The main difference is for SOILUHSI (actually SUHSINP), the files read in the final SFA site-wide horizontal hazard curve and the RASCALS model V/H ratios. For the repository, empirical V/H ratios are not used, because the motion is being calculated at depth.

10GHAZ.03B\

In this folder the conditioned for extreme hazard Point A hazard curves are used and the V/H is constrained to a minimal value of 0.5.

SUHSINP and SOILUHSI are run for each velocity profile, and the directory naming convention is the same as the RASCALS point source calculations, with A replaced with V for vertical (i.e. VM1P02P6.B1 for UMT, magnitude 6.0, mean of all 3 soft zones).

The subfolders are: VSI.###

= .003 = 0.3 Hz, .005 = 0.5 Hz, .010 = 1.0 Hz, .020 = 2.0 Hz, .050 = 5.0 Hz, .100 = 10.0 Hz, .200 = 20.0 Hz, .300 = 30.0 Hz, .500 = 50.0 Hz, .PGA = 100.0 Hz, .PGV = PGV

For each frequency SUHSINP and SOILUHSI are run for various conditioned Point A fractile curves.

SIMNVH.IN is the SUHSINP input file.

SUHSINP reads in the SFA site-wide horizontal fractile curve for the given frequency, the conditioned Point A RASCALS calculated spectra, for the given magnitude, the empirical horizontal spectra for the given magnitude, the RASCALS calculated V/H ratios and empirical

calculated V/H ratios for a given magnitude. The choice of ground motion level to use and the weights are determined from tables D-21. As with the SFA calculations, the weights in table D-21 are based on the contributing earthquakes for each frequency in table D-13, such that the resulting magnitude is equal to the controlling magnitude at each frequency and AFE given in table D-21 (third column). When the controlling magnitude is greater than 7.0, one-hundred percent weight was given to a magnitude 7.0.

TABLE D-21
Weights Utilized in RB V/H Ratios

Freq	AFE	M _w	M	weight	M	weight	
0.3	1.00E-03	7.35	7.0	1.00			
0.3	1.00E-04	7.45	7.0	1.00			
0.3	1.00E-05	7.65	7.0	1.00			
0.3	1.00E-06	7.65	7.0	1.00			
0.3	1.00E-07	7.65	7.0	1.00			
0.5	1.00E-03	7.35	7.0	1.00			
0.5	1.00E-04	7.45	7.0	1.00			
0.5	1.00E-05	7.45	7.0	1.00			
0.5	1.00E-06	7.65	7.0	1.00			
0.5	1.00E-07	7.65	7.0	1.00			
1.0	1.00E-03	7.35	7.0	1.00			
1.0	1.00E-04	7.65	7.0	1.00			
1.0	1.00E-05	6.25	7.0	0.25	6.0	0.75	
1.0	1.00E-06	6.65	7.0	0.65	6.0	0.35	
1.0	1.00E-07	6.65	7.0	0.65	6.0	0.35	
2.0	1.00E-03	7.35	7.0	1.00			
2.0	1.00E-04	6.15	7.0	0.15	6.0	0.85	
2.0	1.00E-05	6.25	7.0	0.25	6.0	0.75	
2.0	1.00E-06	6.25	7.0	0.25	6.0	0.75	
2.0	1.00E-07	6.65	7.0	0.65	6.0	0.35	"P7"
5.0	1.00E-03	5.15	6.0	0.15	5.0	0.85	"P6"
5.0	1.00E-04	6.15	7.0	0.15	6.0	0.85	
5.0	1.00E-05	6.25	7.0	0.25	6.0	0.75	
5.0	1.00E-06	6.15	7.0	0.15	6.0	0.85	
5.0	1.00E-07	6.15	7.0	0.15	6.0	0.85	
10.0	1.00E-03	5.05	6.0	0.05	5.0	0.95	
10.0	1.00E-04	5.85	6.0	0.85	5.0	0.15	
10.0	1.00E-05	6.25	7.0	0.25	6.0	0.75	
10.0	1.00E-06	6.15	7.0	0.15	6.0	0.85	
10.0	1.00E-07	6.15	7.0	0.15	6.0	0.85	
20.0	1.00E-03	5.15	6.0	0.15	5.0	0.85	
20.0	1.00E-04	5.85	6.0	0.85	5.0	0.15	
20.0	1.00E-05	6.25	7.0	0.25	6.0	0.75	
20.0	1.00E-06	6.15	7.0	0.15	6.0	0.85	

Freq	AFE	M_w	M	weight	M	weight	
20.0	1.00E-07	6.15	7.0	0.15	6.0	0.85	
30.0	1.00E-03	5.15	6.0	0.15	5.0	0.85	
30.0	1.00E-04	5.85	6.0	0.85	5.0	0.15	
30.0	1.00E-05	6.25	7.0	0.25	6.0	0.75	
30.0	1.00E-06	6.15	7.0	0.15	6.0	0.85	
30.0	1.00E-07	6.15	7.0	0.15	6.0	0.85	
50.0	1.00E-03	5.15	6.0	0.15	5.0	0.85	
50.0	1.00E-04	5.85	6.0	0.85	5.0	0.15	
50.0	1.00E-05	6.20	7.0	0.20	6.0	0.80	
50.0	1.00E-06	6.15	7.0	0.15	6.0	0.85	
50.0	1.00E-07	6.15	7.0	0.15	6.0	0.85	
100.0	1.00E-03	5.15	6.0	0.15	5.0	0.85	
100.0	1.00E-04	5.85	6.0	0.85	5.0	0.15	
100.0	1.00E-05	6.15	7.0	0.15	6.0	0.85	
100.0	1.00E-06	6.15	7.0	0.15	6.0	0.85	
100.0	1.00E-07	6.15	7.0	0.15	6.0	0.85	

Based on probability levels magnitude 7 is used for frequencies 0.3 Hz, 0.5 Hz, 1.0 Hz, and 2.0 Hz, PGV, and magnitude 6 is used for frequencies 5.0 Hz, 10.0 Hz, 20.0 Hz, 30.0 Hz, 50.0 Hz, and 100 Hz (PGA). Input files for SUHSINP/SOILUHSI exist for all frequencies for each magnitude, but only the ones described above are utilized and have been checked.

For 0.3 Hz and 0.5 Hz, which use only one magnitude (M7.0, see Table D-19), the weighting used in the SUHSINP input file is straightforward. For the other frequencies, which involve multiple magnitude inputs with weights, a variable weighting must be used. The weights for magnitude are interpolated for AFE of the hazard curves.

SUHSINP v1.0 writes out the SOILUHSI v1.0 input file MNVH.IN, for the mean. SOILUHSI is run, and the output file MNVH.OUT is the adjust hazard curve.

The variable weighting was calculated in the folder:

\10GHAZ.03B\VFTPENB.ENV\HAZUHS\VHWTS2

INTERPOL is used to interpolate the assigned weights for AFE to the Horizontal Hazard curve (HUMN.OUT). The weights are derived from table D-21. The INTERPOL input file is INTERMN.IN. The Interpolated weights are then combined in the Excel file WTSMN.XLS.

FRACTILE and HAZUHS are run exactly the same as the horizontal, the only difference is that the vertical adjusted hazard curves are read in. For horizontal the directories began with FCT, for vertical they begin with VFT. Again, magnitude 7 is used for frequencies 0.3 Hz, 0.5 Hz, 1.0 Hz, and 2.0 Hz, PGV, and magnitude 6 is used for frequencies 5.0 Hz, 10.0 Hz, 20.0 Hz, 30.0 Hz, 50.0 Hz and 100 Hz (PGA). Otherwise, the naming convention, folder names, and process is the same as the horizontal described above.

The

The final vertical hazard curves and UHS in the folder VFTPENB.ENV are submitted to the TDMS (DTN: MO0801HCUHSREB.001 [DIRS 184803])

Repository Time Histories

Time history development for the repository block (Section 6.5.5.4) are exactly the same as for the SFA, described earlier. The only difference are the seed time histories and of course, the targets are the UHS developed for the repository. Only one set of three-component time histories are developed for AFE 10-3, 5E-4, 10-4.

The seed time histories listed in table D-22.

TABLE D-22
Summary of RB Seed Time Histories

Repository	Earthquake - Station	Time History M	Time History D	Time History Path
10-3 Set 1	NORTHRIDGE - MEL CANYON	6.7	52	nrcwus.cd\rock\m65d050.100\mel\h1.a02
5E-4 Set 1	NORTHRIDGE - MEL CANYON	6.7	52	nrcwus.cd\rock\m65d050.100\mel\h1.a02
10-4 Set 1	Chi Chi - TCU015	7.6	43.75	nrcwus.cd\rock\m75d010.050\tcu015-n.at2

The folders are:

Match.fn1\AFE\REP1H.1, REP1H.2, REP1V5 (for repository block, set 1, horizontal 1, horizontal 2, vertical, respectively).

(AFE: 5E-4= 5×10^{-4} , 10-3 = 10^{-3} , 10-4= 10^{-4})

The targets are interpolated in the folder TARGET.REP.

The target spectra (design spectra) are submitted to the TDMS (DTN: MO0707DSRB5E4A.000 [DIRS 183130], MO0707DSRB1E4A.000 [DIRS 183129], MO0707DSRB1E3A.000 [DIRS 183128])

The time histories are submitted to the TDMS (DTN: MO0707THRB1E4A.000 [DIRS 183200], MO0707THRB1E3A.000 [DIRS 183196], MO0707THRB5E4A.000 [DIRS 183200])

APPENDIX E
TECHNICAL REVIEW OF THE STOCHASTIC POINT-SOURCE
GROUND MOTION MODEL

APPENDIX E

Review of validation of point-source stochastic ground motion model.

Reviewer: Richard Lee, Los Alamos National Laboratory, Los Alamos, NM

According to Model Validation Checklist (BSC 1098) the key elements to model validation are the following:

1. identification of corroborating /supporting data, models, or information used to complete model validation activities
2. level of model importance and required level of confidence
3. results of validation activities
4. model validation criteria explicitly specified. Criteria must address adequacy of the scientific basis and accuracy of the model consistent with intended use.
 - a. the criteria used to establish the adequacy of the scientific basis for the model must be explicit, consistent with the intended use of the model, and justified in the documentation.
 - b. the criteria used to demonstrate that the model is sufficiently accurate for its intended use must be consistent with parameter uncertainties and must be justified in the documentation.

Comments:

1. With the exception of items identified below, the point-source stochastic ground motion model validation meets the key elements (listed above) of the Model Validation Checklist (BSC 1098).
2. Section 7.2 Acceptance Criteria: model produces response spectra that are in reasonable agreement with observed data “as judged by the modeler” is probably not acceptable. I suggest changing the criteria to be the judgment of ground motion experts and that the approval of this report signifies that these criteria have been met in the view of the report originators, the technical checker and independent technical reviewers who evaluated the adequacy of model validation. See the validation summary similar to that developed for the RVT- equivalent linear site response model of (“Development of Earthquake Ground Motion Input for Preclosure Seismic Design and Postclosure Performance Assessment of a Geologic Repository at Yucca Mountain”).
3. Section 7.3.1. The primary element of the validation of the point-source stochastic ground motion model is the comparison of the model predictions to recorded earthquake spectra. The validation does this for fifteen earthquakes that produce a wealth of strong motion data used in engineering design. The modeling includes a large range in magnitude (M5.3-M7.4) and distance from 1-400 km in a variety of crustal models and several site conditions. This comparison goes well beyond typical validation studies of comparing ground motions for a single well-recorded earthquake and incorporates comparisons for a large number of earthquakes identifying strengths and weaknesses including inherent conservatism with use of the methodology. Since the comparisons have already

- been completed for 15-earthquakes, I suggest that the document be expanded to include descriptions (figures) of the other earthquake components as was done for the Northridge earthquake. Specific sections should be appended to Section 7.3.1 for each earthquake identified in Table 7-4. As for the Northridge example, each earthquake model should be accompanied by source, path and site descriptions (or at least complete references to adopted models) and a discussion of the individual earthquake bias. This effort should only be a “cut” and “paste” effort from the earlier Brookhaven work.
4. The last paragraph of Section 7.3.1.1 describes issues related to the use of synthesized site profiles versus a smoothed median spectrum. This section needs to be expanded somewhat and should describe the correlation model used to develop the simulations. Because the “issue” is left hanging, additional material should be provided to indicate whether there is a resulting significant “bias” introduced by the approach.
 5. 7.3.1.1 Northridge earthquake: How was rise-time used in the stochastic model?
 6. Section 7.3.1.1 Figures 7-3, 7-4 and 7-5 should be 7-2, 7-3 and 7-4 respectively. Then there is no Figure 7-5; i.e., there is a jump in Figure numbers.
 7. I suggest that the earthquake comparisons (Section 7.3.1) be updated to include the 1999 M 7.6 Chi-Chi and 1999 M7.1 Hector Mine earthquakes and any other more recent earthquakes producing applicable engineering data.
 8. I believe that the validation approach using the empirical ground motion prediction model (Section 7.3.2) is probably unnecessary. The key validation is a comparison to the recorded response spectra of major earthquakes as done in Section 7.3.1. It seems that a comparison to an empirical model is a step removed from the desired comparison (which is already completed). To avoid issues related to how the empirical regressions were done, supporting empirical data magnitude and distance, and the inevitable comparisons for magnitudes and distances not supported by the empirical data, I suggest that this section be removed entirely.
 9. The validation using spectral shapes (Section 7.3.3) is also an appropriate and important comparison that compensates somewhat for the lack of well recorded strong motion earthquakes in other tectonic environments such as the eastern United States.
 10. Section 7.3.1.1; last par. Discussion emphasizes the result of using randomized profiles tends to bias the results as compared to a smoothed base-case model especially for rock sites. The paragraph concludes that use of median estimates (in velocity) would improve the data fits. This bias should be more completely described and simulated velocity profiles should be discussed.
 11. Section 7.4: Where are the Little Skull Mountain earthquake spectra and model plots?
 12. Other than the Little Skull Mountain earthquake, all of the modeled earthquakes had mechanisms that were strike-slip, thrust or reverse. The dominant YMP sources are normal-oblique faulting. A critically important element of the validation is the successful modeling of strong ground motion from a normal faulting source. Unfortunately this data is not yet available however there are other events such as the 1999 Chi-Chi and 1999 Hector Mine earthquakes that

have produced significant strong motion data that can be modeled. There is no compelling reason to believe that other than a modification of the stress parameter, normal faulting earthquakes can be modeled adequately with the stochastic ground motion model, however the eventual normal faulting event that is well recorded should be part of the future model validation.

11/28/07

Responses to review comments by Richard Lee on the validation of the stochastic point-source ground motion model.

1. No response needed.
2. We agree with the comment and the text has been amended.
3. We agree and text and figures for the additional 15 earthquakes has been added to the text.
4. This issue is considered outside the scope of this study and considered not to be significant to the validation of the point-source model. The randomization approach used in the Silva et al (1996 [DIRS 110474]) study is an earlier version of approach described in Section 6.4.2.10.
5. This sentence has been deleted from the text as was not used in the stochastic model.
6. The figure numbers have been corrected
7. We agree that adding comparisons for these more recent earthquakes would be useful. We will attempt to include these comparisons in the next revision of this report.
8. We agree with the reviewer and have deleted this section from the text.
9. No response needed.
10. We will attempt to resolve this issue in the next revision of this report.
11. The requested plots have been added to the text.
12. We agree with the reviewer. We will attempt to include these comparisons in the next revision of this report.

01/02/08- I agree with the responses (above) to my stochastic model review comments of
11/24/07- Richard Lee

Supplemental Earthquake Ground Motion Input for a Geologic Repository at Yucca Mountain, NV

APPENDIX E

Approved by Richard C. Lee
Richard C. Lee 2/17/08

Review of validation of point-source stochastic ground motion model.

Reviewer: Richard Lee, Los Alamos National Laboratory, Los Alamos, NM

According to Model Validation Checklist (BSC 1098) the key elements to model validation are the following:

1. identification of corroborating /supporting data, models, or information used to complete model validation activities
2. level of model importance and required level of confidence
3. results of validation activities
4. model validation criteria explicitly specified. Criteria must address adequacy of the scientific basis and accuracy of the model consistent with intended use.
 - a. the criteria used to establish the adequacy of the scientific basis for the model must be explicit, consistent with the intended use of the model, and justified in the documentation.
 - b. the criteria used to demonstrate that the model is sufficiently accurate for its intended use must be consistent with parameter uncertainties and must be justified in the documentation.

Comments:

1. With the exception of items identified below, the point-source stochastic ground motion model validation meets the key elements (listed above) of the Model Validation Checklist (BSC 1098).
2. Section 7.2 Acceptance Criteria: model produces response spectra that are in reasonable agreement with observed data "as judged by the modeler" is probably not acceptable. I suggest changing the criteria to be the judgment of ground motion experts and that the approval of this report signifies that these criteria have been met in the view of the report originators, the technical checker and independent technical reviewers who evaluated the adequacy of model validation. See the validation summary similar to that developed for the RVT- equivalent linear site response model of ("Development of Earthquake Ground Motion Input for Preclosure Seismic Design and Postclosure Performance Assessment of a Geologic Repository at Yucca Mountain").
3. Section 7.3.1. The primary element of the validation of the point-source stochastic ground motion model is the comparison of the model predictions to recorded earthquake spectra. The validation does this for fifteen earthquakes that produce a wealth of strong motion data used in engineering design. The modeling includes a large range in magnitude (M5.3-M7.4) and distance from 1-400 km in a variety of crustal models and several site conditions. This comparison goes well beyond typical validation studies of comparing ground motions for a single well-recorded earthquake and incorporates comparisons for a large number of earthquakes identifying strengths and weaknesses including inherent conservatism with use of the methodology. Since the comparisons have already